FUNCTIONAL IMAGING TECHNIQUES TO PERSONALISE ONCOLOGICAL TREATMENTS

RACHEL ANNE PEARSON

SUBMITTED FOR THE DEGREE OF DOCTOR OF PHILOSOPHY

Date of Viva 24 April 2017

Northern Institute for Cancer Research

Newcastle University

Abstract

Biomarkers are an emerging concept in oncology and are required for stratified medicine. Prognostic and predictive biomarkers forecast outcome and guide therapy. Biological properties of tumours can be visualised using newer functional MRI or PET-CT techniques, which complement the structural information provided by contrast-enhanced CT/MRI. Specifically, the unique properties of the research PET tracer 18F-flurothymidine (FLT PET-CT), and diffusion-weighted (DW-MRI) and dynamic contrast-enhanced magnetic resonance imaging (DCE-MRI) have shown promise in identifying early treatment responders after chemotherapy or radiotherapy. The increasing sophistication of radiotherapy techniques calls for better understanding of tumour biology so that this information can be integrated into individualised treatment plans.

This dissertation describes studies aimed to improve knowledge of how to employ functional imaging techniques to individualise treatments for oncology patients. A portfolio of early phase clinical trials was established to evaluate imaging biomarkers in several solid tumour settings; pancreatic, thyroid, oropharyngeal and bladder cancer patients were studied. Additionally, data from a preclinical study evaluating the administration of thymidine phosphorylase to optimise FLT PET scanning are presented.

Acknowledgements

I am very grateful to have had the support of many people within Newcastle University and the Newcastle upon Tyne Hospitals NHS Foundation Trust, without whom this project would not have been possible. Thank you to the patients and relatives who gave of their time to participate in the studies.

Specifically, I would like to thank my university supervisors Prof Herbie Newell, Prof Ruth Plummer and Dr Ross Maxwell for their guidance and encouragement. I have been very fortunate to have been given the freedom to steer the direction of the clinical studies towards my particular research interests. I am grateful to the many educational and management opportunities that undertaking the PhD within this team has given me and appreciate the inclusion at, and encouragement to actively participate, in many UK meetings.

Additionally, I'd like to thank Prof Josef Vormoor, Prof Steve Wedge and Prof Alan Boddy for their annual panel reviews and general mentoring. For collaboration, supervision and education of the preclinical work: Dr Phil Berry, Mr Martin Galler, Dr Ian Wilson, Dr Gilberto Almeida, and Dr Huw Thomas. For their guidance with the imaging acquisition and analysis: Dr Pete Thelwall, Dr Fiona Smith, Prof Andy Blamire and Dr Ross Maxwell at the Centre for In Vivo Imaging at Newcastle University. For contribution to data analysis undertaken within the FLAIRE project, Mr Dominic Kite, medical student. For administrative support: Mrs Lishan Sung, Mrs Viv Sewell, Mrs Sandra Cartwright, Mrs Sandra Blackwood, Mrs Beverly Hailstone and Mr Josef Hoben.

A specific thank you to Dr George Petrides, radionuclide radiologist for his guidance, reporting of many scans late on a Friday afternoon, and continued enthusiasm for the projects. Also to Dr Ian Driver, Dr Tamir Ali, Miss Elizabeth Howell and the nuclear medicine technologists within the department of Nuclear medicine, and Drs Andy McQueen, Piotr Pieniazek and Phil Haslam in Radiology. Also, Dr Helen Turner and Dr Babet Disep, Consultant Pathologists who performed Ki-67 testing in the MARBLE trial.

Drs Charles Kelly, John Frew, Ujjal Mallick and Kate Sumpter kindly agreed to take on the role of Principal Investigator for the clinical trials and I am grateful to the

additional support from the head and neck, urology, thyroid, and hepatobiliary MDT members, and the Northern Centre for Cancer Care Clinical Director Dr Ian Pedley. For day-to-day assistance running the PET and MRI clinical trials particularly during the periods of my maternity leave: Mr Jim Snell, Mr Chris Barron, Dr Julie Charlton, Mrs Jill McKenna, Mr Steve Harris, Mrs Sarah Atkinson, Dr Noor Haris and Miss Ayesha Clark. Within radiotherapy physics: Mrs Gill Lawrence, Mrs Hazel McCallum, Mr Chris Walker, Mr Nick Willis, Mrs Tracy Wilkes and Mr Jonathan Wyatt.

Thank you also to PET-NET solutions for providing the FLT radiotracer; Dr Bridget Bax at St George's Hospital for the thymidine assays; Dr Eric Aboagye and Dr Kathrin Heinzman at Imperial College for undertaking the thymidine phosphorylase animal work; and Dr Rohini Sharma and Dr Amar Challapalli for inviting us to collaborate on the pancreas study.

Finally, I'd like to thank my husband for his unwavering support, our three children, and my parents.

.

Table of Contents

List of Tables

List of Figures

Chapter 1 Introduction

1.1 Stratified Medicine

The National Institute for Health (NIH) and Food and Drug Administration (FDA) view stratified medicine as core to the progress of healthcare (Hingorani *et al.*, 2013). The term “Stratified Medicine” refers to customising treatments according to tumour biology and other patient characteristics using clinical biomarkers. The process of identifying specific treatments for particular tumour types has been used for many years in the field of oncology although the phrase “stratified medicine” has only been coined in recent times. One of the best examples dates back to 2002: the Her 2-positive genotype in breast cancer identifies patients who respond to treatment with trastuzumab (NICE, 2002).

Biomarkers are an emerging concept in oncology and are required for stratified medicine. Various definitions exist for the term biomarkers and Trusheim *et al* have described a biomarker as

> “a characteristic that is objectively measured and evaluated as an indicator of normal biological processes, pathogenic processes or pharmacological responses to a therapeutic intervention” (Trusheim *et al.*, 2007).

Different classes of biomarker influence patient care at different stages in the management pathway. Prognostic and predictive biomarkers can forecast outcome and guide therapy. Her-2 can be classified as both a poor prognostic biomarker, and a good predictor of response to trastuzumab treatment. Positive prognostic biomarkers forecast a favourable prognosis and may influence management strategies to avoid overtreatment. In these situations patients may have a good outcome with minimal intervention. Poor prognostic biomarkers may lead to intensification of treatment to try and overcome the anticipated poor outcome. In a patient who is unsuitable for intensive treatment, an acknowledgement of poor response to treatment, independent of the type of treatment, could direct the patient towards best supportive care or experimental medicines at an early opportunity. The former may improve quality of life for the patient by minimising the side-effects of a futile therapy.

Clinical biomarker data may be derived from genes, proteins, histology or imaging, and may involve invasive or non-invasive procedures. Biopsies, blood samples and body fluid examinations are invasive procedures, and can provide information on molecular processes in conjunction with the “gold standard” pathological data. However, the techniques rely on procedures which can range from the minimal intervention of venepuncture, to a more invasive surgical biopsy under general anaesthetic. Invasive procedures are not always feasible, may result in patient discomfort, and are dependent on staffing and equipment resources. Furthermore, data obtained from a single sample is specific to the biopsy site and may overlook tumour heterogeneity and changes with time.

Functional imaging technologies offer an appealing alternative to invasive procedures. Non-invasive methodologies have the advantage of providing information on the entire tumour and, if present, the extent of metastatic disease, with minimal patient discomfort. Drawbacks include: the challenges of validating new techniques; generating reproducible results; the additional time spent by the patient and staff performing and processing the results of often complex investigations; and the high cost of serial scans.

Three functional imaging techniques described in this thesis belong to a group of emerging imaging modalities with promising applications in early response assessment or radiotherapy treatment planning: 18F-fluorothymidine positron emission tomography (FLT PET-CT); diffusion-weighted magnetic resonance imaging (DW-MRI); and dynamic contrast-enhanced magnetic resonance imaging (DCE-MRI). Each of these techniques is described in turn, followed by details on the potential clinical applications and background to the clinical trials. To conclude this introduction, an outline of the dissertation is presented.

1.2 Positron Emission Tomography (PET)

1.2.1 Overview of PET

CT and routine MRI are established imaging modalities which provide anatomical information on cancers. Biological properties of tumours can be visualised using newer functional MRI or PET-CT techniques. For many tumour sites, PET-CT is a valued imaging modality for diagnosis, prognosis, treatment-planning and response assessment. PET uses radiotracers which produce a pair of gamma rays when a

positron interacts with an electron inside the patient. The gamma rays travel in opposite directions and are detected using a ring of detectors within the PET machine. ^{18}F-Fluorodeoxyglucose (FDG) is the most widely used PET-CT tracer. “Hot spots” or areas of increased avidity on FDG PET-CT scans represent increased tumour metabolism. Because tumours are composed of cells which are metabolically active and proliferating, uptake of glucose can be high. FDG is preferentially taken up by tumour cells following intravenous injection.

The areas of maximum uptake are usually expressed as the SUVmax which is an abbreviation for Standard Uptake Value. SUVs represent the ratio of radiotracer concentration within a region of interest (ROI) normalised to lean body mass, total body weight or surface area, with a decay correction applied. The SUV is related to normal tissue or background tissue uptake by using the computer software to manually define the ROIs over normal tissue and the area of increased tumour uptake. If the SUV in the tumour is higher than the normal tissue, it is considered raised. Although SUVmax (maximal pixel in the ROI) is the most commonly reported quantitative measure in FLT PET, there are other quantitative PET parameters, for example total lesion glycolysis (TLG), metabolic tumour volume (MTV), proliferative tumour volume (PV), *K*i, and other SUV parameters, which may provide more robust measurements of tumour activity (Zaidi and El Naqa, 2010; Arens *et al.*, 2014; Gallamini *et al.*, 2014).

Although static measures or SUV measurements are convenient to acquire and easy to process, more complex image quantification can be performed using different models. Compartmental modelling facilitates the understanding of tracer kinetics; Mankoff *et al* define compartmental modelling as

> “a method to condense vast amounts of data into biologically meaningful parameters” (Mankoff *et al.*, 2006).

*K*i represents a net irreversible rate constant and requires a dynamic scanning component which, although it provides large amounts of data, is less convenient for the patients, because it requires considerable additional time on the scanning couch and serial blood measurements.

A limitation of FDG PET-CT scanning for early response assessment is the so-called “tumour- stunning” effect which results in false negative results. This occurs in part

due to the effect of chemotherapy on tumour metabolism; bone marrow activation following myelosuppressive treatment or growth factor administration may also influence FDG uptake (MacManus *et al.*, 2007). The data on optimal interval between last day of chemotherapy and FDG PET-CT scanning is inconclusive although the latest European Association of Nuclear Medicine (EANM) guidelines state that a minimum of 10 days is probably sufficient (Boellaard *et al.*, 2015). Prolonged inflammation occurs following radiotherapy and has commonly been reported in head and neck cancer where an interval of two to three months is advised before FDG PET-CT scanning (Andrade *et al.*, 2006; Boellaard *et al.*, 2015). Although FDG uptake reflects the metabolic activity of a cell it is not specific to cancer cells and false positive results may occur in the presence of active infection or inflammation. In addition, early treatment effects may be missed prompting interest in the development of alternative PET tracers which do not have these limitations. In the last ten years, there has been increasing interest in the use of ^{18}F-fluorothymidine (FLT), a proliferation PET imaging biomarker.

1.2.2 18F-Fluorothymidine PET-CT

Langen and colleagues first described ^{18}F-fluorothymidine (FLT) in 1969 but it was not until twenty years later that a radiolabelled form of the nucleoside which could measure tumour proliferation using PET was reported (Langen *et al.*, 1969; Martiat *et al.*, 1988). ^{11}C-Thymidine was also identified as a proliferative biomarker but its short half-life and rapid degradation was expected to limit the clinical applications and FLT was proposed as a suitable alternative PET radiotracer (Shields *et al.*, 1998). FLT sensitivities and SUVs are lower than for FDG, and consequently it is generally reported that FDG is superior to FLT for tumour staging and detection. An important role for FLT is likely to be determining response assessment.

As a thymidine analogue, FLT is a proliferation imaging biomarker of neoplasia. FLT and circulating endogenous thymidine enter the cell by carrier-mediated mechanisms as well as by simple diffusion (Kong *et al.*, 1992). Cytosolic S-phase-specific thymidine kinase 1 (TK1) monophosphorylates FLT via the salvage pathway leading to intracellular trapping as the fluorine substituent prevents incorporation into DNA (Figure 1-1) (Shields, 2012). The *de novo* pathway utilises thymidylate synthase (TS) to catalyse the reductive methylation of deoxyuridine monophosphate to thymidine monophosphate, and imaging FLT uptake may provide a measure of the relative

contribution of the DNA salvage pathway. Levels of TK1 are almost undetectable during the growth-arrested phase of the cell cycle but are considerably increased during S-phase, and hence uptake of FLT is thought to reflect the fraction of tumour cells in S-phase (Sutterluety *et al.*, 1998). It has been shown that there is a positive correlation between cell growth, FLT avidity and TK1 activity (Rasey *et al.*, 2002). Malignant cells are proliferating and therefore levels of TK1 and the uptake of FLT are higher in these cells than normal cells. FLT is metabolised in the liver to a glucuronide which is excreted in the urine, therefore uptake is also seen in the liver, kidney and bladder. Approximately 25 – 30% of FLT is metabolised by 60-minutes post injection of radiotracer, and this radioactivity should be taken into account when considering kinetics for image analysis (Kenny *et al.*, 2005; Shields *et al.*, 2005).

Figure 1-1: Pathways for Cellular FLT Uptake and Metabolism (Shields, 2012).

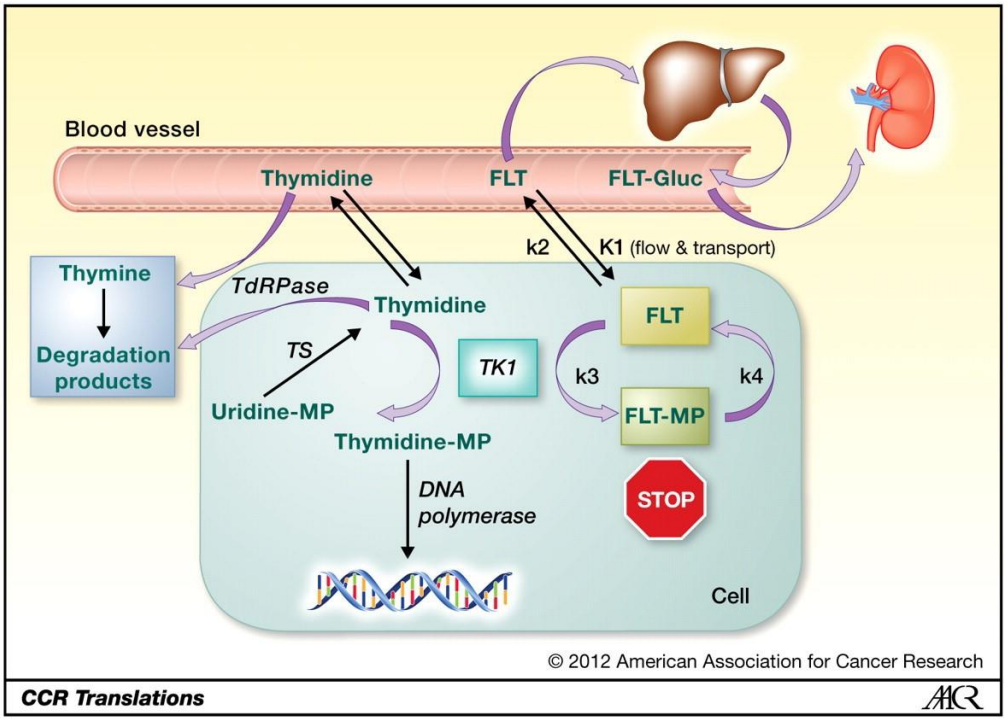

Information on total blood radioactivity, plasma radioactivity and plasma parent FLT fraction can be derived from frequent arterial and venous blood sampling. These parameters have been recorded in many studies over the last decade and have improved the understanding of FLT kinetics. Radiotracer uptake in a tissue is dependent on delivery of FLT via the bloodstream. At any one time, quantification of

transport and tissue retention can be described using a two compartmental model as described by Aboagye and Price for FDG (Aboagye and Price, 2003) and shown in Figure 1-2: K_1, the influx rate constant from capillary to tissue, K_2, the efflux rate constant from tissue to capillary, K_3, the rate of FLT phosphorylation and K_4, the rate of dephosphorylation. The aim of the compartmental model is to estimate flux of FLT from blood through the pathway into the tissue.

Figure 1-2: Kinetic FLT model: Four rate constants describe kinetic transfer rates between the 2 compartments. FLTMP _ FLT-monophosphate; FLTDP _ FLT-diphosphate; FLTTP _ FLT-triphosphate; FLT-gluc _ FLT-glucuronide; Qe _ exchangeable tissue compartment; Qm _ compartment of trapped FLT phosphorylated nucleotides; CpFLT _ concentration of FLT in arterial plasma; Cmet _ concentration of metabolites in arterial plasma (Mankoff et al., 2005)

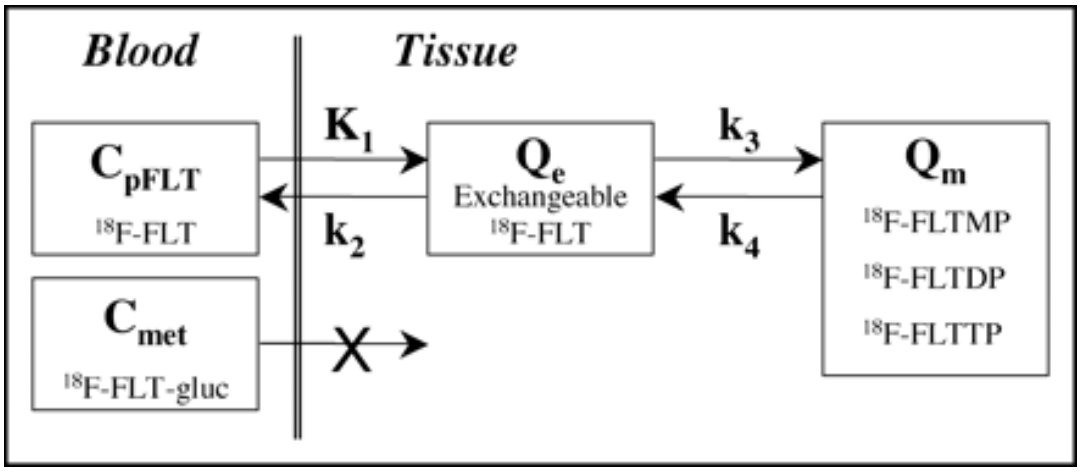

Uptake of FLT is high in proliferating tissues, therefore activity within the bowel, bone marrow, liver, spleen and lymph nodes is often physiological, although can be misleadingly reported as pathological. FLT uptake is regulated by several factors: nucleoside transporters, TK1, ATP, levels of endogenous thymidine and the relative contributions of the salvage and *de novo* pathways providing thymidine for DNA synthesis. The transporters include equilibrative nucleoside transporters 1 and 2 (ENT1 and 2) and concentrative nucleoside transporters 1 and 3 (CNT1 and 3) (Barthel *et al.*, 2005; Perumal *et al.*, 2006; Zhang *et al.*, 2012a). ATP is the co-substrate of TK1 (Barthel *et al.*, 2003; Leyton *et al.*, 2005). TK1 activity requires ATP and a fall in ATP levels might explain a reduction in TK1 catalytic activity, despite an increase in protein expression (Munch-Petersen *et al.*, 1995). High levels of endogenous thymidine antagonise FLT uptake and this was recently demonstrated (Zhang *et al.*, 2012a). Tumour models which displayed high FLT uptake had very low

levels of intrinsic thymidine compared to tumours with low FLT avidity. This result raises the possibility of increasing FLT uptake by thymidine depletion. However, because levels of thymidine are 320-fold lower in humans than in rodents, caution should be exercised when extrapolating results from preclinical studies. Reasons for false-negative FLT PET scans include small tumours due to partial volume effects, low grade tumours or low proliferative activity (Herrmann *et al.*, 2008; Quon *et al.*, 2008).

5-fluorouracil (5FU) is a cytotoxic agent used in the treatment of many cancers. It acts by interfering with the activity of TS by preventing binding of deoxyuridine monophosphate. Tumours treated with 5FU which rely on the *de novo* pathway for thymidylate synthesis may compensate by increasing TK1 activity to enhance the salvage pathway. In this context, FLT PET imaging has demonstrated a flare in FLT uptake in both xenografts and in breast cancer patients early after the administration of 5FU (Wells *et al.*, 2003; Lee *et al.*, 2010; Plotnik *et al.*, 2012). In the clinical setting, FLT PET may therefore be used to measure TS inhibition in patients treated by 5FU and similar acting drugs, by demonstrating increased FLT uptake.

1.2.3 Preclinical Data and Clinical Studies

There is a growing body of evidence supporting the use of FLT PET-CT in the assessment of tumour responses to treatment, although trials are still early phase and the number of patients in each study is generally less than 30. Shields and colleagues studied FLT uptake in preclinical tumour models and a non-small cell lung cancer patient, and found that the FLT was preferentially taken up by both proliferating normal cells and by tumours (Shields *et al.*, 1998). Following this demonstration of FLT uptake in human tumours, studies have concentrated on tumour sites where neighbouring physiological uptake of FLT is low, for example breast, lung, rectal and oesophagus cancers, head and neck cancer and glioma (Vesselle *et al.*, 2002; Buck *et al.*, 2003; van Westreenen *et al.*, 2005; Been *et al.*, 2006; Saga *et al.*, 2006; Linecker *et al.*, 2008; Muijs *et al.*, 2011; Han *et al.*, 2012). Barthel and colleagues published one of the first preclinical studies in 2003 which established a place for FLT PET in monitoring tumour response to treatment, in which RIF-1 tumour-bearing mice treated with the thymidylate synthase inhibitor 5-FU showed a fall in FLT uptake following treatment (Barthel *et al.*, 2003).

Breast cancer has been studied extensively by FLT PET-CT; FLT PET identified primary and nodal masses of breast cancer in feasibility studies in 2005 (Kenny *et al.*, 2005; Been *et al.*, 2006). Pio *et al* reported one of the first response studies; fourteen breast cancer patients attended for 45-minute long dynamic FDG and FLT-PET scans before and after 5-weeks of chemotherapy. The post treatment FLT PET scans predicted eventual tumour response (Pio *et al.*, 2006). Similarly, Kenny and colleagues demonstrated FLT had the potential to be a very early response marker. They studied thirteen breast cancer patients undergoing FEC chemotherapy (5FU, epirubicin, cyclophosphamide) and performed FLT PET-CT scans before starting treatment and 1-week after. Results were compared with clinical response after 9 weeks of treatment. In the 6 patients who showed a considerable reduction in tumour size, there was a significant fall in the FLT PET uptake on the scan performed 1 week after treatment (Kenny *et al.*, 2007). This finding was supported by other feasibility studies which studied alternative chemotherapy regimens involving capecitabine, doxorubicin, docetaxel and paclitaxel (Monazzam *et al.*, 2007; Kenny *et al.*, 2009). Preclinical studies reported similar results in a breast mouse model with trastuzumab treatment, and an *in vitro* MCF-7 model treated with doxorubicin and docetaxel (Dittmann *et al.*, 2009; Shah *et al.*, 2009).

Tumours are not homogenous entities. Imaging intra-tumour heterogeneity using FLT PET-CT has been described by Willaime *et al* and using scanning data from eleven breast cancer patients, twenty-eight textural descriptors were studied on a baseline and follow-up scan, and repeatability measurements performed. Tumours which responded clinically to treatment had higher levels of highly proliferative cells and developed more homogeneity than non-responders (Willaime *et al.*, 2013). This modification to tumour textural features by treatment may have clinical significance if applied to radiotherapy volume definition and could be explored in future studies.

Visualizing response to neoadjuvant therapy was reported by Ott *et al* in a series of gastric cancer patients in 2011. FDG, FLT PET, and Ki67 immunohistochemistry were compared with clinical and histopathological response, and survival. FLT PET detected all 45 tumours, whereas fourteen tumours were missed by the FDG PET (Ott *et al.*, 2011). On multivariate analysis, FLT uptake 2-weeks after initiation of therapy was shown to be the only imaging parameter with significant predictive

impact; high FLT SUVmean 14 days post treatment correlated with increased risk of death.

Yue *et al* conducted a study of serial FLT scans on 20 oesophageal squamous cell cancer patients undergoing radical radiotherapy. All patients had a baseline scan then a further 1-3 scans during the treatment delivery period. During radiotherapy, SUVmax and proliferation target volume decreased; midway through treatment there was almost complete absence of proliferating tumour. In bone marrow, there was a reduction in proliferation after one treatment and complete absence after one week of radiotherapy (Yue *et al.*, 2010).

In 2002, FLT uptake was reported in pancreatic cancer cell lines SW-979 and Bx-Pc-3 using an *in vitro* model. Levels of TK1 were higher in the malignant cells than in tissue from normal pancreatic tissue or chronic pancreatitis (Seitz *et al.*, 2002). The greatest levels of TK1 mRNA were recorded in the SW-979 cell line and high performance liquid chromatography (HPLC) analysis detected FLT metabolism after an incubation period of 60-minutes.

Quon *et al* studied FLT and FDG PET-CT scanning in five patients with pancreatic cancer (Quon *et al.*, 2008). Tumour maximal SUV values were higher on the FDG scans. The primary lesion was identified in only 2 / 5 patients using visual interpretation of the FLT studies, and in all five of the FDG images. As tracer activity could only be distinguished from background activity in two patients the authors concluded that FLT PET-CT was not useful in the investigation of pancreatic cancer patients due to high physiological uptake in the liver obscuring the tumour signal.

Herrmann *et al* reported more success with FLT PET imaging in pancreatic cancer. They obtained a sensitivity of 74% in a series of 25 patients. Mean tumour size was 4 cm (range 1.2 - 8.5), mean FLT SUVmax of pancreatic lesions was 2.9 (median 2.7, range 1.1 - 6.5) and the mean FDG SUVmax 7.2 (median 6.5, range 2.1 - 17.8). FLT PET correctly identified 4 / 6 true-negative scans and FDG PET CT 1 / 6. Receiver-operating characteristic analysis to distinguish benign from malignant lesions provided a cut-off value of SUVmax = 2 for FLT (AUC 0.59) and SUVmax = 3.5 for FDG (AUC 0.84) (Herrmann *et al.*, 2012). The authors of this study do not give specific details of the tumours that were missed by the FLT PET scans, although

pointed out that they were surprised the sensitivities were not lower given that the cohort of patients studied had smaller tumours than in their pilot study.

The difficulty of identifying tumour with FLT PET within a location which itself has high physiological FLT uptake is not limited solely to the pancreas. FLT uptake in hepatic metastases can be obscured by the FLT avidity associated with normal FLT metabolism to the FLT-glucuronide. Gray *et al* devised a filter in breast cancer patients where tumours can be difficult to characterise due to high FLT uptake within the nearby major blood vessels and liver. Gray *et al* added to existing segmentation models with their non-linear filter, and using a dynamic scan of 90 minutes they generated time activity curves for each tissue type and compared these with predefined kinetic properties of FLT (Gray *et al.*, 2010). Each image voxel was assigned to a specific tissue type, tracer intensity derived from normal tissues was removed, leaving only voxels containing tumour with a signal. The filter was validated using scans from fifteen patients with breast cancer and then tested in a patient with liver metastases.

1.3 Magnetic Resonance Imaging (MRI)

Magnetic resonance imaging (MRI) uses the magnetic properties of hydrogen nuclei to generate an image which changes according to the chemical and physical environment. Protons in body water line up with or against the magnetic field $B_{0,}$ according to their energy. Radiofrequency (RF) irradiation causes a change in the alignment, and subsequent decay generates an RF signal which is displayed as an image (Alonzi and Hoskin, 2006). The majority of protons in the body are present in water, and the MR signal from body water varies in different tissues. Diffusion weighted magnetic resonance imaging (DW-MRI) and dynamic contrast-enhanced MRI (DCE-MRI) are functional techniques which detect changes in proton MR signals reflecting biological changes that occur in tissues. Biological changes may be identified earlier than anatomical ones and it is this functionality which is appealing to exploit therapeutically. Similar to PET, these modalities are being extensively evaluated across different tumour sites as markers of early treatment response. Additionally, DW-MRI and DCE-MRI are being investigated in the detection of tumours, planning radiotherapy treatment, and surveillance following treatment, but are not widely used, and are generally employed in the research setting.

1.3.1 Diffusion-Weighted MRI (DW-MRI)

DW-MRI is a non-invasive imaging modality which is sensitive to the diffusion of water molecules (Le Bihan *et al.*, 1988). Endogenous contrast between tissues is depicted due to differences in water molecule movement. The organisation of cells and the proportion of extracellular space is reflected in the extent of water diffusion shown in diffusion-weighted MR images. MR images are made sensitive to diffusion by applying magnetic field gradients during a specific period of the MR pulse sequence. The amount of diffusion weighting depends on the duration and magnitude of the applied gradient, numerically given as the *b*-value. Qualitative assessment using visual inspection requires at least two *b*-values which adequately suppress background signal to allow detection of signal intensity in the tumour; however, the degree of signal intensity is influenced not only by diffusion but also the T2 tissue value, known as T2 shine-through (Heijmen, 2012).

Diffusion coefficients were reported in the 1960s and much of the initial work established a role for DW-MRI in diagnosing cerebral ischaemia (Stejskal and Tanner, 1965; Chenevert *et al.*, 1990; Johnston *et al.*, 2007). Quantification of diffusion measurements, using the apparent diffusion coefficient (ADC), is increasingly used to evaluate treatment effects. It was not until the National Cancer Institute (NCI) held a consensus meeting in 2008, as part of the International Society for Magnetic Resonance in Medicine Meeting, that recommendations for the use of DW-MRI as a cancer imaging biomarker were agreed (Padhani *et al.*, 2009). Since then, there has been considerable interest in the potential role of DW-MRI in the field of oncology, and the number of clinical trials evaluating DW-MRI in cancer management are growing in number.

1.3.2 Dynamic Contrast Enhanced MRI (DCE-MRI)

One of the first uses of dynamic contrast-enhanced magnetic resonance imaging (DCE-MRI) was to assess blood flow within the myocardium and pulmonary vasculature, but it is increasingly being used to evaluate malignant tumours (Hendee and Morgan, 1984; Lallemand *et al.*, 1985; Yang and Knopp, 2011; Khalifa *et al.*, 2014). The technique involves rapid acquisition of images through a region of interest following intravenous administration of a gadolinium-based contrast agent. The contrast agent induces changes in the MRI signal dependant on its concentration,

which provides an *in vivo* assessment of tissue blood flow and / or permeability. Tumours have structurally and functionally abnormal vasculature (Maiorana and Gullino, 1978; Mahadevan and Hart, 1990). The blood vessels are leaky, dilated, and grow in a disorganised fashion, taking up contrast more readily than normal tissues (Carmeliet and Jain, 2000; Folkman, 2002; Verma *et al.*, 2012; de Haas *et al.*, 2014).

Perfusion changes due to compromised blood flow following effective cancer treatment can be assessed by a range of techniques. Semi-quantitative approaches measure signal intensity in low temporal resolution / high spatial resolution images over time. Contrast agent uptake curves vary according to the vascular properties supplying the tumour. Commonly measured parameters include initial area under the curve (iAUC), the time to peak (TTP) and the slope of the washout curve (Yankeelov and Gore, 2009). Fully quantitative methods involve more complex kinetic modelling of data acquired from high temporal resolution images, and describe the exchange of contrast between plasma and the extravascular extracellular space (EES) (Abramson *et al.*, 2013). Kety pioneered a model of gas uptake within pulmonary vasculature which has been extended to extracellular tracers used in other anatomical regions (Kety, 1951). Tofts' is the most widely used DCE-MRI kinetic model and uses the parameters described in Table 1-1 (Tofts *et al.*, 1999).

Table 1-1: Parameters of DCE-MRI

Symbol	Parameter
K*trans*	Volume transfer constant between blood plasma and extravascular extracellular space (min^{-1})
V*e*	Fractional volume of extravascular extracellular space (Ve = Ktrans / Kep)
K*ep*	Rate constant of exchange between extravascular extracellular space and plasma (min^{-1})
V*p*	Fractional plasma volume

1.4 Tumour Response Assessment

Determining response to cancer treatment has traditionally relied on evaluating volumetric tumour changes using anatomical imaging modalities: Ultrasound, CT or MRI. Response evaluation criteria in solid tumours (RECIST) criteria have been incorporated into clinical trials providing a more consistent approach to treatment assessment. The criteria were first published in 2000 and the updated 2009

guidelines (version 1.1) have been adopted internationally as the gold standard criteria for the evaluation of solid tumour burden. Table 1.2 and Table 1.3 summarise RECIST v1.1 Criteria (Eisenhauer *et al.*, 2009). One perceived limitation of RECIST is that it is based on a linear model which assumes tumours are spherical and symmetrical, and uses the sum of the longest diameters. Volumetric measurements can be undertaken but are more complex and may use manual and semi-automated methods (Wang *et al.*, 2011; Lin *et al.*, 2012; Welsh *et al.*, 2012; Zhao *et al.*, 2013). Large validation studies of these techniques may influence how tumour burden is assessed in the future, but currently the standard is linear assessment.

Perhaps a more pertinent limitation of RECIST relates to the structural as opposed to the functional nature of the assessment. Changes in tumour size are usually not detected until several weeks after commencing treatment whereas functional or biological assessments can be performed earlier. Discontinuing ineffective therapies could spare patients unnecessary side-effects and direct them towards more effective treatments, or permit entry into a clinical trial. Functional imaging provides information on the biological properties of tumours. In an era when targeted and often cytostatic therapies are being introduced into clinical practice, absence of tumour progression may also be considered a response to treatment. PET measures change in the biology of the tumour, as opposed to tumour shrinkage, and patients could be denied an effective treatment if the biological change in the tumour is ignored.

Table 1.2: RECIST v1.1 Target lesion evaluation

Response	Definition
Complete Response (CR)	Disappearance of all extranodal target lesions. All pathological lymph nodes must have decreased to <10 mm in short axis.
Partial Response (PR)	At least a 30% decrease in the Sum of the Longest Diameter (SLD) of target lesions, taking as reference the baseline sum diameters
Progressive Disease (PD)	SLD increased by at least 20% from the smallest value on study (including baseline, if that is the smallest). The SLD must also demonstrate an absolute increase of at least 5mm.
Stable Disease (SD)	Neither sufficient shrinkage to qualify for PR nor sufficient increase to qualify for PD

Table 1.3: RECIST 1.1 Non-target lesion evaluation

Response	Definition
Complete Response (CR)	Disappearance of all extranodal non-target lesions All lymph nodes must be non-pathological in size (<10 mm short axis). Normalization of tumour marker level
Non CR/Non PD	Persistence of one or more non-target lesion(s) and/or maintenance of tumour marker level above the normal limits
Progressive Disease (PD)	Unequivocal progression of existing non-target lesions. (Subjective judgement by experienced reader)

The PET-imaging field is less developed than CT and MRI, and there is a lack of consensus on how to approach response assessment including how to segment images, the number and site of lesions which should be selected for response assessment, which metrics to use, and when to schedule the scan in relation to treatment. Image quality is affected by a number of variables including the injected dose of radiotracer, patient habitus and reconstruction method. Image segmentation is the process of defining a region of interest (ROI) using a specific model and is hampered by low spatial resolution and noisy images. Various segmentation methods exist, including clustering, edge detection and region growing, but the most commonly applied is thresholding. This requires selection of a threshold value which distinguishes lesion foreground from background noise to define a ROI (Zaidi and El Naqa, 2010).

Wahl *et al* published a comprehensive review of how to approach treatment response using FDG PET-CT with the introduction of the PERCIST criteria in 2009 (Wahl *et al.*, 2009). Drawing on the framework of RECIST, PERCIST was proposed as criteria that could be implemented in clinical trials and possibly clinical practice. These criteria assess the metabolic burden of the tumour and define three groups: responders; stable disease; and progressive disease (Eisenhauer *et al.*, 2009; Wahl *et al.*, 2009). When grouping patients as responders or non-responders, a patient with stable disease is often classed as a non-responder (Vallius *et al.*, 2016). Defining stable disease as a treatment "response" could be argued in view of the natural history of cancer cells which is to continually proliferate and grow in size. In the clinical setting, a patient with stable disease and acceptable treatment-related toxicities will be

continued on treatment on the grounds that it is holding the disease. This argument may hold more weight in the palliative setting than in the context of neoadjuvant chemotherapy (NAC) which aims to downsize the extent of disease and reduce the burden of micro-metastatic disease.

Response assessments may be qualitative or quantitative. Visual qualitative analysis of the images by a PET-trained radiologist or physicist can provide binary or continuous assessments; a continuous assessment may use a visual assessment scale with several points, in contrast to the yes/no binary result which states the presence or absence of a response. Qualitative assessments rely on the expertise of the reporter, and considers factors specific to the disease process, for example patterns of spread and knowledge of normal variants and artefacts. Limitations of this particular approach include limited reproducibility studies and early responses may be missed on visual inspection. Quantitative parameters have the advantage of detecting more subtle changes in uptake than can be reliably detected visually by the observer and, importantly, these changes can be quantified. EORTC guidelines recommend a 20 – 25% fall in SUV as a cut-off value for a treatment-related effect, and the PERCIST guidelines refer to a ≥ 35% change in SUV_{max} (Wahl *et al.*, 2009; Skougaard *et al.*, 2013; Aras *et al.*, 2016). Reports in the literature are varied between tumour types. In lymphoma patients, SUV declines of > 65.7% after 2 - 3 cycles of chemotherapy predict better progression free survival, in contrast to oesophago-gastric tumours where a fall of 25 – 35% can predict pathological response to neoadjuvant chemotherapy (Weber *et al.*, 2001; Lin *et al.*, 2007; Ott *et al.*, 2008; van Heijl *et al.*, 2011).

The authors of the PERCIST criteria emphasise the importance of consistent scanning approaches between baseline and response scans within radiology departments. An appreciation of test-retest reproducibility figures is important when quantifying responses, because inherent biological variation, altered scanning protocols, variation in time from injection between the baseline and response scans and calibration can all affect SUV measurements. A lack of appreciation of the measurement errors that exist can lead to misinterpretation of PET images and compromise patient care. In addition to standardising response assessments, consideration should therefore be given to the acquisition of the scan. Involvement of the radiographers, physicists and radiologists is crucial to ensure reproducible results

which can be compared between study centres. Calibration tests of PET scanners using phantom measurements should be implemented in advance of the opening of a multi-centre trial involving various scanning systems. Reproducibility measurements have been incorporated into the design of many recent clinical trials with two baseline measurements. In one study, no major differences were encountered with calibration and cross-calibration enabling the clinical trial set-up process to continue with the confidence that reliable results could be expected (Bouchet *et al.*, 2013).

1.5 Image-guided Dose-escalated Radiotherapy

Accelerated repopulation of tumour cells during radiotherapy is recognised as one of the important causes of radio-resistance and consequent treatment failure. With Intensity Modulated Radiotherapy (IMRT) it is possible to deliver optimised photon beams with non-uniform fluences, allowing simultaneous delivery of different doses to various subvolumes within the target. The steep dose gradients allow higher radiotherapy doses to be delivered to certain areas of the gross tumour volume (GTV) and minimises doses to the normal tissues, defined as organs at risk (OAR).

Increased uptake of the radiotracer on PET-CT has the potential to identify tumour subvolumes with high levels of metabolically active proliferating cells which can be targeted for radiotherapy boosting in an attempt to improve the outcome for the patient. Areas of high metabolism, proliferation and hypoxia are demonstrated by avidity of the FDG, FLT or ^{18}F-fluoromisonidazole (FMISO) tracers, respectively (Thorwarth *et al.*, 2007; Zygogianni *et al.*, 2012). FDG PET-based dose escalation studies have been reported in the literature, mainly involving head and neck, and lung cancers (Geets *et al.*, 2007; Madani *et al.*, 2007a; Duprez *et al.*, 2011; Fodor *et al.*, 2011; Moller *et al.*, 2011; Chatterjee *et al.*, 2012). Some are theoretical planning studies but others have been performed in patients, demonstrating feasibility of a PET-CT guided treatment approach and acceptable toxicity. Currently, there is no consensus on the best segmentation methods to define tumour subvolumes suitable for dose painting, although some clinical trials have used the SUV50%max isocontour (Madani *et al.*, 2007a; Madani *et al.*, 2011).

It is clear that different tracers can be used to measure and exploit different functional properties of tumours. These imaging biomarkers have the potential to modify radiotherapy treatment planning, in addition to chemotherapy or novel agent

selection. To date, studies focusing on each of these areas are small in number and size.

1.6 Ki-67

Ki-67 is a histopathological marker of cellular proliferation and indicator of biological aggressiveness. It is expressed only by cells actively undergoing the G1, S, G2 and M stages of the cell cycle (Proctor *et al.*, 2010). Ki-67 has prognostic value in head and neck and non-small cell lung cancers, and gliomas (Vesselle *et al.*, 2008; Warth *et al.*, 2014; Chen *et al.*, 2015a). According to the literature, Ki-67 score is reported as high when labelling index is greater than 20 – 45% expression (Popov *et al.*, 1997; Wu *et al.*, 2000; Bertz *et al.*, 2014; Ding *et al.*, 2014; Krabbe *et al.*, 2014; Wu *et al.*, 2015b). The relationship between Ki-67 and FLT PET-CT imaging has been investigated in a number of studies, and is discussed further in Chapter 2.

1.7 Clinical Trials

The clinical context and motivation to undertake the studies which are reported in this dissertation are described below, under each trial heading.

1.7.1 MARBLE - Bladder Cancer

Bladder cancer affects 350 patients in Newcastle every year, but the patients are under-investigated and outcomes remain poor. Overall five-year survival figures are around 50%, and only 10 – 30% for the more advanced tumours. The MARBLE trial has studied patients with muscle-invasive bladder cancer. In the UK, bladder cancer is the fourth most common cancer in men, and the eleventh in women. Between 2009 and 2013 a mean of 6254 men and 2363 women were diagnosed with bladder cancer each year in the UK (NICE, 2015). The median age of patients diagnosed with bladder cancer is 65-years and more than 70% of patients are over 60-years of age; patients often have co-morbidities which affect their fitness for treatment. Muscle-invasive bladder cancer (MIBC) accounts for approximately 30% of cases, the majority having non muscle-invasive disease. For many years, definitive treatment of MIBC has consisted of surgical removal of the bladder, known as radical cystectomy (RC) preceded by neoadjuvant chemotherapy (NAC). The NAC is given to patients with good performance status and confers a 5 – 7% survival benefit (Sherif *et al.*, 2004; Vale, 2005). In our institution, it is delivered as three or four

cycles of split-day gemcitabine 1250mg/m^2 and cisplatin 35mg/m^2 chemotherapy on days 1 and 8 of a 21-day cycle. Patients are routinely re-staged to confirm suitability for surgery, after two or three cycles of chemotherapy, with CT of chest, abdomen and pelvis. In light of recent studies indicating equivalence in outcome, patients are now offered radical radiotherapy with concurrent chemotherapy as an alternative to surgery (Choudhury and Cowan, 2011; James *et al.*, 2012; Smith *et al.*, 2013; Ploussard *et al.*, 2014). Response rates to NAC are approximately 40 – 60%. Pathological complete responses to chemotherapy are associated with improved outcomes compared to patients with residual disease at time of RC (Grossman *et al.*, 2003; Sonpavde *et al.*, 2009; Meeks *et al.*, 2012).

In the MARBLE study, the feasibility and utility of serial DW-MRI and DCE-MRI scans was assessed. Some patients are unable to tolerate an MRI so a small study (MARBLE-FLT) to evaluate if FLT PET-CT might be an alternative functional imaging modality in bladder cancer is reported. In the context of bladder, the clinical literature is sparse and the utility of this PET tracer unknown.

1.7.2 THRIFT – Thyroid Cancer

Most thyroid cancers are carcinomas. Although differentiated thyroid cancer (DTC) accounts for less than 1% of all malignancies, it is the commonest endocrine neoplasm. 2000 cases are diagnosed and 250 deaths recorded annually in England and Wales (Perros *et al.*, 2014). Papillary and follicular subtypes are the commonest DTC pathologies accounting for approximately 80% and 5 – 20%, respectively. Treatment usually consists of total thyroidectomy, radio-iodine ablation (RIA) and thyroid stimulating hormone (TSH) suppression. Follow-up is long-term surveillance of serum thyroglobulin levels (Tg). Prognosis of treated patients is generally good, with 10-year survival figures of 80 – 90% (Mazzaferri and Massoll, 2002).

A minority (5 – 20%) develop loco-regional recurrence or metastatic disease (lung, bone, liver, brain in decreasing frequency). If Tg levels are elevated, neck ultrasound scan (USS) +/- fine needle aspirate (FNA) and ^{131}iodine whole-body scan (WBS) are arranged. Initial treatment of iodine-avid disease is ^{131}iodine therapy. Bulky or iodine-refractory disease is usually referred for surgical excision, or debulking if this is not possible. FDG PET-CT is increasingly being used in iodine-negative DTC to localise recurrent disease (American Thyroid Association Guidelines Taskforce on Thyroid *et*

al., 2009). A meta-analysis of 17 studies comprising 571 patients with recurrent or metastatic DTC and iodine-negative WBS concluded an overall sensitivity of 0.94 (95% CI 0.87 - 0.97) and specificity of 0.84 (95% CI 0.72-0.92) for FDG PET-CT (Dong *et al.*, 2009)).

For patients with recurrent disease, 5 – 20% die of local cervical involvement. Timely management of local disease in fit patients with distant involvement is therefore important (Perros, 2007). External beam radiotherapy is reserved for unresectable disease or patients with co-morbidities that render them inoperable. If radical treatment is proposed, IMRT is recommended.

The THRIFT study investigated if differentiated thyroid cancers were FLT-avid and if FLT could be used to guide radiotherapy dose escalation.

1.7.3 FLT – Pancreatic adenocarcinoma

Adenocarcinoma of the pancreas is the 4th commonest cause of cancer death worldwide (Sultana *et al.*, 2007). Tumours typically present with vague symptoms and are often advanced at presentation. This renders the vast majority of tumours (up to 80%) inoperable at the time of diagnosis. Surgical resection is the only curative option, but relapse rates are high. Palliative chemotherapy has been shown to confer a median survival benefit of two months with gemcitabine. The addition of nab-paclitaxel or an alternative regimen of folfirinox (5FU, oxaliplatin and irinotecan) have recently demonstrated improved survival. However, due to aggressive tumour biology, median survival is less than a year, even with palliative chemotherapy (Klein *et al.*, 2002; Lamarca *et al.*, 2016). Because of the low response rate, it is even more important to identify non-responding patients at the earliest opportunity to maximise quality of life by sparing unnecessary toxicity from an ineffective treatment.

The FLT-pancreas study evaluated FLT PET-CT as a surrogate biomarker of early response to treatment.

1.7.4 FLAIRE - Oropharyngeal Cancer

Squamous cell carcinomas of the head and neck region (HANSCC) account for approximately 2% of all cancers diagnosed, and 1% of cancer deaths. They are the 14th commonest cancer in the UK and there is a male preponderance. In 2013, there were 7591 cases diagnosed, and 1426 deaths (CRUK, 2016). Overall 5-year survival

figures for tumours which have spread to local structures or into the regional lymph nodes are 50% and is influenced by human papilloma virus (HPV) status and other factors such as tumour stage and co-morbidities.

The oropharynx extends between the soft palate superiorly, hyoid bone inferiorly, and anteriorly it communicates with the oral cavity. Cancers of the oropharynx are mostly tumours of the base of the tongue and tonsillar region, although may arise on the soft palate, and pharyngeal walls (Gunn *et al.*, 2013). The lymphatic drainage of the neck consists of six main lymph node regions: levels I – V and the retropharyngeal lymph nodes. Cancers of the oropharynx typically drain to ipsilateral levels II and III, although large or midline tumours may spread to contralateral lymph nodes. Histologically, the vast majority of tumours of the oropharynx are squamous cell carcinomas. Traditionally, a large proportion of tumours were alcohol- and tobacco-related but the demographics have changed and there are more middle-aged non-smoking males affected by these tumours. The incidence of HPV-positive oropharyngeal cancers has risen considerably in the last two decades. In 1984, 16% of oropharyngeal cancers were HPV-positive, rising to > 70% in 2004 (Pytynia *et al.*, 2014). The HPV-positive tumours are recognised as a distinct entity with differing biological behaviour and responses to treatment. HPV-positivity confers a survival advantage: overall 3-year survival is 85% in HPV-positive tumours; 52% in HPV-negative tumours (Ang *et al.*, 2010).

Tumours may present with pain, difficulty eating, weight loss, mouth ulceration, a neck lump or earache. Clinical assessment includes panendoscopy of the pharynx, biopsy of any abnormal regions, and a CT or MRI. In cases where the site of the primary disease is uncertain, an FDG PET-CT scan will be performed. The main treatment options for locally advanced tumours are radical chemoradiotherapy or surgery. Radiotherapy treatment in our institution consists of 65-Gy in 2.167-Gy fractions to the primary tumour and metastatic cervical lymph nodes, and 54-Gy in 1.8-Gy fractions to at-risk cervical lymph nodes. Fractions are delivered once daily, 5-days a week. Concurrent intravenous cisplatin chemotherapy 40 mg / m^2 is administered once-weekly throughout radiotherapy, in patients with good performance status. Typical follow-up comprises relevant medical history and head and neck examination (inspection, palpation and flexible nasendoscopy) at two-monthly intervals for the first 12-months then three and four-monthly intervals for the

next 12 – 24 months respectively. FDG PET-CT scans are acquired three months following completion of radiotherapy to assess radiological response to treatment.

The FLAIRE study investigated the feasibility of serial FLT PET-CT scanning in patients undergoing chemoradiotherapy. The prognostic and predictive potential of FLT as an imaging biomarker was evaluated. A planning substudy assessed the technical feasibility of generating FLT-guided dose escalated radiotherapy plans.

1.8 Aims and Objectives

This dissertation describes studies aimed to improve knowledge of how to employ functional imaging techniques to individualise treatment for oncology patients. A portfolio of early phase clinical trials was established to evaluate FLT PET-CT, DW-MRI and DCE-MRI as imaging biomarkers in several solid tumour settings. Specifically, the unique properties of these techniques have shown promise in identifying early treatment responders after chemotherapy or radiotherapy. The increasing sophistication of radiotherapy techniques calls for better understanding of tumour biology so that this information can be integrated into individualised treatment plans. Prior to incorporation into clinical practice, these functional techniques require iterative clinical validation; firstly to establish that they can measure the biological process; secondly that the measurement has clinical relevance; and thirdly that it is logistically feasible to undertake in the clinical setting. Consequently the swift translation of clinically validated research findings into patient benefit may be a real possibility. The clinical studies address specific imaging questions at different stages of the clinical pathway. Reasons for selecting the various tumour sites are described below. Given the size of the north east population and for practical reasons, several tumour sites were selected to enable recruitment to a number of small studies, rather than one large study of a single tumour type.

This first chapter has introduced how novel functional imaging techniques may have a role in the early assessment of treatment response, and in radiotherapy treatment planning. Fundamental principles of FLT PET-CT, DW-MRI, and DCE-MRI have been described. The clinical trials involved patients with oropharyngeal, bladder, thyroid and pancreatic cancers; therefore, a brief overview of these disease sites has been given to provide context for the research projects.

FLT PET is a research tracer, with demonstrated limited utility in some tumour sites, and is yet to be studied in others. Chapter 2 investigated if transitional cell carcinomas of the bladder and differentiated thyroid cancers were FLT-avid, and could be usefully imaged with FLT PET-CT.

Chapter 3 presents data from a collaborative project with Imperial College Healthcare NHS Trust. Pancreatic cancers are FLT-avid and this is one of the first studies using FLT PET-CT as a predictor of early response to treatment in advanced pancreatic cancer. Neoplasia in the liver and pancreas may be obscured by high levels of the FLT radiotracer in surrounding tissues. A filtering algorithm to improve visualisation of tumours using FLT PET-CT has been developed by the collaborators and this was the first study to evaluate its use in pancreatic cancer. Full details of the study are provided in the published manuscript (Challapalli *et al*., 2015).

In Chapter 4 results from the FLAIRE study which investigated FLT PET-CT as an imaging biomarker to predict early treatment responses in oropharyngeal cancer, are reported. Head and neck cancers have been studied by a number of research groups investigating FLT PET-CT, and FLAIRE was designed to study one sub-site: oropharyngeal cancers. The optimal time-point for response assessment imaging is unknown, hence serial imaging was undertaken. At the end of the chapter, data from a radiotherapy planning study incorporating FLT PET-CT images are presented.

Despite advances in understanding of tumour cell proliferation and how this is represented on FLT PET-CT images, not all tumours are FLT-avid. Chapter 5 provides results from related pre-clinical experiments conducted by the imaging research group on how to optimise FLT PET-CT scanning in tumours which do not take up FLT.

Chapters 6 and 7 report the evaluation of functional MRI in bladder cancer patients. The role of DW-MRI and DCE-MRI as surrogate markers of early treatment response in bladder cancer are presented from the MARBLE study.

Chapter 8 gives an overview of the results of the studies and the appendix contains further quantitative data and selected case reports from the MARBLE study.

Chapter 2 Exploring the utility of 18F-fluorothymidine PET in transitional cell carcinoma of the bladder and differentiated thyroid cancer

2.1 Introduction

PET-CT is a valued imaging modality for diagnosis, prognosis, treatment-planning and response assessment in many tumour sites. However, it is not routinely used in bladder cancer. Thus, there is potentially an unmet clinical need for PET imaging in bladder cancer and hence the MARBLE-FLT study was performed. In thyroid cancer, FDG PET-CT scans are used to localise and stage iodine-negative thyroid cancer. FLT PET-CT has been investigated in a variety of tumour sites, but the literature base in thyroid cancer is sparse (Herrmann *et al.*, 2012; Nakajo *et al.*, 2013; Belohlavek *et al.*, 2014; Lee *et al.*, 2014a). To assess whether there may be a role for FLT PET-CT in thyroid cancer, it must first be established if thyroid cancer takes up FLT. The THRIFT study was designed to explore the utility of FLT PET-CT in differentiated thyroid cancer. In this chapter, results from the MARBLE-FLT and THRIFT studies are presented.

2.2 MARBLE-FLT - Background

Although PET-CT imaging of bladder cancer is not routinely used in the UK, the landscape is beginning to change. In the metastatic setting, there is increasing interest in using FDG PET-CT, and the most recent NICE guidelines recommend consideration of FDG PET-CT staging in patients who have a high risk of metastases (NICE Guideline 2 Bladder Cancer: Diagnosis and Management). Evaluation of primary disease is hampered due to FDG excretion via the urinary system which pools in the bladder and can mask tumours within the bladder wall. Some research groups have reported attempts to overcome the technical limitations. Urinary catheterisation with retrograde irrigation, and forced diuresis with intravenous fluids and injection with the diuretic furosemide, have been shown to improve the detection of tumours (Kosuda *et al.*, 1997; Koyama *et al.*, 2003; Kamel *et al.*, 2006; Anjos *et al.*, 2007; Kibel *et al.*, 2009; Garcia Vicente *et al.*, 2011). These methods have drawbacks which include lengthy patient visits, more input from scanning staff, and invasive procedures which exposes patients to infection risks. Development of a scanning protocol which is practical to deliver, tolerable for patients and sufficiently

sensitive and specific to detect bladder lesions is required before FDG PET-CT imaging could become part of the patient pathway.

There are no reports of imaging primary bladder tumours with 18F-fluorothymidine (FLT) PET-CT. Therefore, to investigate the potential utility of FLT-PET CT in this tumour setting, a PET imaging sub-study was included in the MARBLE protocol.

2.3 MARBLE – FLT – Objectives

The MARBLE-FLT study aimed to develop a scanning protocol which was tolerable for patients, could overcome the interaction with background signal from FLT in urine to enable the detection of primary bladder tumours, and investigate the utility of FLT-PET-CT in the assessment of primary and metastatic transitional cell carcinoma of bladder tumours.

2.4 MARBLE - FLT - Methods

2.4.1 Study Participants

This prospective feasibility study was conducted in accordance with The Code of Ethics of the World Medical Association (Declaration of Helsinki) for experiments involving humans. Ethical approval was gained from the local ethics committee (REC reference 13/NE/0007 and IRAS project ID 100429) and adopted onto the UK clinical research network (CRN) Portfolio (ID 14489). The study was sponsored by Newcastle upon Tyne Hospitals NHS Foundation Trust (NUTH) and was undertaken at the Northern Centre for Cancer Care (NCCC), Freeman Hospital, Newcastle upon Tyne, UK. Participants were identified in the NUTH Uro-oncology Multidisciplinary Team Meeting.

Eligibility criteria were:

- T2 -T4a N0 - 2 M0 muscle-invasive bladder cancer according to UICC TNM Seventh Edition
- residual disease post transurethral resection of bladder tumour (TURBT) determined by examination under anaesthetic at time of TURBT or on staging CT
- patients scheduled to receive three or four cycles of neo-adjuvant or down-staging cisplatin-based chemotherapy followed by radical cystectomy or radiotherapy

- participating in the MARBLE study

After written informed consent, five MARBLE patients were recruited to the MARBLE-FLT sub-study between 7 June 2013 and 22 July 2015.

2.4.2 Diuretic Scanning Protocol

The scanning protocol was based on a diuretic and delayed scanning regimen reported by Anjos *et al*, incorporating the specifics of FLT dosimetry (Anjos *et al.*, 2007). The protocol involved acquisition of three PET-CT scans over the bladder: Scan 1: 30-minute dynamic PET acquisition over the bladder immediately before and during FLT administration (collection of FLT kinetic data); Scan 2: whole body PET-CT scan 60-minutes post FLT administration (to look for FLT-avid metastatic disease); and Scan 3: delayed scan, 135-minutes after FLT administration, which aimed to unmask a bladder tumour by sufficiently diluting the FLT concentration within the urine in the bladder. Figure 2-1 demonstrates the scanning protocol. If the tumours were not identified there was REC approval to modify the scanning protocol as required.

2.4.3 PET Scanning Details

18F-Fluorothymidine was obtained from PETNET Solutions, Nottingham. FLT was manufactured according to standard protocol (> 95% radiochemical purity). All PET-CT scans were performed on the same Siemens Biograph 40 TruePoint PET-CT scanner. Initially, a topogram and low-dose bladder CT were acquired after requesting the patient to void. This was followed by a dynamic 30-minute bladder PET scan. 2.59 MBq/kg (max dose 222 MBq) 18F-FLT was administered intravenously 30-seconds after starting the dynamic acquisition, followed by 10ml saline flush. The patient dismounted the scanning couch and was instructed to drink at least 600ml of water. After an uptake period of 60-minutes, a repeat topogram and static eye-to-thigh PET-CT scan was acquired with 6-minutes per bed position (CT for attenuation correction: 45 mAs effective; 3 mm slices; pitch 1.0; 120 kV). Four or five bed positions were acquired in each patient (according to patient size), imaging in a caudal-cranial direction, resulting in scan times of 24 – 30-minutes. Twenty mg of furosemide was administered as a bolus intravenous injection followed by a 20-ml saline flush 5-minutes before the end of the scan acquisition. The patient returned to the uptake bay and was encouraged to drink 1.5 litres over 45-minutes and void urine

frequently. A third and final topogram and static PET scan was then acquired over the bladder after a total time of 137-minutes. (Figure 2-1). Total radiation dose per scan visit was calculated as 15.21 mSv (Table 2-1). PET images were reconstructed using an iterative process (OSEM); 2 iterations 8 subsets, 168 x 168 matrix; filter Gaussian 5 mm; zoom = 1; pixel size = 4.07 mm. All FLT PET-CT scans were reported by a PET-approved radiologist within three days of the scan. Any unexpected findings were discussed with the Principal Investigator and actioned accordingly.

Table 2-1: Radiation dose per MARBLE-FLT PET-CT scan

Procedure	No of procedures	Estimated procedure dose (mSv)
FLT injection – max 222 MBq	1	7
CT bladder	2	1
CT eye-to-thigh	1	4.2
Topogram	3	0.67
	Total	**15.21 mSv**

Figure 2-1: MARBLE-FLT diuretic scanning protocol

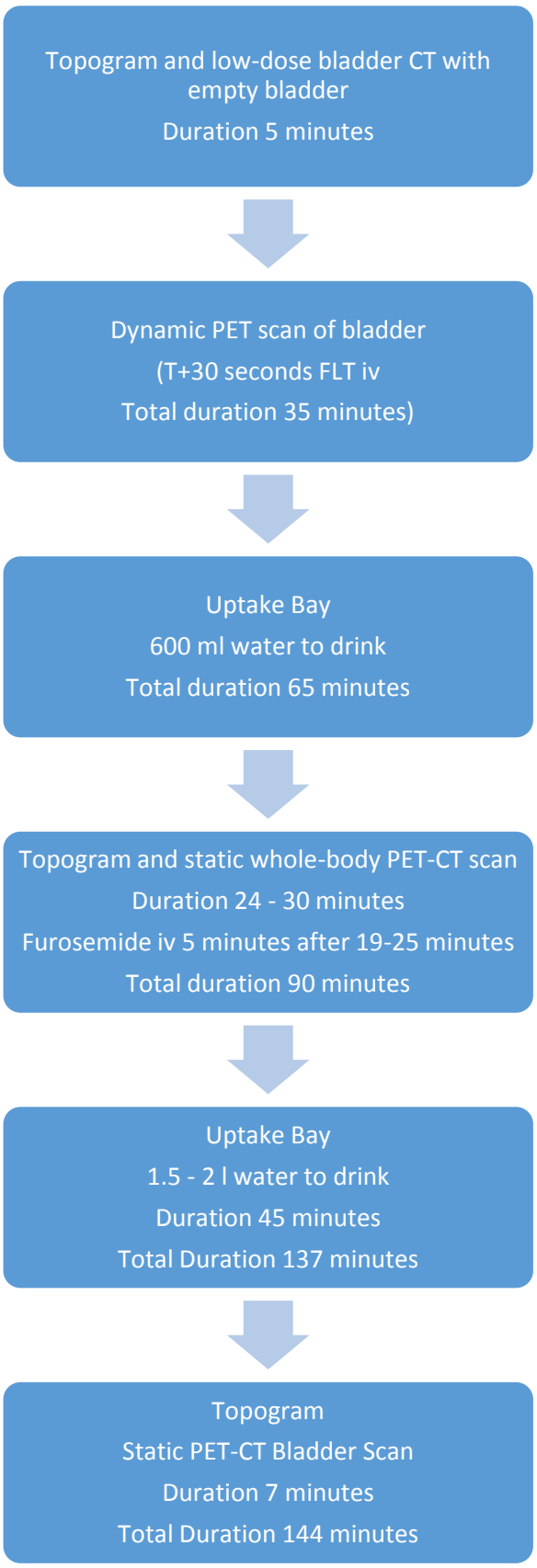

2.4.4 18F-FLT PET-CT analysis

After reconstruction, standardized uptake value (SUV) PET images were obtained using the HERMES Hybrid Viewer 2D v2.2 software (www.hermesmedical.com) correcting for body weight, injected dose and radiotracer decay. For consistency, all scan times refer to the scan start time. Using the PET and CT data sets, regions were drawn around the bladder, excluding any tumour pathology and including only bladder activity, slice-by-slice; the regions were summed together to create a volume of interest (VOI). For each patient, the bladder mean, max and peak standardised uptake values (SUVmean, max, peak kBq/ml) were noted. Regions of interest (ROIs) were then drawn around identified tumour tissue on PET-CT imaging to determine the tumour SUVmax and SUVmean. Tumour SUVmax was defined as the maximum signal intensity within a tumour and SUVmean referred to the mean value within a defined ROI. Separate volumes were drawn on both the whole body PET images and the late static images following the diuresis and fluid challenge.

Physical measurements such as signal-to-noise (SNR), contrast, and the coefficient of variance in the background (CV) are useful in characterising PET image quality and comparing results between studies (Akamatsu *et al.*, 2012). Detailed analysis was performed by Mr Nick Vennart, Medical Physicist and Dr George Petrides, Consultant Radionuclide Radiologist to determine the contrast and signal-to-noise ratios as described by Akamatsu *et al*.

$$SNR_{\max} = \frac{S_{\max} - B_{av}}{B_{SD}} \qquad \text{Equation 1}$$

The signal (S_{max}) was the maximum SUV measured in the bladder tumour. The average and standard deviation (SD) background (B_{av} and B_{SD}) denote the average and SD SUV measured in the normal bladder, respectively. The Contrast and Coefficient of Variance (CV) were calculated by:

$$Contrast = \frac{S_{\max}}{B_{av}} \qquad \text{Equation 2}$$

$$CV = \frac{B_{SD}}{B_{av}} \times 100\% \qquad \text{Equation 3}$$

To track FLT uptake over time within bone, a circular ROI was placed over the fifth lumbar vertebra (L5) and SUVmax recorded on each scan. A two-tailed paired Students t-test was performed to determine any statistically significant difference between the results.

2.5 MARBLE – FLT - Results

2.5.1 Study population

Participant characteristics and tumour details are described in Table 2-2. The study population was representative of patients treated with neoadjuvant chemotherapy in our institution. The range of Ki-67 scores determined was 45 – 90%.

Table 2-2: MARBLE-FLT patient characteristics

	MAR002	MAR003	MAR004	MAR007	MAR016
Gender	M	M	M	F	F
Age	67	53	72	53	68
TNM	T3N1	T3N1	T2N0	T4N0	T4N1
Ki-67 of tumour biopsy at TURBT	90	70	70	75	45

2.5.2 Evaluation of primary bladder tumour

Urinary activity of FLT was highest in all patients 30-minutes following injection of FLT (Table 2-3). None of the primary tumours were discernible from urinary activity at this time-point. Mean reduction in bladder SUVmean between the whole body scan at 60 minutes, and the delayed static at 137-minutes, was 73% (range 52 – 86%, $p < 0.01$, Table 2-4, Figure 2-2). In the whole body FLT PET images, two of the primary tumours (MAR007 and MAR016) were visible despite high urinary FLT concentrations. Both these tumours were large and extended beyond the bladder wall into neighbouring pelvic structures. Following the trial diuresis and hydration protocol, the patients were rescanned a mean of 45-minutes later, FLT activity within the bladder decreased, and bladder tumours were identified in four of the five patients. In MAR004, the urinary FLT SUVmax remained high at 11 and tumour could not clearly be identified. At the final time-point, mean tumour SUVmax was 7.7 (range 4.4 – 11, Figure 2-3). Mean bladder SUVmax was 7.6 (range 5.4 – 11). Because all patients had primary tumours in-situ, sensitivity of the protocol for detecting the

primary was 80%, and positive predictive value 100%. Figures 2-4 to Figure 2-11 illustrate the fall in FLT uptake within the bladder on a *per* patient basis.

Table 2-3: MARBLE-FLT bladder SUVmax at serial time-points

Interval after FLT injection (minutes)	MAR002	MAR003	MAR004	MAR007	MAR016
30	109	94	556	21	35
60	61	32	28	22	86
137	5.4	5.9	11	9.4	6.8

Table 2-4: MARBLE-FLT serial activity of FLT within urine in the bladder and tumour at 60 and 137-minutes for 2.59 MBq / kg injection. * not visualised

		MAR002	MAR003	MAR004	MAR007	MAR016
Bladder (60-minutes)	**Mean**	24	24	22	12	33
	Max	61	32	28	22	86
	Dev	16	5.4	3.9	5	16
	Peak	58	32	27	21	74
Bladder (37-minutes)	**Mean**	4.2	4.6	8.2	5.6	4.6
	Max	5.4	5.9	11	9.4	6.8
	Dev	0.64	0.6	1	1.6	0.56
	Peak	5.1	5.5	9.8	8.4	6.2
Bladder dilution (% fall between 60- and 137-minutes)	**SUV Max (%)**	93	94	61	59	93
	SUV Mean (%)	82	81	63	52	86
Tumour (60-minutes)	**Mean**	*	*	*	2.6	4.9
	Max	*	*	*	4.6	7.7
	Dev	*	*	*	0.77	1.1
	Peak	*	*	*	3.8	6.8
Tumour (137-minutes)	**Mean**	6.6	2.9	*	3.7	5.3
	Max	11	4.4	*	6.3	8.6
	Dev	1.4	0.77	*	1.2	0.99
	Peak	9.7	3.5	*	5.5	7.7

Figure 2-2: MARBLE-FLT urinary FLT activity following diuresis, oral hydration and delayed scanning

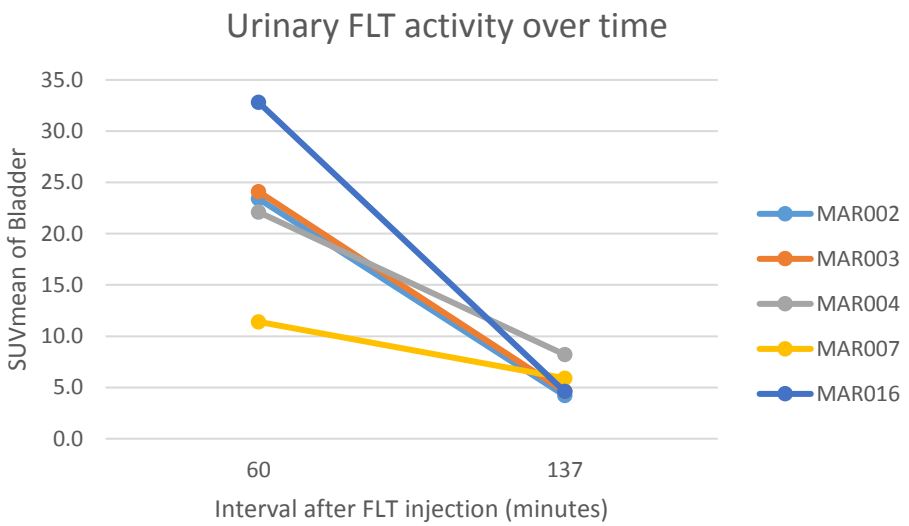

Figure 2-3: MARBLE-FLT tumour and bladder FLT SUVmax at 137 minutes

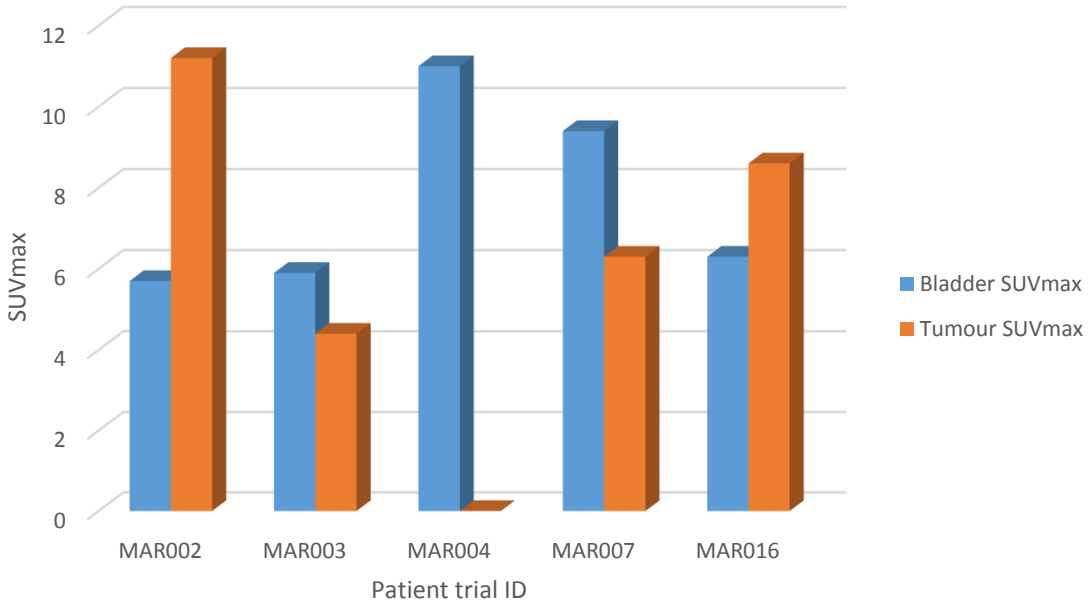

Figure 2-4: MAR002 - FLT PET CT at level of bladder at 30-minutes. Bladder tumour not identifiable due to high urinary activity of FLT SUVmax 109, (arrowed).

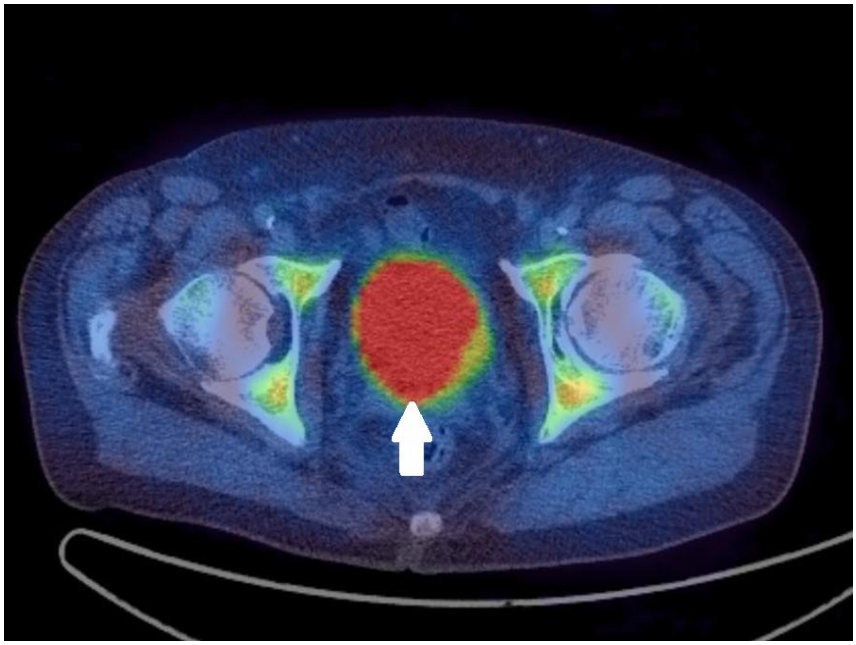

Figure 2-5: MAR002 - FLT PET CT at level of bladder at 137-minutes post injection of FLT. Bladder tumour clearly visualised, SUVmax 11 (arrowed). Urinary activity had decreased (SUVmax 5.4). Note also the increase in FLT uptake within proliferating bone marrow compared with previous image (arrowed).

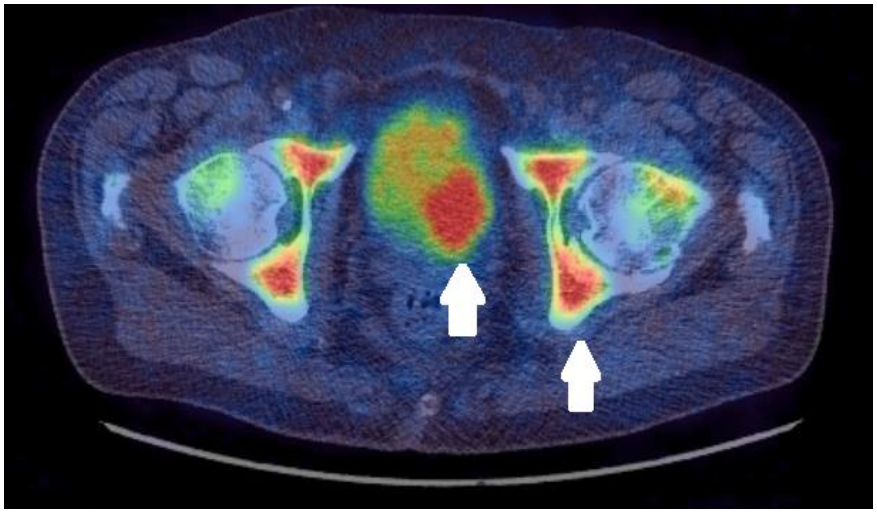

Table 2-5: MAR002 – Change in urinary radioactivity with time. Tumour visualised when FLT-intensity was sufficiently diluted within bladder.

Interval post injection of FLT	Urine		Tumour	
	SUVmax	SUVmean	SUVmax	SUVmean
30-minutes	109	31	-	-
60-minutes	61	23	-	-
137-minutes	5.4	4.2	11	6.6

Figure 2-6: MAR003 – Bladder SUVmax 94 at 30-minutes,

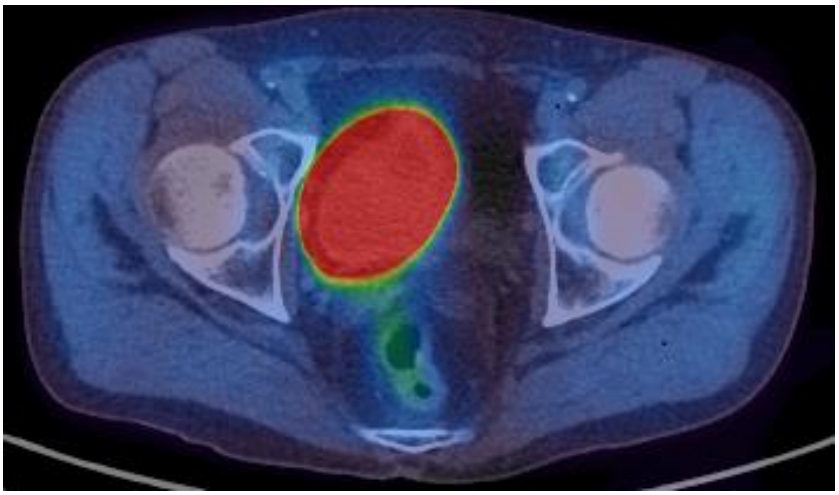

Figure 2-7: MAR003 – Bladder SUVmax 5.9 at 137-minutes. Tumour (arrowed) identified on CT portion of scan as thickening of left posterolateral wall of bladder, with less FLT uptake than nearby urine.

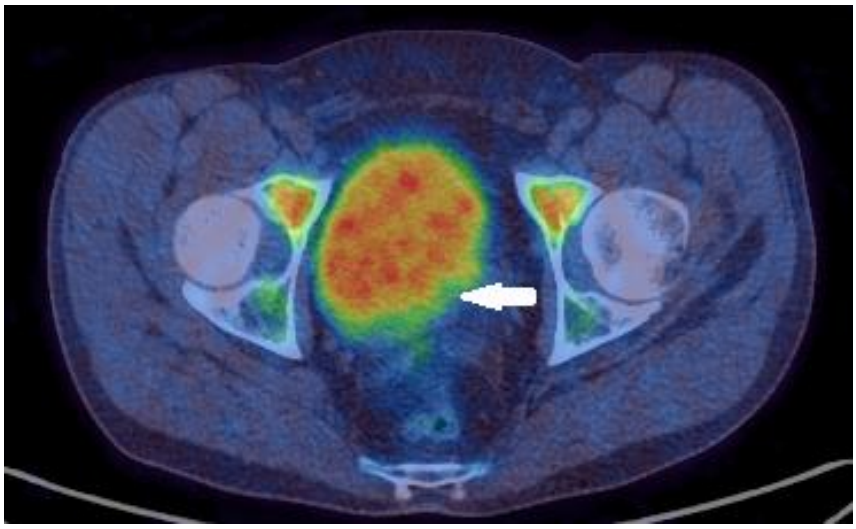

Figure 2-8: MAR004 – Tumour not visible on FLT PET-CT scan 30-minutes post FLT injection, Bladder SUVmax 555.7.

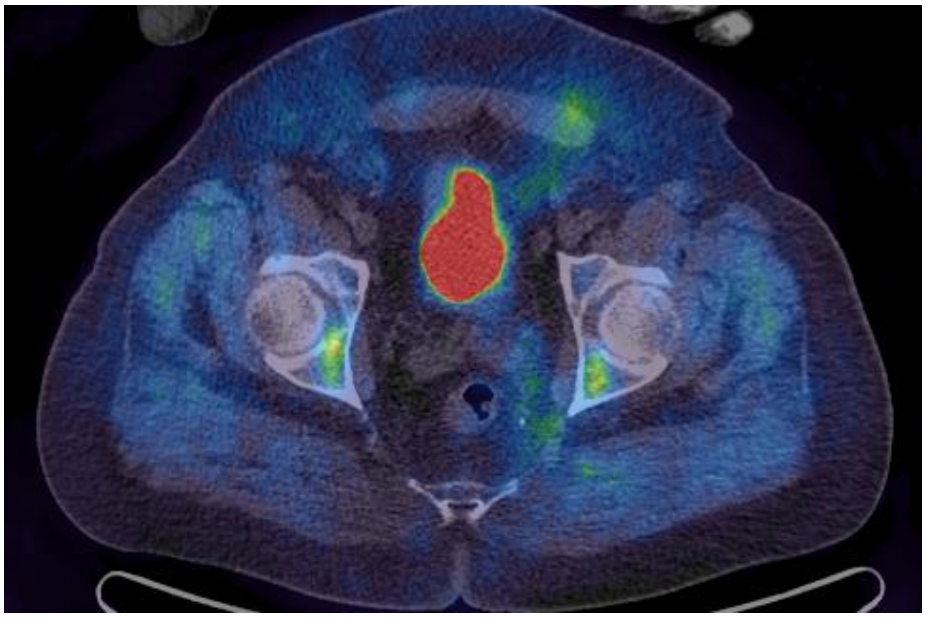

Figure 2-9: MAR004 – Tumour at 137 minutes (arrowed) identified in left lateral bladder wall on CT portion of scan but not clearly distinguishable from bladder on delayed PET imaging. SUVmax bladder 11.4.

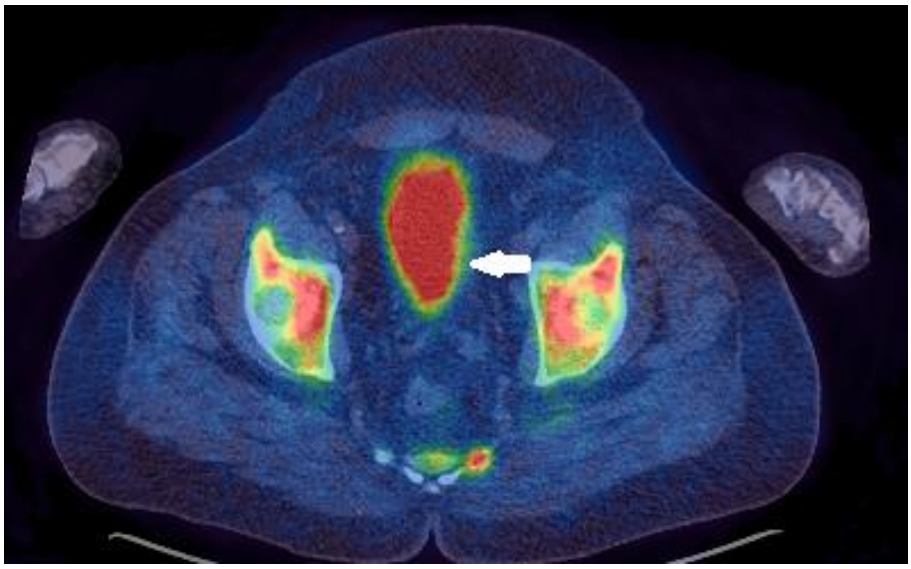

Figure 2-10: MAR007 – bladder at 60-minutes post injection of FLT, bladder SUVmax 21.8 (green arrows), tumour SUVmax 4.5 white arrow)

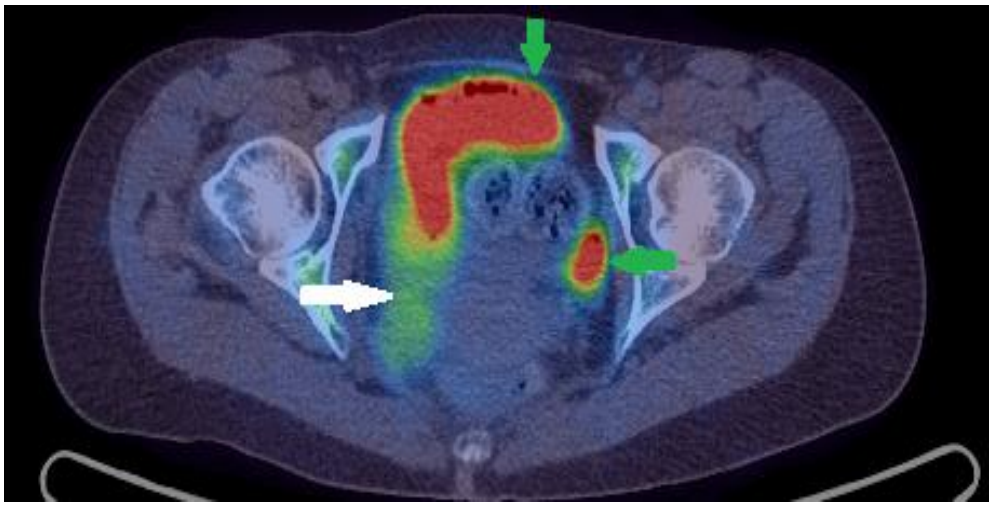

Figure 2-11: MAR007 – tumour at 137-mins post injection at the level of the tumour (ROI 1), bladder SUVmax 9.4, tumour SUVmax 6.3

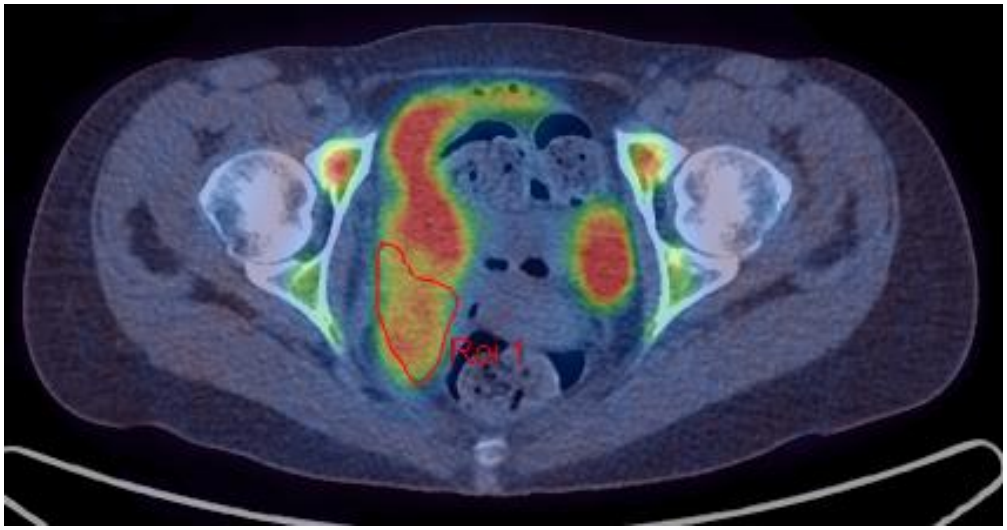

2.5.3 Evaluation of nodal and metastatic disease

Three patients (MAR002, MAR003 and MAR016) were node positive on staging CT or MRI, and FLT PET-CT (Table 2-6). Not all lymph nodes seen on CT were FLT-avid, (e.g. MAR002 external iliac), and a para-aortic lymph node group observed on FLT PET-CT was not identified on staging (MAR002 para-aortic) (Figure 2-15 - Figure 2-16). Between 60 and 137 minutes, SUVmax in the internal iliac lymph node in MAR003 increased from 1.9 to 3.6. The images from 60 and 137-minutes in MAR016 clearly identify the FLT-avid right external iliac lymph node, with SUVmax

6.6 and 6.4, respectively (Figures 2-12 to 2-14). For FLT detection of nodal disease, sensitivity was 67%, specificity 100%, positive predictive value 100% and negative predictive value 67%.

Figure 2-12: MAR016 – coronal and sagittal fused PET-CT showing FLT-avidity in the wall of the bladder and right external iliac lymph node, in keeping with sites of known TCC bladder (arrowed). Physiological uptake identified within pelvic bones and lumbar vertebrae.

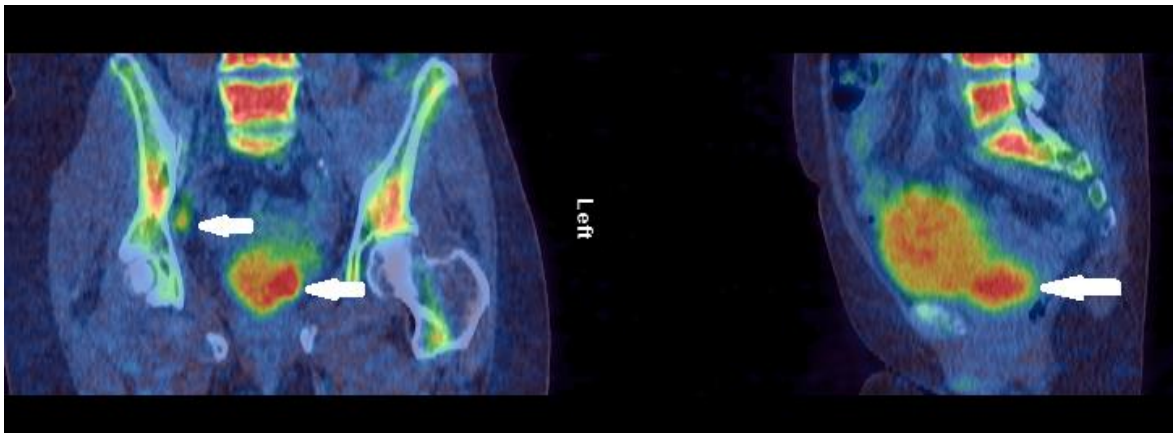

Table 2-6: MARBLE-FLT node status according to imaging modality. + = node positive, - = node negative, †External iliac LN not FLT-avid.

Imaging modality	MAR002	MAR003	MAR004	MAR007	MAR016
CT	+	+	-	-	+
MRI	-	-	-	-	+
FLT PET-CT	+	+	-	-	+
(Site, SUVmax at 60 minutes)	*†Para-aortic, SUVmax 5*	*Internal iliac, SUVmax 1.9*			*External iliac, SUVmax 6.4*

Figure 2-13: MAR016 – axial and coronal CT images demonstrating right iliac lymph node (red arrows) and primary tumour in posterior bladder wall (white arrows). In coronal images the right kidney and ureter are dilated. A percutaneous nephrostomy tube was inserted to drain the poorly functioning right kidney (see Figure 2-18).

Figure 2-14: MAR016 – coronal CT (left panel) and coronal fused PET-CT (right panel) 60-minutes post injection of FLT. Red arrows denote iliac lymph node which was FLT-avid (SUVmax was 6.6 at 60-minutes). White arrows indicate primary tumour in posterior bladder wall visible on CT but obscured on FLT PET-CT. Blue arrows denote left kidney and left ureter with physiological FLT uptake. This is not seen in the right kidney and right ureter due to the obstructing tumour causing hydronephrosis (seen in Figure 2-13)

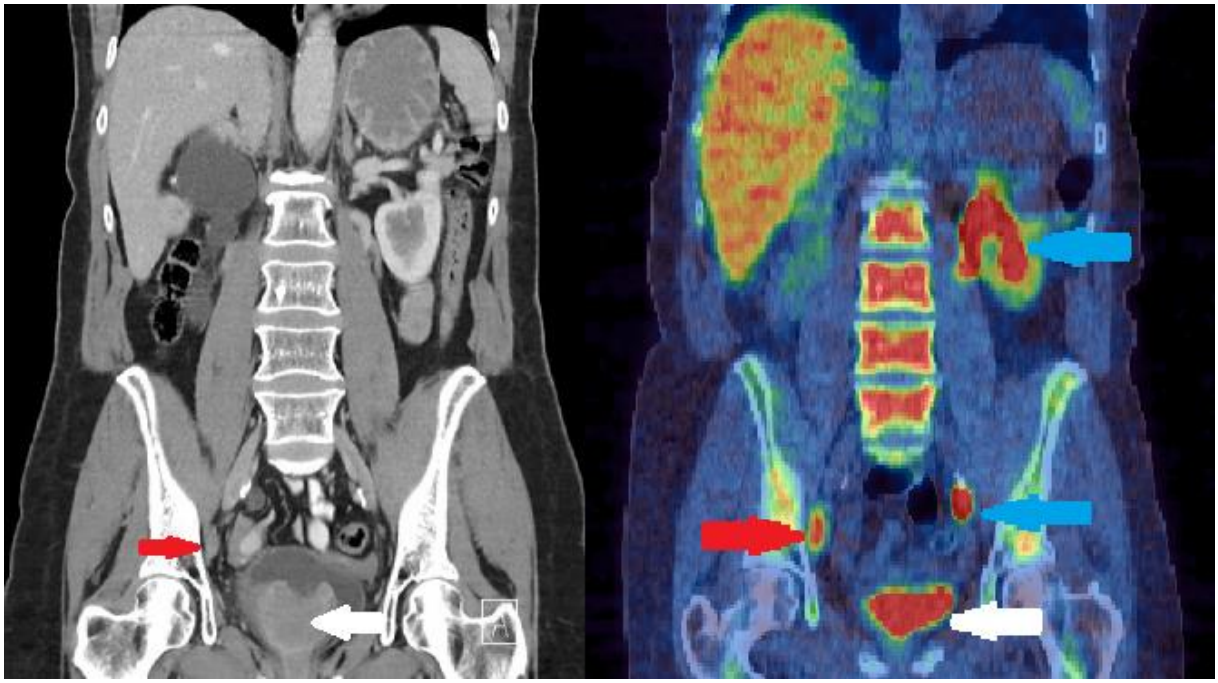

Figure 2-15: MAR002 – CT and FLT PET-CT images showing para-aortic lymph node, SUVmax 4.98 at 60 minutes (red arrow)

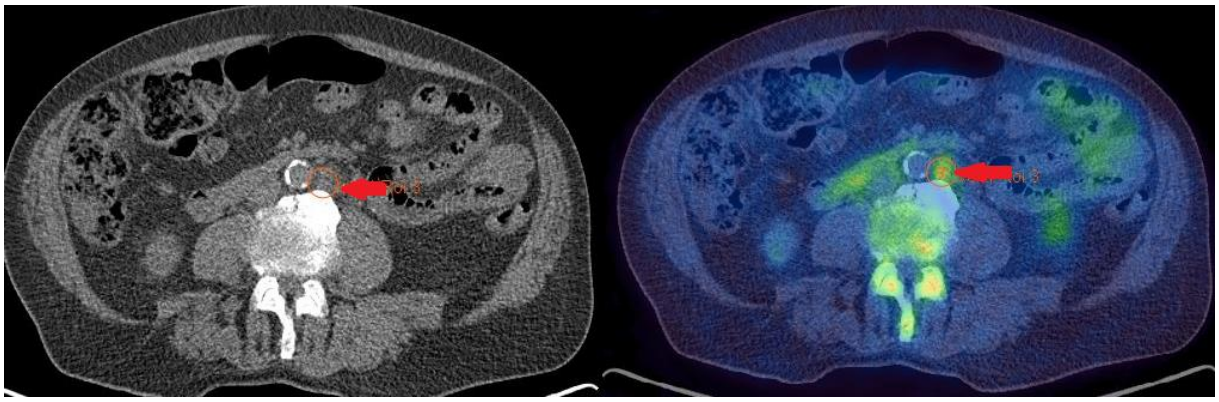

Figure 2-16: MAR002: Static MIP (Maximum Intensity Projection) image of FLT PET-CT 60-minutes post injection. High urinary FLT activity seen in bladder. Prolonged accumulation of FLT within left kidney (blue arrow) resulting in slower elimination of FLT identified due to an obstructing left bladder wall tumour. Four FLT-avid para-aortic lymph nodes (circled in red).

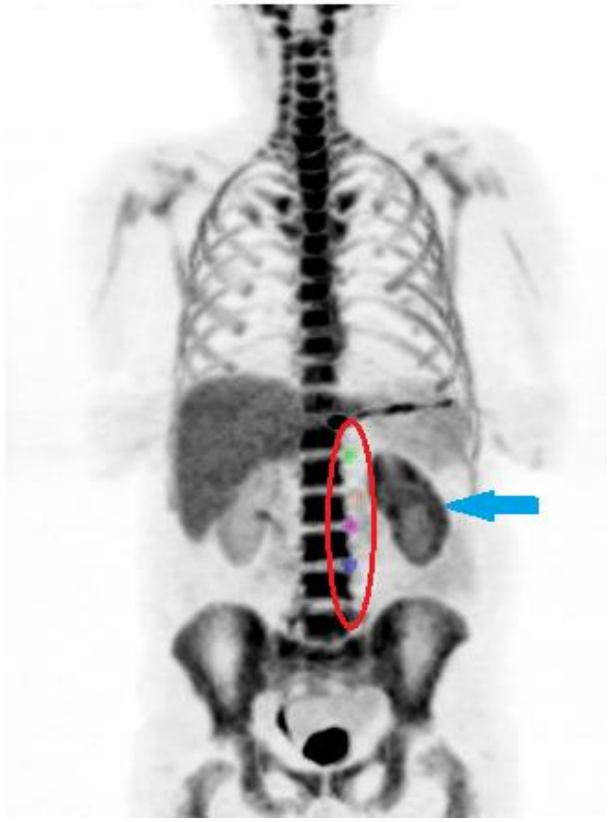

2.5.4 FLT PET-CT image quality

The SNRs and contrast values for the tumour and bladder background were highest for patients MAR002 (11 and 2.7) and MAR016 (7.3 and 1.9) on the delayed static scan at 137-minutes (Table 2-7). Similarly, the reduction in the coefficient of variance for the bladder background was also highest for patients MAR002 and MAR016. In patient MAR004, the tumour was not clearly visualised on any of the PET-CT imaging sequences. A reduction of 32% in the CV was noted for this patient. In patient MAR003, in spite of a large (81%) reduction in the bladder activity, the bladder tumour SUVmax was similar to the bladder SUVmean and, therefore, the SNR favoured the normal bladder (-0.5).

Table 2-7: MARBLE-FLT PET-CT image quality – SNR and Contrast values for tumour/bladder

Variable	MAR002	MAR003	MAR004	MAR007	MAR016
SNR Delayed Static	11	-0.5	0.0	0.5	7.3
Contrast Delayed Static	2.7	0.9	0.0	1.1	1.9
CV Whole Body (%)	68	22	18	43	50
CV Delayed Static (%)	15	13	12	28	12
Reduction in CV (%)	77	42	32	35	76

2.5.5 Additional findings

In two patients (MAR002 and MAR016), a marked difference in the FLT excretion between each kidney was observed on the whole body static PET-CT at 60-minutes. In MAR002, an obstructing tumour in the left side of the bladder caused dilatation of the left ureter and renal pelvis resulting in slower elimination of the FLT compared with the right kidney and this is clearly seen in Figure 2-16. In MAR016, the right kidney was drained by a nephrostomy tube into an external catheter bag. Urinary excretion is indicated by the blue arrows in Figure 2-14. The tumour with highest SUVmax was recorded in the patient with the highest Ki-67 score (MAR002). The tumour with the second highest SUV_{max} was recorded in the patient with the lowest Ki-67 score.

The SUV_{max} values of L5 increased as the interval between FLT injection increased (Figres 2-17 and 2-18).

Figure 2-17: MARBLE-FLT change in SUVmax uptake in fifth lumbar vertebra (L5) over time

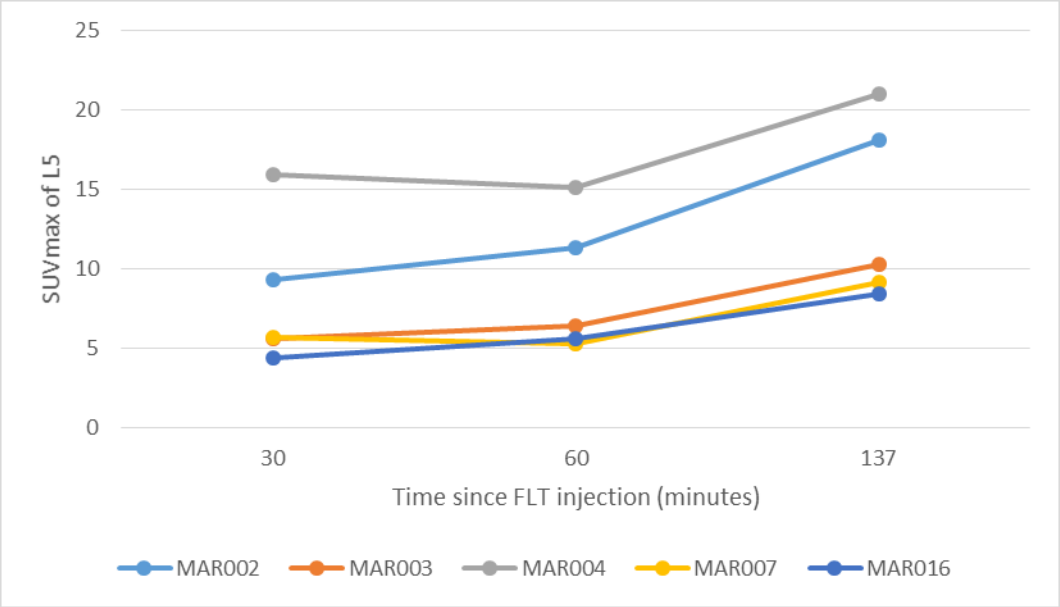

Figure 2-18: MAR016 - Physiological uptake observed in ureter (white arrow) and within fifth lumbar vertebra (L5) at 60 minutes, SUVmax 5.6 (green arrow). Nephrostomy tube draining right kidney (red arrow).

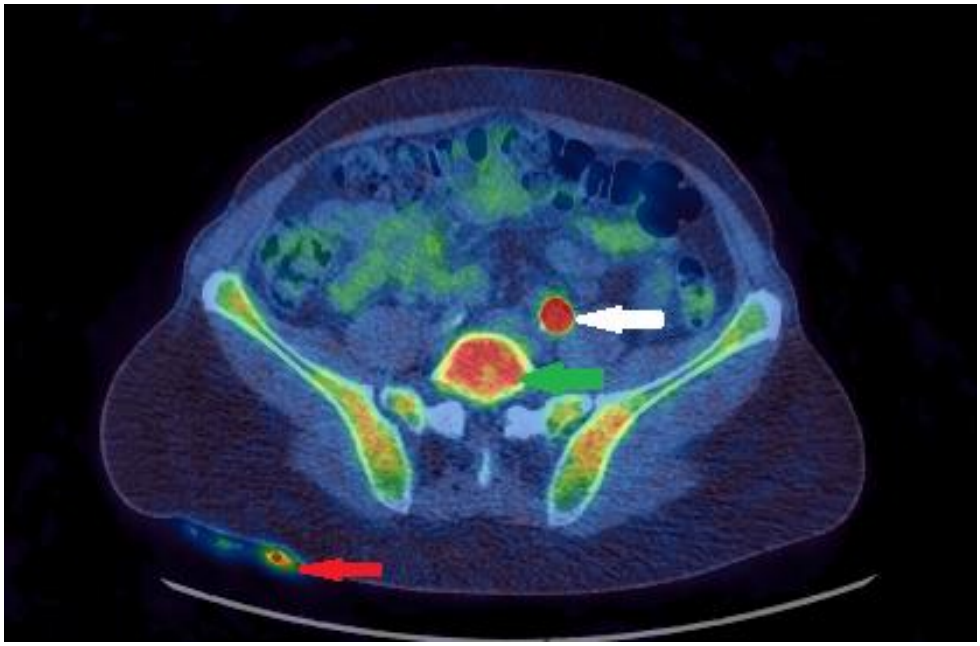

2.6 MARBLE - FLT - Discussion

2.6.1 Imaging of the primary bladder tumour

FDG PET-CT is used routinely for staging and response evaluation in tumour sites such as lung, lymphoma, and colorectal but not in muscle-invasive bladder cancer (MIBC) (Barrington and Scarsbrook, 2013). Less than 50% sensitivities for both CT and FDG PET-CT have been reported, questioning the added benefit of PET (Swinnen *et al.*, 2010). One of the limitations of the earlier studies was the lack of CT scan performed alongside the PET. With the addition of CT images, the diagnostic accuracy of the PET increases (Lu *et al.*, 2011). Previous studies report mainly nodal or metastatic disease with PET. Presumably one of the reasons for the lack of data on primary tumour imaging relates to the technical challenges. The MARBLE-FLT study sought to overcome some of the perceived limitations of using renally-excreted PET tracers in bladder cancer.

To improve visualisation of bladder pathology an enhanced imaging protocol which employed oral hydration, intravenous diuretic and triple-time-point imaging was developed in our institution, specifically for FLT. The protocol aimed to reduce background activity in soft tissues, reduce the activity in the excretory system and increase tumour to background contrast. A degree of variability in the urinary bladder SUV_{max} readings was observed and may be accounted for by inter-patient variation in urinary clearance. The accumulation of activity in the bladder, as indicated by the bladder SUVmean and SUVmax, decreased in all patients over time. Furthermore, it was possible to define a tumour volume and determine SUVmax for FLT-avid bladder wall tumours in four of the five patients studied. The primary tumour SUVmax values using FLT-PET imaging ranged from 4.4 to 11.2 and interestingly, were comparable to those found in similar studies using FDG-PET imaging, where SUVmax ranged from 5.0 – 10.1 (Anjos *et al.*, 2007), and SUVmean 5.3, range 1.3 – 11.7 (Nayak *et al.*, 2013). In their study, Nayak *et al* included low and high grade bladder tumours, and did not report any relationship between FDG SUVmax and grade of tumour. In comparison, all tumours in the MARBLE-FLT study were high grade with high Ki-67 scores. In other tumour settings, FLT SUVmax values are generally lower compared with FDG SUVs. For example, Hoshikawa *et al* reported mean FLT SUVmax was 5.65 in 43 head and neck tumours compared with mean FDG SUVmax of 10.9 (Hoshikawa *et al.*, 2011). In 20 non-small cell lung cancer patients, median FLT SUVmax was 6

compared with median FDG SUVmax of 14 (Everitt *et al.*, 2014). To our knowledge there are no similar studies which have reported FLT-avidity in MIBC, raising its potential as an imaging biomarker of proliferation in this tumour group. Further data, in particular within-patient comparisons, are required before concluding that bladder FLT values are similar to FDG values. The literature is sparse regarding FLT PET imaging of urothelial tumour xenografts; Allen *et al* reported FLT tumour uptake in the urothelial UMU-C cell line reduced after treatment with pegylated arginine deiminase and the anti-folate drug pemetrexed, suggesting that FLT PET could be used as an early surrogate response marker (Allen *et al.*, 2014).

It is not possible to comment on the FLT time to peak within tumour or urinary bladder with the current data from the MARBLE-FLT study. To track tumour kinetics, time-activity curves need to be generated from serial time-points, and a longer dynamic scanning sequence should be acquired. Over time the bladder becomes more distended so unless repeated CT scans are acquired, the CT component will not match the PET images and the composition of tissues within the region of interest will change. Also, patients may find it uncomfortable lying for a longer scan and bladder filling contributes to this discomfort. Additionally, smaller tumours are susceptible to partial volume effects which influences the validity of results.

The interval between FLT injection and PET scanning is one of a number of factors which are thought to influence quantitative measurements such as SUVmax. To date, the optimal interval between FDG injection and scanning is 45 – 60 minutes, but is unknown for all radiotracers and tumour types. The uptake of FDG may continue to rise for up to 500 minutes in some tumour types (Hamberg *et al.*, 1994). For consistent results, SUV measurements should be taken when the tracer uptake reaches a plateau. In head and neck cancer, static imaging should begin after an uptake period of 45 – 60 minutes (Menda *et al.*, 2009). In high grade gliomas for example, FLT tracer uptake peaks at 5 – 10 minutes and remains stable for up to 75 minutes (Chen *et al.*, 2005).

Delaying the imaging of the tumour region in the MARBLE-FLT study allowed more time for the diuresis and hydration protocol to reduce the urinary concentration of FLT, but did not appear to be at the expense of tumour FLT uptake. Only two of the primary tumours were identified on the 60-minute scan, but in these, the SUVmax on the

delayed static scan was higher, suggesting the tumour time-activity curve plateau had not been reached.

Attempts to overcome the technical limitations of imaging pelvic tumours with FDG PET-CT have been reported in a number of studies in the last twenty years. Retrograde irrigation of the urinary bladder using a catheter reduced urinary activity of FDG, but not low enough to reveal the primary tumour (Kosuda *et al.*, 1997). A similar technique was recommended by a Spanish group who imaged over 50 patients with known pelvic malignancies (Garcia Vicente *et al.*, 2011). Following FDG injection, patients were catheterised after voiding, and the bladder was irrigated with 250ml of saline whilst supine. If bladder radioactivity persisted on scanning, the procedure was repeated. If activity was localised to the posterior bladder wall, the patient was moved into the prone position. Another group reported the elimination of FDG activity within the bladder and easy visualisation of uterine or ovarian masses after 30 minutes of continuous bladder irrigation (Koyama *et al.*, 2003).

A number of research groups have reported higher sensitivities for diuretic FDG PET-CT (Nayak *et al.*, 2013). Furosemide is a loop diuretic which lowers the urinary tract activity of FDG without significantly affecting blood activity (Ceriani *et al.*, 2011). A study by Kamel *et al* involving 32 patients with abdomen-pelvic tumours concluded that forced diuresis using furosemide, intravenous fluids and three voiding episodes eliminated any significant FDG activity from the bladder in 97% of cases (Kamel *et al.*, 2006). In addition to using a diuretic, varying the degree and route of hydration has been addressed (Kamel *et al.*, 2006; Anjos *et al.*, 2007; Ceriani *et al.*, 2011). In a study reported by Ceriani *et al*, 120 cancer patients attending for a follow-up FDG PET-CT were assigned to one of four different hydration protocols to investigate the impact on image quality in the bladder. The best results were observed in the group who received 10 mg of intravenous frusemide and 250 ml of intravenous saline.

Delayed imaging enhances the detection rate of bladder lesions. Anjos and colleagues studied 17 patients with a past history of bladder cancer (11 with an intact bladder and 6 post cystectomy). PET-CT acquired three hours after FDG-tracer injection detected all six of the recurrent bladder tumours (Anjos *et al.*, 2007). CT identified 4 / 6 of these tumours. The protocol followed by Anjos *et al* differed from the one used in MARBLE because the tracer involved was FDG, which was administered after a period of pre-hydration with 500 ml of intravenous saline. The

timing of the whole body scan post tracer injection was similar, but furosemide was given at least two hours after tracer injection, followed by oral hydration of up to one litre of water and frequent voiding. Their protocol required more on-bed time (up to 40 minutes) and a scanning visit of four hours. Compared to MARBLE-FLT this research group reported more success in diluting urinary FDG activity levels to background in the eleven patients. The radioactivity administered in MARBLE-FLT was less than that used in many studies; 370 MBq (10 mCi) administered by Anjos *et al*, compared with maximum 222 MBq in MARBLE. Patients with urinary diversions were included in the study reported by Anjos *et al,* but results were less successful. They hypothesised that a larger dose of diuretic and a greater delay before scanning could improve these results.

Voiding before scanning usually leaves a small residual volume of urine within the bladder, therefore, radiation dose to the urinary bladder will be reduced several-fold by repeated voiding. Vesselle *et al* reported a 50% reduction in absorbed dose to bladder after requesting patients to void after 2-hours, compared with a single void 6-hours post FLT injection (Vesselle *et al.*, 2003). Frequent micturition was encouraged in MARBLE-FLT and contributed to the fall in bladder radioactivity, and consequently reduced the absorbed dose to bladder.

A meta-analysis of FDG in bladder cancer identified 126 studies but only 6 were eligible for inclusion, totalling 236 patients. Studies were excluded for the following reasons: included other urological tumours; data from sub-analyses were missing; or if numbers of true positives or negatives, and false positives or negatives, were not reported. Three of the studies included patients with bladders intact and reported on identification of bladder lesions, totalling 64 patients; it reported pooled sensitivities and specificities of 90% and 100%. The forest plot of sensitivity and specificity of FDG PET or FDG PET-CT for staging or restaging was 82% and 89% respectively. Four studies used intravenous diuretic and two also used delayed imaging. The meta-analysis concluded that FDG PET provided good diagnostic accuracy of lymph node staging and detection of distant metastases, but larger studies were needed to evaluate the detection of primary tumours (Lu *et al.*, 2011). Included in the meta-analysis were 42 T2 – 3 N0 tumour bladder cancer patients; FDG PET identified both primary tumour and perivesical lymph node metastases using a catheter and diuretic protocol resulting in sensitivity of 70% and specificity 94% (Kibel *et al.*, 2009).

Metastatic disease was identified in 7/42 patients. However, the techniques involved catheterisation and retrograde or continuous irrigation which is uncomfortable for a patient, time-consuming to undertake and invasive with a risk of infection. Furthermore, irrigation of the bladder exposes staff to additional radiation. Therefore, it is desirable to develop a technique which maintains accuracy without subjecting the patient to the aforementioned risks. Harkirat *et al* reported excellent washout of FDG following 1500ml oral hydration, 0.5 mg/kg furosemide intravenous injection and delayed scanning 150 – 180 minutes after FDG injection. Bladder lesions were detected in 13 of 22 bladder preserved patients (Harkirat *et al.*, 2010). The MARBLE-FLT scanning acquisition protocol used here was similar to that reported by Harkirat *et al.*

Although the number of patients was small in the MARBLE-FLT study, initial results suggest that the use of a diuresis and hydration protocol can considerably reduce the activity in the bladder to allow quantitative visualisation of FLT-avid neoplasia arising in the bladder wall, as other groups have demonstrated with FDG.

2.6.2 Imaging nodal disease with FLT PET-CT

Compared to primary tumour assessment, FDG PET-CT to evaluate nodal disease is more frequently reported, but the literature is varied with sensitivities and specificities ranging from 33 – 70% and 87 – 100%, respectively. In the MARBLE-FLT study, sensitivity for nodal detection was 67% with a specificity of 100%. The FLT PET-CT scan in MAR002 identified FLT-avid para-aortic lymph nodes on the whole-body scan, which were visible on the accompanying CT, but had not been size-significant at the time and were not reported as being involved by cancer. In this particular case, the treatment intent changed from radical to palliative. PET-CT is not routinely used in our institution, although with recent changes to NICE guidance for patients at high risk of metastatic disease, it is under evaluation as a staging investigation (NICE, 2015).

Although FLT uptake appeared to have plateaued in one nodal deposit at 137-minutes, in another the SUV increased by a factor of 2. Nayak *et al* reported more intense FDG uptake in a pelvic lymph node following diuresis. They suggest that an alternative to dual-time-point imaging demonstrating that the tracer uptake had not peaked, could be the ‘sun and star’ phenomenon. A possible explanation of this phenomenon is that due

to a considerable amount of activity within the bladder (the sun) in the earlier images, the signal from adjacent smaller nodes (the stars) has been flooded. However, when the bladder activity is reduced, this results in a more accurate estimate of the nodal activity and hence a perceived (pseudo) increase. Delaying the bladder imaging further, and administering greater hydration, is likely to have reduced the urinary activity by a larger magnitude, but at some undefined time-point the signal arising from tumour will also fall with time, challenging image interpretation.

2.6.3 Ki-67

The ability to select which patients are most likely to benefit from particular functional imaging modalities has great appeal. Minimising scanning costs and reducing unnecessary hospital attendances generally lead to increased NHS efficiency and should improve patient care. Ki-67 is an established histological marker of cellular proliferation. Correlating Ki-67 score with FLT PET-CT imaging may identify which patients would be best imaged by FLT. There have been conflicting reports on the relationship between Ki-67 score and FLT uptake. A meta-analysis of 27 studies concluded that there is a correlation, irrespective of tumour type, where average Ki-67 expression is reported, or for whole surgical samples if maximum Ki-67 expression is given (Chalkidou *et al.*, 2012). In MARBLE-FLT, the average Ki-67 score in a biopsy specimen was reported. The correlation of Ki-67 score and FLT PET-CT imaging is strongest in brain, breast and lung cancers (Chalkidou *et al.*, 2012). Further data are required to validate the strength of correlation for other tumour types.

High Ki-67 scores in bladder cancer correlate with poorer outcome (Margulis *et al.*, 2006). In their study, Ki-67 labelling index (LI) was deemed positive if ≥ 20% cells stained positive. Using this criterion, all of the MARBLE-FLT and 17 / 18 of the main MARBLE cohort had Ki-67 scores > 20%. With a small sample size, it is unclear if the Ki-67 results in MARBLE-FLT are typical of the cohort of bladder cancers treated with neoadjuvant chemotherapy because Ki-67 is not routinely tested. Additional data from the aforementioned studies relating to the degree of Ki-67 expression rather than a simple less than or greater than 20 - 25% expression would aid contextualisation of the MARBLE-FLT results.

The prognostic role of Ki-67 in bladder cancer has been studied. Margulis *et al* reported that in 713 bladder cancer patients post-cystectomy, Ki-67 LI > 20% predicted for tumour recurrence (Margulis *et al.*, 2009). More recently, Ding *et al* reported that Ki-67 expression (Ki-67 > 25%) in non-muscle-invasive bladder (NMIBC) cancer could be used as an independent risk factor for recurrence or progression to MIBC (Ding *et al.*, 2014). Combining the Ki-67 score with EORTC risk scores, as suggested by Ding *et al*, could improve risk stratification in early bladder cancers. The EORTC risk tables for predicting recurrence and progression in individual patients with stage Ta or T1 bladder cancer include the following six factors: number of tumours; tumour size; prior recurrence rate; T category; concomitant carcinoma-in-situ; grade (Sylvester *et al.*, 2006). In the clinic, this could lead to the development of an algorithm which selects patients most suitable for particular therapies e.g. neoadjuvant chemotherapy. Further investigation into the utility of FLT PET-CT scanning as an imaging biomarker in bladder cancer, for prognostication and tumour response monitoring is suggested by results of the current study. In particular, a larger study comprising patients with a range of Ki-67 score on bladder biopsy, and scanning at different time-points would be useful to further evaluate the potential utility of FLT PET-CT in this cancer group.

2.6.4 Bone marrow

FLT accumulates in urinary bladder, liver, kidneys and bone marrow in healthy subjects. Vesselle *et al* studied 18 lung cancer patients and reported time-activity curves for normal tissues; two-hour dynamic imaging provided FLT radiation dosimetry in more than 10 organs of the body (Vesselle *et al.*, 2003). The dose administered was similar to MARBLE-FLT, with 2.59 MBq / kg (0.07 mCi /kg), and a maximum dose 185 MBq (5 mCi). The marrow time-activity peak occurred around 25 minutes but remained relatively stable until 100 minutes (Vesselle *et al.*, 2003). This compared with a more rapid peak at two minutes within the liver and kidney, a rapid fall off in kidney, but slower within liver. Interestingly, the bladder time-activity curves showed a slow increase to plateau around 80 minutes. In the MARBLE-FLT cohort, FLT uptake within the fifth lumbar vertebra ranged between SUVmax 5.6 – 15.9 at 30 minutes, to SUVmax 8.4 – 21 at 137 minutes. It is unclear if the peak time-activity curve had been reached for this organ because in four subjects the SUVmax at the final time-point was higher than earlier measurements.

Defined as an organ at risk in terms of its response to radiation, functional bone marrow may be characterised by FLT-PET imaging. Spatial mapping may allow sparing of functional bone marrow in radiotherapy planning to minimise prolonged myelosuppression using highly intensity modulated radiotherapy treatment (IMRT). This may have particular utility in paediatric patients or those who have been heavily pre-treated with myelosuppressive chemotherapy. The greatest bone marrow distribution can be observed within the pelvis and thoracolumbar spines (Hayman *et al.*, 2011). An atlas of marrow distribution from 51 patients with non-small cell lung cancer is available; four sub-group atlases have been devised according to age and sex, due to considerable inter-individual variation in marrow uptake (Campbell *et al.*, 2015). McGuire *et al* have investigated the ability to determine areas of functional bone marrow using bony landmarks on CT, comparing them with FLT PET imaging. They suggest these data could be used in personalised radiotherapy treatment plans of the pelvis to minimise radiotherapy dose to bone marrow (McGuire *et al.*, 2014).

Additionally, there may be interest in quantifying residual bone marrow activity in patients who have previously received chemotherapy, to establish bone marrow tolerance of further lines of chemotherapy. Chemotherapy cannot be delivered until the peripheral neutrophil count, measured from simple venepuncture, is above a defined cut-off level. Despite this safe guard, a considerable number of patients are admitted to hospital within three weeks of receiving chemotherapy with infections that have a 2 – 21% mortality rate which develop when neutrophil counts are lower than 0.5 $x10^9$ per litre. Aggressive management within England has reduced mortality from infections to 5% (NICE, 2012). Current guidelines recommend using primary prophylactic granulocyte colony stimulating factor (G-CSF) if the risk of febrile neutropenia is greater than 20% (Smith *et al.*, 2015). This risk could be further quantified on a per-patient basis by bone marrow mapping using FLT PET-CT. If estimating bone marrow reserve on an imaging map is found to be more accurate than a peripheral blood count, these data could potentially influence patient care: for example the timing of chemotherapy cycles; need for G-CSF. A strong argument against this would be the radiation dose exposure and cost of the FLT PET-CT scan.

2.7 MARBLE-FLT - Limitations

This was a pilot single-institution study with a few patients to collect some preliminary data on MIBC tumours and FLT uptake. Contamination from the neighbouring urine, and small tumour size may have influenced the SUV measurements.

2.8 MARBLE-FLT - Conclusions

Urothelial carcinomas of the bladder are FLT-avid. Dilution of the urinary activity of FLT may improve identification of bladder wall tumours. Although results were not as good as some FDG studies which eliminated urinary radioactivity, the MARBLE method avoided urinary catheterisation and intravenous hydration, and enabled the detection of tumours with 80% sensitivity. Further validation work is required.

2.9 Future Directions

Building on the encouraging results demonstrated in the MARBLE-FLT study, the author has led a funding application to investigate this scanning protocol in muscle invasive bladder cancer using FDG PET-CT. This has been successful and is planned to open in 2017; the HYDRO-FDG study will be a prospective feasibility study which has two phases. The first seeks to establish if urinary concentrations of FDG can be sufficiently reduced to enable evaluation of the bladder wall, in cancer patients who are routinely attending for FDG PET-CT examinations as part of planned surgical work-up. If results are promising, a second phase will evaluate the protocol in bladder cancer patients. Subsequently, a comparative study of FDG and FLT PET-CT could be performed in MIBC.

2.10 THRIFT – Background

Limited data are available on FLT in the context of differentiated thyroid carcinoma (DTC). The THRIFT study sought to investigate if differentiated thyroid cancers demonstrated raised FLT uptake and how the images compared to FDG-PET scanning. This is an uncommon clinical scenario with an average of three patients treated *per annum* at the author's institution. A theoretic planning study was included in the design of THRIFT. Similar to the FLAIRE study, in patients with FLT uptake on the PET-CT scan, a simulated radiotherapy plan to boost the excessively proliferating regions of the tumour with a higher radiotherapy dose was planned.

2.11 THRIFT – Objectives

The primary aim of the study was to determine the feasibility of undertaking FLT PET-CT scans in patients with radioiodine-resistant differentiated thyroid cancer. Secondary objectives comprised: (i) determining the feasibility of generating FLT-guided dose-escalation radiotherapy plans; (ii) determining if FLT is effective at localising recurrent disease; (iii) comparing FLT-based RT plans and PET-CT scans with FDG-based RT plans and PET-CT scans; (iv) determining if radiotherapy dose to parotid glands could be reduced further using FLT-guided dose-escalation.

2.12 THRIFT - Methods

On the basis of few differentiated thyroid cancer patients being treated with RT each year, a sample size of 3 patients was agreed. A total of two patients were recruited between May 2014 and November 2015 from the Newcastle upon Tyne Hospitals NHS Foundation Trust thyroid cancer multidisciplinary team meeting.

The eligible patients had histological or cytological evidence of DTC and were scheduled to receive radical radiotherapy to the thyroid bed and neck. Patients attended for a single FLT PET-CT scan in the same visit as the radiotherapy planning CT scan. The PET-CT scan was acquired on a Siemens Biograph 40 TruePoint PET-CT, with the patient immobilised in a customised radiotherapy shell, in the radiotherapy planning position. 2.59MBq/kg FLT (maximum 222 MBq) was injected intravenously and after 45 - 60 minutes uptake time a static PET-CT scan was acquired. A low-dose attenuation correction CT scan extending from the base of skull to the carina was followed by the PET acquisition with 6 minutes per bed-position; CT for attenuation correction: 45mAs effective; 3mm slices; pitch 1.0; 120kV. In addition, contrast-enhanced CT images of the head and neck region using 100ml of Omnipaque 300 were acquired for anatomic correlation and to aid tumour localisation for radiotherapy planning (120 mAs effective; 3mm x 274 slices; pitch 1.5; rotation 0.5s; 120kV). PET images were reconstructed using an iterative process (OSEM) 2 iterations 8 subsets, 168 x 168 matrix; filter Gaussian 5mm; zoom = 1; pixel size = 4.07mm. The maximum total effective dose within the study period was 9.9 mSV of which 8 mSv was additional to routine care (Table 2-8).

Table 2-8: THRIFT radiation exposure for study participants

Procedure	No of procedures	Estimated procedure dose (mSv)
FLT injection – max 222 MBq	1	7
CT base of skull to carina	1	0.7
Contrast-enhanced planning CT base of skull to carina	1	1.9
Topogram	1	0.3
	Total	**9.9 mSv**

2.13 THRIFT – Results

Two patients with pT3N1b papillary thyroid carcinoma with recurrence after total thyroidectomy, level VI neck dissection, radioiodine ablation, surgery and radioactive iodine therapy were recruited to the study. An example of a post radio-iodine ablation scan from THR002 is shown in Figure 2-19. In the same patient, Figure 2-20 demonstrates a diagnostic whole body scan.

In patient THR001, the primary thyroid tumour had a Ki-67 score of 5.8% and the metastatic tumour forming a right neck lump had a Ki-67 of 5.5% at diagnosis. FDG PET-CT performed six weeks prior to the FLT PET-CT scan, demonstrated marked focal uptake within the thyroid bed (SUVmax 6.9) and right supraclavicular fossa (SUVmax 10.3) consistent with recurrent disease seen on CT (Figures 2-21 and 2-22). FLT PET-CT showed no focal uptake within the thyroid bed or neck.

Figure 2-19: THR002: Whole body scan 7-days post 5 MBq I131 NaI given orally. Small areas of increased uptake seen left neck, posterior left lung and liver. Physiological uptake in mouth, salivary glands, gastro-intestinal tract and bladder.

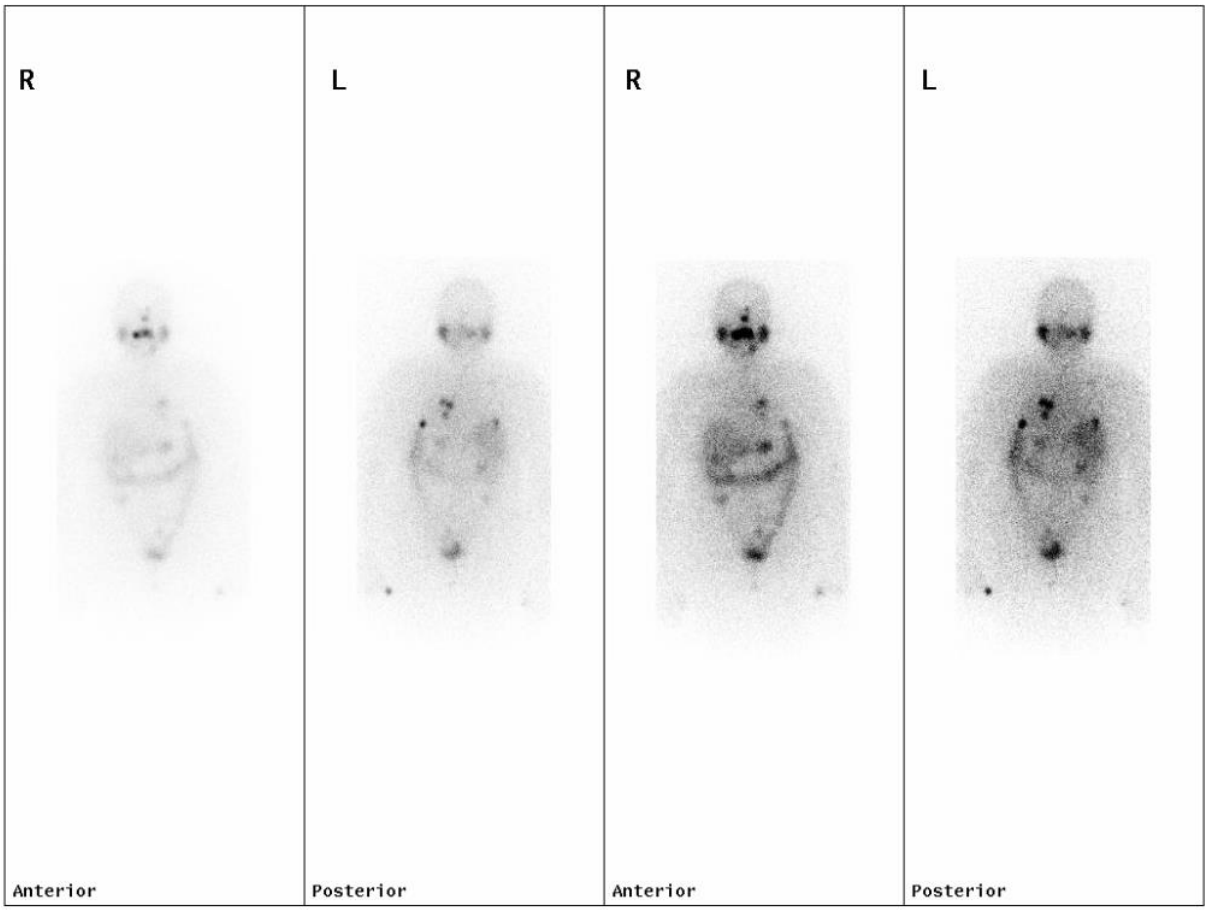

Figure 2-20: THR002: Diagnostic whole body scan demonstrating no abnormal uptake.

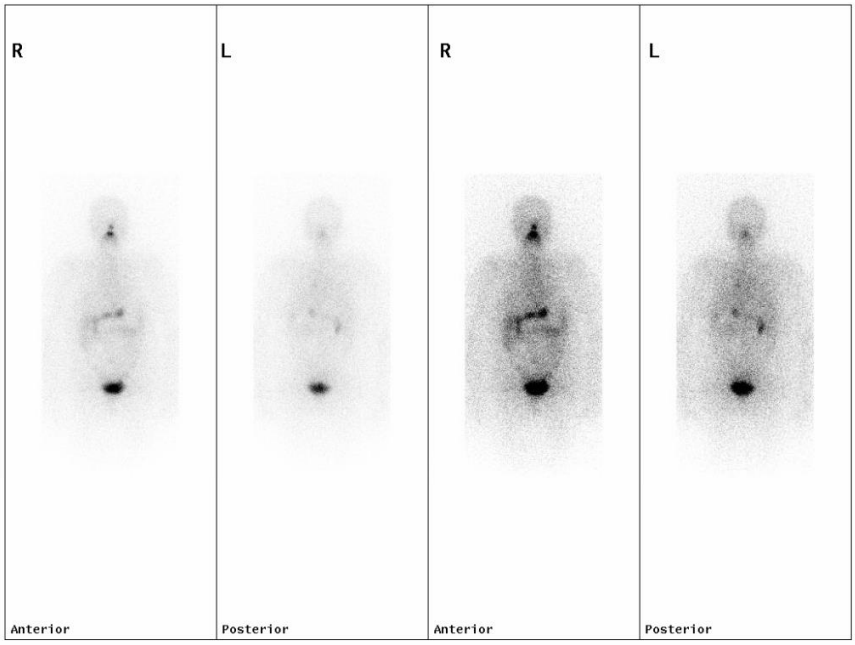

Figure 2-21: THR001 - paired FDG PET-CT (top panel) and FLT PET-CT (bottom panel) images taken 6 weeks apart. FDG PET-CT scan shows marked focal uptake within thyroid bed (SUVmax 6.9) and right supraclavicular fossa (SUVmax 10.3). Raised FLT uptake seen within normal proliferating bone marrow on FLT PET-CT scan but no uptake within thyroid cancer mass.

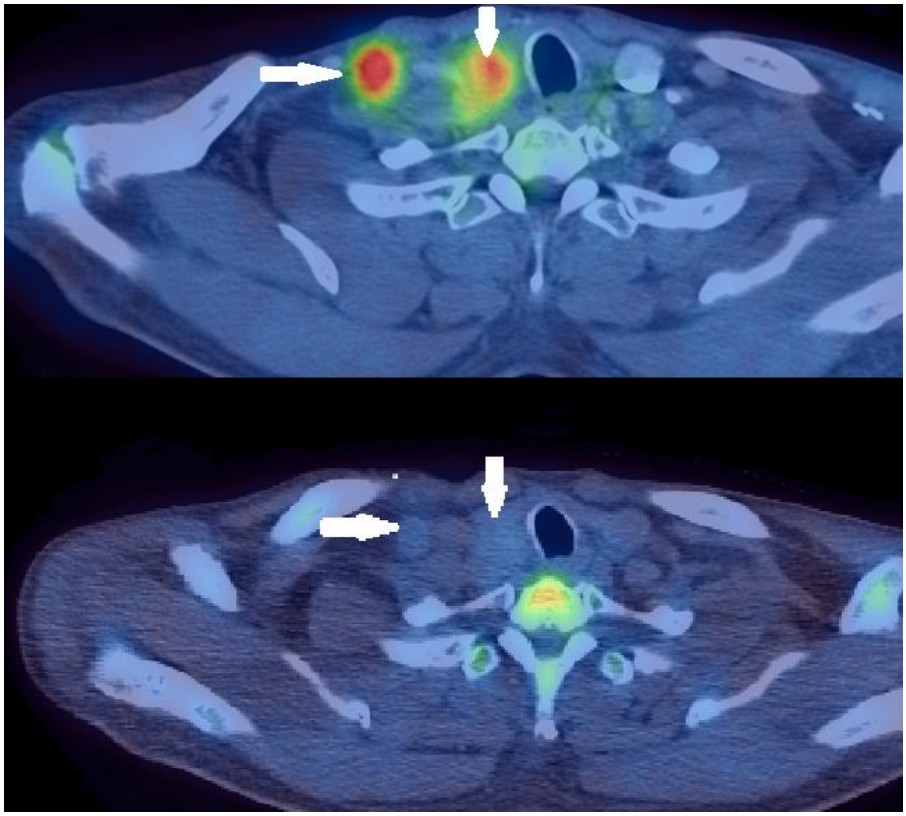

Figure 2-22: THR001 – FDG MIP demonstrating increased FDG uptake in right sided cervical lymph nodes.

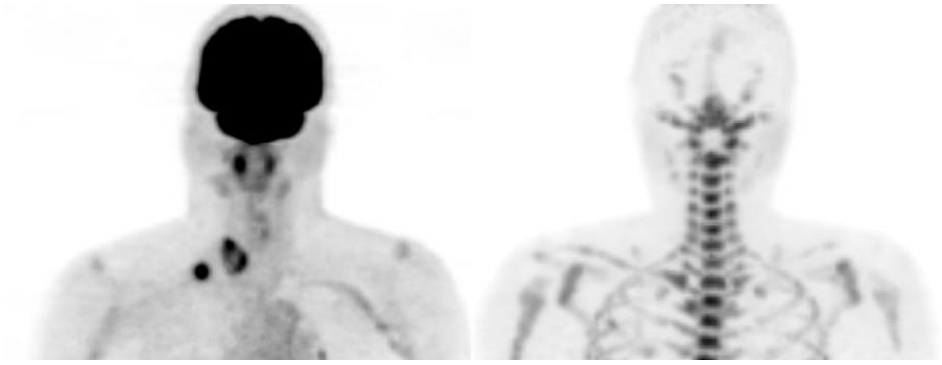

In Patient THR002 Ki-67 was 20% and mild FLT uptake was present at the site of the recurrent disease in the thyroid bed (SUVmax 2.5). CT demonstrated a 4 cm recurrence within the left thyroid bed, measuring 4 x 3.7 x 3.4 cm (Figures 2-23 and 224). Additionally, widespread intrapulmonary metastases, measuring up to 1.2 x 1.2cm were present. Recurrent disease was confirmed histologically following

debulking of the locally recurrent tumour. The pulmonary lesions did not take up FLT. No FDG PET-CT scan was available for comparison in this patient.

High dose radical radiotherapy was delivered to both patients; 66-Gy in 30 fractions to FDG-avid disease (in THR001), 60-Gy to thyroid bed (THR001 and THR002) and 54-Gy to bilateral neck (THR001 and THR002), as routine practice. A slice from the TomoTherapy IMRT radiotherapy plan is seen in Figures 2-25 and 2-26).

Figure 2-23: THR002: Recurrent tumour mass in left thyroid bed on axial CT (red arrow) and on FLT PET-CT (white arrow).

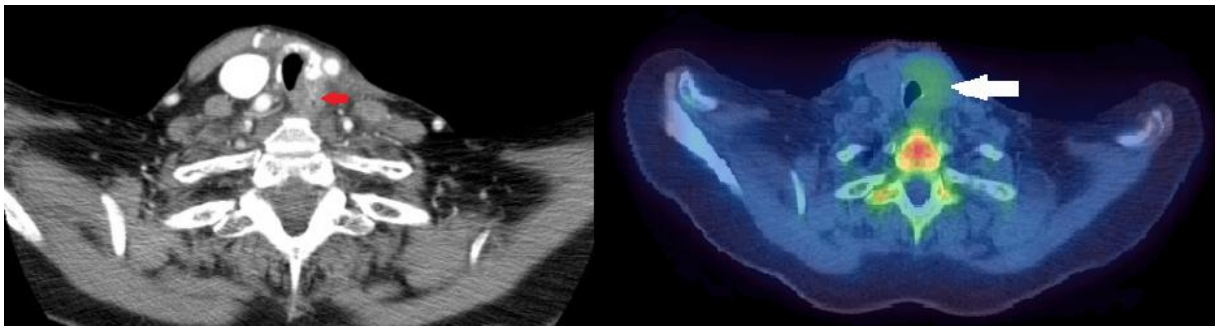

Figure 2-24: THR002: Recurrence identified within left thyroid bed on coronal CT (denoted by red arrow).

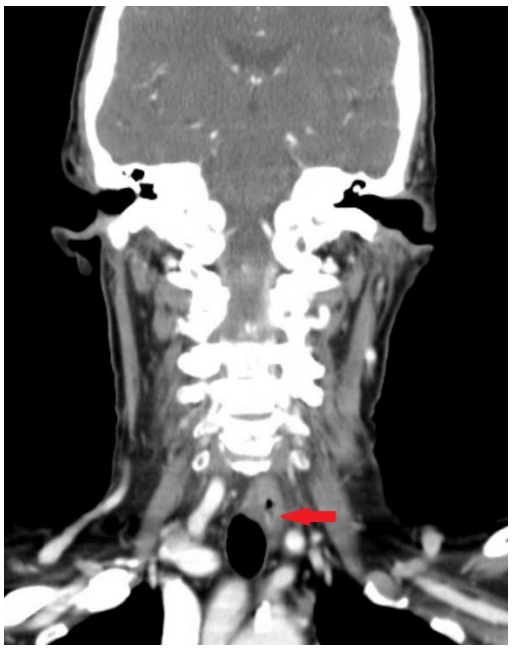

Figure 2-25: THR001 - TomoTherapy plan at level of thyroid bed.

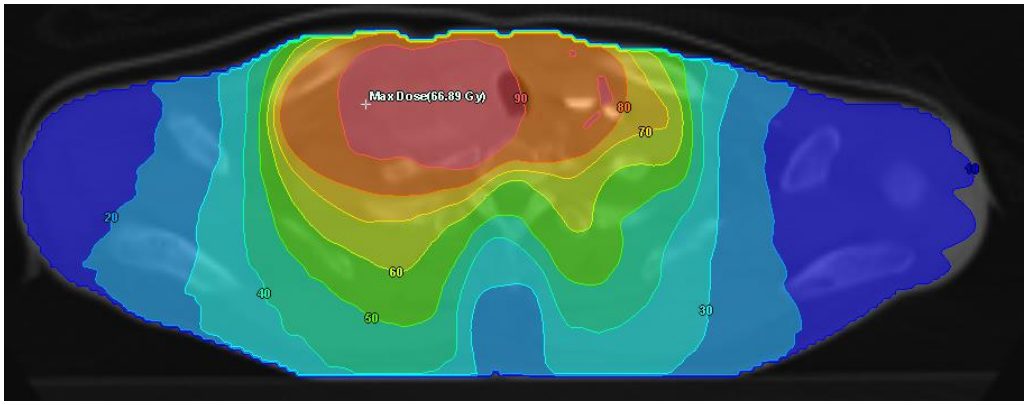

Figure 2-26: THR001 - target volume (left panel) and scale depicting isolines in absolute dose in Gy (right panel)

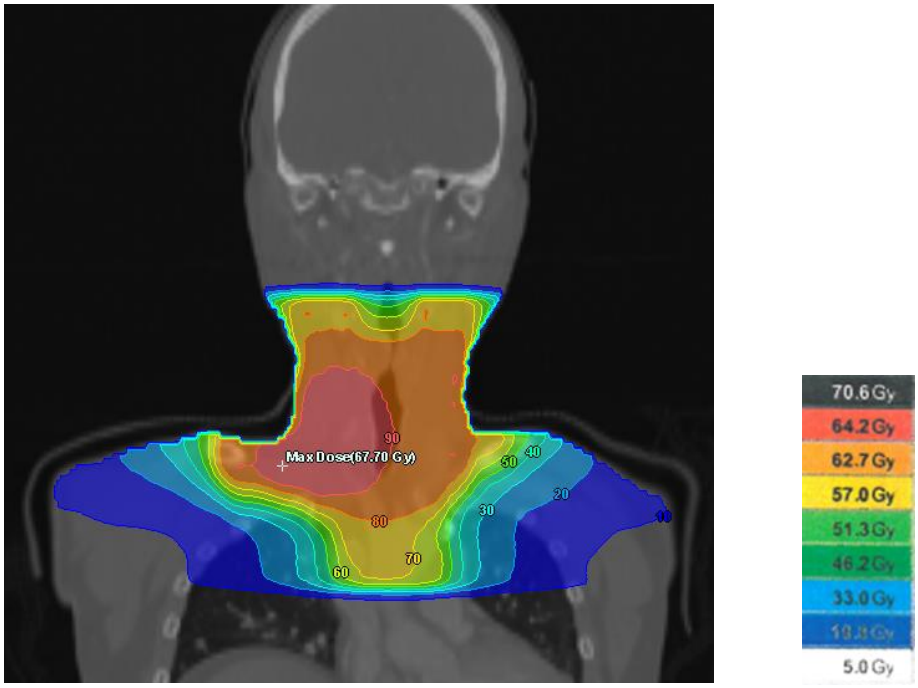

2.14 THRIFT – Discussion

2.14.1 FLT scanning in DTC

To date, there is limited knowledge of the biological behaviour of FLT in differentiated thyroid cancer (DTC) patients. The cohort of patients under investigation in THRIFT had radio-iodine refractory disease, which was confirmed radiologically by FDG PET-CT in one case, and histologically in the other. The FLT PET-CT was falsely negative in one case, and of uncertain significance in the other. To our knowledge there are no other studies reporting FLT accumulation in this group of patients. One previous

study has examined FLT uptake in DTC patients at an earlier stage in the treatment pathway; Nakajo *et al* compared FLT PET-CT scanning with FDG PET-CT and I^{131} WBS in 20 patients undergoing follow-up following total thyroidectomy (Nakajo *et al.*, 2013). Thirteen of the 20 patients were found to have histologically-confirmed nodal or distant metastases on FDG PET-CT or I^{131} WBS scanning. The FLT PET-CT scans correctly identified nine of 13 patients with metastatic disease but with a specificity of only 29%, the diagnosis was wrong in nine of the 20 patients, questioning the suitability of this scanning modality in this group of patients.

2.14.2 Comparison of FLT accumulation and Ki-67 score

In the patient with Ki-67 20 – 25%, mild FLT uptake was identified, with SUV_{max} 2.4. No uptake was seen in the patient with Ki-67 score of 5%. The literature is conflicting regarding the relationship between Ki-67 and FLT PET-CT, as discussed earlier in this chapter. This may in part be due to the variation in methods and reporting of Ki-67 score (Chalkidou *et al.*, 2012). The meta-analysis concluded that only Ki-67 maximum measurements from a whole surgical specimen correlate with FLT. Previous studies which reported Ki-67 maximum scores from biopsy samples did not have a significant correlation. However, studies which report average Ki-67 expression independent of the nature of the sample (biopsy or whole specimen) demonstrated good correlation. Ki-67 average expression was reported for all THRIFT specimens. Mild FLT uptake was observed in the patient with the higher Ki-67 over expression (20 - 25%), and none was seen in the patient with low Ki-67 score. Despite only two results from THRIFT, the evidence from the literature suggests that in thyroid tumours with higher Ki-67 average expression scores FLT PET-CT may hold some utility. Although the THRIFT study was seeking to establish utility in the DTC cancer group, for FLT-PET scanning, it may be more appropriate to investigate the utility according to Ki-67 score than tumour type. Larger studies are clearly required to evaluate the role of FLT PET-CT in DTC patients, with a range of Ki-67 scores. Anaplastic thyroid cancers are aggressive undifferentiated tumours which, on the basis of high Ki-67 scores, are likely to have more FLT uptake and would be interesting to image using FLT PET-CT.

2.14.3 Comparison of FLT and FDG PET-CT scanning

One case report describes high FDG and low FLT uptake in a patient with papillary thyroid cancer (Nakajo *et al.*, 2012). Ki-67 was 1.9% in this patient. The investigators concluded the low FLT uptake (SUVmax 3) related to the low proliferative index of the tumour. In contrast, the FDG SUVmax was 19.7 for FDG highlighting the different biological properties reflected by the tracers (Nakajo *et al.*, 2012). A further study by this research group evaluated FDG and FLT PET-CT scanning in the post-operative setting. They reported sensitivity and accuracy of 92% and 90% for FDG PET-CT, which was superior to FLT, with sensitivity and accuracy 69% and 55%, on patient-based analysis (Nakajo *et al.*, 2013).

FDG PET-CT is not performed routinely in our institution to guide radiotherapy planning in thyroid cancer. In some patients the scan has been performed for staging and treatment planning purposes but is not usually acquired in the treatment planning position. In THR001, the avid lesions identified on the FDG PET-CT (Figure 2-21) were used to guide radiotherapy volume definition.

2.14.4 Suitability of FLT PET-CT to guide radiotherapy volume definition

Consistent with low proliferative indices, FLT PET-CT scans acquired in the two patients with recurrent DTC did not have sufficient uptake required to guide RT volume definition, thus the radiotherapy dose planning study was not undertaken.

2.15 THRIFT - Conclusions

The THRIFT study generated insufficient data to draw conclusions from FLT PET-CT scanning in refractory differentiated thyroid cancer. However, in tumours with higher average Ki-67 expression (allowing for intratumour heterogeneity), or anaplastic carcinomas, FLT may have more utility. The scope of this initial study did not allow us to investigate the role of FLT PET-CT in early assessment of radiotherapy response.

A small number of studies have demonstrated that pancreatic cancers are FLT-avid. In the next chapter, one of the first studies to assess FLT PET-CT as an imaging biomarker of early response is presented.

Chapter 3 ^{18}F-FLT PET-CT for assessment of treatment response in exocrine carcinoma of pancreas

3.1 Introduction

The majority of pancreatic cancer patients are inoperable at presentation due to local spread or distant metastatic disease. Median survival is only 6-12 months and chemotherapy response rates are low (Sultana *et al.*, 2007; Gong *et al.*, 2016). Because of the low response rate, early identification of non-responding patients could spare individuals unnecessary toxicity from an ineffective treatment.

The average Ki-67 index of pancreatic cancers is relatively high at 37%, therefore FLT PET-CT imaging may have potential utility (Klein *et al.*, 2002). However, imaging of pancreatic or liver tumours may be obscured by physiological uptake of FLT in the liver and bowel. The two-compartment model assume no local metabolism of FLT other than phosphorylation, however hepatic metabolism of FLT produces FLT-glucuronide, limiting the application of the model (Muzi *et al.*, 2005a). Our collaborators at Imperial College developed a PET scanning protocol and associated mathematical filtering algorithm to assist visualization and quantification of neoplastic tissue. A detailed report of the study can be found in the published manuscript (Challapalli *et al.*, 2015).

Quantification of response to treatment requires a metric, which in the context of FDG PET-CT are standardised uptake values (SUVs). However, SUVs may over-simplify the data, therefore, there is renewed interest in compartmental modelling which uses dynamic imaging and measurement of the blood activity concentration input function over time. One aspect of this research project was the collection of dynamic PET data and the application of a compartmental model. Analysis of Imperial College and Newcastle patient data and PET image data analysis was carried out by the Imperial College team, led by Professor Eric Aboagye. The Newcastle laboratory work described below was undertaken by Dr Phil Berry, Mr Martin Galler and Dr Rachel Pearson. Miss Elizabeth Howell, Dr Pearson and the Imperial College team performed the kinetic filtering and gamma counting which is described.

3.2 Objectives

The primary objective was to explore the ability of FLT PET-CT to detect an early tumour response following one cycle of chemotherapy in locally advanced or metastatic carcinoma of the pancreas. Secondary objectives included investigating if early response to chemotherapy correlated with clinical response using conventional imaging (RECIST criteria) after 3-4 cycles; deriving PET kinetic and voxel-wise parameters for pre-treatment scans and an early follow-up time point; and analysing the metabolism of FLT during the PET scan

3.3 Methods

3.3.1 Patients

The study opened to recruitment on 13 October 2011 at the Newcastle upon Tyne Hospitals NHS Foundation Trust (REC 10/H0707/50; R and D Ref 5626); the project was sponsored by Imperial College Healthcare NHS Trust. Eligibility criteria required a diagnosis of histologically proven carcinoma of the pancreas; locally advanced or metastatic disease; patients who were planned for treatment with gemcitabine-based chemotherapy; and at least one measurable pancreatic lesion with smallest dimeter ≥ 2 cm. After informed written consent patients were scheduled for two dynamically-acquired FLT PET-CT scans; the first scan was performed no more than two weeks before starting treatment, and the second scan no more than 20-days after commencing the first cycle. Routine interval staging by CT chest, abdomen and pelvis was conducted after cycle three of chemotherapy.

3.3.2 Scanning protocol

PET scans were acquired on the same Siemens Biograph 40 TruePoint PET-CT scanner, Campus for Ageing and Vitality, Newcastle University. Each scanning visit lasted approximately two-hours. Patient images were acquired over 66-minutes from injection of FLT (not more than 222 MBq, 7 mSv) and reconstructed as a dynamic series. Venous blood samples were collected prior to FLT injection, and at 2.5, 5, 10, 30 and 60-minutes post injection, for analysis of FLT and metabolite radioactivity. A diagnostic quality CT of the pancreas (120 kV, 300 mA, 1.35 pitch, 0.8 sec/ rotation) was acquired to enable correction of the PET data for photon attenuation in the body and for defining abdominal structures.

3.3.3 Sample analysis

Preliminary work to refine plasma extraction of “cold” and “hot” FLT, and experiments to establish the sensitivity of the HPLC instruments to detect FLT and FLT-glucuronide, using synthetic FLT-glucuronide had been undertaken. Blood samples were transported to the Northern Institute of Cancer Research, Newcastle University. Plasma samples were prepared for high performance liquid chromatography (HPLC) and gamma counting. One millilitre (ml) of whole blood and 1 ml plasma were assayed for levels of radioactivity. One ml of plasma was assayed for parent FLT and the presence of the metabolite FLT-glucuronide (Figure 3-1). Gamma counting of whole blood and plasma was performed in the Department of Nuclear Medicine, Royal Victoria Infirmary, Newcastle upon Tyne (Figure 3-2).

Figure 3-1: FLT metabolism to FLT-glucuronide

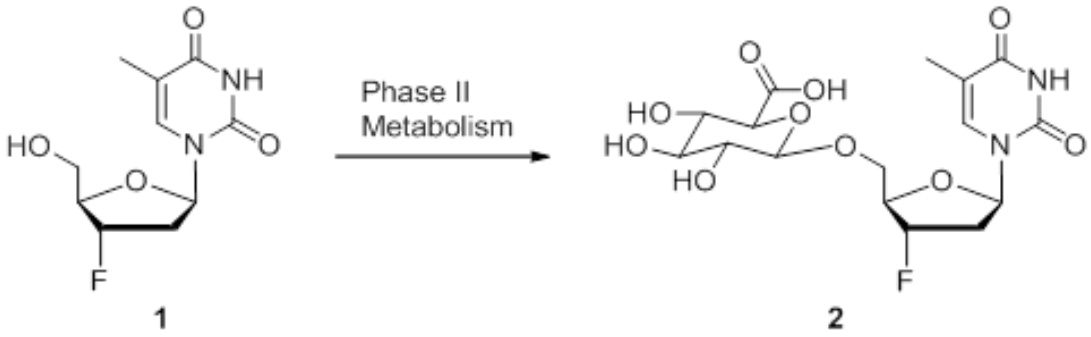

3.3.4 Image Processing

For the filtering of images, time-activity curves were derived from images of tumour regions and normal proliferative tissue regions within the vertebral bone marrow, and included a total activity arterial blood curve. The curves for each voxel were compared with predefined classes and only the voxels identified as tumour-like were saved in the post-filter image. By this process physiological uptake was removed.

Figure 3-2: FLT-Panc flow chart for processing pancreatic images. (CPM = counts per minute)

3.4 Results

3.4.1 Study participants

Six patients were recruited to the study in Newcastle between 13 October 2011 and 20 June 2013 (Table 3-1). Nineteen patients were recruited by the team at Imperial College. A total of 20 patients attended for both the baseline and post-treatment FLT PET-CT scan. Following restaging investigations after three cycles of chemotherapy, 7 / 20 (35%) patients had progressive disease. A summary of results from the work undertaken in Newcastle and main study findings are reported in this chapter. Full details of the study can be found by referring to the manuscript produced by the collaboration (Challapalli *et al.*, 2015).

Table 3-1: Characteristics of FLT-Panc patients recruited in Newcastle

Study ID	Gender	Age (yrs)	Stage	Location of primary	Plasma metabolite detected	FLT PET CT Response	Overall RECIST response	PFS (mths)
1	F	63	Locally Advanced	Head	Yes	No	PD	1.8
2	M	64	Metastatic	Body	No	N/A	PD	5.7
3	F	60	Metastatic	Tail	Yes	No	PD	2.6
4	M	59	Locally Advanced	Head	Yes	No	PD	4.8
5	F	84	Metastatic	Head	Yes	No	SD	12.7
6	M	54	Locally advanced	Head	Yes	Yes	SD	8.3

3.4.2 HPLC and gamma counting analysis

Decreasing gamma counts, reflecting a fall in radioactivity over time in both whole blood and plasma, were observed. Results from the gamma count of one patient's samples are shown in Table 3-1 and Figure 3-3. Mean blood to plasma activity ratio was 0.86 (Table 3-3, n = 3).

Table 3-2: FLT-Panc radioactivity detected by gamma counter in whole blood and plasma from 2.5 to 60-minutes after FLT injection in one patient

		Time (min)	Count	Count per minute (CPM)	At measurement Activity (Bq/ml)	Decay Corrected At point of injection (Bq/ml)
1	**Blood**	2.5	31915	28243	2765	7838
2	**Blood**	5	31269	20547	2011	6138
3	**Blood**	10	31926	16994	1664	5142
4	**Blood**	30	30956	9834	963	3039
5	**Blood**	60	30683	6576	644	2097
6	**Plasma**	2.5	31833	29761	2913	9571
7	**Plasma**	5	31244	21399	2095	6959
8	**Plasma**	10	31172	17227	1686	5679
9	**Plasma**	30	30830	10304	1009	3472
10	**Plasma**	60	30810	7303.3	715	2538

Figure 3-3: FLT-Panc FLT activity in blood and plasma over time in one patient measured by gamma counter at 5 time-points.

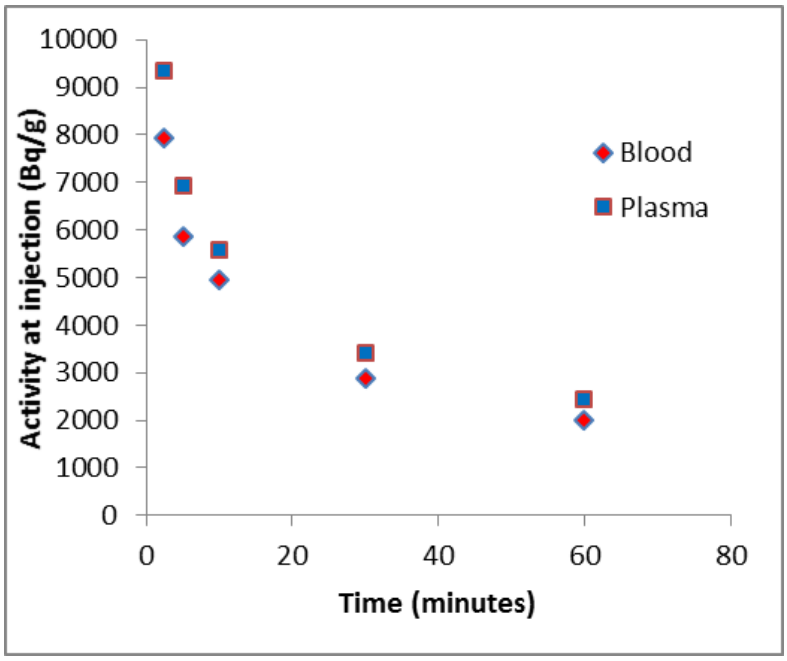

Table 3-3: FLT-Panc gamma counter: comparison of blood to plasma activity

Patient ID	**N001_1**	**N001_2**	**N002_1**	**(Muzi *et al.*, 2005b)**
Blood to plasma activity ratio (mean ± SD)	0.85 ± 0.03	0.87 ± 0.03	0.86 ± 0.04	0.96 ± 0.07

HPLC analysis was more challenging and the threshold for detecting activity and the glucuronide metabolite varied. Alterations were made to the assay to increase the sensitivity of the HPLC; the volume of blood drawn was increased to provide 3 – 4 ml of plasma, the volume used for gamma counting was reduced and the volume injected onto the HPLC column was doubled. Glucuronide was detected as a peak on chromatograms as shown in Figure 3-4, in 5 / 10 of the samples. HPLC at the 10-minute venous blood time-point showed the FLT peak at 1.71 minutes, similar to that obtained at 2.5-minute and 5-minute time-points. The FLT-glucuronide peak eluted at 1.1 minutes, consistent with the synthetic glucuronide peak recorded at 1.1 minutes.

Reasons for not detecting the metabolite were: technical problems with the Posi-Ram radiodetector (n = 2); noise interference on chromatogram around the retention time (n = 1); reason unknown, potentially lack of metabolism, (n = 2).

Figure 3-4: FLT-Panc HPLC trace of FLT and FLT-glucuronide

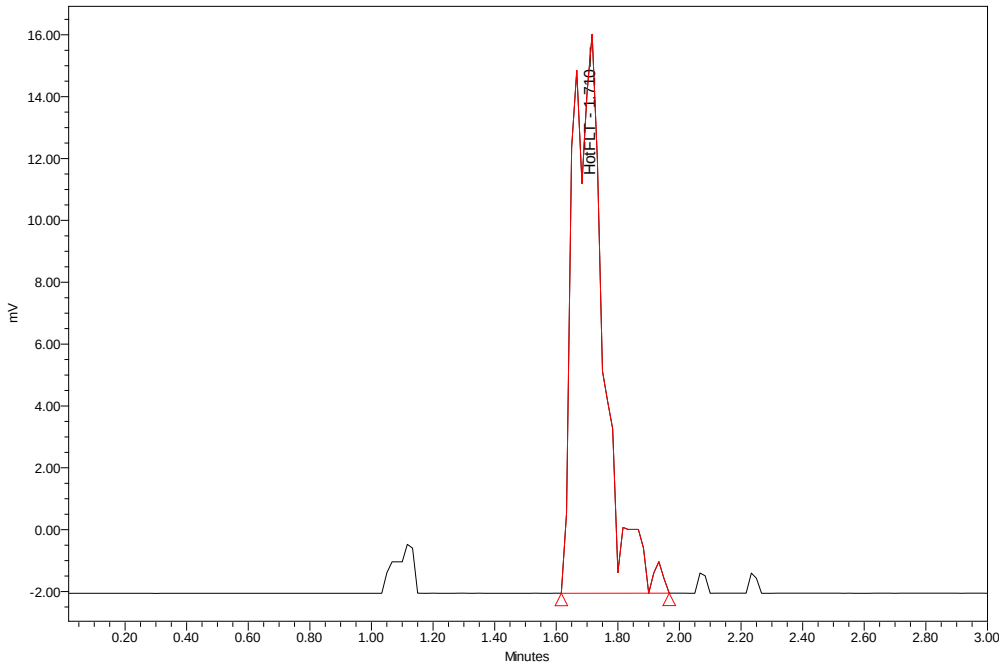

3.4.3 FLT PET-CT scans

Primary and metastatic lesions greater than 2 cm diameter were visualised on the PET-scan after kinetic filtering. Smaller lesions were not identified. Figures 3-5 and 3-6 illustrate examples of a CT and FLT PET-CT scan showing multiple liver metastases and a tumour in the pancreatic tail.

Figure 3-5: FLT-Panc CT image of bulky tumour in the tail of pancreas (denoted by red arrow), and multiple liver metastases.

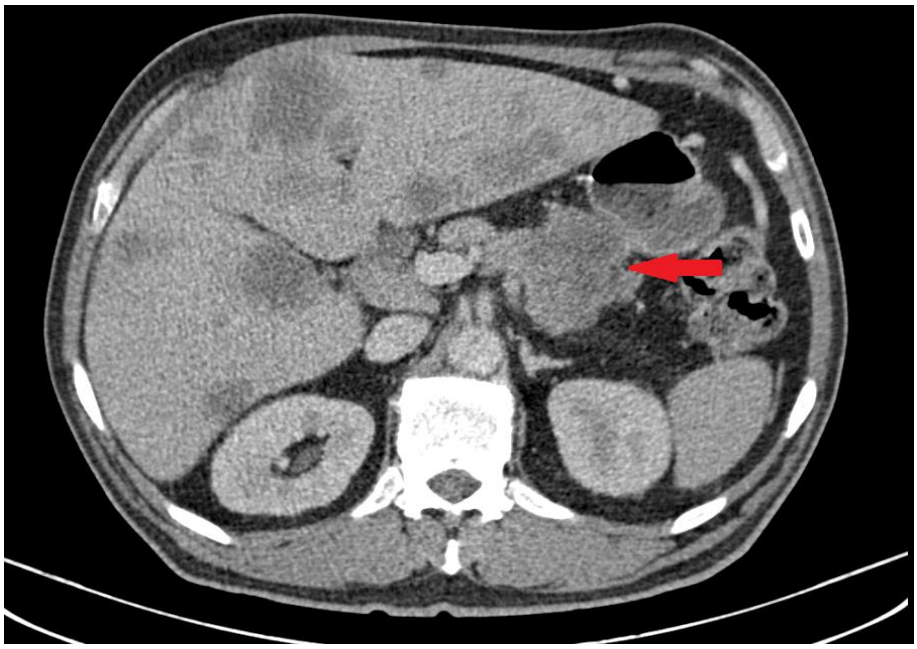

Figure 3-6: FLT-Panc FLT PET-CT scan demonstrating high physiological uptake within liver and vertebral bone marrow, moderate uptake within kidneys and pancreatic tail.

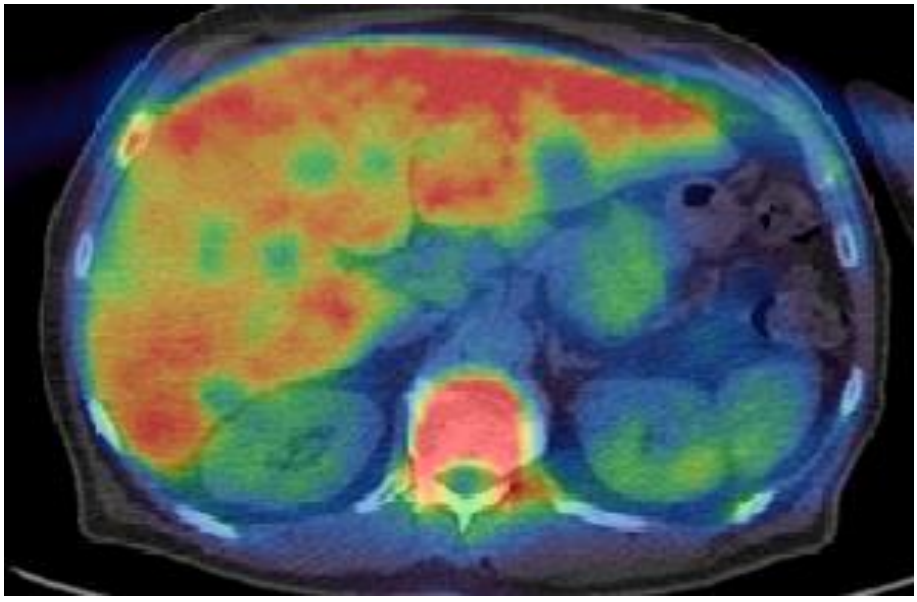

Maximum SUV on the second scan significantly increased in patients with progressive disease (p = 0.04) and an example of this is shown in Figure 3-7 and 3-8. FLT uptake was raised on the second scan in all tissues; however, there was also an increase in the size of the primary tumour on CT. ROC analysis demonstrated that a threshold SUVmax increase of > 12% resulted in sensitivity, specificity and positive

predictive value of 71%, 100% and 100%, respectively, for predicting disease progression, but not survival (p = 0.0001).

Figure 3-7: FLT-Panc pre-chemotherapy FLT scan of a patient with progressive disease. Arrow denotes primary tumour in the tail of the pancreas. SUVmax 1.96

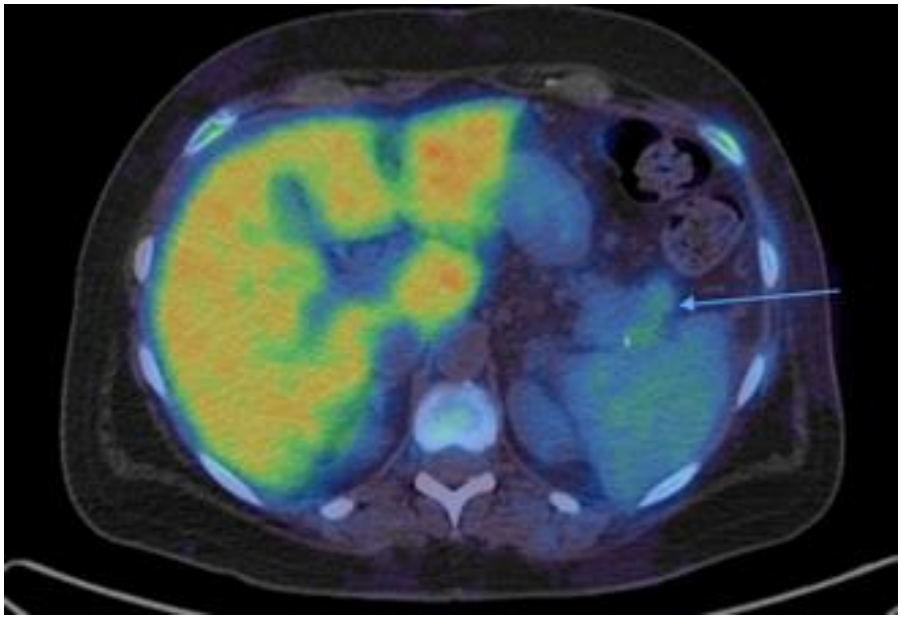

Figure 3-8: FLT-Panc post-chemotherapy FLT PET-CT in a patient with progressive disease. Arrow denotes raised FLT uptake in the pancreatic tail. SUVmax 3.74

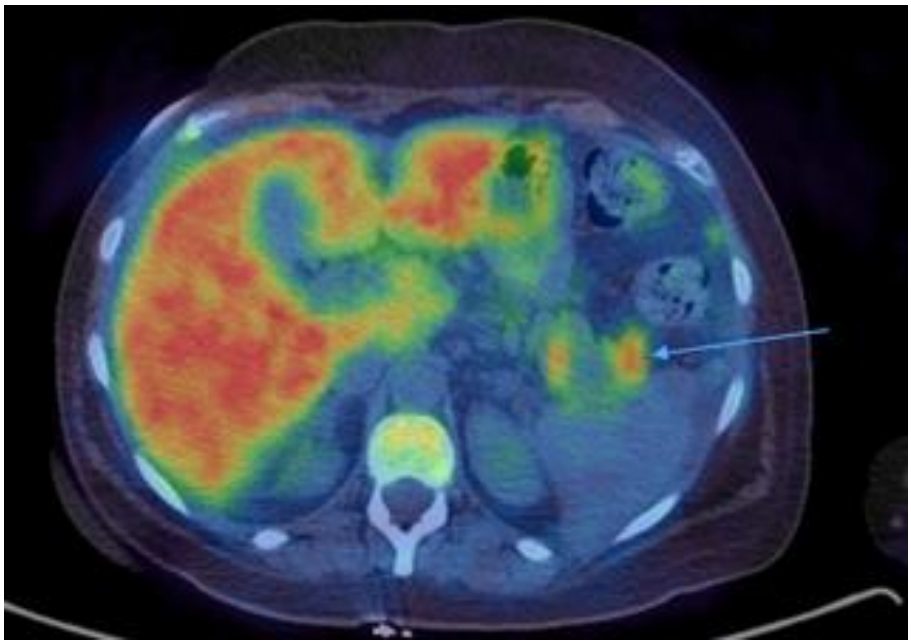

The FLT PET-CT scans of a patient who had radiological stable disease after three cycles of chemotherapy are shown in Figure 3-9 and Figure 3-10. The primary

tumour had poor FLT uptake, but high physiological uptake is seen in surrounding bowel, bone marrow and renal collecting system. After one cycle of chemotherapy, there was no FLT uptake within the visualised bone marrow.

Figure 3-9: FLT-Panc FLT PET-CT scan pre-chemotherapy in a patient with stable disease. Blue arrows indicate poorly FLT-avid tumour in the head of pancreas which is stented, and high physiological uptake in vertebral bone marrow.

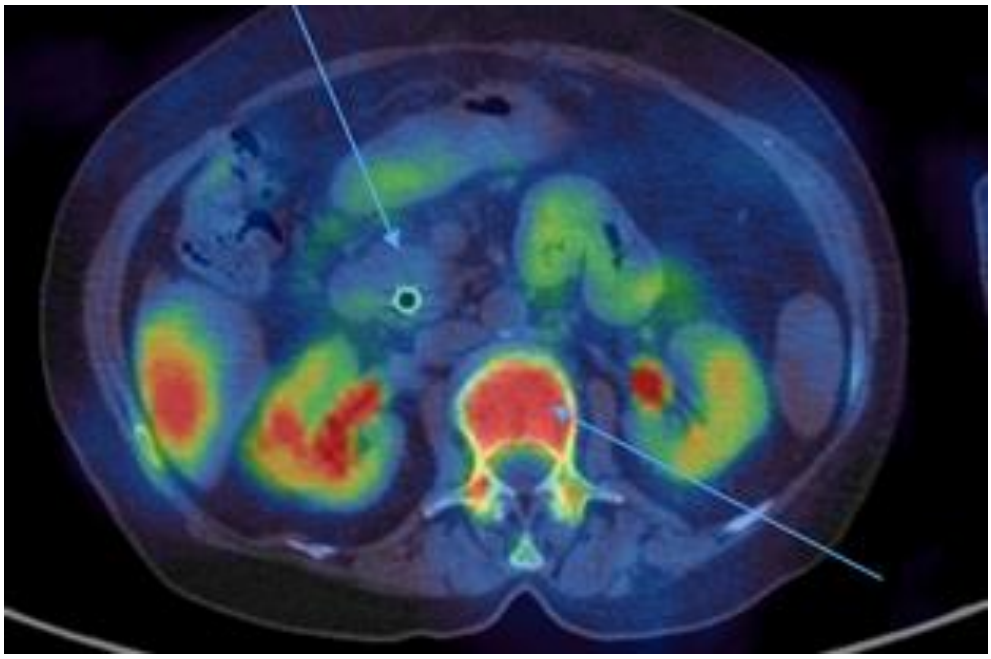

Figure 3-10: FLT-Panc FLT PET-CT scan post chemotherapy in patient with stable disease. Blue arrows indicate tumour within the head of pancreas and vertebral bone marrow with absence of FLT-uptake.

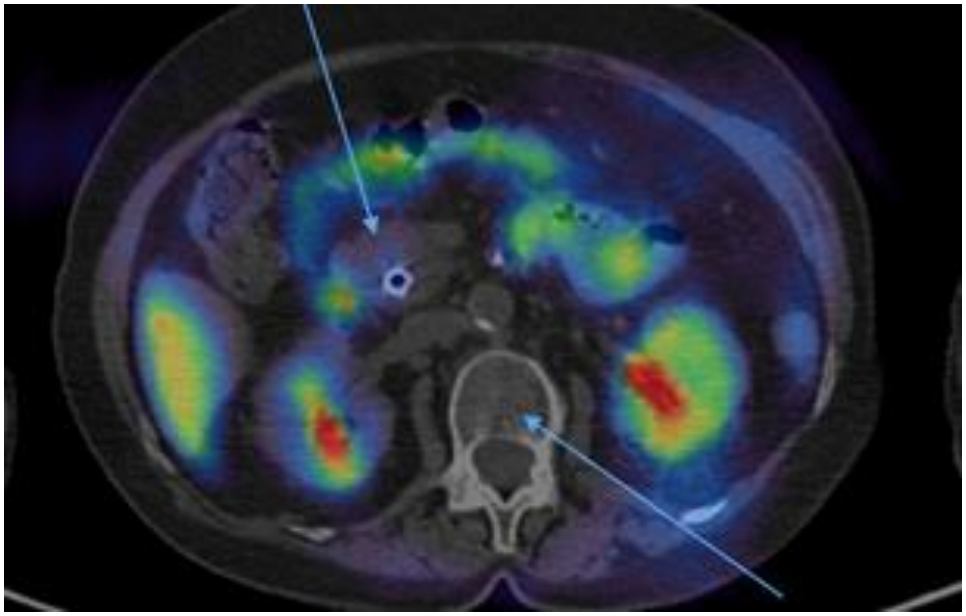

3.5 Discussion

In the context of early response assessment, this is one of the first studies to report on the potential of FLT PET-CT scanning in pancreatic cancer. The scans identified patients who ultimately progressed on treatment, using simplified SUVmax measurements. FLT PET-CT is reported to be superior to FDG PET-CT in distinguishing benign from malignant pancreatic tumours; however, the study was small and a recent review concluded that the role for FLT PET-CT in pancreatic cancer is likely to be in detecting responses to treatment (Lamarca *et al.*, 2016; Vineeth Kumar *et al.*, 2016).

A limitation of FLT PET-CT imaging of advanced pancreatic cancer is the high physiological uptake of the tracer in surrounding tissues. Application of a specifically designed kinetic filter to compensate for uptake due to hepatic glucuronidation of FLT improved visualisation of primary and secondary tumours > 2cm in size.

Following chemotherapy, there was no uptake of FLT within visualised bone marrow in one of the patients. The myelosuppressive effect of chemotherapy is well known; however, the complete absence of proliferation on FLT scan was unexpected. Menda *et al* reported an average reduction in SUV of 12% (range -52% to +16%) in non-irradiated bone marrow of a group of head and neck cancer patients undergoing chemoradiation. Within the irradiated field, the average fall in SUV of bone marrow was 76%. It would be interesting to explore the intra- and inter-variation in peripheral blood counts in study patients to determine if there is an association with the FLT PET-CT imaging metrics after treatment. Leimgruber *et al* studied the effect of two platinum-based chemotherapy regimens on the bone marrow and spleen of 60 non-small lung cancer patients receiving radiotherapy (Leimgruber *et al.*, 2014). The patients received either cisplatin / etoposide on weeks 1 and 5 of the radiotherapy, or weekly cisplatin / paclitaxel chemotherapy. Outside of the radiotherapy field, they found that FLT changes preceded neutrophil count reductions, but did not find a direct correlation between the two. FLT uptake within bone marrow decreased in the cisplatin / etoposide group to 31% on week 2 with recovery at week 4, whereas the cisplatin / paclitaxel group showed a more gradual decline. Interestingly, spleen uptake decreased in both groups on week 2 with a rebound increase at week 4.

It is important to fully understand kinetics and metabolism when developing clinical radiotracers, particularly for quantitative assessments. Dynamic imaging analysis requires a model input function derived from measurement of metabolites. These analysis methods are more complex to undertake and require longer scan times (up to 120-minutes); therefore, several research groups are investigating if simpler methods of analysis are sufficient to quantify FLT uptake. In humans, hepatic glucuronidation of FLT produces metabolites which influence the total radioactivity kinetics. Muzi *et al* reported 25 – 35% underestimation of FLT flux using simplistic modelling, indicating that more complex models are required (Muzi *et al.*, 2005b).

Quantification of FLT-glucuronide in our study proved challenging, with some patient samples yielding no detectable level even at 60-minutes. The fall in FLT radioactivity over time is in keeping with those cited in the published literature (Muzi *et al.*, 2005b; Shields *et al.*, 2005). Furthermore, results for whole blood and plasma were similar, suggesting that whole blood analysis, which is more practical to undertake, may be sufficient. Approximately 30% of FLT was metabolised to the glucuronide, similar to data reported by Shields *et al (Shields et al., 2005).* Further work is needed to establish whether the variation in results obtained in our study correspond to patient status or to limitations in our techniques.

3.6 Conclusions

Results from this study suggest FLT PET-CT could be used as an early response biomarker in the context of advanced pancreatic cancer. Larger studies are required to validate these findings.

A tumour group which has been more frequently studied are head and neck cancer patients. In the next chapter, a single-centre study (FLAIRE) evaluating the feasibility of serial scanning in oropharyngeal cancer patients undergoing chemoradiotherapy is reported.

Chapter 4 FLAIRE: Using 18F-FLT PET CT to assess response on imaging to radiotherapy and guide future dose escalation to resistant areas in the radiotherapy treatment of locally advanced oropharyngeal cancer: a pilot study

4.1 Introduction

4.1.1 18F-FLT as an imaging biomarker in head and neck cancer

Outcomes for locally advanced oropharyngeal cancers are influenced by HPV status. Overall five-year survival of HPV-negative tumours is less than 50%, but for HPV-positive tumours is more than 70% (Huang *et al.*, 2015). Many patients receive primary treatment with chemoradiotherapy which is delivered over six weeks. Currently treatment is assessed by clinical examination upon completion of radiotherapy, and radiologically using FDG PET-CT three months after radiotherapy. In our institution, approximately 10% of patients require surgical salvage following radiotherapy. If an imaging biomarker could predict at an early time-point which patients are less likely to respond to treatment, theoretically there is time to adjust a radiotherapy treatment plan to improve the outcome. The FLAIRE trial has investigated FLT PET-CT as an imaging biomarker in patients with oropharyngeal cancer using serial scans at different stages of the radiotherapy treatment pathway.

For the initial staging of head and neck squamous cell carcinoma (HANSCC), FLT does not perform any better than FDG (Heuveling *et al.*, 2011), (Linecker *et al.*, 2008). One of the reasons for this is that FLT uptake is lower than FDG uptake. However, consistent with other tumour sites, FLT is an appealing tracer to further investigate in the early response setting, due to greater specificity than FDG; for example, false positive results seen on FDG PET CT relating to inflammation or infection of the biopsy site are reportedly not seen on the FLT scans (van Waarde *et al.*, 2004; van Westreenen *et al.*, 2005). Studies have shown that the degree of proliferation in a tumour reduces after radiation but may vary after chemotherapy (Atkinson *et al.*, 2008; Agool *et al.*, 2011). Accelerated repopulation of tumour cells is a mechanism for treatment resistance. Various radiotherapy schedules and the addition of systemic treatments are being investigated to overcome this effect. FLT imaging has the potential to monitor proliferative activity and may identify patients in need of treatment schedule modifications.

Although SUVs are the most commonly used quantitative measure in FLT and FDG PET-CT, there is a lack of consensus on the most robust method of assessing treatment response on PET-CT scans. Progress has been made in FDG PET-CT with the development of the PERCIST criteria, but these are not universally adopted and have not been translated to FLT imaging. Volume of interest (VOI) metrics influence SUVmean (SUVpeak and max to a lesser extent), and therefore quantitative analysis. VOI can be manually drawn or automatically calculated. Merging refers to the inclusion of multiple areas of separate anatomical uptake in a single VOI and limits the usefulness of automatic methods.

4.2 Objectives

The primary objective of the FLAIRE study was to determine the technical feasibility of FLT PET-CT for detecting changes in cell proliferation during radiotherapy. Secondary objectives included evaluating the role of FLT PET-CT as a prognostic biomarker, and as a surrogate early response biomarker using triple-time-point imaging. Following completion of radiotherapy, the utility of FLT PET-CT at detecting residual disease at an earlier time-point (six weeks post RT) than routine FDG PET-CT (12-weeks post RT) was studied.

Methods of measuring SUV using automated and manual VOI to propose a consistent semi-automated technique to calculate SUVmean/peak were investigated; as a result, the contouring tool was proposed to overcome merging and be used as a less operator-dependent, and more reliable and time-efficient assessment of treatment response than manual methods.

4.3 Methods

4.3.1 Patients

The FLAIRE study was granted ethical approval by Newcastle and North Tyneside 1 NRES Committee North East on 9 October 2012 (REC 12/NE/0346); sponsored by Newcastle upon Tyne NHS Foundation Trust (R and D Ref 6096); and adopted onto the UK CRN (Portfolio ID 13992). Eligibility criteria included newly diagnosed oropharyngeal squamous cell carcinomas that were to be treated with radical radiotherapy (RT) or chemoradiotherapy (CRT) as the primary treatment. After informed written consent, eighteen participants were recruited between 4 June 2013 and 3 February 2015. Recruitment to the study was halted for nine months between

May 2014 and February 2015 due to relocation of the PET-CT scanner on the Newcastle University Campus for Ageing and Vitality.

Radiotherapy was planned using a contrast-enhanced CT scan +/- MRI acquired in the radiotherapy planning position. Three-dimensional conformal or intensity-modulated radiotherapy plans were generated, delivering a standard dose of 65-Gy in 30 fractions to the primary tumour and metastatic cervical lymph nodes, and 54-Gy in 30 fractions to at-risk cervical lymph nodes, with an overall treatment time of 41 days. Serial FLT PET CT scans were performed before (FLT1), during (FLT2) and after (FLT3) chemoradiotherapy. No patients were treated with FLT PET-CT guided radiotherapy.

4.3.2 Response Assessment

FLT scans were compared with response assessed clinically six weeks post-treatment, and on conventional CT and FDG PET-CT imaging 12 weeks post-treatment. Treatment response was defined as tumour shrinkage on clinical examination and minimal or absence of FDG uptake on 12-week post RT FDG PET-CT. Non-responders had stable or progressive disease on clinical and radiological assessment.

4.3.3 18F-FLT PET-CT scanning details

18F-Fluorothymidine was obtained from PETNET Solutions, Nottingham. All PET-CT scans were performed on the same Siemens Biograph 40 TruePoint PET-CT scanner. 2.59 MBq / kg (max dose 222 MBq) 18F-FLT was administered by intravenous injection followed by 10 ml saline flush and an uptake period from time of injection of FLT to start of emission scan of 45 – 60-minutes. The uptake periods for follow-up scans were timed to be comparable to the baseline scan. Patients were immobilised supine on a flat couch-top wearing a customized thermoplastic radiotherapy shell. Static acquisition of PET emission images extended from vertex to aortic arch with 6-minutes per bed position (CT for attenuation correction: 45 mAs effective; 3 mm slices; pitch 1.0; 120 kV). Contrast-enhanced CT images of the same region head and neck region using 100 ml of Omnipaque 300 were acquired for anatomic correlation and to guide tumour localisation for radiotherapy planning (120 mAs effective; 3 mm x 274 slices; pitch 1.5; rotation 0.5s; 120 kV). PET images were reconstructed using an iterative process (OSEM) 2 iterations 8 subsets, 168 x

168 matrix; filter Gaussian 5mm; zoom = 1; pixel size = 4.07 mm. Duration of PET-CT and radiotherapy scan was approximately 18-minutes. Total radiation dose per scan was calculated as 12 mSv, and total radiation exposure due to research scans was 36 mSv (Table 4-1). All FLT PET-CT scans were reported by a PET-approved radiologist within three days of the scan. Any unexpected findings were discussed with the Principal Investigator and the Head and Neck Multidisciplinary Team (MDT).

FLT PET-CT scans were performed no more than three weeks prior to starting RT (FLT1), in the second week of RT (FLT2) and six weeks after the end of RT (FLT3).

Table 4-1: FLAIRE radiation dose for study participants from research FLT PET-CT scans

Procedure	No of procedures	Estimated procedure dose (mSv)
Contrast-enhanced CT scan of head and neck	3	3
Attenuation Correction CT of FLT PET-CT	3	2
FLT Injection - 2.59 MBq/kg (max 222 MBq)	3	7
	Total	**36 mSv**

4.3.4 18F-FLT PET-CT analysis

After reconstruction and correction for body weight, injected dose and radiotracer decay, standardized uptake value (SUV) PET images were obtained using the HERMES GOLD^{TM} software (www.hermesmedical.com). Regions of interest (ROI) were placed over tumour foci and SUVs recorded. Data were collected on all primary tumours, the primary or nodal tumours with the highest SUVmax on each scan, and up to four involved lymph nodes in each participant. Tumour SUVmax was defined as the maximum signal intensity within a tumour, SUVmean referred to the mean value within a defined ROI, and SUVpeak was the mean value for a 1cm^3 sphere centred on the voxel of maximum uptake.

FLT responders were defined by a reduction in primary or lymph node tumour SUVmax of ≥ 25 % after one week of treatment, based on reproducibility data in the literature (de Langen *et al.*, 2009). Post-treatment FLT responders had no significant FLT uptake above adjacent background or blood pool, and non-responders had residual uptake.

4.3.5 Developing a consistent PET methodology for quantitative assessment of FLT PET

Volumes of interest (VOI) were defined over tumour foci using 11 SUV selection metrics (nine automated, two manual). The automated methods were based on SUV 3, 4 or 5 above background, and 40 /50 /70 % of SUVmax using a threshold SUV of 3 or 4. VOIs were redefined manually if they merged with neighbouring FLT-avid sites to create individual lymph node volumes. A second manual contour was defined using the contrast CT and FLT-PET-CT scans. Data on tumour volume and SUVmax / mean / peak were collected for the two most avid lesions on each scan. To determine which SUV threshold generated a VOI closely fitting the manually-defined VOI, an iterative process using different SUV thresholds was followed.

4.4 Statistical analysis

Due to the feasibility study design, no formal power calculations were used. The number of patients included in the study was based on the expected number that could be recruited in a timeframe of three years, funds available, and ethical considerations. Statistical analyses were performed using IBM SPSS Version 22.0. Correlation was assessed using Pearson's correlation, and Wilcoxon signed-rank or paired *t*-tests evaluated differences between paired parameters. Mann-Whitney U and Kruskal-Wallis tests evaluated the differences between SUV parameters according to T-stage and HPV status. Overall survival (OS) extended from date of consent into the study until date of death or study closure on 31 July 2016. SigmaPlot 12.5 generated dot histograms and ROC analyses. MedCalc easy-to-use statistical software (https://www.medcalc.org) was used for the diagnostic test evaluations. A two-sided *p*-value of less than 0.05 was considered significant.

4.5 Results

4.5.1 Patient characteristics

Eighteen patients were recruited from two Foundation Trust multidisciplinary team meetings: Newcastle Upon Tyne Hospitals NHS Foundation Trust (13 / 18 patients) and City Hospitals Sunderland NHS Foundation Trust (5 / 18). All patients had histologically or radiologically confirmed oropharyngeal squamous cell cancers. One patient was excluded from further evaluation due to the baseline scan being

performed after one fraction of radiotherapy, therefore 17 patients with oropharyngeal tumours were evaluable and participant characteristics are listed in Table 4-2.

Table 4-2: FLAIRE patient characteristics and events. †MDT consensus-metastatic neck nodes arose from oropharyngeal primary.

	n	%
Gender		
Male	14	82.3
Female	3	17.6
Age (years)	Mean 58.1, Median 59	Range 45 – 74
Tumour Location		
Base of Tongue	9	52.9
Tonsil	7	41.2
Unknown†	1	5.9
T stage		
T1/2	11	64.7
T3/4	6	35.3
N-stage		
N0/N1	2	11.8
N2a/b	8	47
N2c	7	41.2
7th ed TNM stage		
II	1	5.9
III	1	5.9
IVA	15	88.2
HPV status		
Positive	14	82.4
Negative	3	17.6
Primary Treatment		
Chemoradiotherapy (CRT)	16	94.2
Radiotherapy alone	1	5.8
No. of weekly chemotherapy cycles	Median 6	Range 3 – 6
Overall radiotherapy treatment time (days)	Median 41	Range 40 - 41
No. of tumour-related events (n = 4 in 2 patients)		
Primary radiotherapy failure	1	5.9
Loco regional recurrence	0	0
Distant metastases	2	11.8
Tumour-related death	2	11.8
Treatment response		
Responder	16	94.2
Non-responder	1	5.8

Fourteen tumours were HPV-positive, and three were HPV–negative. All but one patient received concurrent weekly cisplatin chemotherapy.

4.5.2 Patient outcomes

Median time between diagnostic biopsy and entry into the study was 3 weeks (range 1 – 7). Study participants were followed up for a median of 31 months (range 16 - 37) from date of entry in the study to study end date of 31 July 2016, or date of death. Twelve study participants required hospital admission for treatment of acute radiotherapy-related toxicities. Eight patients required nasogastric feeding, and six were fitted with a percutaneous endoscopic gastroscopy tube prior to treatment in anticipation of requiring supplementary feeding. The remaining three patients maintained sufficient oral intake during radiotherapy. Mean weight loss between baseline and 6 weeks after RT was 11% (range 3 – 17%) and from baseline to 12 weeks after RT was 13% (range 1 – 20%).

There were 16 treatment responders (Figure 4-1) and one non-responder, who was HPV-negative (Figure 4-2) on the 3 month post RT FDG PET-CT scan. Two patients have died of distant metastatic disease. In one case, although the oropharyngeal tumour and neck nodes responded clinically and radiologically, the FDG PET-CT scan revealed bone metastases. As the patient was not staged with a PET-CT scan prior to treatment it is unclear if these metastases were new. This patient was diagnosed with liver metastases six months later, and died 12-months after diagnosing the bone metastases. The other patient who died did not respond to radiotherapy, therefore proceeded to salvage surgery after the post treatment FDG PET-CT scan. More than 24-weeks had elapsed from diagnosis to an effective treatment. The patient developed metastatic disease in paraspinal tissues and bones after 18-months, and died five months later. For the entire cohort, overall 1-year survival was 100%, and 2-year survival 88%.

Figure 4-1: FLAIRE FDG PET-CT scan pre- (left panel) and post- (right panel) RT in a treatment responder. FDG-avid right tonsillar mass and right level II lymph nodes on left panel pre-treatment. No FDG-avid uptake on FDG-PET CT 12 weeks after treatment (right panel).

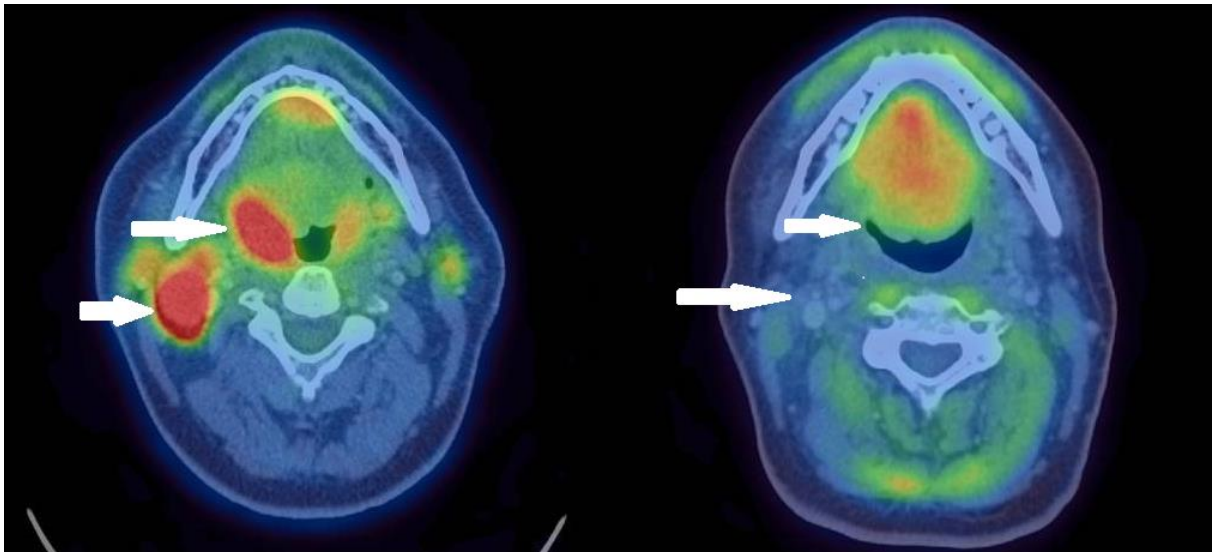

Figure 4-2: FLAIRE FDG PET-CT post RT in non-responding primary tumour. No pre-RT FDG PET-CT was available for comparison. Marked FDG uptake (SUVmax 11.5) can be observed at the site of the bulky right sided tongue tumour which crosses the midline. No significant FDG uptake was identified within the neck; however, a 14 x 10mm right level 2 LN had reduced in size compared with radiotherapy planning MRI

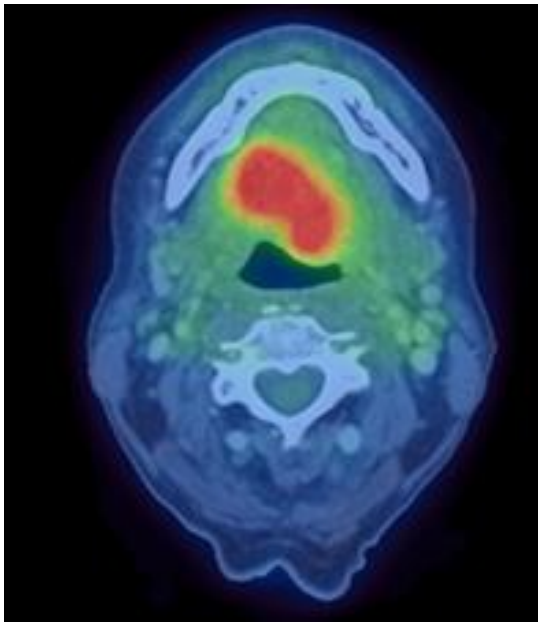

Figure 4-3: FLAIRE Kaplan-Meier plot of overall survival from consent into study until study closure or date of death.

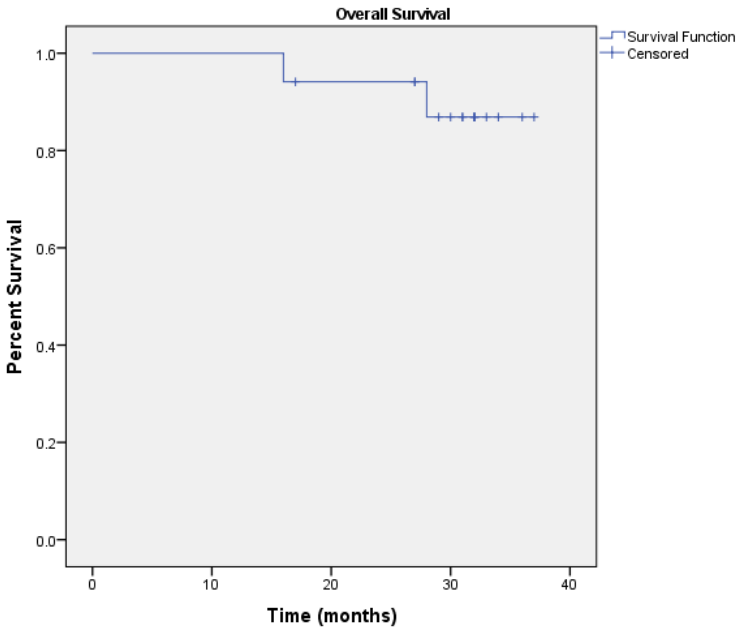

4.5.3 Baseline 18F-FLT PET-CT SUV parameters

18F-FLT PET-CT scans were acquired a median of 14 days (range 4 – 21) prior to commencing radiotherapy treatment. In fourteen patients (82%), there was raised FLT uptake within both the primary and lymph node regions, consistent with findings on CT and MRI. In seven (50%) of these patients, the primary tumour SUVmax was of greater magnitude than the SUVmax of the lymph nodes. The remaining three patients had either neck-only or neck-negative disease. The highest SUVmax results for each participant from the baseline scan are displayed in Table 4-3. A trend was observed between higher T-stage and higher SUVmax, but this was not significant (Figure 4-4). The outlier with T4 disease in Figure 4-4 with a low SUVmax of 5.5 had the primary in-situ but bilateral neck dissections had been undertaken. There was a negative correlation between SUVmax of the primary tumour and the SUVmax of the most avid lymph node group (Pearson correlation -0.57, $p = 0.03$, $n = 14$) displayed in Figure 4-5. In the three patients who attended for the pre-treatment FDG and FLT PET-CT scans, the uptake of FDG was higher than the uptake of FLT within tumour tissues (Table 4-4).

Table 4-3: FLAIRE highest FLT SUVmax in primary and lymph node groups recorded across the study cohort.

SUVmax	Median	Range	n
Highest SUVmax lesion (primary or nodal metastatic deposit)	8.1 ± 1.4	5.6 – 10.3	17
SUVmax of primary tumour	6.7 ± 1.9	4.6 – 10.3	16
Second highest SUVmax lesion	6.2 ± 1.5	3.4 – 8.7	15
SUVmax of most FLT-avid lymph node group	7 ± 2	2.4 – 9.7	15

Figure 4-4: FLAIRE summary statistic of FLT SUVmax of primary tumour according to size of tumour: T1 (n = 3), T2 (n = 7), T3 (n= 1), T4 (n =5).

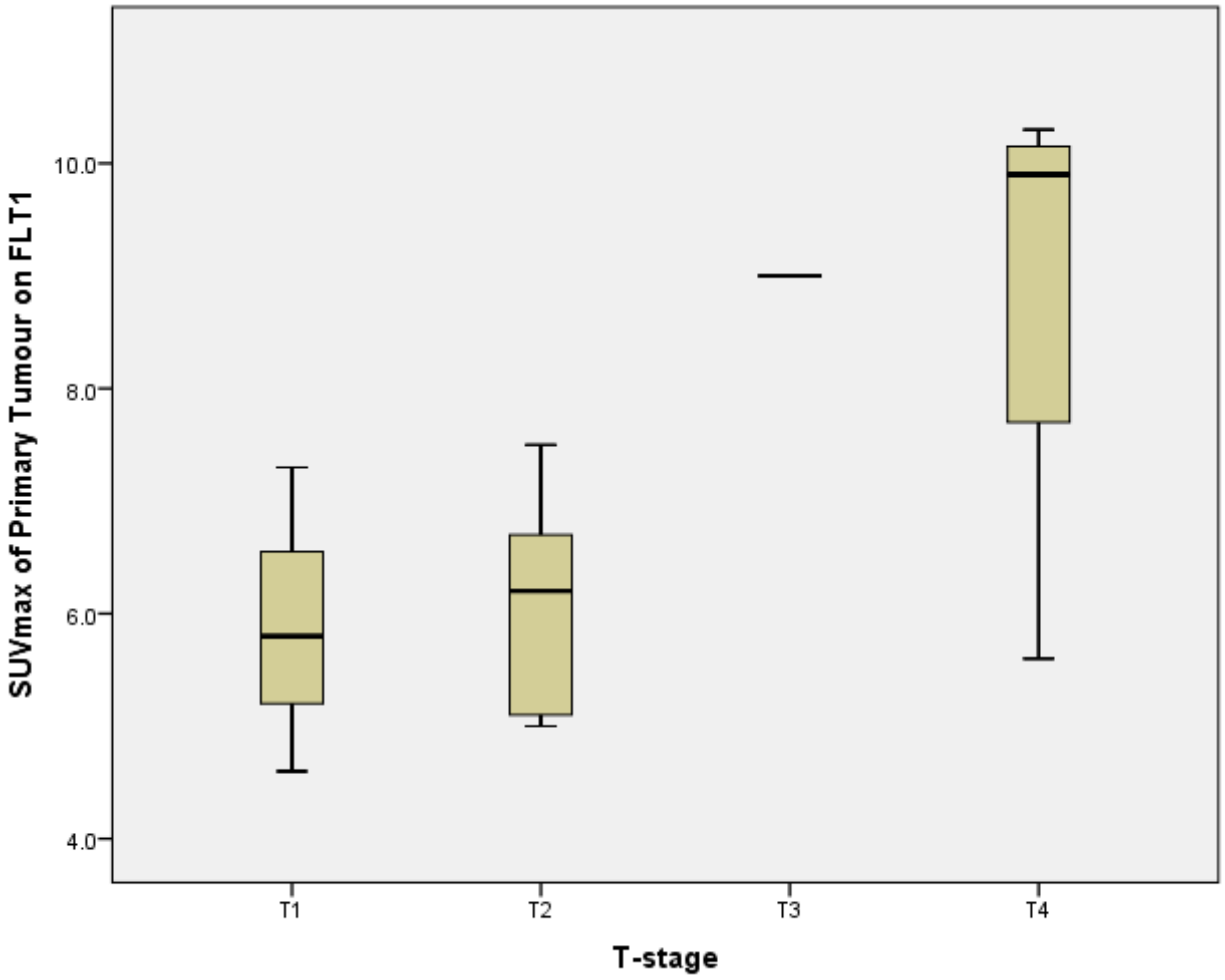

Table 4-4: FLAIRE comparison of baseline FLT and FDG SUVmax of primary and nodal tumours:

Study ID	Primary		Lymph node	
	FLT SUVmax	FDG SUVmax	FLT SUVmax	FDG SUVmax
3	-	-	9.7	15.7
5	5.8	10.1	8.6	20.1
6	6.6	14.9	8.6	18.7

Figure 4-5: FLAIRE negative correlation observed between the SUVmax of the primary tumour and the SUVmax of the most avid lymph node group on the baseline FLT scan (Pearson correlation r = -0.57, p = 0.03, n = 14).

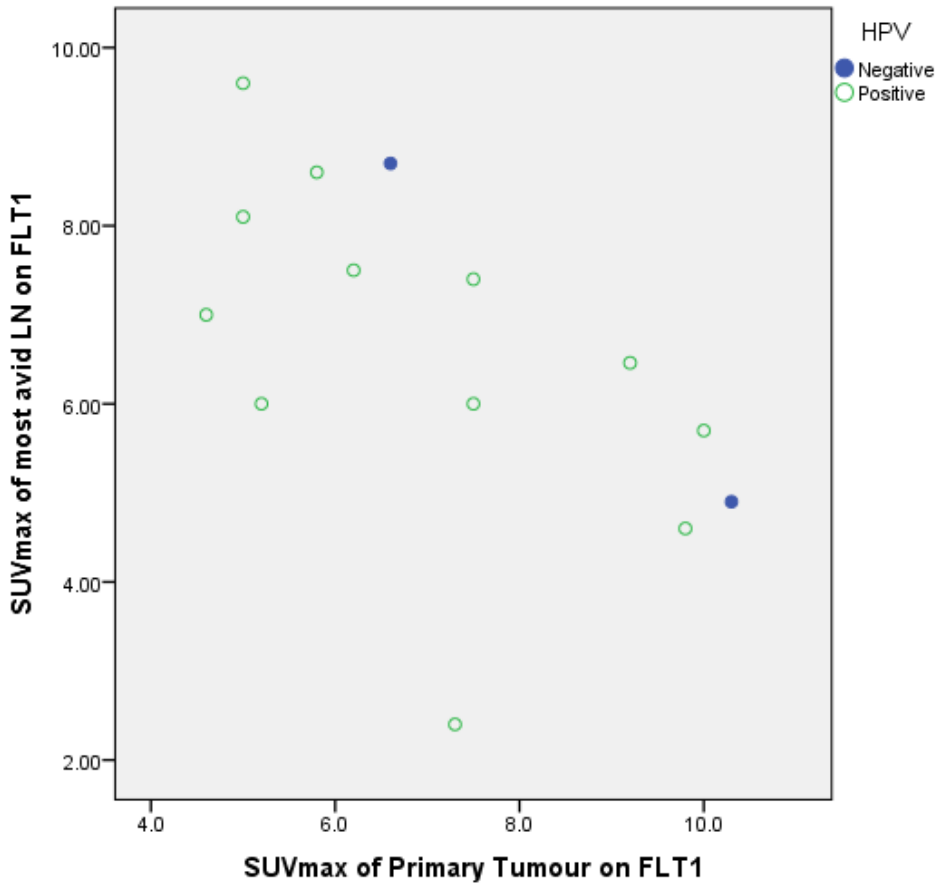

The three HPV-negative cases had primary tumour baseline SUVmax values of 6.8, 8.7 and 10.3. Two patients developed distant metastases and died within the study period. Using ROC analysis the pre-treatment FLT PET SUVmax of the most avid lesion gave a cut-off value of 9.9 for development of metastases (p = 0.02, sensitivity and specificity of 100%, Figure 4-6, Figure 4-7). The small number of events occurring precluded further analysis exploring a relationship between pre-treatment SUV parameters and outcome.

Figure 4-6: FLAIRE dot histogram of pre-treatment FLT-PET SUVmax of most avid lesion in patients who are disease-free (black dots) and those who have developed metastases (white dots).

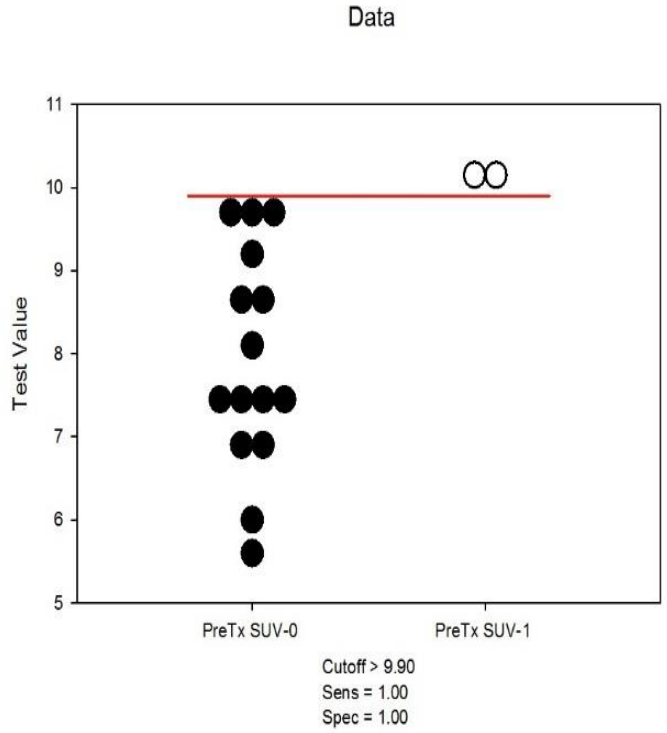

Figure 4-7: FLAIRE ROC curve indicating a cut-off of 9.9 gives sensitivity and specificity of 100%, (p = 0.02, area under ROC curve = 1).

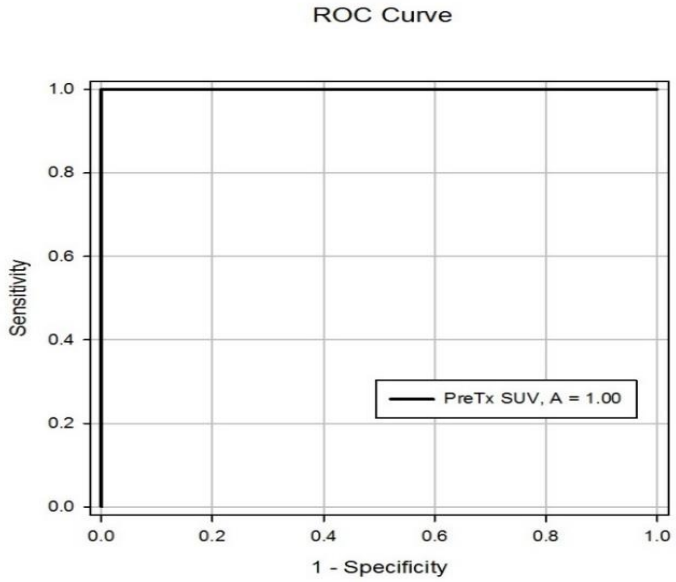

4.5.4 Early response assessment using 18F-FLT PET-CT

All participants were scheduled for the second FLT PET-CT scan during the second week of radiotherapy, after a median 15.2-Gy (range 10.8 – 52-Gy; median 7 fractions; range 5 – 24, n = 17). Reasons for the second scan occurring later than planned were as follows: FLT production failure (n = 1); and patient unable to attend for scan (n = 2). Median uptake time of 18F-FLT was 49 minutes for all scans; median difference between uptake times for the first and second FLT PET-CT scans was 0 minutes (range 0 - 5).

Figure 4-8 illustrates a visual decrease in FLT uptake within a right tonsillar tumour on the second FLT PET-CT scan. A significant decrease in SUVmax was observed in all tumours between the baseline and second FLT scan ($p < 0.001$) in Figures 4-9 and 4-10. Changes in the SUVmax of primary and nodal lesions between FLT1 and FLT2 are displayed in Table 4-5. Differences in the magnitude of SUVmax changes were observed; in some patients there was a greater change within the primary tumour, whilst in others the greater change was observed in a nodal deposit (Table 4-6 and Figure 4-10). There was noticeable intra- and inter-subject variation. Results for the primary tumour and most FLT-avid tumour on the baseline scan are presented. Considering only the patients who were scanned during the second week of radiotherapy (i.e. who had received ≤ 19.5-Gy; 5 – 9 fractions of radiotherapy; n = 14), and only the single most FLT-avid lesion on the baseline scan were studied, there was a median fall in SUVmax of 49.5% (range 13 – 70).

Figure 4-8: FLAIRE FLT PET-CT scans acquired before (left panel) and during (right panel) radiotherapy. 61-year-old female with T1N1 right tonsillar carcinoma. On the pre-treatment scan, primary tumour SUVmax 5.8, decreased to SUVmax 1.9 after six fractions of RT.

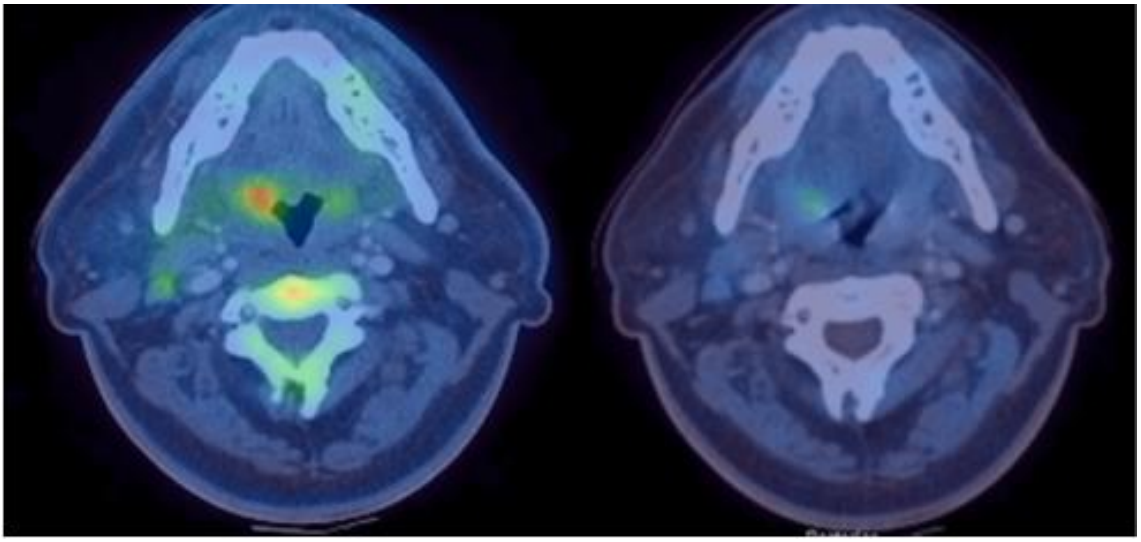

Figure 4-9: FLAIRE boxplot of median SUVmax of the primary tumour between baseline (SUVmax 7.3 on Scan FLT 1) PET and after a median of 7 fractions (SUVmax 4 on Scan FLT 2, n = 13, p = 0.001).

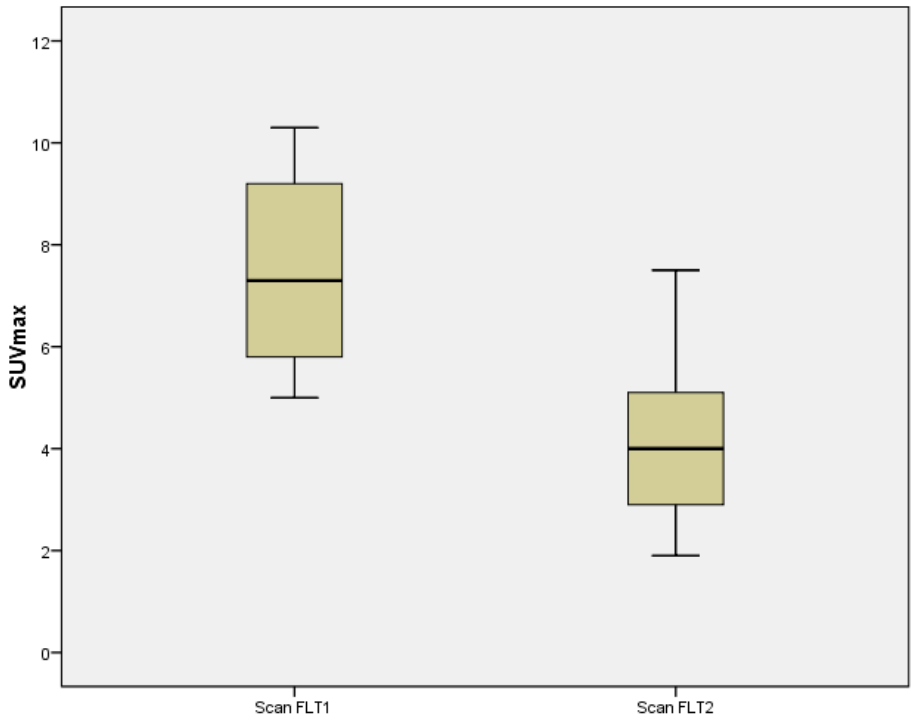

Table 4-5: FLAIRE SUVmax changes in primary and lymph node regions before and during RT (FLT1 and FLT2 respectively) after a median of 7 fractions of radiotherapy.

SUVmax parameter on FLT1 and FLT2	Median	Range	n
Most FLT-avid lesion on FLT1	8.3 ± 1.4	5.6 – 10.3	14
Most FLT-avid lesion from FLT1 on FLT2	4.1 ± 1.8	2.6 – 8.2	14
Percent change in SUVmax of most FLT-avid lesion on FLT1	50 ± 18 %	13 – 70 %	14
SUVmax of primary tumour on FLT1	7.3 ± 1.9	5 – 10.3	13
SUVmax of primary tumour on FLT2	4 ± 1.8	1.9 – 8	13
Percent change in SUVmax of primary tumour between FLT1 and FLT2	51 ± 17 %	13 – 67 %	13
Percent change in SUVmax of most avid LN group on FLT1	49 ± 17 %	15 – 77 %	12
Greatest percent change in SUVmax of primary or most avid LN group on FLT1	59 ± 10 %	49 – 79 %	14
Least percent change in SUVmax in a LN region	43 ± 19 %	15 – 73 %	12

Figure 4-10: FLAIRE SUVmax of primary tumour during treatment decreased in all patients. Dashes indicate the treatment non-responder.

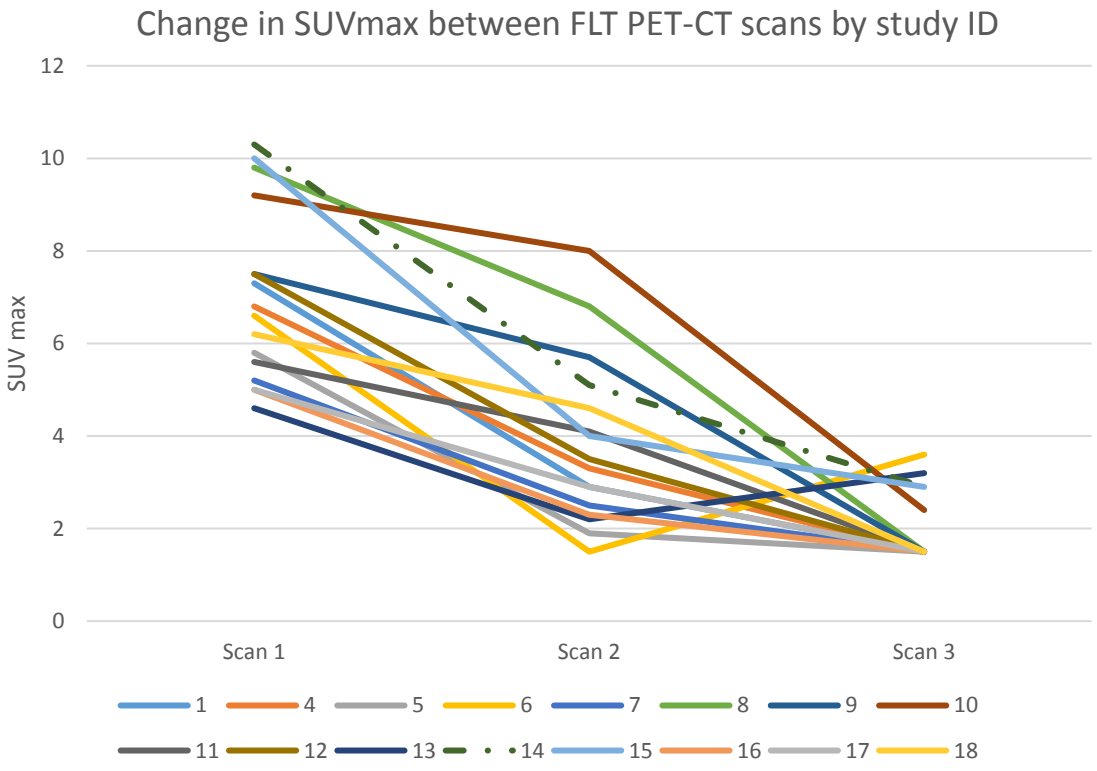

Moreover, despite a generally linear relationship between the SUVmax of the primary on the first and second FLT scans, there was no clear relationship between percentage change in SUVmax in these tumours or of the most avid FLT tumours, and the baseline SUVmax value (Figure 4-11 and Figure 4-12)

Table 4-6: FLAIRE baseline and on-treatment characteristics of primary and nodal lesions performed during week 2 of RT (n = 14)

Study ID	Lesion 1			Lesion 2			Primary	
	Site	FLT1 SUV_{max}	% change FLT2	Site	FLT1 SUV_{max}	% change FLT2	FLT1 SUVmax	% change FLT2
1	Primary	7.3	60	Level II Ipsi	2.4	38	7.3	60
3	Level III Ipsi	9.7	49	Level II Ipsi	8.7	59	-	-
4	Primary	6.8	51	-	-	-	6.8	52
5	Level II Ipsi	8.6	70	Level II Ipsi	7.1	79	5.8	67
8	Primary	9.8	31	Level III Contra	4.6	46	9.8	31
9	Primary	7.5	24	Level II Ipsi	7.4	49	7.5	24
10	Primary	9.2	13	Level II Contra	6.5	77	9.2	13
11	Primary	5.6	27	-	-	-	5.6	27
12	Primary	7.5	53	Level II Ipsi	6.0	73	7.5	53
14	Primary	10.3	50	Level II Contra	4.9	57	10.3	51
15	Primary	10.0	60	Level III Ipsi	5.7	68	10.0	60
16	Level II Ipsi	9.6	15	Level III Ipsi	6.2	23	5.0	54
17	Level III Ipsi	8.1	48	Primary	5.0	42	5.0	42
18	Level II Ipsi	7.5	50	Primary	6.2	26	6.2	26

Figure 4-11: FLAIRE scatter plot illustrating no clear relationship between change in SUVmax and baseline SUVmax.

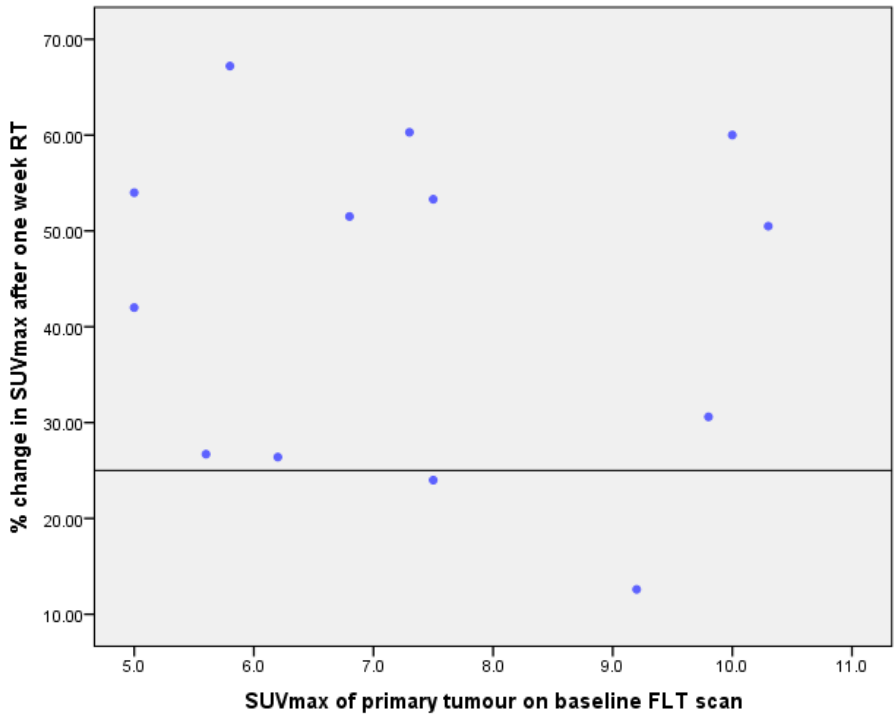

Figure 4-11 illustrates the percentage changes in primary tumour SUVmax after one week of RT, with reference line at 25%. Patients 9 and 10 lie below the line. In four patients, the percentage decrease in SUVmax was less than 25% in either the primary tumour, or most avid metastatic nodal disease. These patients would be classed as PET non-responders and further details are listed in Table 4-7. All of these patients were treatment responders on the 3-month post RT FDG PET-CT scan.

In the one treatment non-responder, there was a 50% fall in FLT SUVmax of both the primary and most FLT-avid nodal disease, similar to the cohort median value of 51% and 49%, respectively. However, in one group of lymph nodes in this patient, the percentage fall in SUVmax was 23% on the second FLT scan.

Table 4-7: FLAIRE characteristics of FLT PET-CT non-responders, defined by a decrease in SUVmax of less than 25% in one lesion.

Study ID	**9**	**10**	**13**	**14**	**16**
Stage	IVA (T2N2b)	IVA (T4N2b)	IVA (T1N2c)	IVA (T4N2c)	IVA (T2N2b)
HPV status	+	+	+	-	+
Treatment response	R	R	R	R	R
No. of weekly cycles chemotherapy	6	6	5	4	3
Primary tumour SUVmax	7.5	9.2	4.6	10.3	5
Highest SUVmax (site) on FLT1	7.5 (Primary)	9.2 (Primary)	7 (Level II ipsilateral LN)	10.3 (Primary)	9.6 (Level II ipsilateral LN)
Most avid LN SUVmax	7.4	6.5	7	4.9	9.6
No. of fractions of RT delivered at time of FLT2	7	7	13	8	6
% change in SUVmax of primary	24%	13%	53%	50%	54%
% change in SUVmax of most avid LN	49%	77%	43%	57%	15%
Smallest % change in SUVmax	16%	13%	20%	23%	15%

Figure 4-12: FLAIRE plot demonstrating lack of relationship between highest SUVmax at baseline and percentage change in SUVmax after one week of CRT (n = 13), and RT (n = 1), according to anatomical site (primary n = 9, lymph nodes n = 5).

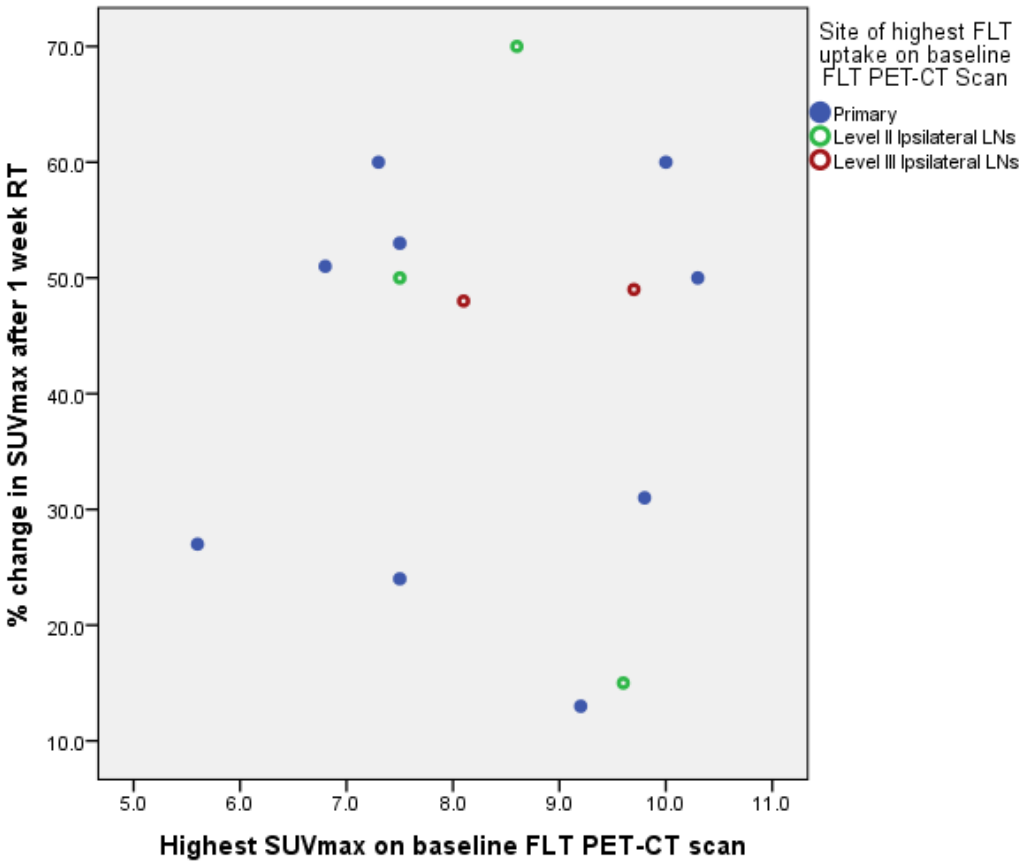

To investigate how the timing of the FLT PET-CT scan after a specific number of radiotherapy fractions affected the percent change in SUVmax, Figure 4-13 demonstrates there was no clear relationship in this cohort.

Considering an SUVmax assessment of the primary tumour where < 25% change determined non-response, sensitivity was 0% and specificity 83%, with a negative predictive value of 91% (Table 4-8). There were two false-positive results, and one false-negative result.

Figure 4-13: Percentage change in SUVmax of most avid FLT region according to number of fractions of RT delivered (n = 16, red marker indicates treatment non responder).

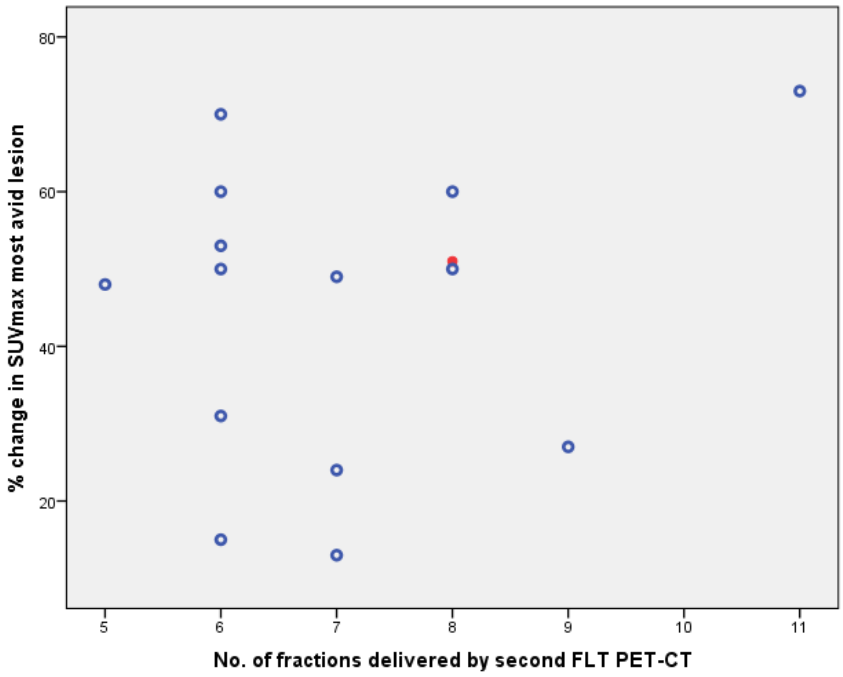

Table 4-8: FLAIRE diagnostic test evaluation of change in SUVmax of primary tumour on FLT2 (n = 13), and SUVmax of the most FLT-avid lesion (n = 14)

Statistic	Primary	Most Avid
Sensitivity	0%	0%
Specificity	83%	77%
Positive Likelihood Ratio	0	0
Negative Likelihood Ratio	1.2	1.3
Disease Prevalence	8%	7%
Positive Predictive Value	0%	0%
Negative Predictive Value	91 %	91%

4.5.5 Delayed response assessment using 18F-FLT PET-CT

Fourteen patients attended for FLT3. Reasons for three scans not being obtained were: patient declined (n = 2); and PET-scanning facilities not available (n = 1). To evaluate the role of FLT PET-CT at detecting residual disease post radiotherapy, the post-treatment scans were acquired a median of 6 weeks (range 6 – 8) following

completion of RT; a median of 11 weeks (range 8 – 13, n = 14) after the second FLT PET-CT scan; and a median of 5 weeks (range 4 – 8) before the post-treatment FDG PET-CT. Median difference in uptake times between the first and third FLT PET-CT scans was 1.5 minutes (range 0 – 7).

In 5 / 14 cases there was evidence of residual FLT uptake within areas of previous known disease (Table 4-10). Correlation with the CT images identified lymph nodes which were either decreasing in size, or appeared reactive, suggesting treatment response. In the patient who was classed as a non-responder due to uptake on FDG PET-CT, FLT uptake within the primary was low with SUVmax 2.9. In all patients with FLT uptake, the intensity had decreased serially on each scan. FLT3 scans identified four false-positive and no false-negative results (Table 4-9).

Table 4-9: FLAIRE diagnostic test evaluation of FLT3

Statistic	Value
Sensitivity	100%
Specificity	69%
Positive Likelihood Ratio	3.2
Negative Likelihood Ratio	0
Disease Prevalence	7%
Positive Predictive Value	20%
Negative Predictive Value	100%

Table 4-10: FLAIRE details of patients with FLT uptake within the oropharynx and/or neck on post treatment FLT PET-CT scan

Pt ID	Pre-treatment FLT	During RT FLT	Post RT FLT	Post RT FDG	Outcome
6 **T2N2b** **HPV+**	Primary SUV_{max} 6.6, 24 x 12mm Level II LN SUV_{max} 8.6, 25 x 20mm	Primary No uptake 14 x 18mm Level II SUV_{max} 2.1, 12 x 12mm	Primary SUV_{max} 3.5, 10 x 15mm Level II SUV_{max} 5.3, 12 x 13mm Mild widespread FLT uptake within pharynx, SUV_{max} 3.5	No focal FDG-avid disease 9mm level II, not FLT-avid	Examination at time of post RT FLT scan showed response to treatment. Widespread mucositis. USS R neck LN post FDG scan showed response to treatment. No evidence recurrence after 30 months follow-up
10 **T4N2b** **HPV+**	Primary SUV_{max} 9.2, 48 x 38mm R level II LN SUV_{max} 6.5, 15 x 7mm R level III SUV_{max} 4.1, 12 x 8mm	Primary SUV_{max} 8, 42 x 41mm LN no FLT uptake R level II 11 x 4mm R level III 12 x 6mm	Primary SUV_{max} 2.4, 12 x 12mm R level III/IV SUV_{max} 3.8, 10 x 5mm Multiple small LN SUV_{max} <2.5	No focal FDG uptake	Examination at time of post RT showed oedema of epiglottis and arytenoids but no residual disease. No evidence recurrence after 28 months follow-up.
13 **T1N2c** **HPV+**	Primary SUV_{max} 4.6, 16 x 13mm L level II SUV_{max}7, 18 x 15mm	Primary SUV_{max} 2.2, 16 x 12mm L level II SUV_{max} 5.6, 12 x 12mm	Primary SUV_{max} 3.2, 13 x 12mm L level III necrotic, SUV_{max} 2.5, 11 x 8mm R level III SUV_{max} 5.2, 10 x 7mm R level IV SUV_{max} 4.2, 9 x 5mm	Mild FDG uptake within site of primary, no CT abnormality, suggestive of post RT changes	Examination at time of post RT FLT and FDG scan showed oedema but no residual disease. No evidence recurrence after 26 months follow-up.
14 T4N2c **HPV-**	Primary SUV_{max} 10.3, 44 x 37mm L level II SUV_{max} 4.9, 18 x 14mm R level II SUV_{max} 4.4, 24 x 22mm L level III SUV_{max} 3.9, 12 x 9mm	Primary SUV_{max} 5.1, 48 x 36 L level II SUV_{max} 2.1, 16 x 15mm R level II SUV_{max} 2, 21 x 23mm L level III SUV_{max} 2.8, 8 x 12mm	Primary SUV_{max} 2.9, 30 x 39mm L level II No uptake, 7 x 7mm R level II necrotic, no FLT uptake, 13 x 16mm R level 1b SUV_{max} 2.1, 7 x 4mm (likely reactive)	Marked FDG uptake in primary No FDG-avid LNs R level II necrotic, smaller	Examination at time of post RT showed oedema. FDG PET-CT delayed 3 weeks due to perforated bowel. Examination after FDG PET-CT showed residual disease. Proceeded to salvage surgery, upT3, 45mm primary, ypN0 neck LNs left 20/20, right 21/21 No evidence recurrence disease after 26 months follow-up
15 **T4N2b** **HPV+**	Primary SUV_{max} 10, 42x45mm L level III SUV_{max} 5.7, 22 x 25mm L level II SUV_{max} 3.9, 20 x 24mm	Primary SUV_{max} 4, 37 x 25mm L level III SUV_{max} 1.9, 23 x 19mm L level II SUV_{max} II 16 x 19mm	Primary SUV_{max} 2.9, 10 x 10mm R level II SUV_{max} 3.7, 10 x 8mm L level II No uptake, 16 x 14mm Multiple small bilateral LNs SUV_{max} < 2.5	Primary not FDG-avid, not visible on CT Mild FDG uptake bilateral neck nodes L level II 10 x 15mm New focal FDG uptake R pubic bone SUV_{max} 9.5, T4 SUV_{max} 3, faint uptake in small pulmonary nodules	Examination at time of FLT and FDG scans no residual disease Multiple bone, lung, liver metastases 5 months after FDG PET-CT Died secondary to metastatic disease 12 months after FDG PET-CT, 18 months after diagnosis

4.5.6 Semi-automated contouring of FLT PET-CT avid regions

Twenty-nine primary and nodal lesions were selected for contouring using an automated thresholding technique or manual delineation. The automated contouring methods resulted in merging of adjacent involved lymph node groups generating a composite SUV value which represented the group rather than the individual lymph nodes (Figure 4-14). To facilitate the calculation of changes in SUV parameters within each lymph node, 38% (11 / 29) of these lesions required manual contouring. In a comparison of the nine automated techniques a threshold of 40% SUVmax using SUV threshold 4 returned the least usable data (16/36 invalid); this compared with SUV 3, 70% of SUVmax using SUV threshold 4 and 3.5 where 7/36 results were invalid. Data were considered invalid if no measurement could be recorded by the HERMES software. Consistent with previous SUVmax results, the SUVmean and SUVpeak of lesions decreased on treatment. Furthermore, the volume of these lesions with a known FLT concentration also decreased (Table 4-11 and Figure 4-15). The number of lesions detected by the automated methods decreased on the second FLT PET-CT scan due to reduced concentration of the FLT-tracer, hindering quantitative assessment of both the SUV change and volume. A mean automated threshold of 63% using SUV threshold 4 most accurately defined the lesions which were manually contoured (Table 4-12). The author acknowledges the contribution from Mr Dominic Kite in the automated contouring of lymph nodes to generate SUV values.

Figure 4-14: FLAIRE 3-D reconstructions demonstrating 'merging': manual VOIs for a chain of adjacent lymph nodes with uptake (left panel); an automated VOI encompassing the entire same area (right panel)

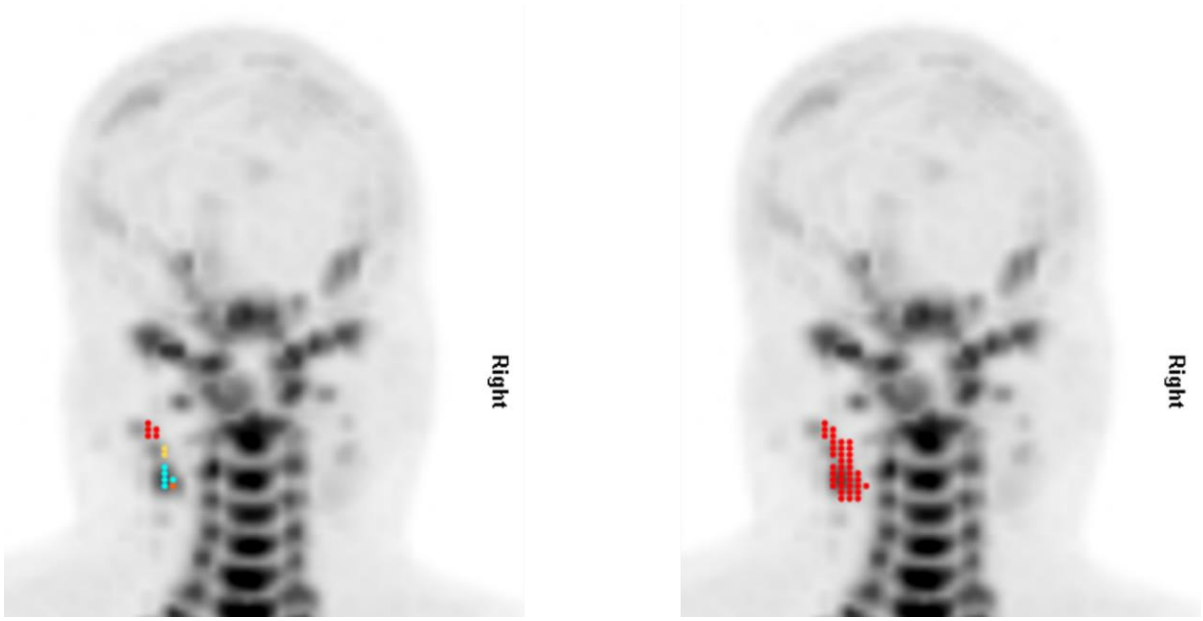

Table 4-11: FLAIRE comparison of SUV max / mean / peak on FLT PET-CT scans of 29 primary and nodal regions before (Scan 1) and during (Scan 2) treatment. (ROI = region of interest within primary or nodal disease).

	No. of ROIs	Mean ± SD	Range
Scan 1 SUVmean	129	5.8 ± 1.1	3.4 - 8.1
Scan 1 SUVmax	145	8.2 ± 1.5	5.6 - 10.3
Scan 1 SUVpeak	112	7.5 ± 1.5	4.8 - 9.5
Scan 1 volume (cm^3)	129	8.6 ± 9.3	0.2 - 49
Scan 2 SUVmean	76	4.2 ± 1.1	2.3 - 6.7
Scan 2 SUVmax	88	5.6 ± 1.6	3.1 - 8.2
Scan 2 SUVpeak	64	5.3 ± 1.4	3.3 - 7.2
Scan 2 volume (cm^3)	76	5.4 ± 5.9	0.1 - 27

Figure 4-15: FLAIRE box plots demonstrating a decrease in SUV mean / max / peak between the baseline and second scan in 29 primary and nodal regions.

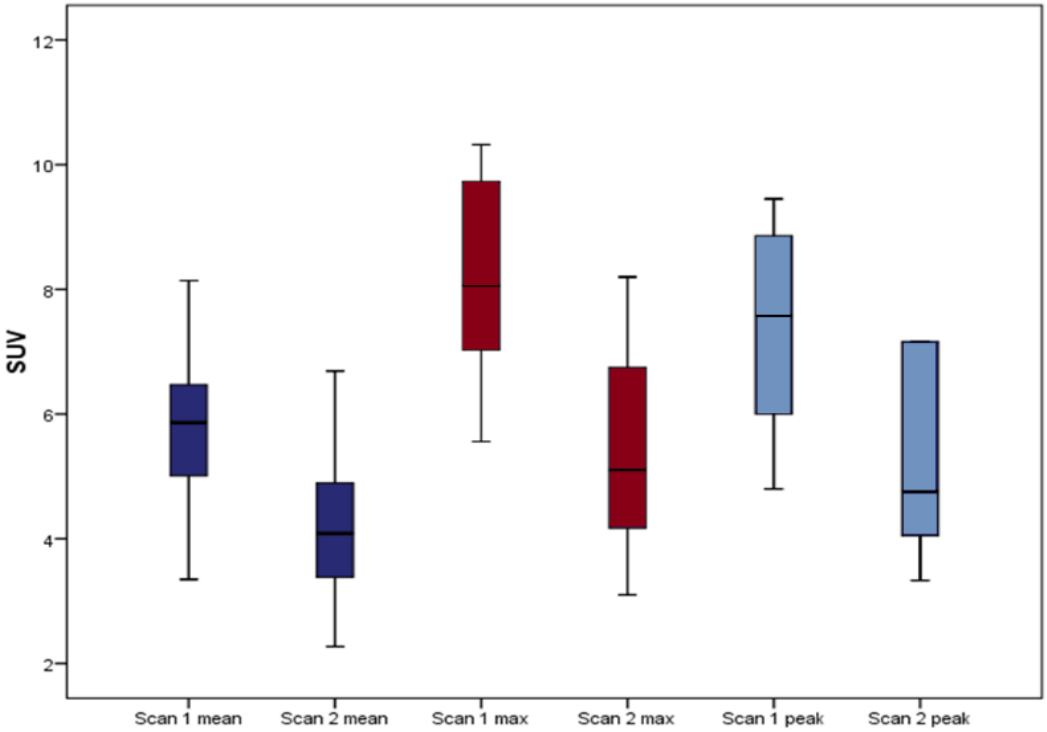

Table 4-12: Comparison of manual and semi-automated VOIs

Study ID	SUVmax	SUVmean		Volume (cm3)		Threshold SUVmax (%)
		Manual	Automated	Manual	Automated	
1_1	7.3	5.5	6.1	1.3	0.8	67
3_1	9.7	6.6	7.7	2.4	1.5	64
7_1	6	4	4.9	1.5	0.6	67
12_1	7.8	5.9	6	11.6	11.3	67
13_1	7	6	6	0.6	0.6	70
13_2	5.6	4.9	4.7	0.2	0.4	70
15_1	19	6.8	6.9	17.4	16.6	53
16_1	9.6	6.9	6.9	2.7	2.8	55
16_2	8.2	6.3	6	1.6	2.2	60
17_1	8.1	6.2	6.2	1.4	1.5	60
mean	8.8	5.9	6.1	4.1	3.8	63.3

4.5.7 Additional FLT PET-CT Findings

Several interesting additional findings are detailed below.

Bone Marrow Proliferative Changes

In all patients, absence of proliferating bone marrow clearly identified the radiotherapy field on the scan performed during RT (FLT2). Figure 4-16 illustrates an example of this.

Figure 4-16: FLAIRE pre-treatment FLT PET-CT image of 51-year-old male with TxN2b oropharyngeal cancer (left panel) and FLT PET-CT acquired in same patient after 7 fractions of radiotherapy demonstrating absence of FLT uptake in the bone marrow within the radiotherapy field (right panel).

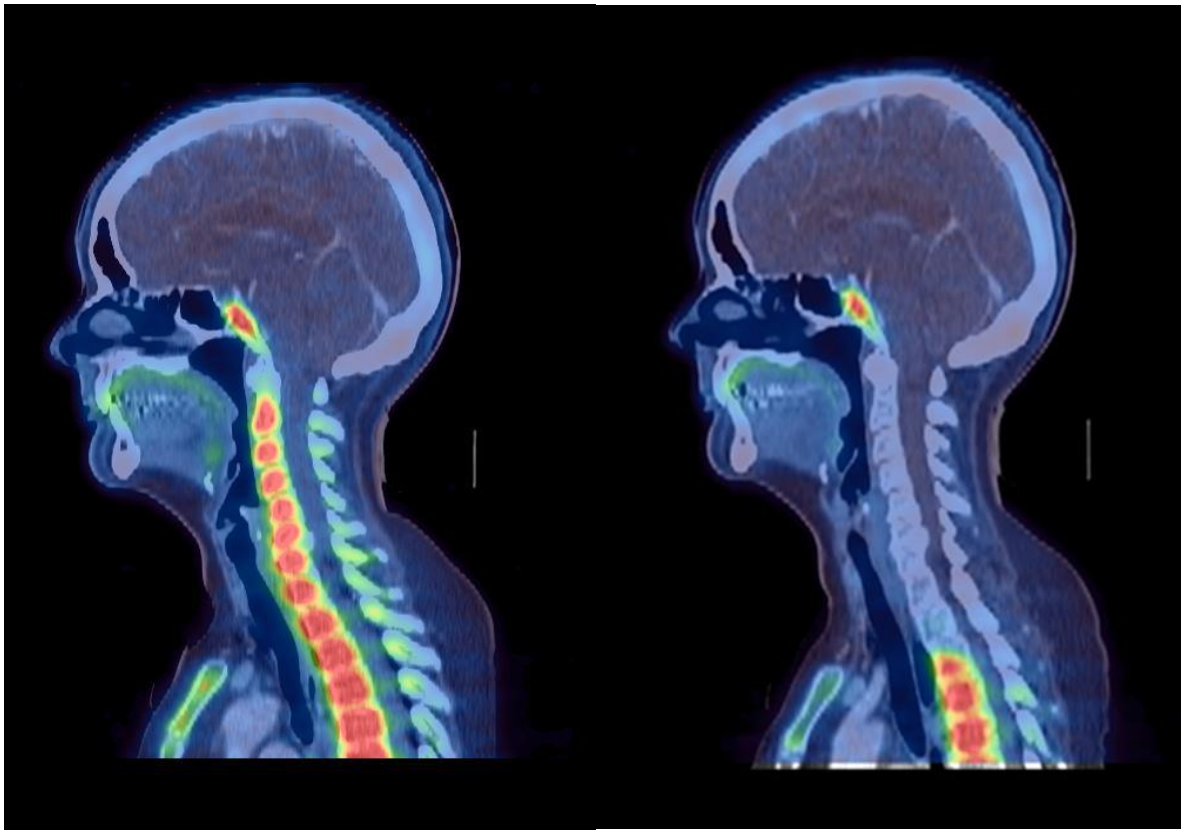

Dental uptake

Baseline FLT PET-CT scan demonstrated raised FLT-uptake on the both sides of the neck in one patient who had been staged by conventional imaging with unilateral neck disease. Therefore, the patient was investigated further with FDG PET-CT and this showed unilateral neck disease (Figure 4-17).

Additional questioning revealed a history of multiple dental extractions 5-days prior to the FLT scan. The FLT uptake within left-sided neck nodes was deemed to be reactive, because there was no FDG uptake on the FDG PET-CT. In a further patient, staged as T2 N0 right oropharyngeal cancer, the FLT PET-CT scan demonstrated increased avidity in group of small lymph nodes posterior to right mandible and increased uptake left maxilla, out of keeping with the anticipated spread of the original cancer. This patient also had a history of tooth extraction.

Figure 4-17: FLAIRE 53-year-old man with T1N2b squamous cell carcinoma of right base of tongue. FLT PET-CT scan (left panel) showed FLT avidity in bilateral level II lymph nodes (SUVmax 8.3 right level II, 7.1 left level II) and staging FDG PET-CT scan (right panel) acquired after a 6-day interval, showed an extremely avid 3 cm right level II neck node (SUVmax 20.1) and marked FDG uptake at the right tonsil (SUVmax 10.1).

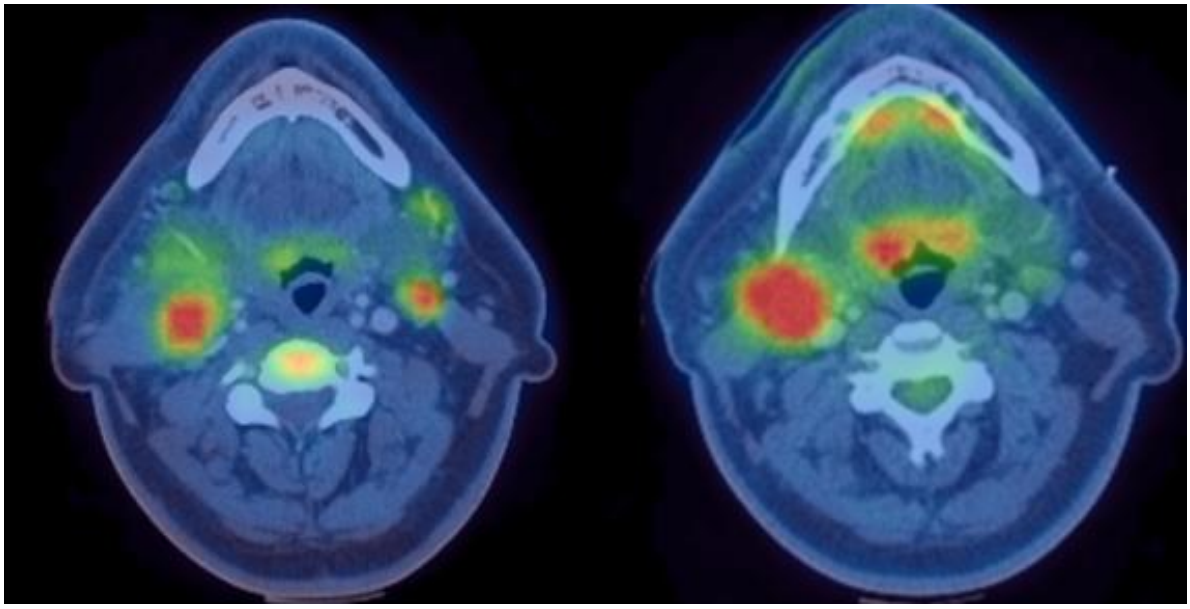

Active Shingles Infection

In one study participant with T2 N2b right tonsil HPV-negative cancer (Figure 4-18), a cluster of lymph nodes with increased FLT uptake were seen in the left axilla and pre-pectoral region (SUVmax 3.1). The lymph nodes were borderline by size criteria (maximum 24 x 10 mm dimension) and suspicious by position. An FDG PET-CT to evaluate these lymph nodes further was performed 6-days later and demonstrated FDG-negative axillary lymph nodes (Figure 4-19). On the day of the FDG PET-CT scan the patient reported a resolving painful erythematous pruritic rash on the back. The rash was consistent with *varicella zoster* infection and had developed in the T10

dermatome 8-days prior to the baseline FLT scan. The lymph nodes were not FLT-avid on the second FLT scan which was performed later than planned in the fourth week of RT. The fatty hilum of these lymph nodes on CT implied a benign nature and the consensus was that the axillary and pre-pectoral lymph nodes were most likely to be reactive from the shingles infection, and non-metastatic.

Figure 4-18: FLAIRE FLT PET-CT scans of T2 N2b primary tumour in the right tonsil and level II lymph nodes

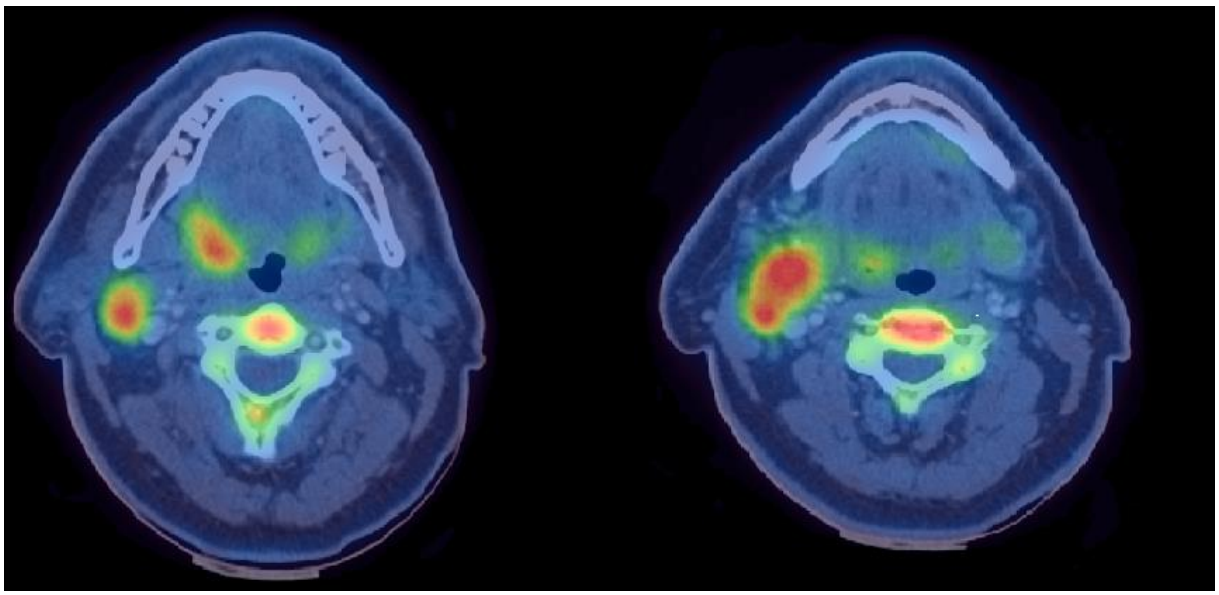

Figure 4-19: FLAIRE Left axillary LN, FLT-avid pre-treatment (top panel, red arrow denotes axillary LN) and not FDG-avid on pre-treatment FDG PET-CT (lower panel)

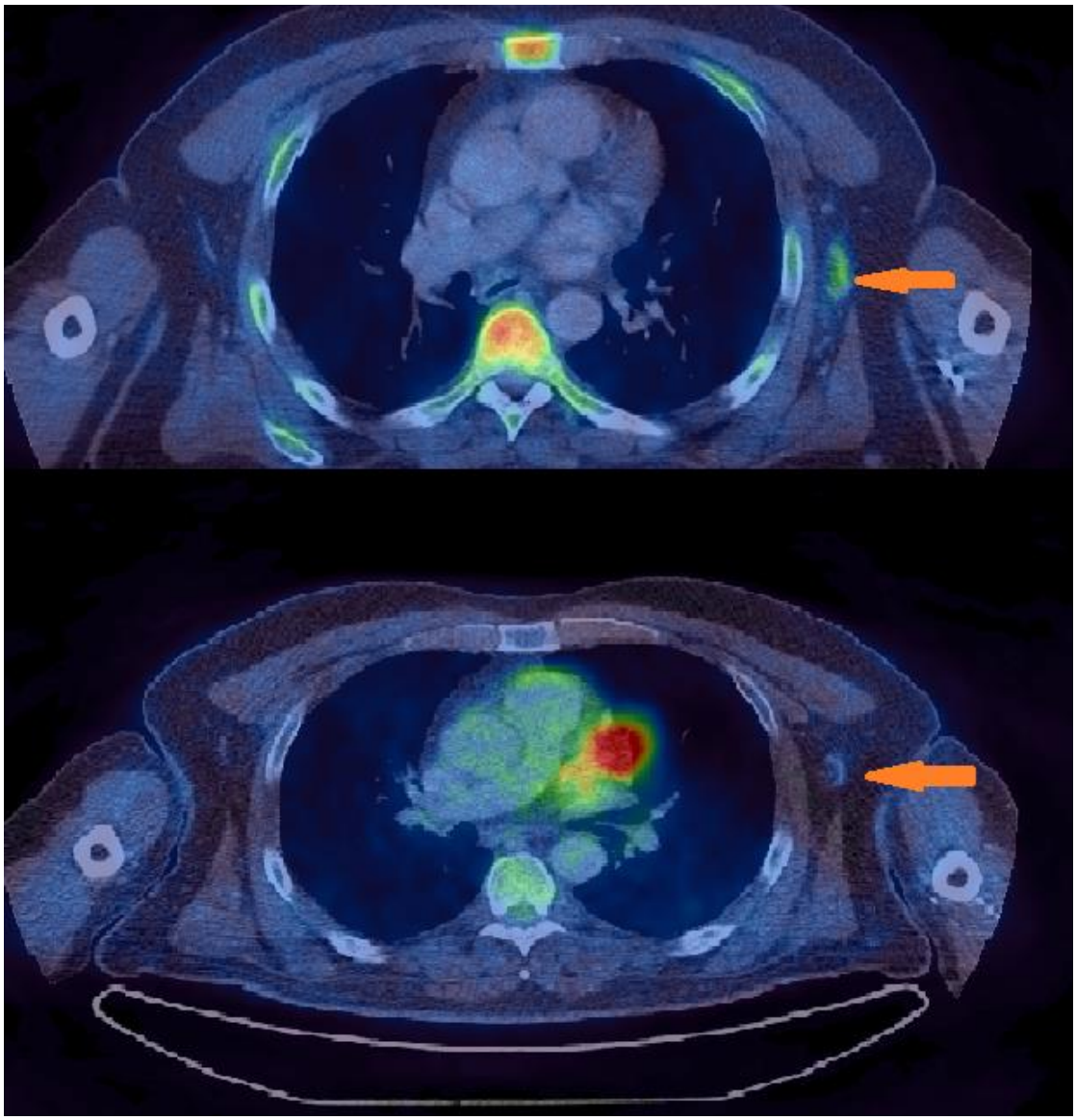

4.6 Discussion

One of the key objectives of the FLAIRE study was to assess if serial PET scans involving a novel research tracer could be undertaken in patients undergoing radical chemoradiotherapy treatment. The study was logistically challenged by the location of the PET-CT scanner on a different site to the radiotherapy machines; FLT is a research PET tracer and was only produced one or two days a week, 160-miles away; a high number of different professional disciplines were required for each scan; in addition to the general recruitment hurdles that all clinical trials face. Few patients who were approached turned down the study. Patients tolerated the scans

well and were interested in the results. All oropharyngeal tumours were FLT-avid. FLT uptake was lower than FDG in the three patients who had similar timed FDG PET-CT scans, consistent with the literature (Troost *et al.*, 2009; Hoshikawa *et al.*, 2012) (Troost *et al.*, 2009; Hoshikawa *et al.*, 2012).

4.6.1 Early response assessment using 18F-FLT PET-CT

In all primary and involved lymph node regions, there was a fall in the SUVmax value after one week of chemoradiotherapy. This finding is in accordance with reports from the literature suggesting proliferation changes in response to radiotherapy or chemotherapy can be quantified at an early stage using FLT PET-CT, not only in head and neck cancer (HANSCC), but in other tumour sites including breast, lymphoma, sarcoma, lung, pancreatic and oesophageal carcinomas. (Troost *et al.*, 2010; Yue *et al.*, 2010; Herrmann *et al.*, 2011b; Benz *et al.*, 2012; Contractor *et al.*, 2012; Kishino *et al.*, 2012; Hoeben *et al.*, 2013; Inubushi *et al.*, 2013; Sanghera *et al.*, 2014; Challapalli *et al.*, 2015). The median magnitude of the fall in SUVmax after one week of radiotherapy was 49% and 51% in SUVmax of the lymph nodes and primary, respectively, in FLAIRE patients. This pattern was reported by Troost *et al* who were one of the first research groups to study oropharyngeal cancer patients (Troost *et al.*, 2010). In the initial phase of their study involving ten patients, mean pre-treatment FLT SUVmax values of 4.7 decreased to 2 after one week of radiotherapy. A similar study of 48 head and neck cancer patients who were imaged during the second week of radiotherapy reported a median fall in SUVmax of 45%, which is supported by the FLAIRE study findings (Hoeben *et al.*, 2013). In head and neck radiotherapy another study demonstrated a greater than two-fold reduction in SUV after 1 week, and more than four-fold reduction after 4 weeks of treatment (de Langen *et al.*, 2009). The quantification of the decrease is not always straightforward as there can be increased uptake in tonsillar tissue due to proliferation of inflammatory cells. The tumour subvolumes with highest proliferative activity may also change in size and shape.

The patient who did not respond to radiotherapy exhibited a change in SUVmax of the primary tumour of greater than the median value, therefore is not defined as a non-responder according to the 25% response criterion. However, the absolute value of SUVmax may be more important than the relative change in predicting eventual responses to treatment, in addition to tumour characteristics; this patient had T4 disease, was HPV-negative, and a baseline SUVmax of 10.3. Therefore, this patient

had poor prognosis disease. Conversely, the tumour may have initially responded well to the radiotherapy and subsequently developed radioresistance. Potentially this could be overcome by a boost radiotherapy dose to the primary tumour. More detailed understanding of the proliferation changes on FLT PET-CT imaging during chemoradiotherapy and the development of radioresistance will influence the timing of strategies to overcome this.

The specificity of the second FLT PET-CT was 83%, and negative predictive value was 91%, but the sensitivity and positive predictive value were 0%. This is consistent with findings by Kishino *et al* who recorded negative predictive values of 100% and high specificity (72%) in their cohort of 28 patients with head and neck squamous cell cancer which were superior to FDG PET-CT assessments (Kishino *et al.*, 2012). The mid-treatment imaging was performed at a later time-point; after a median of 40-Gy the FDG PET-CT had high sensitivity and high negative predictive values of 100%, but low specificity (19%) and a low positive predictive value of 17%. One of the limiting factors in their study was the inclusion of multiple primary sites, and an advantage of FLAIRE and work reported by Troost *et al* is the evaluation of only oropharyngeal cancers (Troost *et al.*, 2010).

Larger decreases in FLT tumour uptake have predicted for better outcome in the literature. Hoeben *et al* demonstrated that a fall greater than the median value of 45 % related to improved 3-year survival of 88% compared with 63% (Hoeben *et al.*, 2013). Similarly, Arens *et al* reported a reduction in SUV above the median value predicted better 4-year survival (90% versus 53% 4-year survival, $p = 0.04$) in head and neck cancers (Arens *et al.*, 2014). In the current study, only two patients have developed metastatic disease, and in one the metastases may have been there at baseline, hence it is not possible to comment on the relationship between the change in proliferative activity and development of metastatic disease. Extending the follow-up period may increase the number of events, and enable further evaluation.

Relating treatment response to eventual outcome has been reported in a variety of other tumour sites. FLT SUV decreases of greater than 30% in non-small cell lung cancer patients after one week of erlotinib treatment showed significantly longer progression free survival (Kahraman *et al.*, 2011) than smaller decreases in SUVmax. In mucosal melanoma, Inubushi *et al* reported a 35% reduction in SUVmax predicted better local control (Inubushi *et al.*, 2013).

The optimal timing for an FLT tumour response assessment scan in unknown. A decision to scan in the second week of radiotherapy would allow time for an alternative treatment plan to be generated and delivered, if the sensitivity and positive predictive value could be improved. Hoeben *et al* reported difficulty quantifying uptake due to a reduced signal to noise ratio, therefore imaging after this early time-point may add little information (Hoeben *et al.*, 2013).

4.6.2 Predictive and prognostic value of pre-treatment 18F-FLT PET-CT

The FLAIRE study investigated the potential of FLT PET-CT to predict clinical outcome of oropharyngeal squamous cell carcinoma treated with chemoradiotherapy. The patient characteristics of the study cohort are typical of patients with oropharyngeal cancer in the UK, thus conclusions may be applicable to the wider patient population. The response rate to treatment in the FLAIRE cohort was similar to data recorded locally (94% vs 90%).

All tumours were FLT-avid. The highest SUVmax values for each patient ranged from 5.6 – 10.3 which is consistent with reports in the literature; mean SUV_{max} of 19 head and neck cancer patients was 5.8 (range 1.5 – 11.7) and of 10 oropharyngeal cancers mean SUVmax was 7.6 (range 3 – 11) (Linecker *et al.*, 2008; Troost *et al.*, 2010).

Biological behaviour may differ between primaries and lymph nodes, as may their response to treatment. In 53% of the study cohort, the lymph node metastases were more FLT-avid than the primary tumours. Diagnostic biopsies of the primary tumour performed prior to the scan may have influenced this result due to reducing the volume of viable tumour evaluable to image; therefore, the result may differ if patients are scanned prior to the diagnostic tonsillar biopsy.

A trend was observed between higher T-stage and higher SUVmax. To our knowledge this is not widely reported in the literature; Troost *et al* did not include T4 oropharyngeal tumours in their study, and there was only one T4 oropharyngeal cancer in Kishino *et al*'s work (Troost *et al.*, 2010; Kishino *et al.*, 2012). Only Hoeben *et al* reported no correlation between CT and PET tumour volumes and SUVmax. They included seven T4 head and neck cancers in their cohort of 48 patients, which consisted of 27 oropharyngeal primaries (Hoeben *et al.*, 2013).

Eighty-four percent of the FLAIRE study cohort were HPV-positive and 2-year survival in the 15 study participants was 88%. Similarly high survival rates have been reported in the literature in HPV-positive patients treated with chemoradiotherapy. In a landmark paper by Ang *et al*, 3-year survival of HPV-positive patients was 82% compared to 57% among HPV-negative patients, identifying HPV as a prognostic biomarker. Similarly, Lill and colleagues reported 2 year-survival of 100 % in HPV-positive patients and 30% in HPV-negative patients and Bossi *et al* reported not only better survival outcomes in HPV-positive patients than HPV-negative patients but that treatment with chemoradiotherapy rather than surgery conferred a survival benefit (Ang *et al.*, 2010; Lill *et al.*, 2011; Bossi *et al.*, 2014). It is important, therefore, to account for HPV status when investigating tumours or the head and neck. Differences in FDG PET imaging parameters according to HPV-status were investigated by Tahari *et al* (Tahari *et al.*, 2014). They observed greater metabolic parameters and larger primary tumours in the HPV-negative patients. Additionally, HPV-positive nodal metastases tended to be larger and have higher glycolytic indices compared to patients with HPV-negative disease. The FLAIRE cohort was too small to derive similar FLT-data according to HPV-status.

Currently, there have been too few events in the follow-up period, to evaluate robustly the relationship between baseline SUV parameters and outcome; however, pre-treatment SUV max above 9.9 predicted for metastatic disease and death within two-years of diagnosis. A larger study with longer follow-up would increase the number of events and may confirm the initial results. In some clinical scenarios, this information could sway the clinician to intensify treatment: adding in chemotherapy or a biological agent; using multimodality treatment; or dose-escalating radiotherapy. Conversely, a baseline SUVmax associated with a better prognosis may enable de-escalation of the treatment plan to reduce the considerable long term morbidity associated with current treatments.

Reports in the literature are varied when considering the predictive potential of FLT PET-CT scans. A correlation between pre-treatment SUV parameters and eventual outcome has been reported. Hoeben *et al* studied more than fifty patients with HANSCC (52% oropharynx, HPV status unknown, 50% had advanced stage IVA, 31% were treated with chemoradiotherapy). All tumours were detected by FLT PET, as shown in the FLAIRE study. Baseline SUVmax below 6.6 predicted better

locoregional control (LRC) and disease-free survival (DFS) in patients treated with radiotherapy alone. In contrast, SUVmax below 6.6 predicted worse LRC and DFS in patients treated with chemoradiotherapy. Three-year LRC was 100% if SUVmax was equal to or higher than 6.6 in patients receiving CRT, compared with 57% ($p = 0.04$) if SUVmax was below 6.6. If these results are reproduced in larger studies, a pre-treatment SUVmax below 6.6 may select out the patients who do better with radiotherapy alone. Hoshikawa *et al* studied more than 50 patients with HANSCC treated with CRT over a seven-year period. FDG and FLT PET-CT scans were performed in all patients. On univariate analysis they demonstrated FLT PET SUV_{max} and total lesion proliferation (TLP) correlated with LRC and overall survival (OS). Multivariate analysis demonstrated that total TLP was an independent factor for LRC, and that SUVmax predicted OS (Hoshikawa *et al.*, 2015). Despite correlations of FDG SUV_{max} with OS and tumour lesion glycolysis (TLG) with LRC, they observed that FLT-derived parameters were superior to FDG-PET parameters in predicting clinical outcome. Linecker *et al,* provided additional data that high FDG and FLT uptake correlates with poor outcome (Linecker *et al.*, 2008).

The potential of FLT PET-CT as a prognostic imaging biomarker has been investigated in several other malignancies. In thirteen patients with head and neck mucosal malignant melanoma (MMM) pre-treatment SUVmax values of ≥ 4.3, age ≥ 80 years, gross tumour volume ≥ 39ml, sinonasal primary tumour site and absence of involved lymph nodes predicted better overall survival (Inubushi *et al.*, 2013). Conversely, Hermann and colleagues demonstrated the predictive potential of FLT PET in non-Hodgkin's lymphoma patients undergoing R-CHOP chemotherapy. Pre-treatment SUV mean and max values were lower in the group who completely responded, compared with the non-complete responders (Herrmann *et al.*, 2011a). In some primary sites, FLT PET-CT imaging holds less appeal due to surrounding high physiological uptake which may mask tumours. For example, Zhou *et al* reported no role for pre-treatment FLT PET-CT imaging of metastatic gastric carcinoma, favouring instead the FDG tracer. Sensitivity of FLT PET was 30 % due to high background hepatic uptake (Zhou *et al.*, 2013). This topic was discussed in more detail in Chapter 3.

4.6.3 Delayed response assessment using 18F-FLT PET-CT

Newcastle upon Tyne Hospitals NHS Foundation Trust audit data and clinical experience suggest as many as 40% of head and neck squamous cell cancer patients will have residual disease on clinical examination six weeks following radiotherapy. By 10-12 weeks FDG PET-CT demonstrates that approximately 10% of patients have residual disease prompting further treatment, usually surgery. If a response biomarker could predict at six weeks what is seen at twelve weeks, then potentially the 10% of patients requiring salvage therapy could be identified and treated earlier in the pathway. Delaying the FDG PET-CT until 12 weeks after the end of treatment reduces the rate of false-positives, arising from post-treatment inflammation (Porceddu *et al.*, 2005) (Schoder *et al.*, 2009).

The motivation to determine response to radiotherapy and inform patients and therapy decisions earlier drove one of the secondary objectives in FLAIRE. In practice, however, these patients are often struggling to maintain nutrition and coping with the acute toxicities of chemoradiotherapy, and so may not be fit enough for alternative treatments.

FLAIRE demonstrated that at six weeks post treatment, 5 / 14 (36%) of participants had evidence of FLT uptake, which is similar to the clinical findings from local audit data. One of these five patients had residual disease on the FDG-PET performed two-months later, and proceeded to surgery. Similarly, Kishino *et al* reported persistent FLT accumulation in 37% of head and neck cancer patients five weeks (range 3 – 11) following radiotherapy which was associated with adverse outcomes at three years, compared with patients with no FLT-avid disease (Kishino *et al.*, 2012). The negative predictive value of the post-treatment FLT PET-CT scan was 100% but the positive predictive value was only 20%. The high negative predictive value of this test is appealing in the context of identifying responders to treatment six weeks earlier than current practice, and being able to inform patients of this encouraging news at a time when acute treatment-related toxicities are at their most challenging. For the smaller proportion of patients with positive results, 80% will be told at a later time-point that disease has responded, following the FDG PET-CT. Potentially there could be implications for clinical practice in identifying treatment responders at six weeks avoiding the need for a 12 –week FDG PET-CT scan, if the findings were to be reproduced in larger prospective studies.

4.6.4 Developing a semi-automated contouring threshold for consistent quantitative assessment of FLT PET-CT images

Currently, there is no consensus on the best segmentation methods to define tumour subvolumes suitable for response assessment or radiotherapy dose painting; however, several clinical trials use the SUV 50%max isocontour (Madani *et al.*, 2007a; Madani *et al.*, 2011). The automated-thresholding contouring technique may be of limited value in the patients with neighbouring involved lymph node regions because not all lymph nodes are measured individually. Currently there is also no consensus on which tumour deposits to evaluate or how many; however, if there is general agreement that only the most avid lesion is selected for evaluation on serial scans, and the chosen parameter is SUVmax, an automated technique may be sufficient.

For the degree of uptake demonstrated in this study an automated threshold of 63% of SUVmax provided a measure of SUV parameters and tumour volume, which related to manual contouring on contrast-enhanced CT images. A semi-automated quantitative technique based on SUVmax could be applied in the assessment of treatment response and warrants further investigation with a larger dataset. Applying the derived automated threshold of 63% of SUVmax to define ROIs may be more suited to radiotherapy definition than to response assessment using FLT PET-CT. This is described in more detail below. Moreover, there may be more potential using an automated contouring method with other tracers which have a higher tissue concentration at baseline, or which show a smaller decrease on treatment, e.g. FDG.

4.6.5 Additional FLT PET-CT Findings

Varicella zoster (VZ) is a common viral infection which in the immunocompetent is rarely serious. In patients undergoing chemotherapy, the infection may become life-threatening and it is important to diagnose. In the FLAIRE study, lymphadenopathy secondary to *VZ* was FLT-avid, but not metabolically-avid when imaged on FDG PET-CT six days later. Cutaneous manifestations of *VZ* have been reported on FDG PET-CT but are few in number (Muzaffar *et al.*, 2013). Because of the clinical significance of untreated VZ in immunocompromised patients, it is important to distinguish the cause of increased uptake secondary to infection, as opposed to skin metastases. To our knowledge there are no reports of FLT-uptake in *VZ* infection.

Although FLT has been heralded by many as being a more specific radiotracer in relation to inflammation, FLAIRE demonstrated uptake in both *Varicella zoster* infection and following dental extraction; the latter is more relevant as this is a common occurrence in patients being prepared for head and neck radiotherapy. Troost *et al* reported that FLT PET-CT had specificity 17% and positive predictive value of 38%; therefore, it could not discriminate between metastatic and reactive cervical lymph nodes in HANSCC (Troost *et al.*, 2007). This is in contrast to findings by other research groups (van Waarde *et al.*, 2004; van Westreenen *et al.*, 2005). A common drawback of many of the FLT imaging studies, including the Troost study, is the small number of patients (n = 10), but without larger studies these results are the data we have to build on.

4.6.6 Limitations of the study

The study population included small patient numbers and a follow-up time which was too short to comment on three-year outcomes, for comparison with similar studies. The number of non-responders was too small to enable detailed evaluation of FLT PET-CT as an early response imaging biomarker. Unlike several other studies, heterogeneity of results was reduced by limiting the inclusion criteria to only oropharyngeal cancers.

4.7 Conclusions

Although the cost of repeated FLT PET-CT scans is a not insignificant consideration, the technical feasibility of undertaking repeated scans was demonstrated, and provides preliminary data for further work. FLT PET-CT during chemoradiotherapy treatment can identify early changes in tumour and bone marrow proliferation. Pre-treatment high tumour SUVmax may predict for poor outcome. FLT PET-CT may not discriminate between reactive and metastatic lymph nodes prompting additional diagnostic procedures. There may be a role for post-treatment FLT PET-CT imaging to identify treatment responders at an earlier stage than is currently undertaken. A semi-automatic contouring algorithm has been proposed to identify tumour volumes which will be explored in the radiotherapy setting in the next section.

4.8 Radiotherapy planning study

4.8.1 Introduction

Intensity Modulated Radiotherapy (IMRT) has been widely used in head and neck cancer for over a decade due to the ability to deliver highly conformal treatment to malignancies which often lie adjacent to critical normal tissues. Sharp fall-offs in radiotherapy dose lower the exposure to organs at risk. Additionally, IMRT permits the escalation of dose to improve tumour control without excessive toxicity to surrounding healthy structures. Locoregional failure tends to occur within the high-dose gross tumour volume (GTV) lending weight to the argument for radiotherapy dose escalation to the GTV (Leclerc *et al.*, 2013; De Felice *et al.*, 2015). Dose escalation strategies include a simultaneous boost (SIB), altered fractionation and adaptive replanning, guided by on-treatment imaging. Conventional fractionation for head and neck cancers is 70-Gy in 35 fractions, or 65-Gy in 30 fractions; recently, studies have shown an acceptable toxicity profile with boost doses of up to 70-Gy in 30 fractions (Miah *et al.*, 2012). Altered fractionation schedules can be logistically challenging to implement (Leclerc *et al.*, 2013); adaptive replanning is not routine practice. Due to the ultimate dose constraints of surrounding tissues, an alternative strategy is aimed at delivering high doses of radiotherapy to a tumour subvolume with increased radioresistance e.g. areas of hypoxia, excessive metabolism or proliferation. Functional imaging (FI) can provide this biological information. The most commonly used FI technique to inform RTP is ^{18}FDG PET-CT. Alternative PET tracers are ^{18}F-fluoromisonidazole, which provides tumour hypoxic measurements, and ^{18}F-FLT which characterises tumour proliferation. Dose-painting tumour subvolumes to different doses using molecular imaging is an expanding area of radiotherapy research. Within the FLAIRE study, a SIB approach to 75-Gy in 30 daily fractions, guided by FLT imaging, was investigated.

4.8.2 Objectives

The main purpose of the planning study, which was a substudy of the main FLAIRE study, was to investigate if the FLT PET-CT scans performed before and during RT could guide GTV definition and generate an additional radiotherapy plan (Plan 2). As this was a dose planning exercise, none of the FLT-guided radiotherapy plans were used to treat patients.

4.8.3 Methods

All patients underwent a radiotherapy planning scan as described in Section 4.3.3. Target volumes were defined on radiotherapy planning workstations using ProSoma Treatment Planning programme v 3.3 (MedCom, Darmstadt, Germany) and Oncentra MasterPlan version 4.3 (Elekta, Stockholm, Sweden) according to the ICRU 50 and 62 definitions. Plan 1 GTVs and CTVs were defined using clinical examination findings, diagnostic CT/MRI imaging, and a radiotherapy planning CT ± MRI acquired in the radiotherapy planning position; 65-Gy in 30 fractions to the high dose CTV, and 54-Gy in 30 fractions to the electively treated nodal levels (Table 4-13). The high dose CTV included the GTV with a 10mm margin, involved lymph nodes with a 5mm margin, and adjacent lymph nodes at high risk of involvement. The low dose CTV included contralateral lymph node regions at risk of metastatic involvement, and ipsilateral lower cervical lymph nodes not encompassed within the high-dose CTV. Lymph node regions were contoured using the consensus guidelines for delineation of neck node levels (Gregoire *et al.*, 2014). A 3 mm margin was added to the CTV to account for set-up inaccuracies and patient motion to create a PTV. Spinal cord, parotid and submandibular glands, larynx, thyroid gland, brain stem and mandible were delineated as organs at risk (OAR). A 3mm margin was added to define a planning organ at risk volume (PRV).

Dose planning exercise to create FLT-guided dose-escalated plan

Using HERMES GOLD^{TM} software (HERMES Medical Solutions, Stockholm, Sweden) one operator with eight years radiotherapy planning experience delineated the (GTV-P) of the primary tumour and all metastatic lymph nodes on fused PET and contrast-enhanced CT images. A simultaneous integrated boost volume was defined by the 70% isocontour (GTV70%). Preliminary work to derive tumour subvolumes derived from 80% of SUVmax proved challenging for the HERMES software due to the small size of the volumes. Subvolumes defined by 70% of the SUVmax were larger and were therefore selected for further evaluation. A 5mm margin was added to the GTV70% to create a boost PTV (PTV-75). High- and low-dose PTVs, organs at risk and any planning structures were copied from Plan 1. A total dose of 75-Gy was prescribed to PTV-75, 65-Gy to high-dose PTV and 54-Gy to low-dose PTV, using 6 MV photons.

Table 4-13: Radiotherapy plans details

	Imaging datasets required	Timing of RT plan	Max prescription
Plan 1 (No Boost)	Routine planning CT ± MRI	Pre-treatment	High dose CTV – 65 Gy Low dose CTV – 54 Gy
Plan 2 (Boost)	Routine planning CT ± MRI + pre-treatment FLT PET-CT	Pre-treatment	Boost PTV – 75 Gy High dose CTV – 65 Gy Low dose CTV – 54 Gy

Two single-phase inverse radiotherapy plans using TomoTherapy IMRT were created for three patients, using a 2.512cm jaw width, a couch pitch of 0.287 and a modulation factor of 2.4 by Mr Jonathan Wyatt, Research Radiotherapy Physicist. Table 4-14 lists the dose constraints. In the optimization process, the following dose-volume constraints were used: D99%, D95%, D50%, D5% and D2%. D99% was defined as the minimum dose the hottest 99% of the volume received and D50% was defined as the median dose the PTV received.

Table 4-14: FLAIRE radiotherapy dose constraints for organs at risk (*where achievable)

		Dose Constraint (Gy)
Spinal Cord	**Maximum**	47
	PRV maximum	48
Brainstem	**Maximum**	52
	PRV maximum	53
Parotid	**Ipsilateral mean***	26
	Contralateral mean	26
Larynx	**Mean**	40
Mandible	**D1cc**	64

4.8.4 Results

Using IMRT with integrated simultaneous boost, simulated dose escalation plans to PTV-75 (defined by GTV 70% of the primary tumour SUVmax and 5mm margin) for three patients were achieved. In one case, FLT-avid lymph nodes were adjacent to

the primary tumour and a second boost volume was defined. Radiotherapy dosimetry parameters for Plan 1 (no boost) and Plan 2 (boost) are shown in Table 4-15. All the boost PTV 75 volumes and the FLA001 PTV 54 failed the maximum doses clinical requirements. This was inevitable due to the dose tail which can be seen on the dose volume histogram where there are different dose levels in volumes that are adjacent to one another. Sparing of organs at risk was similar between the two dose levels. The mean PTV 75 volume of 12.5 cm^3 was considerably smaller than the mean PTV 65 volume of 372 cm^3. A single slice from Plan 1 and Plan 2 for each patient are shown in Figure 4-20 - Figure 4-27. Boost plans had marginally longer delivery times (mean 0.1 minute longer).

Table 4-15: FLAIRE radiotherapy dose parameters for plan 1 (no boost) and plan 2 (simulated dose escalated plans with subvolume boost to 75-Gy)

		Patient 1 T1 N1		Patient 2 T2N2b		Patient 3 T4N2b	
		No Boost	Boost	No Boost	Boost	No Boost	Boost
Spinal Cord	**Maximum**	30.1	28.5	29.7	29.9	31.9	28.8
	PRV maximum	32.6	31.0	31.6	34.2	39.0	33.8
Brainstem	**Maximum**	25.4	23.5	21.5	22.3	26.7	25.5
	PRV maximum	29.9	27.7	25.7	25.4	31.8	29.3
Parotid	**Contralateral mean**	24.4	24.0	23.2	23.2	42.9	41.6
	Ipsilateral mean	40.3	41.8	34.3	37.3	34.8	34.0
Submandibular	**Contralateral mean**	50.3	47.9	53.6	53.3	64.7	64.5
	Ipsilateral mean	64.6	64.6	64.6	68.6	64.7	64.5
Larynx	**Mean**	53.2	54.4	47.8	50.0	47.4	50.4
Mandible	**D1cc**	64.7	65.4	64.9	65.6	65.0	65.2
	Mean	43.3	43.3	43.5	44.2	49.6	50.8
	D2	64.6	64.8	64.8	65.0	65.0	65.1
Primary Tumour Volume (cm^3)	**PTV 75**	-	6.5	-	9.9	-	21.2
	PTV 65	277.3	277.3	361.8	361.8	753.2	753.2
	PTV 54	265.5	265.5	167.1	167.1	-	-

Figure 4-20: FLAIRE Patient 1 - TomoTherapy Plan 1 for 61-year old with T1 N1 right tonsil HPV-positive cancer. FLT SUVmax of primary 7.3.

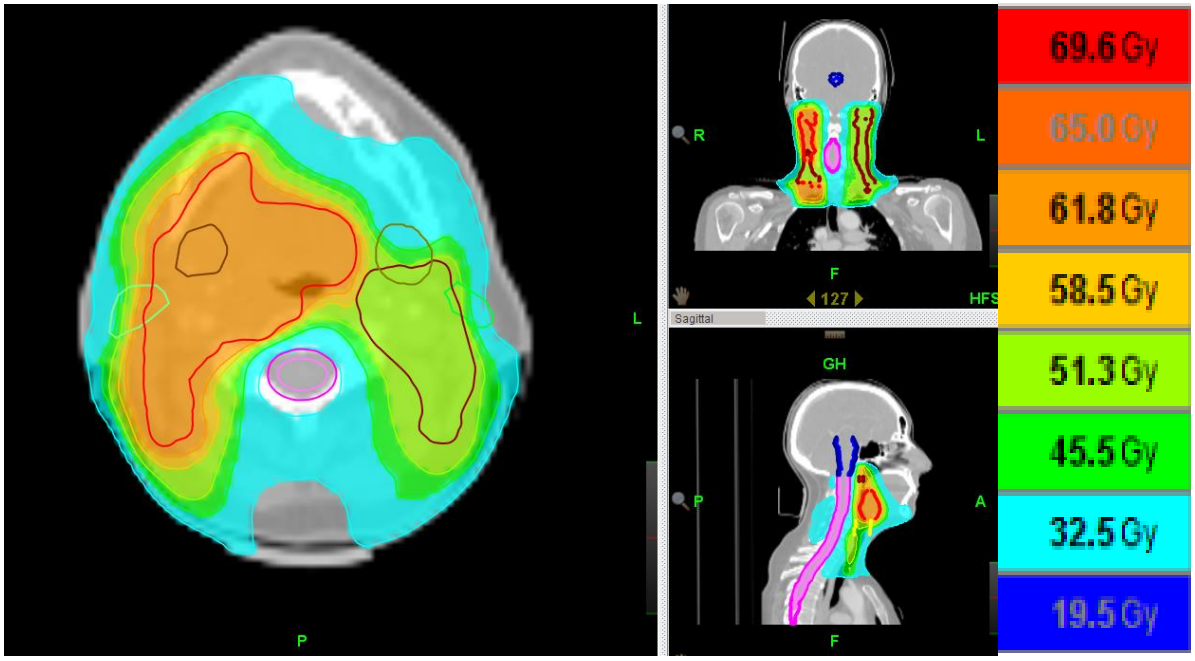

Figure 4-21: FLAIRE Patient 1 – TomoTherapy Plan 2 for 61-year old with T1 N1 right tonsil HPV-positive cancer. FLT SUVmax of primary 7.3.

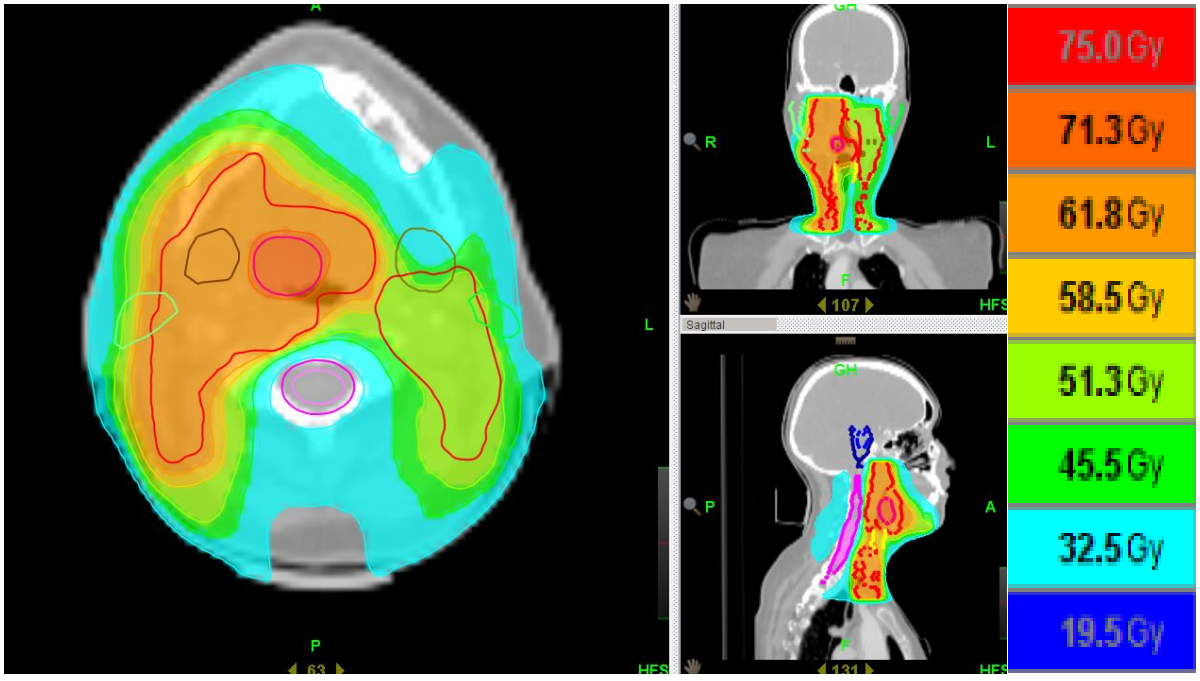

Figure 4-22: FLAIRE Patient 1 - Dose volume histogram (DVH) (SMG = submandibular gland)

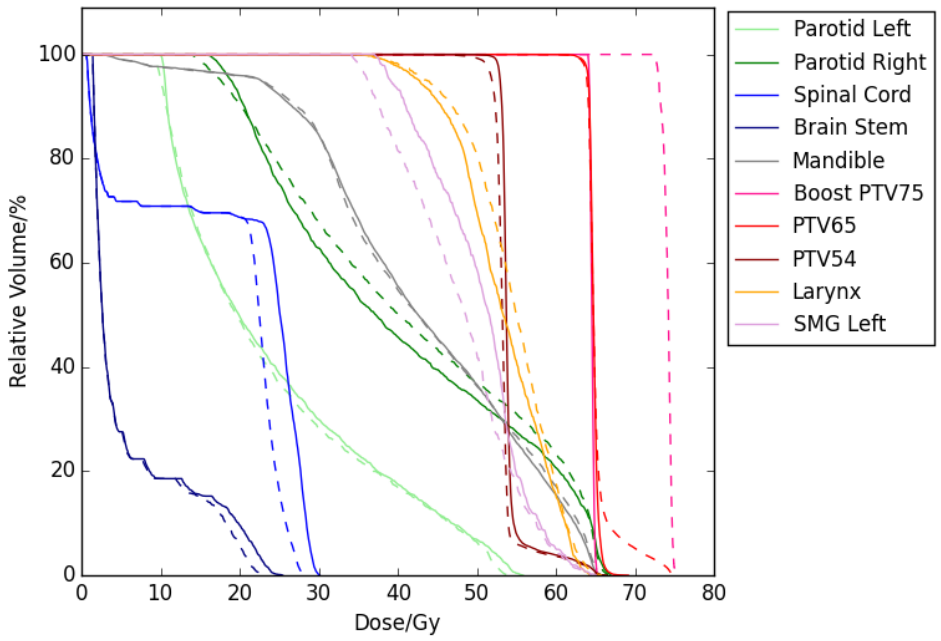

Figure 4-23: FLAIRE Patient 2 – TomoTherapy Plan 1 in 59-year old with T2 N2b left base of tongue HPV-positive cancer. FLT SUVmax of primary 7.5, and SUVmax 6.9 of left level II lymph nodes.

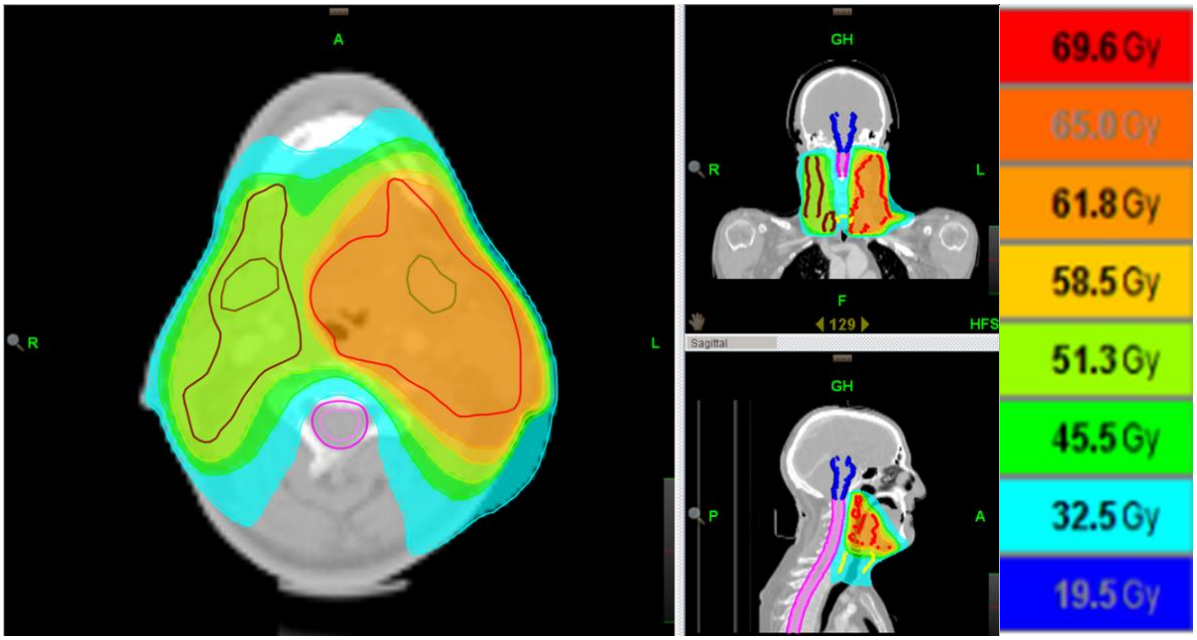

Figure 4-24: FLAIRE Patient 2 – TomoTherapy Plan 2 in 59-year old with T2 N2b left base of tongue HPV-positive cancer. FLT SUVmax of primary 7.5, and SUVmax 6.9 of left level II lymph nodes.

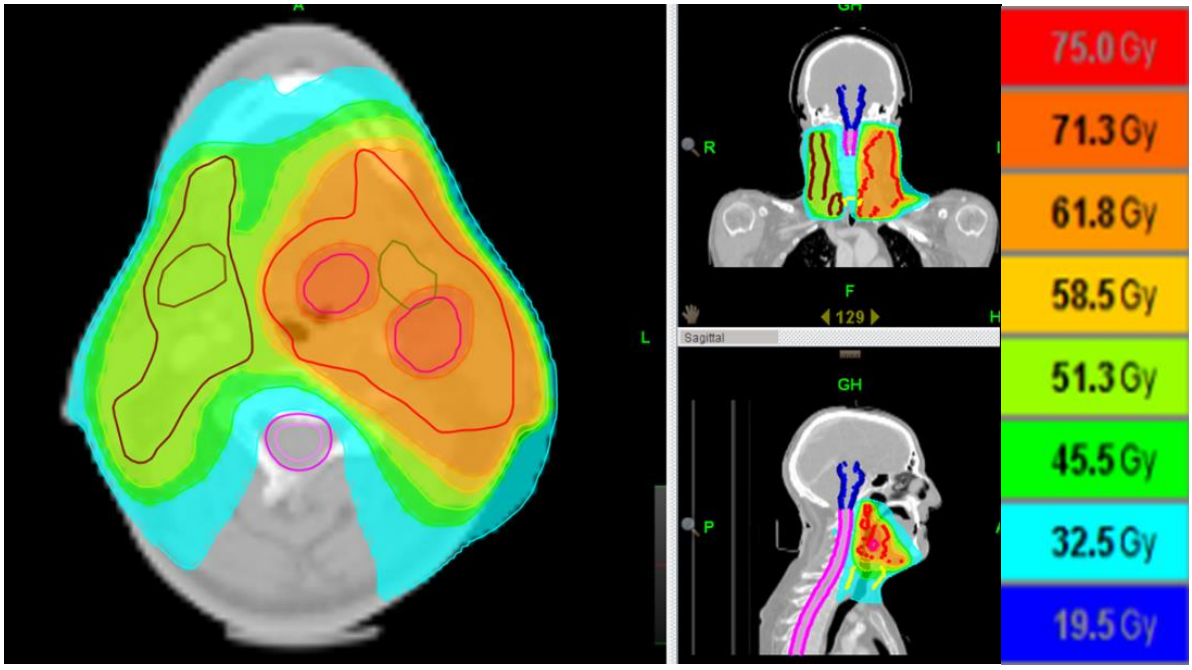

Figure 4-25: FLAIRE Patient 2 - DVH for primary tumour (SMG = submandibular gland)

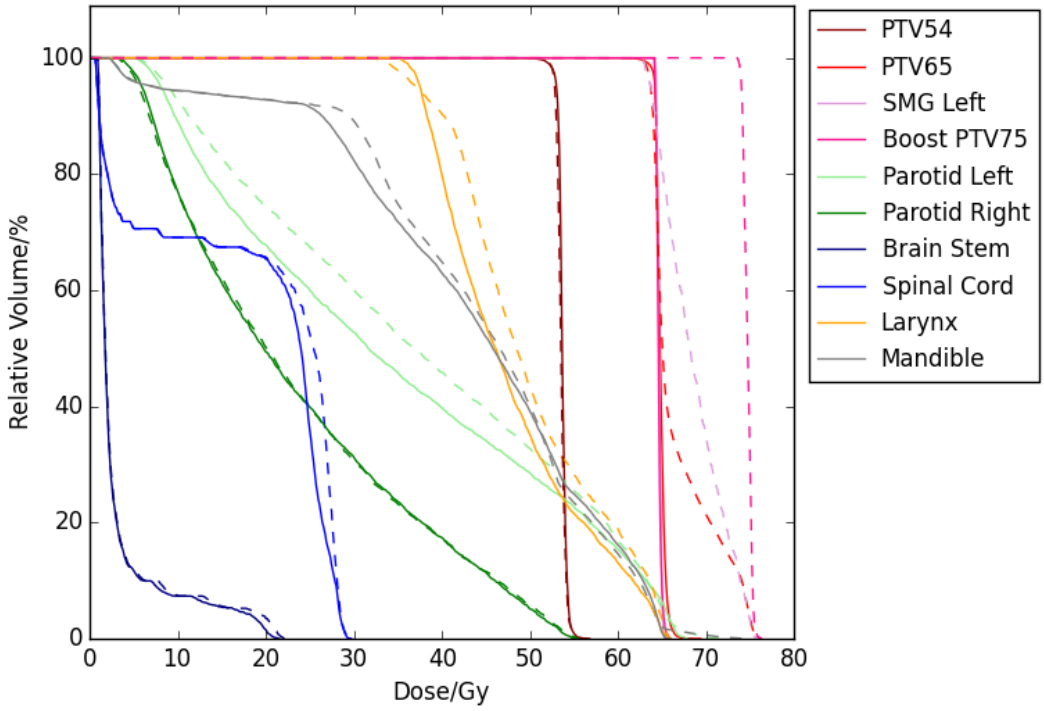

Figure 4-26: FLAIRE Patient 3 – TomoTherapy Plan 1 in 57-year old with T4 N2b left base of tongue HPV-positive cancer. FLT SUVmax of primary 9.2.

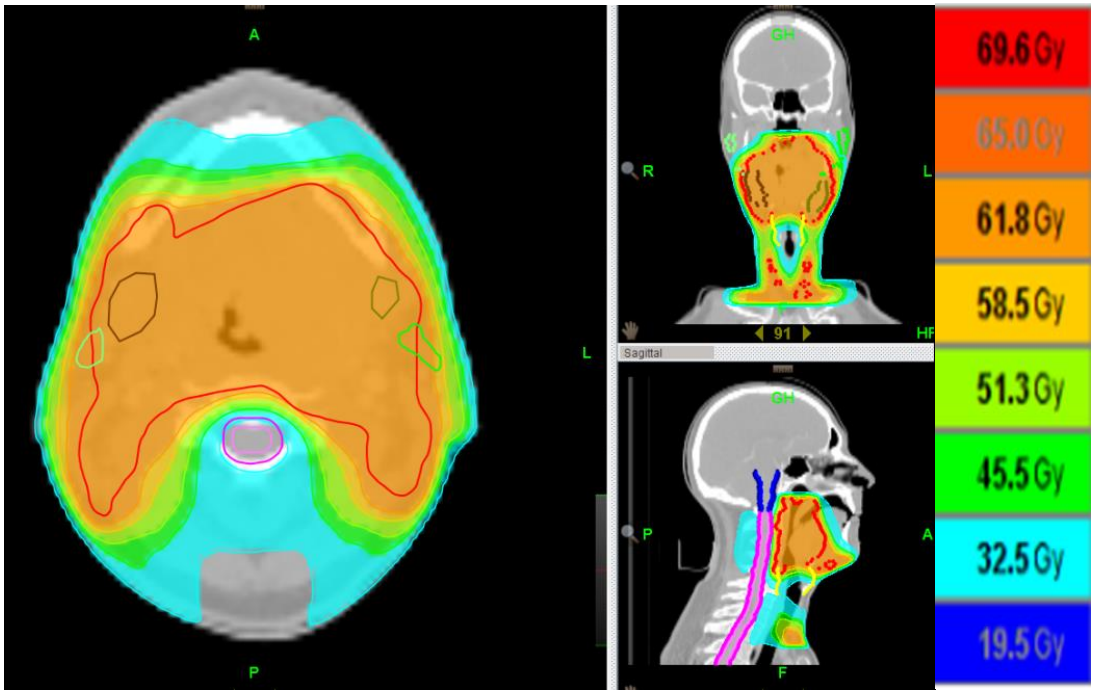

Figure 4-27: Patient 3 – TomoTherapy Plan 2 in 57-year old with T4 N2b left base of tongue HPV-positive cancer. FLT SUVmax of primary 9.2.

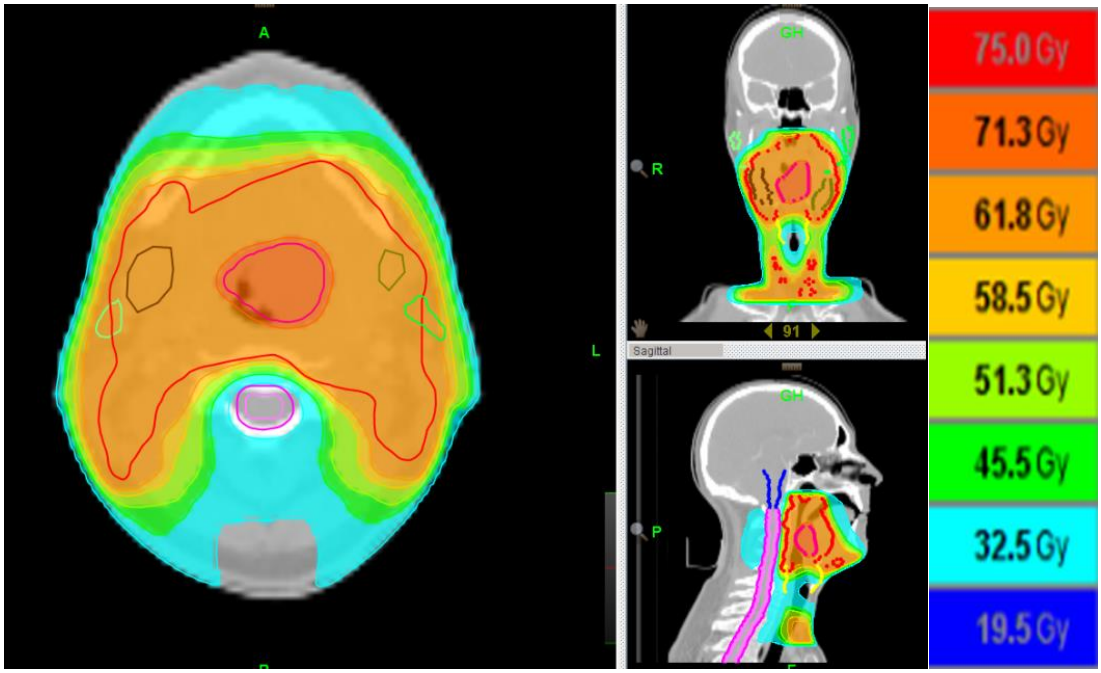

Figure 4-28: FLAIRE Patient 3 – DVH

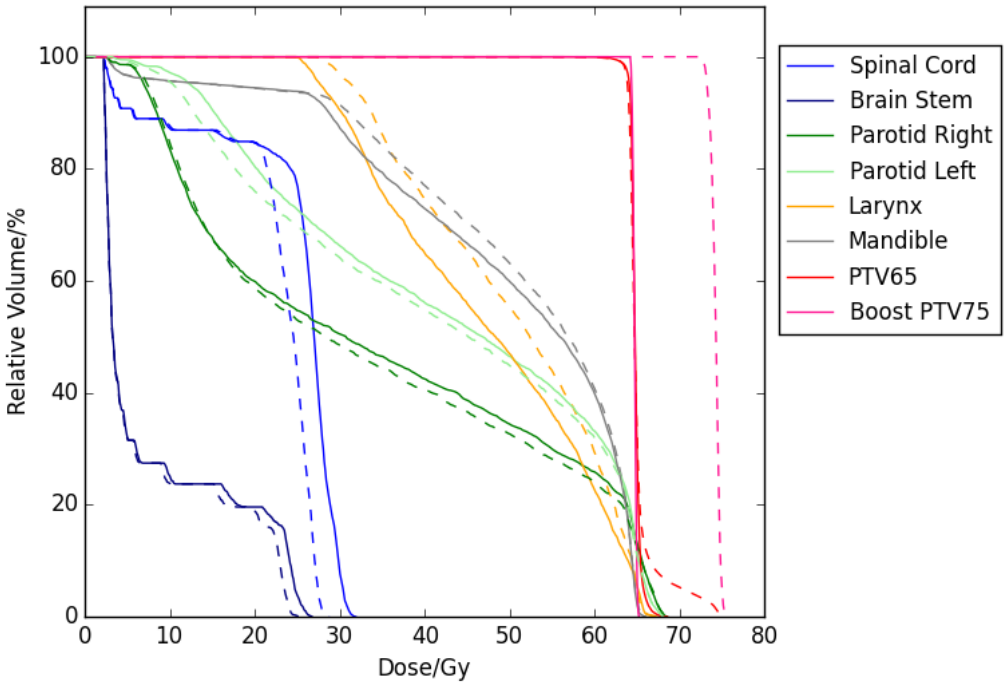

4.8.5 Discussion

Salvage surgery in the head and neck for locoregional failure following radiotherapy is technically more challenging and associated with greater morbidity (De Felice *et al.*, 2015). Dose escalation to overcome radioresistance and treatment failure is a promising area of radiotherapy research. In this small feasibility study, pre-treatment FLT PET-CT scans were used as a boost delineation tool. It was technically feasible to generate radiotherapy plans for patients with T2-4 N0-2b disease, which delivered 75 Gy to a proliferative subvolume defined by 70% SUVmax of the primary tumour. Using IMRT, the volume of tissue that would be irradiated to 75-Gy was small, and compared with the conventional plan (Plan1), did not increase dose delivered to organs at risk for any of the patients in this study. However, if the boost PTV overlapped the OAR the dose could substantially increase.

During radiotherapy, the tumour shape and volume may change. As discussed previously, biological changes within the tumours are also observed. Quantification of a decrease in proliferation is not always straightforward as there can be increased uptake in tonsillar tissue due to proliferation of inflammatory cells. The tumour subvolumes with highest proliferative activity may also change in size and shape (de

Langen *et al.*, 2009; Troost *et al.*, 2010). One method to correct for these changes is the generation of an adaptive radiotherapy plan, as described by Troost *et al*. This research group reported on an adaptive IMRT treatment plan with a SIB to a patient with a T3 N0 oropharyngeal tumour. The primary tumour proliferative subvolume was defined by 80% of the SUVmax and was defined on a pre-treatment FLT scan, and on a scan obtained during the second week of RT. A total dose of 74-Gy to the overlapping GTV volumes was planned, and total dose of 71-Gy to any areas of mismatch (Troost *et al.*, 2010). Other research groups have looked at SIB using alternative PET tracers. In head and neck cancer, a number of studies investigating radiotherapy dose-escalation to FDG or FMISO-avid subvolumes have been reported. A boost dose of up to 84-Gy in a tumour hypoxic region was reported by Lee *et al*, and dose of 80.9-Gy to an FDG-subvolume was tolerated in a Phase 1 study by Madani *et al.* However, other studies report the maximal tolerated dose to be lower, and have limited the dose escalation to 68 – 75-Gy (Lauve *et al.*, 2004; Guerrero Urbano *et al.*, 2007; Lee *et al.*, 2008; Madani *et al.*, 2011; Miah *et al.*, 2012). Higher T-stage is a risk factor for late side-effects in altered fractionation highlighting the importance of patient selection for dose adaptive strategies (Lassen *et al.*, 2011). In addition to the total radiation dose, overall treatment time, fractionation schedule, fraction size, and concomitant systemic treatment are known to influence the tumour response and the toxicity of normal tissues (Orlandi *et al.*, 2010).

Accurate determination of tumour extent from molecular imaging is challenging. Validating new techniques with histopathological correlation is important to consider when there is uncertainty. Daisne *et al* studied laryngeal cancer patients and showed that FDG-PET delineation demonstrated a closer match to resected tumour volume, than CT or MRI. In their study, each modality overestimated the tumour size by 29%, 65% and 89% respectively. Despite this, all modalities failed to delineate an area of macroscopic superficial mucosal extensions (Daisne *et al.*, 2004). FDG PET-CT volumes have been shown to be smaller that CT and MRI-defined volumes in a number of other studies. This translates to dosimetric advantages to organs at risk (Leclerc *et al.*, 2015). An important consideration when reducing the size of the GTV, is the risk of geographical miss resulting in treatment failure. Studies which have reported on recurrences following RT have shown these tend to occur within the high dose PET-GTV (Madani *et al.*, 2007b; De Felice *et al.*, 2015; Leclerc *et al.*, 2015).

Dose escalating a subvolume using molecular imaging, without reducing the size of the GTV defined by CT or MRI is one potential strategy to overcome this challenge, and was investigated in the FLAIRE substudy.

An additional consideration with functional imaging is the accurate segmentation of PET images. Various methods have been reported: manual delineation using a window-level setting to threshold the volume and straightforward visual interpretation; threshold-based methods e.g. fixed threshold of SUV 3 or fixed percentage of the maximum signal intensity, e.g. 80% as used by Troost *et al*; volumes defined using a signal-to-background ratio; a gradient-based method using a watershed transform algorithm and hierarchical clustering analysis; and a fuzzy locally adaptive Bayesian algorithm (Troost *et al.*, 2010; Arens *et al.*, 2014). In a comparison of semi-automatic segmentation algorithms, Arens *et al* observed that a greater than median fall in proliferative volume after 4-weeks of radiotherapy determined by the fuzzy locally adaptive Bayesian method was the best predictor of outcome. Similarly, Zaidi *et al* reported the most accuracy with a variant of the fuzzy clustering-based algorithm (Zaidi *et al.*, 2012). The thresholding auto-contouring method applied in the FLAIRE study was selected for several reasons: the functionality of the HERMES radiotherapy planning workstation facilitated the work; investigator's experience; and the algorithm is independent of the heterogeneity of the tracer uptake within the lesion. A more detailed study and discussion of the various PET segmentation methods is warranted but was outwith the scope of the dissertation.

4.8.6 Conclusions

Pre-treatment FLT PET-CT imaging defined a boost volume for a single-phase inverse-planned simultaneous-boost radiotherapy plan to be delivered using IMRT. Doses to organs at risk were kept within tolerance. For the subgroup of oropharyngeal patients who are predicted to have a poor prognosis, a phase 1 dose escalation study to evaluate acute toxicities would address concerns of safety and feasibility.

Chapter 5 Optimising FLT PET-CT imaging using Thymidine Phosphorylase

5.1 Introduction

One of the fundamental hallmarks of cancer is the ability to sustain proliferation. Proliferation can be assessed histologically using endogenous markers such as Ki-67, proliferating cell nuclear antigen (PCNA) and cyclins; or staining for incorporated exogenous thymidine analogues such as bromodeoxyuridine (BrdUrd) and iododeoxyuridine (IdUrd) (Troost *et al.*, 2009). A strong correlation between the proliferation imaging biomarker 18F -fluorothymidine (FLT) SUV measurements and staining with the exogenous marker IdUrd has been identified, although more research groups have studied Ki-67 (Troost *et al.*, 2009; Chalkidou *et al.*, 2012). Alternative PET tracers for the measurement of tumour proliferation have also been evaluated (Mankoff *et al.*, 2005); however, these remain experimental and only FLT is widely available. There is substantial inter-patient variation using FLT PET-CT that currently limits its utility (Zhang *et al.*, 2012b). Various intrinsic tumour and endogenous factors are thought to influence FLT uptake: the endogenous thymidine concentration; thymidine kinase 1 (TK1) activity or protein levels; thymidine phosphorylase (TP) activity; and equilibrative nucleoside transporter (ENT-1) expression.

Malignant tumours are composed of proliferating cells and FLT is taken up by cells in the synthesis or S-phase of the cell cycle, a process facilitated primarily by ENT-1. Subsequent intracellular phosphorylation by TK1 traps FLT within the cell and levels of TK1 are increased in malignant cells (Shields *et al.*, 1998) (Sherley and Kelly, 1988; Munch-Petersen *et al.*, 1995). Thymidine phosphorylase (TP) catalyses the breakdown of the nucleoside thymidine to the base thymine and deoxyribose phosphate. Recent independent preclinical studies have shown that FLT accumulation in human tumour xenografts can be greater in tumours that express higher levels of TP, and that high levels of tumour TP are associated with low tumour thymidine concentrations (Zhang *et al.*, 2012a; Lee *et al.*, 2014b; Schelhaas *et al.*, 2014a). Thus, in the presence of high TP activity, endogenous tumour thymidine levels are low such that there is less competition with FLT and hence increased uptake of FLT into the tumour cell. Consequently, FLT PET scans should be optimal

in patients with high tumour TP levels. Supporting these preclinical data, Lee and colleagues demonstrated a significant correlation between FLT uptake in patients with non-small cell lung cancer, as measured by FLT PET, and tumour TP expression measured by immunohistochemistry (Lee *et al.*, 2014b). Furthermore, in a pilot pre-clinical study van Waarde *et al* demonstrated that TP administration prior to FLT PET scanning, markedly improved the selectivity of tumour detection (van Waarde *et al.*, 2004). FLT is not metabolized by TP due to the fluorine in the 3-position of the sugar which prevents TP-mediated phosphorylation (Grierson and Shields, 2000). To our knowledge there are no reports of administering TP to humans, to improve FLT PET-CT imaging.

A clinically viable formulation of TP is currently being used to treat patients with mitochondrial neurogastrointestinal encephalomyopathy (MNGIE) (Bax *et al.*, 2013). MNGIE is an autosomal recessive progressive mitochondrial disease which is universally fatal. A mutation in the nuclear *TYMP* gene leads to a reduction in TP resulting in plasma and tissue accumulation of thymidine and deoxyuridine. Much of the initial work on TP administration related to pre-clinical evaluation of Erythrocyte Encapsulated – Thymidine Phosphorylase (EE-TP) in mice and canines. Bax *et al* reported that no serious toxicities were identified which would preclude a clinical trial of EE-TP in MNGIE patients, although infusion-related reactions due to activation of the immune response were a potential concern (Levene *et al.*, 2013). This research group have developed EE-TP as enzyme replacement therapy which is currently the only treatment for MNGIE. The therapeutic procedure involves taking 50ml of venous blood from the patient which is then subjected to a reversible hypo-osmotic dialysis procedure in the presence of TP. After a five hour interval the EE-TP is administered back to the patient as a 50ml volume intravenously. On the basis of these studies, there is a translational opportunity for the administration of TP to patients to optimise FLT PET scanning.

Thymidine phosphorylase is also known as platelet-derived endothelial cell growth factor (PD-ECGF). TP therefore plays a dual role in cancer development and therapy. In some solid tumours it is upregulated, promoting tumour growth and metastasis (Maeda *et al.*, 1996; Ackland and Peters, 1999; Bronckaers *et al.*, 2009; Miszczak-Zaborska *et al.*, 2010). High intra-tumoural levels of TP are associated with higher disease stage and consequently poorer outcomes (Tokunaga *et al.*, 2002; Zhang *et*

al., 2014). It is important therefore, to evaluate the potential impact of exogenous TP on tumour growth. 5-Fluorouracil is a commonly used anti-cancer drug and targets thymidylate synthase, RNA and DNA. TP catalyses the final conversion of the 5-FU pro-drug capecitabine to 5-FU. In breast cancer, higher levels of TP in tumours, have been related to better outcome due to enhanced sensitivity to 5-FU (Fox *et al.*, 1997; Miwa *et al.*, 1998; Gasparini *et al.*, 1999).

5.2 Objectives

The aim of this work was to provide preclinical data to support further clinical studies using FLT PET-CT. The principle objective was to determine if administration of *E. Coli* thymidine phosphorylase to human xenograft models in mice could elevate tumour TP activity, deplete tumour thymidine levels and improve tumour imaging with FLT PET.

5.3 Methods

Professor Herbie Newell and Dr Rachel Pearson designed and co-ordinated the programme of experiments. The cell culture and animal work was conducted by Mr Martin Galler, Mr Huw Thomas, and Mr Ian Wilson at the Northern Institute of Cancer Research, Newcastle University. Dr Bridget Bax and her research group at St George's Hospital, London, undertook the thymidine and thymidine phosphorylase assays. FLT PET imaging was performed by Dr Kathrin Heinzman and Prof Eric Aboagye at Imperial College, London.

5.3.1 Cell culture, treatment and preparation

Cell lines HT29 and SW620 (colon adenocarcinoma), A549 (lung adenocarcinoma) and Calu 6 (lung carcinoma) were selected on the basis of preliminary experiments in our institution demonstrating poor FLT uptake by PET scanning (I Wilson and R Maxwell, unpublished results). Cells were maintained *in vitro* within the exponential growth phase by passage until 80 - 90 % confluent, then trypsinized and viable cell counts determined.

To determine intrinsic tumour thymidine and TP activity levels, and to select a cell line for further evaluation, each cell line was subcutaneously injected into the flank of the hind leg of five male athymic CD1 nude mice. Tumours were freeze clamped and harvested when they reached 10 mm in diameter.

5.3.2 TP Administration

Thymidine phosphorylase dosing calculations were based on the data of van Waarde *et al*, with a starting dose of 20 IU per 20 g mouse (van Waarde *et al.*, 2004). Athymic nude CD1 mice (n = 2 for each group) were injected with 20 IU or 200 IU TP, or control, *via* tail vein. No adverse reactions were observed. Mice were killed after 24 hours and plasma samples sent to St George's Hospital for analysis of plasma thymidine and thymidine phosphorylase.

A second experiment commenced at 1000 IU was not tolerated due to a presumed reaction inducing pulmonary collapse which necessitated a serial dose reduction to 50 IU *per* mouse. A modified formulation of good manufacturing process (GMP) clinical grade TP was used for subsequent experiments. To assess the impact of single dosing versus daily dosing for five days, 50 IU TP was administered and mice were killed at 3, 6, 24 and 48 hours after the single dose, and 3, 6, 24-hours after 5-day dosing.

Three CD1 nu/nu mice bearing SW620 human tumour xenografts were treated with 100, 250, 500 or 1000 IU of TP. The control group were not treated. At 24 hours, mice were killed and a terminal bleed collected. Tumour tissue was excised immediately and frozen. Samples were analysed for thymidine levels and TP activity, and results expressed as mean ± SD, unless indicated otherwise.

5.3.3 Small-animal PET imaging

SW620 tumour-bearing athymic nude mice were imaged using FLT PET. 1000 IU TP were administered to two mice. After TP injections, mice were imaged at 1 or 4 hours using 0.96 MBq FLT and a 60-minute dynamic PET scan acquisition. Two control mice were injected with intravenous PBS and scanned using FLT PET. .

5.4 Results

5.4.1 Variability of thymidine and thymidine phosphorylase levels in lung and colorectal tumour xenografts

Tumour thymidine concentrations varied widely from very high in the SW620 model (mean 2233 ng/g ± 458) to consistently very low concentrations in the HT29 model (mean 0 ng/g ± 0). Levels in A549 and Calu6 were generally low (mean 114 ng/g ±

161 and 166 ng/g ± 152 respectively) but showed some variability. TP activity was lowest in SW620 xenografts (Figure 5-1).

Figure 5-1: Variability in tumour thymidine and TP in four cell lines.

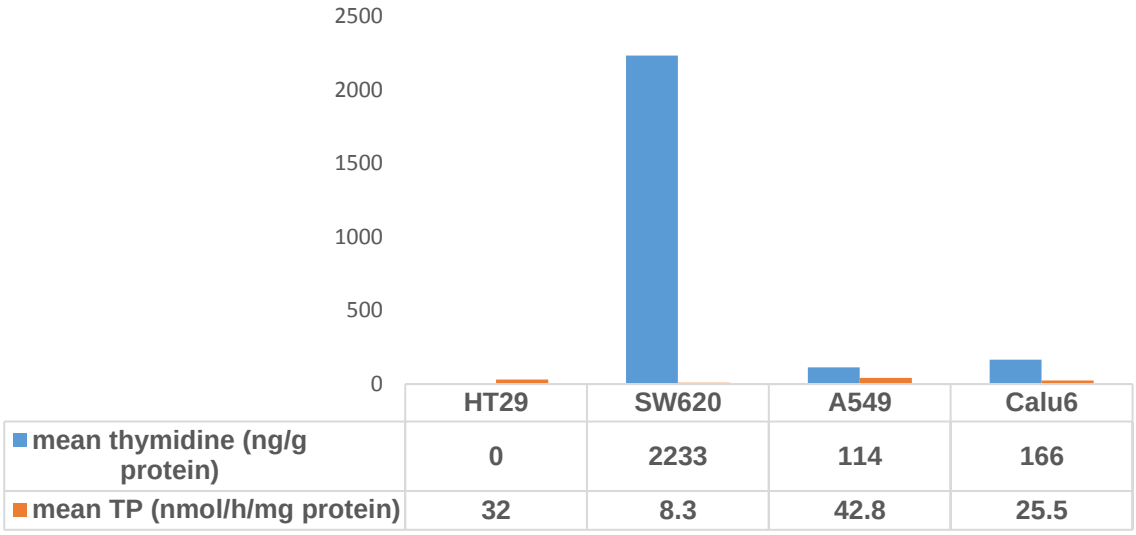

	HT29	SW620	A549	Calu6
mean thymidine (ng/g protein)	0	2233	114	166
mean TP (nmol/h/mg protein)	32	8.3	42.8	25.5

5.4.2 Effect of increasing doses of thymidine phosphorylase on plasma thymidine concentration

For the thymidine and TP assays, the limits of detection were: 0.5 µmol / l for thymidine (tissue and plasma) and 1.2 nmol / ml for TP (tissue and plasma). TP administration of 20 IU produced a 2 – 3 fold increase in TP activity and 200 IU resulted in a 10 – 20 fold increase at 24 hours. Despite the increased plasma TP activity, there was no reduction in plasma thymidine concentration at 24 hours compared with controls (Table 5-1).

Table 5-1: Plasma thymidine and TP levels following increased doses of exogenous TP

Sample ID	Thymidine (µmol/l)	Thymidine phosphorylase activity (nmol/hour/mL)
Control Plasma (1P)	1.0	1.5
Control Plasma (2P)	1.3	1.2
Plasma 20 IU TP (3P)	1.2	3.8
Plasma 20 IU TP (4P)	0.8	2.6
Plasma 200 IU TP (5P)	1.2	9.9
Plasma 200 IU TP (6P)	0.9	22

Figure 5-2: Mean plasma thymidine and TP activity in SW620 tumour-bearing mice (n = 3) 24 hours after increasing doses of TP (100 IU, 250 IU, 500 IU, 1000 IU).

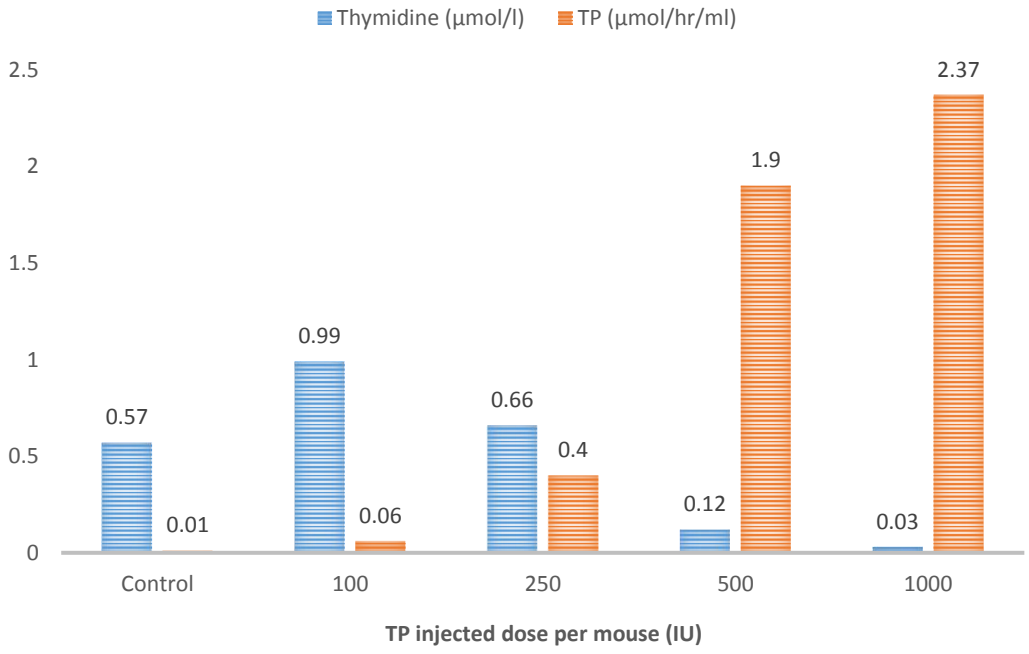

Following further increasing doses of exogenous TP, an increase was seen in the plasma and tumour TP activity which was associated with a fall in plasma thymidine concentrations at 24 hours (Figure 5-2).

In the control animals, mean ± SD tumour thymidine in this experiment was 2966 ± 588 ng/g tissue weight (three replicates), which compares with 2233 ± 458 ng/g tissue wet weight from an earlier experiment. Following 100 IU, 250 IU, 500 IU and

1000 IU TP, mean ± SD tumour thymidine concentrations of 1565 ± 265, 1591 ± 488, 1063 ± 330 and 1085 ± 560 ng/g tissue wet weight were recorded (n = 3).

5.4.3 Plasma thymidine and TP levels following single or serial injections of TP

A single dosing with 50 IU TP per mouse increased plasma TP at 3 and 6 hrs, and depleted plasma thymidine. The plasma TP activity was undetectable at 24 and 48 hours (Figure 5-3). Within tumour tissue, TP activity peaked 3 hours post injection, after single (mean 264 ± 25 nmol / hr / mg protein) and daily dosing (mean 368 ± 43 nmol / hr / mg protein).

Figure 5-3: Mean plasma thymidine (µmol / l) and mean thymidine phosphorylase (µmol / hr / ml) levels at 3 and 6 hours after a single dose of 50 IU TP injection, or 5 daily doses of 50 IU TP. Plasma thymidine was undetectable (< 0.5 µmol / l) at 3 and 6-hours (n = 3).

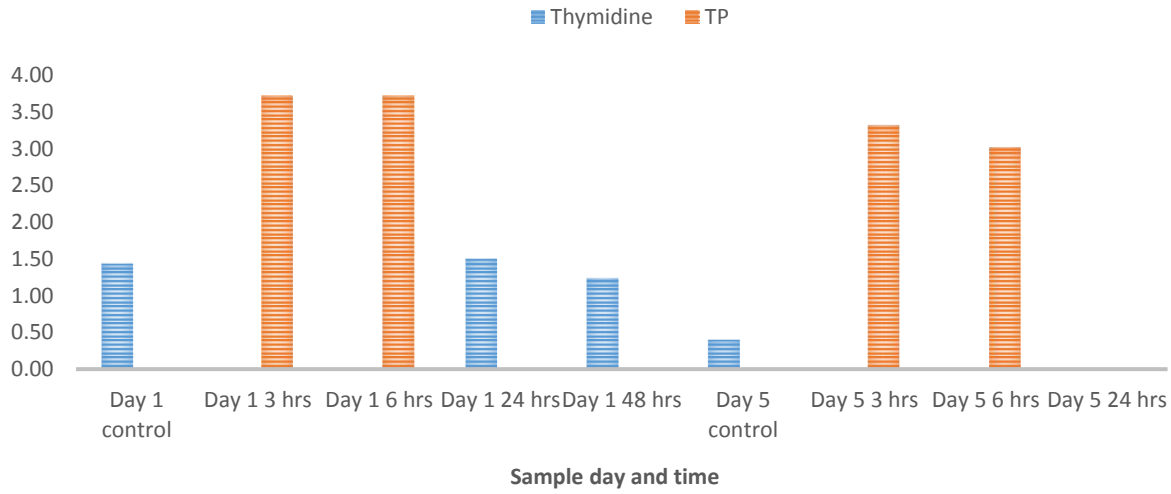

5.4.4 Pilot study to determine the effect of TP administration on SW620 tumour FLT uptake as measured by small-animal PET

The accumulation of FLT was assessed in SW620 tumour-bearing mice and tracer uptake was low. Following injection of 1000 IU TP, there was increased FLT tracer retention within the tumour xenografts, and physiological uptake within bone marrow, gut and spleen (Figure 5-4).

Figure 5-4: FLT PET imaging following 1000 IU TP administration. Top panel – 1 hour after TP injection. Middle panel – 4.5 hours after TP injection. Bottom panel - control, showing uptake within bladder only. The top two panels demonstrate increased tracer retention in tumour, bone marrow, gut and spleen. White arrows indicate the tumour. Red arrow indicates the bladder.

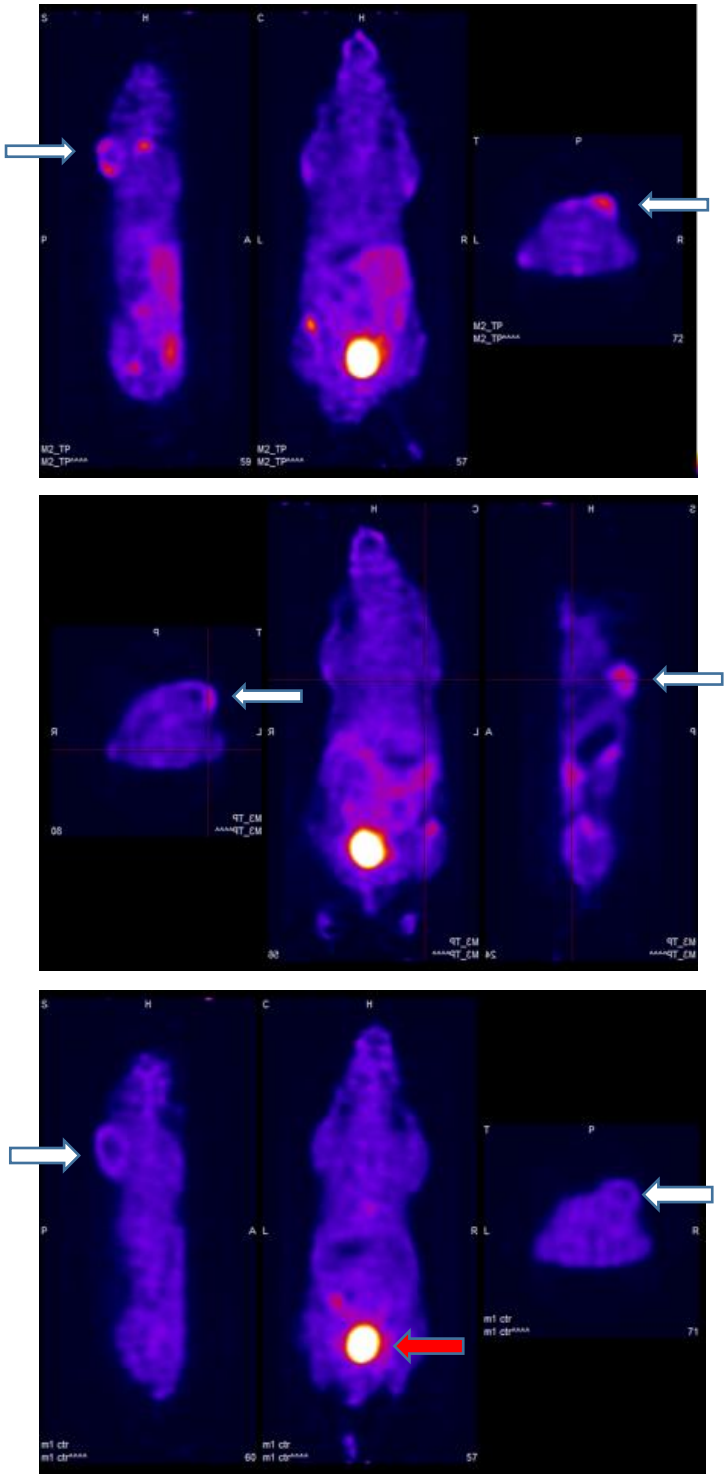

5.5 Discussion

In this study, the principal objective was to evaluate the impact of administering exogenous thymidine phosphorylase on tumour thymidine levels and tumour FLT uptake. First, tumour thymidine and TP activity levels were determined in four different tumour xenografts to select a cell line for further evaluation. Thymidine concentrations in control A549 tumours have been reported to be either low (~1 μM) or higher (~10 μM), with more tumours having lower levels, as in our study (Schelhaas *et al.*, 2014a). Overall, the tumour thymidine concentrations measured in our study were 0 – 2628 ng/g tumour. Similarly, Zhang *et al* reported a comparable range of ~ 100 – 1500 ng/g (Zhang *et al.*, 2012b).

TP expression in tumours is also variable. Of 85 non-small cell lung tumours studied, 45 tested positive for TP (Lee *et al.*, 2014b). In our study, the values obtained for intrinsic tumour thymidine phosphorylase levels in the A549 and HT29 cell lines were high, (42.8 and 32 nmol /h / mg protein respectively) consistent with the literature. TP levels are reported to be high in A549 tumours with a high FLT/ thymidine uptake ratio (Lee *et al.*, 2014b; Schelhaas *et al.*, 2014b). Furthermore, Lee and colleagues reported that TP expression was not associated with age, sex, tumour diameter, histological type or Ki-67 score. In contrast, FLT PET SUVmax correlated with tumour size, % Ki-67 expression and TP score. In our study, the tumour with the lowest TP activity was SW620, which had the highest thymidine level, and hence was selected for further evaluation. Consistent with this finding, SW620 tumours have been reported to show very poor FLT uptake *in vivo* (Lee *et al.*, 2011).

Prior to investigating the effect of TP administration on FLT PET scans the maximal tolerated dose of TP was established in athymic nude mice. The formulation of the TP was changed due to concerns regarding the level of endotoxin present which caused unexpected mouse death immediately following TP injection. Levene *et al* investigated the systemic toxicity of intermittent iv dosing with EE-TP in mice and Beagle dogs (Levene *et al.*, 2013). Temporary immune-based reactions were observed in the dogs. Additionally, this group reported evidence of thrombo-embolic disease in treated and control mice at post-mortem; however, the severity was higher in treated mice and one mouse died of this complication. We considered the reason for early mouse death in our study was due to circulatory collapse secondary to a thrombo-embolic event. With the availability of a newer formulation TP, retitration of

the TP dose was undertaken, with no adverse effects. Going forward the potential of immune-based side-effects should be monitored. Reassuringly, initial clinical work using the newer TP formulation has been reported and no serious adverse sequelae have been observed (Bax *et al.*, 2013). Pharmaceutical companies have recognized the therapeutic potential for erythrocyte–encapsulation of drugs and are investigating its utility providing further support that EE-TP could be incorporated into clinical practice (Bourgeaux *et al.*, 2016).

To evaluate the optimal TP dosing schedule a time-course experiment demonstrated that dosing for 5-consecutive days resulted in higher plasma and tumour TP activity, compared with a single injection. However, this did not affect plasma thymidine levels. Following a single dose of TP, sampling at 3 and 6 hours demonstrated undetectable plasma and tumour thymidine and elevated TP levels, suggesting that the optimal time to image would be during this interval. Furthermore, a single higher TP dose was sufficient to achieve undetectable thymidine levels.

Finally, the impact of administering TP on FLT uptake in a xenograft model was investigated in a pilot experiment and promising data were generated. Administration of TP reduced plasma and tumour thymidine levels in SW620 tumours supporting the inverse relationship between thymidine and TP, and previous studies demonstrating that TP inhibition increases thymidine levels by 3 – 45-fold (Lee *et al.*, 2014b). High tumour TP activity has been associated with a high FLT / thymidine uptake ratio (Lee et al., 2014), and an inverse relationship between intra-tumoural thymidine levels and FLT avidity has been observed (Zhou *et al.*, 2013).

Tumours with low or high TP levels may demonstrate similar FLT uptake, lending support to the argument that many factors influence FLT uptake and that we do not yet fully understand the interactions and relative importance of each. Recently, a multi-centre study has demonstrated that levels of tumour thymidine alone do not account for differences in FLT accumulation in murine cancer models, and a further factor which may influence FLT retention in tissues is thymidine kinase 1 activity or expression (Heinzmann *et al.*, 2016). TP inhibition has been reported to have no effect on TK1 or ENT-1 activity and there is no correlation between TK1 activity and FLT retention in tissues (Brockenbrough *et al.*, 2011; Lee *et al.*, 2014b). In contrast, Rasey *et al* observed that FLT uptake was strongly associated with TK1 expression (Rasey *et al.*, 2002). These authors studied A549 cells and observed that when only

3 – 5% of cells were in the S-phase, TK1 activity was low and FLT uptake was poor. Conversely, when cells were stimulated to divide, there was a strong correlation between TK1 activity and FLT uptake. This correlation is unsurprising, given the well-established relationship between TK1 activity and cell proliferation (Sherley and Kelly, 1988).

Prior to clinical development of exogenous TP to improve FLT PET scanning in patients with cancer, further evaluation of its angiogenic potential at clinical doses is warranted.

5.6 Conclusions

Previous studies have shown that SW620 tumours have high tumour thymidine levels and are poorly FLT-avid, questioning the utility of FLT as a useful radiotracer in this tumour group. In the experiments described in this chapter, endogenous tumour thymidine levels can be reduced by simple thymidine phosphorylase dosing and the SW620 tumours can be visualised on FLT PET. Further work to evaluate FLT PET as an imaging biomarker of response in this cell line is underway by the imaging research group based at Newcastle University, Imperial College and St George's Hospital.

Chapter 6 Diffusion-Weighted MRI as a predictive and early response biomarker in muscle-invasive bladder cancer: MARBLE study

6.1 Introduction

DW-MRI is a non-invasive imaging modality which is sensitive to the diffusion of water molecules (Le Bihan *et al.*, 1988). Quantification of diffusion measurements is increasingly used to evaluate treatment effects. Quantitative measurements in DW-MRI rely on the apparent diffusion coefficient (ADC), a value which reflects the mobility of the water molecules. The ADC is calculated from the exponential decay of signal intensity with increasing *b*-value and illustrated on a map generated by the MRI scanning software, or off-line analysis (Bollineni *et al.*, 2015). The diffusion coefficient is referred to as “apparent” due to the existence of factors other than the movement of water molecules which impact on diffusion: blood flow and diffusion; active transport; and cardiorespiratory movement (Padhani *et al.*, 2009). There is no optimal set of *b*-values for the acquisition of DW-MRI sequences because of the dependence on the tissue under investigation and signal to noise ratio (SNR). Further to a National Cancer Institute (NCI) – sponsored open consensus meeting held during the 2008 International Society for Magnetic Resonance in Medicine Meeting, it was recommended that three or more *b*-values should be used, which includes b = 0 s/mm^2, b ≥ 100s/mm^2 and b ≥ 500 s/mm^2 (Padhani *et al.*, 2009). Table 6-1 summarizes recommended b-values for DW-MRI protocols according to anatomical site. It is widely acknowledged that institutions tend to use their own MRI parameters and this is reflected in the varied *b*-values reported in the literature.

Water molecules move freely within blood vessels and urine, resulting in high diffusion and higher ADC values. In general, tumours have lower ADC values than normal tissues, and threshold values differ between primary sites. Highly cellular tumours have restricted diffusion and are bright on high *b*-value images as a result of high signal intensity which yields a low ADC value. Effective treatment results in tumour necrosis and membrane disruption which increases the extracellular space. This results in increased movement of water molecules and a rise in ADC (Nakayama *et al.*, 2008; Braithwaite *et al.*, 2009).

Table 6-1: *b*-values for qualitative tumour evaluations. Reproduced with kind permission from Professor A Padhani.

***b* Values (sec/mm^2)**	**Anatomic Regions**
> 1000	Brain, prostate, uterus, cervix, lymph nodes
750 – 1000	Brain, neck, breast, chest, general abdomen (including colorectal, pancreas, kidneys, peritoneum), lymph nodes, pelvis (including prostate, uterus, cervix, ovaries, bladder). Also for whole-body imaging (diffusion-weighted whole-body imaging with background body signal suppression)
100 - 750	Liver (primary and metastatic disease)
< 100	Used for the detection of liver lesions (“black blood technique”)

The treatment effect can be measured and is the ratio of change in ADC to the pre-treatment value;

$$Treatment\ Effect = \frac{(post - treatment\ ADC) - (pre - treatment\ ADC)}{pre - treatment\ ADC}$$

Demonstrating a treatment effect at the earliest opportunity could spare patients the unnecessary toxicity from ineffective treatments and contribute to personalised medicine by tailoring therapies. Assessing treatment effectiveness is generally based on criteria which use anatomical measurements. Due to the growing number of cytostatic treatments there is an increasing need to develop useful imaging BM to evaluate treatment responses.

Related to the treatment effect is the coefficient of variation (CoV). The CoV is a statistical term which can be used to compare the degree of variability in one set of results with another, and is the ratio of standard deviation to the mean;

$$CoV = \frac{standard\ deviation}{mean}$$

Repeatability value is defined as the range in which 95% of measurements will fall, (1.96 x CoV), assuming no treatment effect (Morgan *et al.*, 2006).

The MARBLE trial has studied patients with muscle-invasive bladder cancer. As described in Chapter 1, the majority of patients are over 60 years of age which has implications for suitability for treatment due to the presence of co-morbidities. Outcomes remain poor with overall five-year survival figures of 50%, and 10 – 30%

for more advanced tumours (T3 or T4, or lymph node positive) (Stein, 2006; NICE, 2015). For many years, definitive treatment of MIBC has consisted of surgical removal of the bladder, known as radical cystectomy (RC) preceded by three cycles of neoadjuvant chemotherapy (NAC). The NAC is given to patients with good performance status and confers a 5 – 7% survival benefit (Sherif *et al.*, 2004; Vale, 2005). In our institution, patients are routinely re-staged to confirm suitability for surgery, after two or three cycles of chemotherapy, with CT of chest, abdomen and pelvis to exclude progression of disease. Pathological complete responses to chemotherapy are associated with greatly improved outcomes relative to patients with residual disease at time of RC (Grossman *et al.*, 2003; Sonpavde *et al.*, 2009; Meeks *et al.*, 2012). Identifying treatment failures at an early opportunity could direct these patients towards surgical management and not organ preservation with RT. In light of recent studies published since the design of the MARBLE study, patients are now offered radical radiotherapy with or without concurrent chemotherapy as an alternative to surgery (Choudhury and Cowan, 2011; James *et al.*, 2012; Smith *et al.*, 2013; Ploussard *et al.*, 2014).

6.2 Objectives

The MARBLE study was designed to investigate the predictive, prognostic and early response potential of DWI and DCE-MRI in a cohort of bladder cancer patients planned to receive neoadjuvant chemotherapy. The primary objective was to assess the feasibility of performing serial quantitative MRI scans in patients with bladder tumours, prior to and early in the course of cytotoxic treatment. Secondary objectives included determining the repeatability measurement errors for DW-MRI; correlating baseline MRI parameters and Ki-67 with pathological or radiological assessment of response after two or three cycles of chemotherapy, overall survival and progression-free survival; and investigating whether the changes in MRI parameters after one or two cycles of chemotherapy related to treatment response, overall survival and progression-free survival.

6.3 Methods

6.3.1 Study Participants

This prospective study was conducted in accordance with The Code of Ethics of the World Medical Association (Declaration of Helsinki) for experiments involving

humans. Ethical approval was gained from the local ethics committee (REC reference 13/NE/0007 and IRAS project ID 100429). The study was sponsored by Newcastle upon Tyne Hospitals NHS Foundation Trust (NUTH) and was undertaken at the Northern Centre for Cancer Care (NCCC), Freeman Hospital, Newcastle upon Tyne, UK. Participants were identified in the NUTH Uro-oncology Multidisciplinary Team Meeting.

Eligibility criteria were:

T2-T4a N0-2 M0 muscle-invasive bladder cancer according to UICC TNM Seventh Edition (2009) (Table 6-2)

- residual disease post transurethral resection of bladder tumour (TURBT) determined by examination under anaesthetic at time of TURBT
- patients planned to receive three or four cycles of neo-adjuvant or down-staging cisplatin-based chemotherapy followed by radical cystectomy or radiotherapy

Patients were excluded if they were unable to give fully informed consent or unable to tolerate an MRI scan. A sub-group of patients were consented into the MARBLE 18F-FLT Sub-study which was described in Chapter 2.

Table 6-2: TNM staging of bladder cancer. [Guideline] National Comprehensive Cancer Network. NCCN Clinical Practice Guidelines in Oncology: Bladder Cancer V. 2.2015. Accessed: May 14th, 2016.

Primary tumour (T)	
TX	Primary tumour cannot be assessed
T0	No evidence of primary tumour
Ta	Non-invasive papillary carcinoma
Tis	Carcinoma in situ: “flat tumour”
T1	Tumour invades subepithelial connective tissue
T2	Tumour invades muscularis propria
pT2a	Tumour invades superficial muscularis propria (inner half)
pT2b	Tumour invades deep muscularis propria (outer half)
T3	Tumour invades perivesical tissue
pT3a	Microscopically
pT3b	Macroscopically (extravesical mass)
T4	Tumour invades any of the following: prostatic stroma, seminal vesicles, uterus, vagina, pelvic wall, abdominal wall
T4a	Tumour invades prostatic stroma, uterus, vagina
T4b	Tumour invades pelvic wall, abdominal wall
Regional lymph nodes (N)	
Regional lymph nodes include both primary and secondary drainage regions. All other nodes above the aortic bifurcation are considered distant lymph nodes.	
NX	Lymph nodes cannot be assessed
N0	No lymph node metastasis
N1	Single regional lymph node metastasis in the true pelvis (obturator, internal iliac, external iliac, or presacral lymph node)
N2	Multiple regional lymph node metastasis in the true pelvis (obturator, internal iliac, external iliac, or presacral lymph node metastasis)
N3	Lymph node metastasis to the common iliac lymph nodes
Distant metastasis (M)	
MO	No distant metastasis
M1	Distant metastasis

6.3.2 Ki-67 measurements

Ki-67 scores were performed by the NUTH pathology department on the diagnostic biopsy specimens which had been obtained at the time of transurethral resection of bladder tumour (TURBT) prior to chemotherapy. The specimens were fixed in 10% formalin, embedded in paraffin for routine haematoxylin and eosin (HE) and immunohistochemistry (IHC) staining. IHC staining was performed by the immunoperoxidase procedures (avidin-biotin-complex methods) to enable detection of Ki-67 using an automated staining system (Ventana Medical Systems, Inc., Tuscon, AZ, USA) as *per* manufacturer's protocol. The deparaffinized and rehydrated sections were heated to 37°C for 60 min in Tris-EDTA buffer (pH 8.5) for antigen retrieval followed by application of the MIB-1 antibody (MMI 1:100, mouse, monoclonal, Dako, UK). The I-VIEW/DAB detection system was used to detect antigen-antibody complexes. The IHC stained sections were evaluated in a blinded manner without knowledge of the PET-CT findings by one pathologist with 6 years of experience in pathological evaluation, and then reviewed by a second pathologist with 17 years experience. Tumour volume and morphology were recorded across blocks. Mean Ki-67 was calculated in a cut section of multiple blocks from each specimen. All reactive nuclei were considered positive, irrespective of their intensity. IHC was evaluated semi-quantitatively using a scoring system with 5% steps.

6.3.3 MRI Scanning

Each patient was scheduled to attend one baseline and two early response MRI scans; post treatment scans were scheduled 10 -17 days after the first and second cycles of NAC. All MRI scans were performed on the same Siemens 1.5-Tesla Espree system using a body array 6-element design coil with six integrated preamplifiers, and patients were requested to have a comfortably full bladder. T1-weighted, T2-weighted, DW-MRI and DCE-MRI sequences were acquired at each visit, assuming renal function was adequate for contrast (glomerular filtration rate > 30 ml/min) (Figure 6-1). A repeatability DW-MRI was included in the pre-treatment protocol. The coffee-break approach was used which involved the patient dismounting from the scanning couch and returning after a short walk around the scanning department. Images were obtained of the pelvis up to lumbar vertebrae level L3/4, ensuring bladder and local pelvic lymph nodes were encompassed. Images were obtained in two blocks:

- Inferior: symphysis pubis to L5 / S1
- Superior: L5 / S1 to L3 / 4

T1-weighted (repetition time TR 541 / echo time TE 13 ms, 6 mm slices) and T2-weighted (TR 3500 ms / TE 109 ms, 6 mm slices) sequences were anatomically matched to the DW-MRI slices for the analysis. In the first two trial patients, DW-MRI was performed using an imaging sequence with 4mm slice thickness, TR 3200 ms / TE 104 ms, matrix 128x128, and 60 images per series with *b*-values = 200, 800, 1500 seconds / mm^2 and free-breathing. To improve signal to noise ratio, the sequence was modified to 6mm slice thickness, TR 8000 ms / TE 86 ms, matrix 256 x 224 and 26 images per series with *b* = 0, 100, 500, 900 seconds / mm^2. Figure 6-2 demonstrates a higher signal to noise ratio, using *b* = 0, 100, 500, 900 seconds / mm^2. These scanning protocols generated on-bed scan times of 47 minutes for the baseline scan, excluding time off the bed for repeatability measurements, and 30 minutes for the two response scans.

Figure 6-1: MARBLE T2-W sagittal view of tumour within trigone of bladder (denoted by arrow)

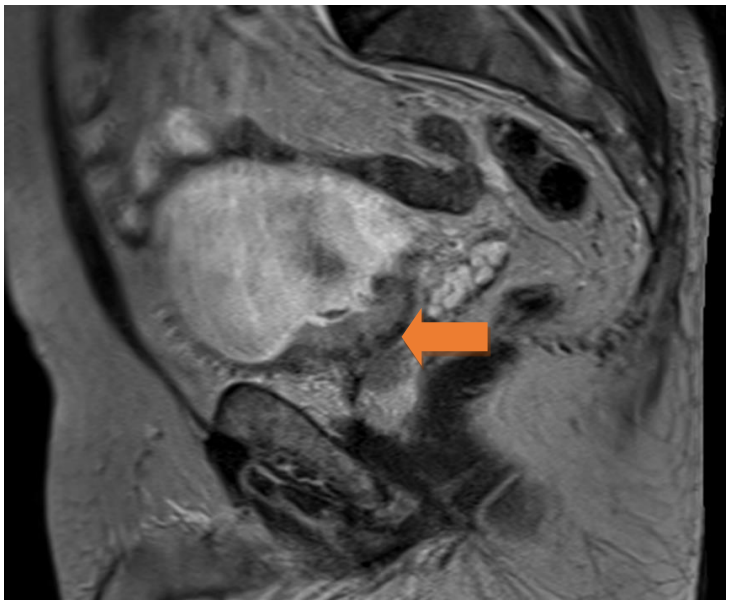

Figure 6-2: MARBLE comparison of ADC maps derived from b-values 200, 800, 1500 (middle panel) and 0, 100, 500, 900 mm/s2 (right panel) resulting in a mean tumour ADC difference of 40%. Left panel shows anatomically-matched T2-W sequence. Tumour indicated by red arrow.

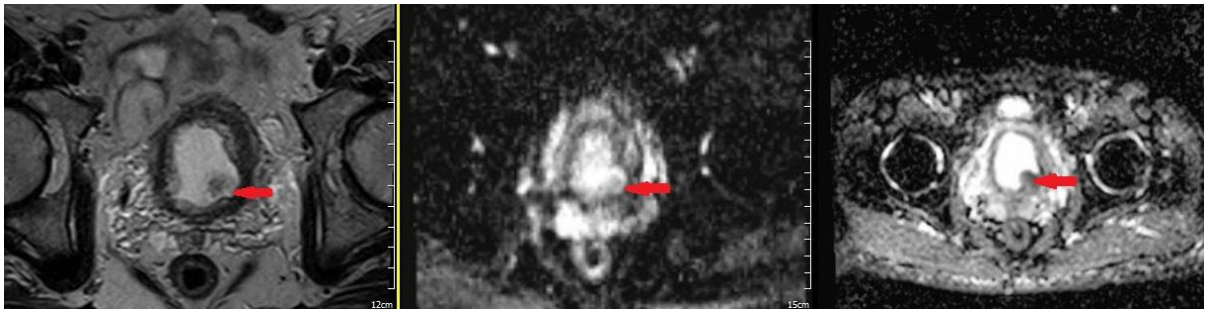

6.3.4 Diffusion-Weighted MRI image analysis

An MRI radiologist with more than twenty years of experience reported all research scans within seven days of the scan being acquired, commenting on structural and functional findings. Incidental findings were acted on by the responsible clinical team and are discussed at the end of this chapter. The diffusion-weighted images were processed in open-source medical image processing software OsiriX v.5.8.2 32-bit, revision 20131218, www.pixmeo.pixmeo.com) by the author who has more than 5 years of experience of target volume definition for radiotherapy planning. A region of interest (ROI) based analysis was used. ROIs were defined manually using the polygon tool on every T2-weighted slice where there was visible tumour or, in the case of the response scans if no overt tumour was identified, the tumour bed. Tumour bed was identified as an area of thickening or enhancement located in the region known to have tumour from previous scans. ROIs were transferred to anatomically-matched DW-MRI sequences. Whole tumour mean, minimum and maximum ADC measurements were derived from the ADC map produced by the MRI Siemens Syngo MR B19. The Siemens system calculated the ADC pixel by pixel by linear regression to yield an ADC map. On a half logarithmic scale, the slope of the signal decay provided the ADC. ROIs on each axial slice were analysed separately then summed to derive volume-based data for whole tumour measurements. Additional assessments of ADCs using the OsiriX plug-in tool using two alternative methods were undertaken; T2-W ROIs were applied to the diffusion sequence opened within 4D-Viewer, and ADC values obtained; secondly, an ADC map was generated, the ROIs applied and measurements recorded. The ADC map is a fit to Si = exp (-bi*D) for signal and monoexponential fit, where Si referred to the signal intensity from images acquired with different diffusion weighting and bi and D the

diffusion coefficient. This is a direct fit if 2 *b*-value images are given, or a least squares fit to log (Si)vs – (bi*D).

A comparison of single-slice and whole tumour mean ADCs was undertaken to evaluate if a measurement taken in the central slice of the tumour volume could be representative of the entire tumour. Where there were an even number of slices, the larger slice was selected. These measurements were systematically compared with ADCs obtained from the whole tumour.

To compare study findings with the literature, a range of normal tissue measurements were obtained. Circular regions of interest of varying diameter were placed over tumour, bladder and femoral head to calculate ADC value, shown in Figure 6-3. Repeatability of the DW-MRI measurements was assessed by comparing volume, mean and minimum ADC values of tumours from the two scans performed at baseline. In view of the variability in mean ADC values which is dependent on *b*-values used, percentage changes in ADCs were analysed, not the absolute values.

The resulting quantitative and qualitative data were compared with clinical outcome and Ki-67 histological data from the initial biopsy specimen.

Figure 6-3: MARBLE ROIs defined on tumour in anterior wall of bladder, ilium and rectus abdominus, on ADC map (left panel) and T2-W MRI (right panel)

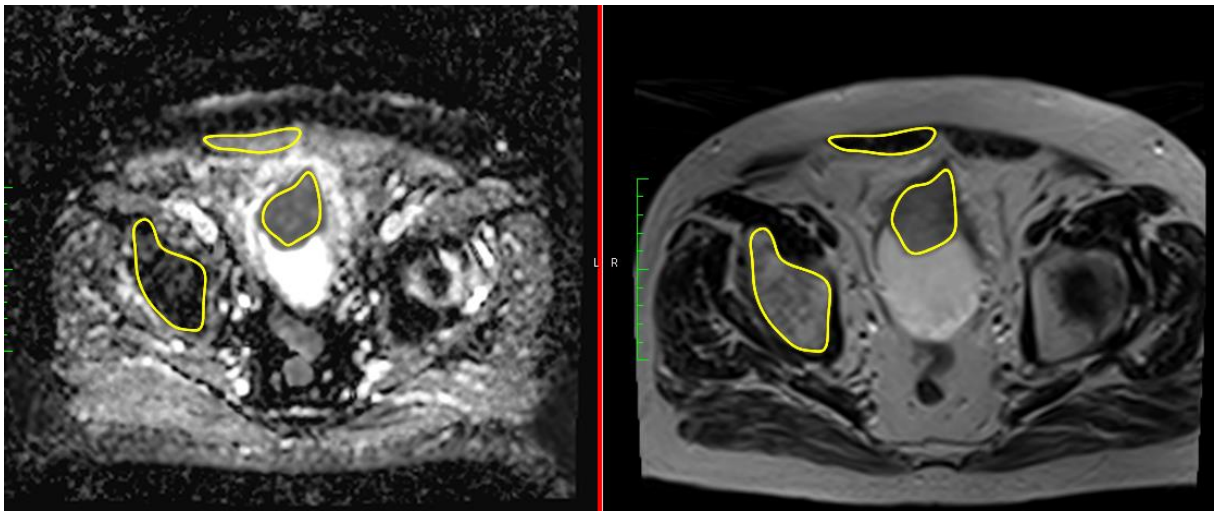

6.3.5 Treatment response evaluation

To compare with the research scans, routine CT scans were acquired pre TURBT and after three cycles of chemotherapy. Participants were defined as either treatment responders or non-responders according to appearances on CT or on the surgical specimen. Radiological treatment responders were defined by shrinkage in tumour

volume measurements, and as non-responders if there was stable or progressive disease on the CT scan. According to RECIST 1.1 criteria, response is defined by a 30% or more decrease in maximal tumour diameter, and no response is less than 30% decrease (Eisenhauer *et al.*, 2009). Maximum primary tumour thickness perpendicular to bladder wall and bladder dimensions were recorded for all scans by the author. An objective pathological assessment of chemotherapy response was undertaken at the time of radical cystectomy or, if the patient had radical radiotherapy, several months later, with a surveillance cystoscopy inspecting the bladder for evidence of neoplasia. Pathological non-responders had ≥ pT2 disease at time of cystectomy (Hafeez *et al.*, 2016). Because pathological grading is the gold standard, where this was available it over-ruled the radiological response if results differed.

6.3.6 Statistical analysis

The demographic, treatment and imaging details of the study participants were analysed using the IBM SPSS v22 statistical package. Mean change and CoV of ADC were calculated and expressed as percentages. Repeatability value was evaluated as = 1.96 x CoV. To test for differences between the baseline, repeated, and first response scans, a paired samples T-test was used. The second response scan data were not normally distributed; therefore the Wilcoxon signed ranks test was applied. Correlation analysis was undertaken to assess the association between the following parameters: Ki-67 score, mean ADC, tumour volume, change in ADC, change in volume between the scans, and length of follow-up. Excluding Ki-67 score, data were not of normal distribution so the Spearman's correlation coefficient was calculated. Findings were considered significant at the 0.05 level (2-tailed). Sigma Plot 12.5 was used to perform ROC analysis and Bland-Altman analysis. ROC curves were used to determine a cutoff value for a clinical test; sensitivity was plotted on the y-axis *versus* 1-specificity on the x-axis. A Bland-Altman plot was used to compare the repeated DW-MRI measurements, and the single versus multi-slice measurements. Horizontal lines were drawn at the mean difference and at the limits of agreement, defined as mean difference plus or minus 1.96 times the standard deviation of the differences, as described by *https://www.medcalc.org/manual/blandaltman.php.*

6.4 Results

6.4.1 Study population

Eighteen patients with muscle-invasive bladder cancer were recruited to the MARBLE trial between 5 April 2013 and 22 October 2015. Patient characteristics and treatment details can be found in Tables 6-3 to 6-5. The majority of patients received two or three cycles of neoadjuvant chemotherapy followed by either radical cystectomy (RC) or chemoradiotherapy (CRT). Three patients were unsuitable for curative treatment due to metastatic or inoperable disease diagnosed on the baseline research scan and continued on palliative chemotherapy. Five patients did not complete the intended courses of chemotherapy for the following reasons: deterioration in performance status and not fit enough to commence chemotherapy (n = 1); allergic reaction to chemotherapy (n = 1); identification on baseline MRI of a fistula between bladder and bowel which was a contra-indication to chemotherapy (n = 1); non-haematological toxicity (n = 2). Fifteen patients received two or more cycles of chemotherapy and attended for one or more follow up research scans. Response evaluation was defined radiologically on CT (n = 10) or pathologically from the surgical specimen (n = 5). Pathological correlation of imaging from radical cystectomy (RC) was available in three patients who completed three cycles of NAC, and in two patients who received two cycles. Overall, there were 11 treatment responders, and 4 non-responders after two or more cycles of chemotherapy. Figure 6-4 summarises the management of the MARBLE cohort of patients. Median follow-up was 13.5 months (range 1 – 40, mean 17.8) from time of consent into the study to last follow-up appointment or date of death (data censored on 24 September 2016).

Table 6-3: MARBLE characteristics of study participants; NAC = Neoadjuvant chemotherapy, S = surgery, CRT = chemoradiotherapy

	n	%
Gender		
Male	12	66
Female	6	33
Age (years)	Mean 59 years	Range 37 – 72 years
T stage		
T2	5	28
T3/4	13	72
N-stage		
N0	12	66
N1	5	27
N2	1	6
Ki-67		
< 70%	4	22
70– 89%	9	50
≥90%	5	28
Definitive Treatment		
NAC - CRT	7	39
NAC - S	5	28
Other	6	33
NAC dose intensity (n = 15)	Median = 3 cycles	Range 2 – 4 cycles
Treatment response (n = 15)		
Treatment responder	11	73
Treatment non-responder	4	27
No. of tumour-related events		
Distant metastases	8	44
Tumour-related death	6	33

Table 6-4: MARBLE characteristics and treatment details of individual study participants: m = male, f = female, NAC=Neoadjuvant chemotherapy, S = surgery, CRT = chemoradiotherapy, Pall CT = palliative chemotherapy, Gem/Cis = gemcitabine and cisplatin chemotherapy, Gem/Carbo = gemcitabine and carboplatin chemotherapy

Patient ID	TNM	Age	Gender	Ki-67	Chemo Regime	Number of cycles	Treatment Details
1	T2N0	67	m	60	Gem/Cis	3	NAC- Surgery
2	T3N1	67	m	90	Gem/Cis	4	NAC-CRT
3	T3N1	53	m	70	Gem/Cis	4	NAC-CRT
4	T2N0	72	m	70	Gem/Cis	3	NAC-CRT
5	T2N0	55	m	90	Gem/Cis	3	NAC-CRT
6	T2N0	43	m	8	Gem/Cis	2	NAC-Surgery
7	T4N0	53	f	75	Gem/Cis	3	Pall CT
8	T3N0	71	m	90	Gem/Cis	4	NAC-CRT
9	T3N1	67	f	85	Gem/Cis	2	NAC-Surgery
10	T3N0	52	f	90	Gem/Cis	0.5	Surgery
11	T2N2	67	m	85	Gem/Cis	4	NAC-Surgery
12	T4N0	66	m	85	Gem/Carbo	0	Nil
13	T3N0	59	m	75	Gem/Cis	3	NAC-Surgery
14	T3N1	45	f	70	Gem/Cis	0.5	Surgery
15	T4N0	37	f	90	Gem/Cis	6	Pall CT
16	T4N1	68	f	45	Gem/Cis	4	Pall CT
17	T3N0	64	m	80	Gem/Cis	3	NAC-CRT
18	T4N0	67	m	30	Gem/Carbo	4	NAC-CRT

Figure 6-4: MARBLE patient Cohort Treatment Pathway

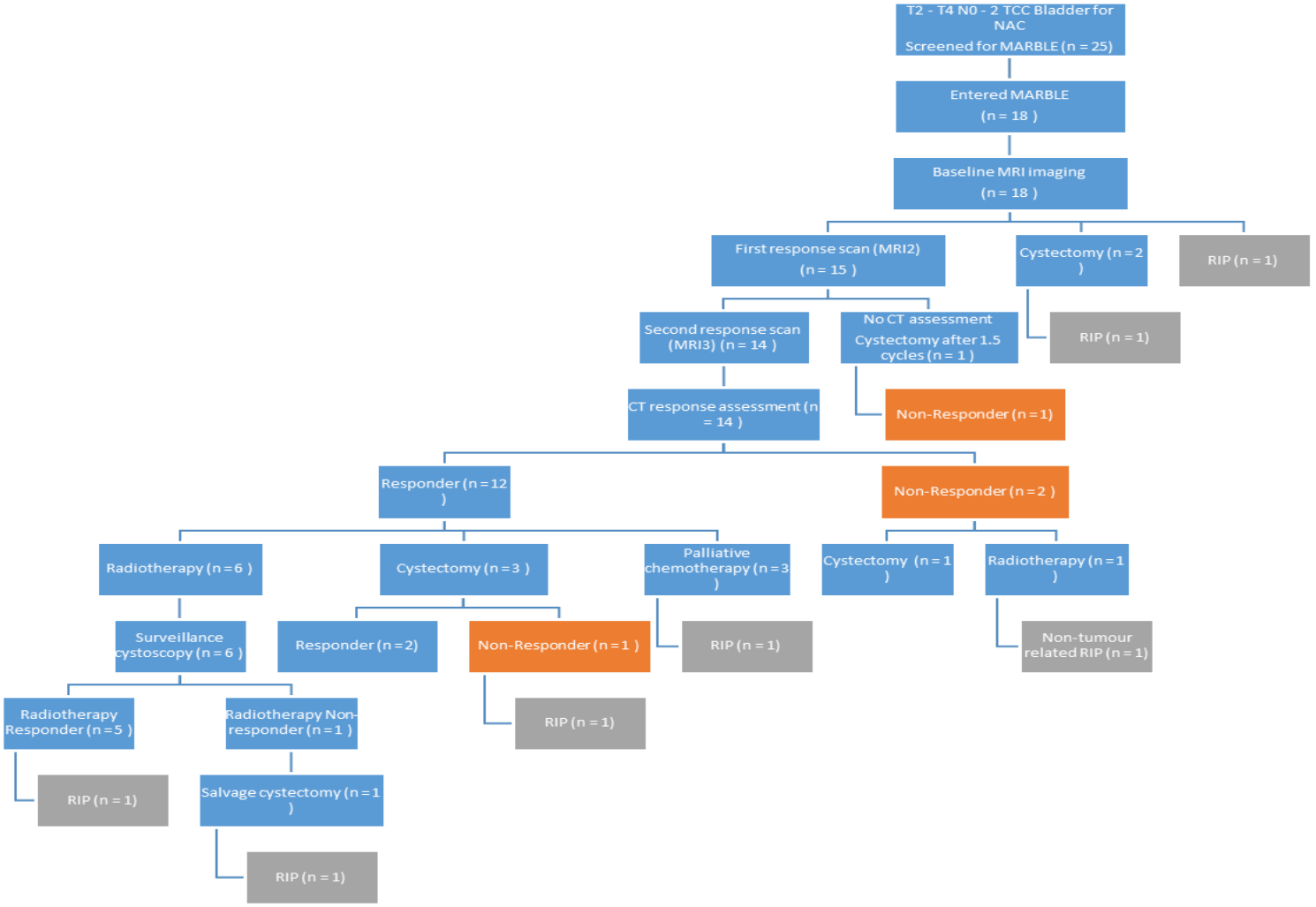

Table 6-5: MARBLE intervals between staging investigations, treatments and follow-up

Time interval	Mean ± SD	Range
TURBT - Consent into study (weeks, n = 18)	6.6 ± 3.9	1 – 18
MRI1 – D1 chemotherapy (days, n = 17)	7.5 ± 5	0 - 14
D1 Cycle 1 chemotherapy – MRI 2 (days, n = 15)	12 ± 2.2	9 – 15
D1 Cycle 2 chemotherapy – MRI 3 (days, n = 14)	12 ± 2	9 – 15
D1 Cycle 1 chemotherapy – restaging CT (weeks, n = 14)	8.4 ± 1.9	6 – 13
MRI 2 – restaging CT (days, n = 14)	49 ± 13	31 - 78
MRI 3 – restaging CT (days, n = 14)	24 ± 12	6 – 57
Restaging CT – surgery (days, n = 4)	31 ± 27	12 – 71
Consent – surgery (weeks, n = 7)	20 ± 17	6 – 56
Consent – last visit or time of death (months, n = 18)	19 ± 11	1 - 40
Consent – date of death (months, n = 7)	15 ± 10	1 - 28
TURBT – date of death (months, n = 7)	17 ± 10	2 – 30
Last day of radiotherapy to check cystoscopy (months, n = 6)	4.2 ± 1.7	2 – 7

6.4.2 Ki-67 measurements

Most cases had a high proliferation fraction and the intensity of the nuclear staining was moderate to strong. The median Ki-67 index was 80% and mean Ki-67 was recorded as ≥ 70% in 14 / 18 (78%) of the tumours. Of these, five had a Ki-67 of ≥ 90%. Only one case (MAR006) had a low number of stained nuclei estimated at 1 – 10%. In this case the areas of highest intensity were evaluated and the percentage of Ki-67 positive cells was visually counted in 1000 cells at high magnification amounting to 8% (Figures 6-5 and 6-6).

Figure 6-5: MARBLE low Ki-67 Score (MAR006 - High grade invasive urothelial carcinoma with squamoid and glandular differentiation, pT2, G2, Ki-67 8%, morphology similar throughout blocks). Left panel: histological specimen of TCC bladder stained with haematoxylin and eosin. Right panel: Ki-67 immunostaining of bladder tumour with a low proliferative rate.

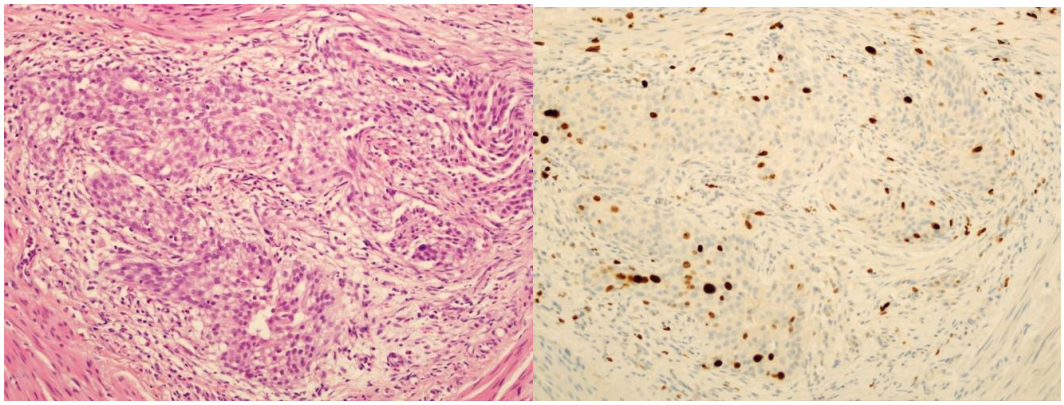

Figure 6-6: MARBLE high Ki-67 score (MAR005 - Invasive high grade urothelial carcinoma, pT2, G3, Ki-67 90%, morphology similar throughout blocks). Left panel: histological specimen of TCC bladder stained with haematoxylin and eosin. Right panel: Ki-67 immunostaining of bladder tumour with a high proliferative rate.

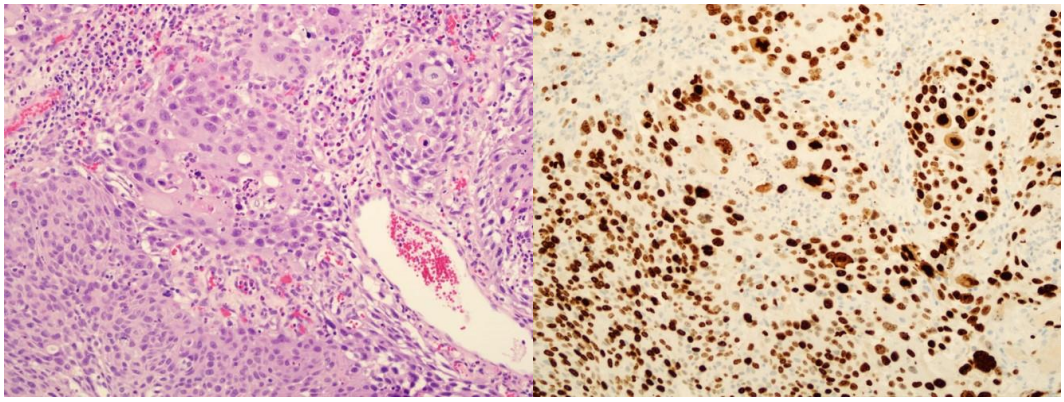

6.4.3 Tumour Response Evaluation

A mean interval of 8.4 weeks (range 6 - 13) elapsed between commencing chemotherapy and the reassessment CT scan, which is typical of routine practice in our institution. Two patients were scanned earlier than planned due to (1) additional information required on liver metastases (refer to Appendix), and (2) early termination of chemotherapy. Twelve tumours exhibited response treatment on radiology; however, one patient had a pT2 tumour at cystectomy so was categorised as a non-responder, similar to other reported studies. Overall, there were 11 responders and 4 non-responders. Three of the non-responders received less than two full cycles of chemotherapy, or carboplatin in place of cisplatin.

Seven patients were operated on, and the number of cycles of chemotherapy delivered was as follows: three cycles (n = 3); two cycles (n = 2); and less than one one full cycle (n = 2). Two of the three patients who received three cycles showed a complete pathological response to treatment. No tumours which were resected showed an increase in pathological size, consistent with the radiology findings.

In the patients who were treated with chemoradiotherapy, mean interval from last day of radiotherapy to first surveillance cystoscopy was 4.2 months (range 2 – 7, n = 6). One patient died before the cystoscopy. Residual disease was identified in one patient who then proceeded to salvage surgery with radical cystectomy. The interval between completion of radiotherapy and cystoscopy was 7 months in this patient. Restaging CT following three cycles of chemotherapy had shown persistent thickening in the region of the known tumour, but overall a response to treatment was recorded, due to a decrease in the number of tumours.

6.4.4 DW-MRI Image Analysis

Qualitative Assessment

If only the T1- and T2-weighted series were studied, lack of bladder distension resulting in detrusor muscle thickening limited detection of the primary bladder tumour in some cases. In each case they were small tumours (stage T2 before TURBT). Review of the DW-MRI and DCE-MRI sequences aided localisation so that all tumours could be contoured on the baseline imaging. Response DW-MRI data following the first cycle of chemotherapy were available in 15 patients, and following the second cycle in 14 patients. Mean interval between day 1 chemotherapy of cycle 1 or 2, and the first and second response MRI scans (MRI2 and MRI3 respectively) was 12 days (range 9 – 15).

Primary tumour

After the first cycle of chemotherapy, tumour shrinkage was identified by the radiologist in 33% of cases (5 / 15). After the second cycle, this increased to 86% (12 / 14), with 14% (2 / 14) stable disease (Table 6-6, Table 6-7). Qualitative assessment of MRI performed after one cycle of chemotherapy predicted 42% (5 / 12) of treatment responders defined by restaging CT performed six weeks later. One non-responder was classified as a treatment responder on both MRI after the second cycle, and CT after third cycle of chemotherapy, due to a decrease in tumour size

from size T3 at baseline. However, because the extent of disease was pT2 at surgery, this determined poor response.

Nodal Disease

Five patients were staged on baseline CT with node positive disease. The size of the involved lymph nodes ranged from 5 mm to 12 mm, and in all but one case, were solitary. MRI imaging identified two of the six nodal deposits. After one cycle of chemotherapy, one lymph node reduced in size by 2mm, and the other from 13 mm to 10 mm. After two cycles, these lymph nodes had shrunk further and were not detected.

Table 6-6: MARBLE qualitative response assessments on serial MRIs and CT after 1, 2, and 3 cycles of chemotherapy respectively. MRI2 = MRI performed after 1 cycle of NAC, MRI3 = MRI performed after 2 cycles.

	MRI2	MRI3	CT
Stable Disease	9	2	2
Response	5	12	12
Unclear	1	0	0
Not performed	0	1	1
Total	15	15	15

Table 6-7: MARBLE individual patient qualitative response assessments: MRI2 = MRI performed after 1 cycle of NAC, MRI3 = MRI performed after 2 cycles, SD = stable disease, R = response, ND = not performed, CR = complete pathological response, U = unable to assess due to lack of bladder distension limiting detection of bladder tumour

Patient ID	Chemo cycles	MRI2	MRI3	Restaging CT	Cystectomy
1	3	SD	R	SD	SD
2	4	R	R	R	
3	4	SD	R	R	
4	3	SD	SD	R	
5	3	R	R	R	
6	1.5	SD	ND	ND	SD
7	3	SD	R	R	
8	4	R	R	R	
9	1.5	R	R	R	SD
11	4	SD	R	R	CR
13	3	SD	R	R	CR
15	6	SD	R	R	
16	4	R	R	R	
17	3	U	R	R	
18	4	SD	SD	SD	

MRI imaging after two cycles of chemotherapy correctly predicted response to treatment in 12 / 14 patients who were subsequently defined by treatment response on CT after three cycles.

Table 6-8 displays the % change in tumour thickness between treatment responders and non-responders after one and two cycles. There was a trend between larger decreases in the responders, and again this was measurable after one cycle as shown in one patient in Figure 6-8.

Table 6-8: MARBLE percentage and absolute change in tumour thickness after 1 cycle (n = 15), and 2 cycles (n = 14) of neoadjuvant chemotherapy.

Tumour thickness	% Change after 1 cycle (absolute change in cm)		% Change after 2 cycles (absolute change in cm)	
	Responders n = 11	Non-responders n = 4	Responders n = 11	Non-responders n = 3
Mean	38 (1.1)	14 (0.2)	59 (1.6)	28 (0.63)
Median	42 (0.8)	12 (0.2)	50 (1.1)	31 (0.4)
Minimum	5.0 (0.1)	0 (0)	31 (0.5)	6 (0.1)
Maximum	86 (2.9)	33 (0.8)	100 (4.4)	58 (1.4)

Quantitative Assessment

There was no significant difference in mean ADC or tumour volume measurements between the baseline and repeated scans (Table 6-9). This was a consistent finding across all tumour sizes. Paired samples correlation was 0.96. Mean change in ADC across the entire tumour between the baseline and repeated scan was 1 ± 4%, generating a CoV of 7.5% and repeatability figure of 14.6%. A Bland-Altman plot showed mean differences between baseline and repeated ADC were mainly within 5% (Figure 6-7).

Table 6-9: MARBLE repeatability data from DWI-MRI (n=16, *b*-values 0, 100, 500, 900 mm/s^2)

	Baseline ADC ($x10^{-3}$ mm^2/s)	Repeated ADC ($x10^{-3}$ mm^2/s)	*p* value	Baseline tumour volume (cm^3)	Repeated tumour volume (cm^3)	*p* value
Mean	1.19	1.20	*p*=0.73	13.5	13.5	*p*=0.65
Range	0.84 -1.59	0.83 -1.47		2.6 - 57	2.5 – 50	

Figure 6-7: MARBLE Bland-Altman plot of mean difference between the baseline and repeated ADC. 95% CI = -0.05 - 0.06, SD = 0.06

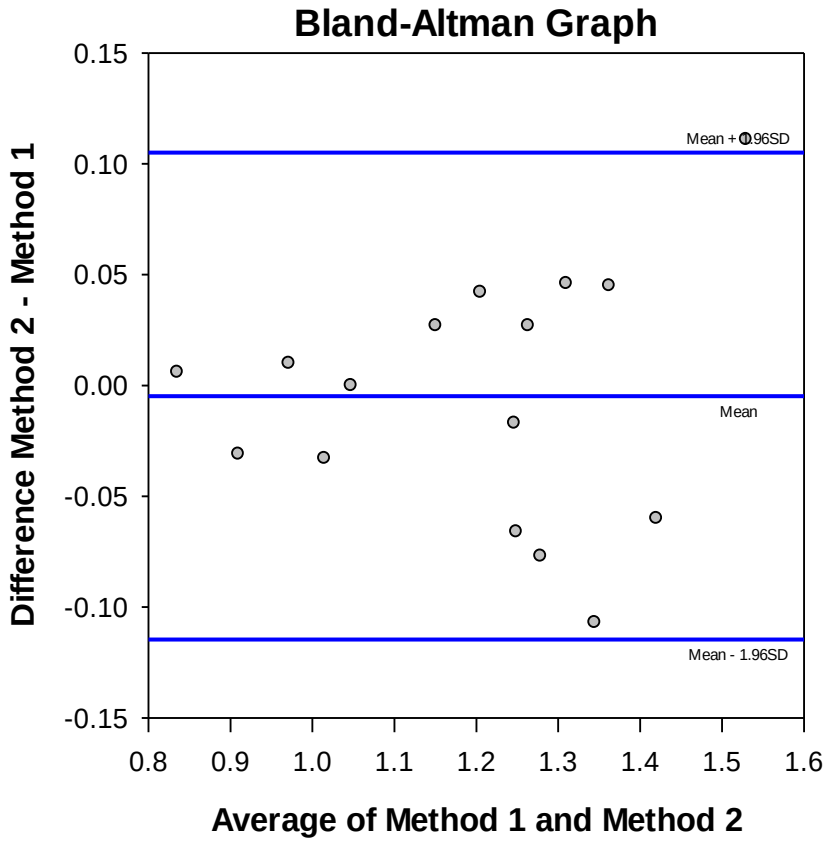

The DW-MRI sequences acquired with *b*-values of 0, 100, 500 and 900 s / mm^2 yielded superior ADC maps for visual assessment of primary tumour response, compared with *b*-values of 200, 800 and 1500 s / mm^2 (Figure 6-2). Further details on the difference in signal intensity according to *b*-value and how the MARBLE results compare to the literature, can be found in the appendix. Although the ADC values were influenced by the two sets of *b*-values, the ratio of bladder tumour to urine was similar. A comparison of the mean ADCs obtained from the three OsiriX analysis methods is also shown in the supplementary data. Overall, there was 3 - 5% difference in mean ADC dependent on the method applied.

Figure 6-8: MARBLE Left hand panel shows tumour in anterior bladder at baseline on T2-W and right panel shows reduction in tumour size after 1 cycle of chemotherapy (white arrow).

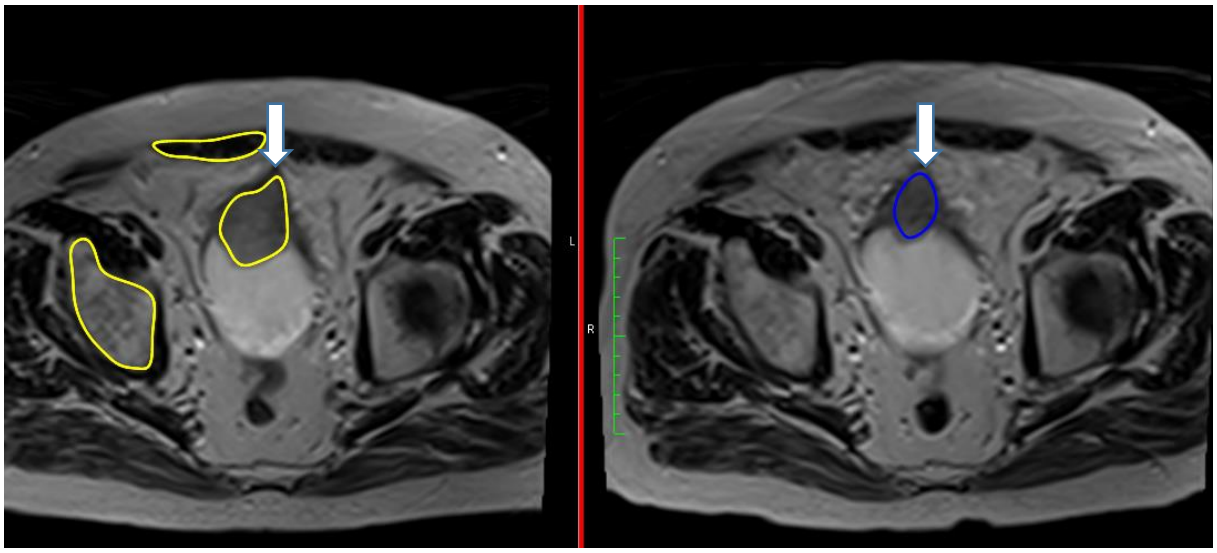

A comparison of single-slice versus whole tumour assessment of ADC revealed a mean difference of 1 ± 4% between the measurements, and this is represented in a Bland – Altman Plot (Figure 6-9).

Figure 6-9: MARBLE Bland-Altman plot showing mean difference between central single-slice and whole tumour measurements (95% CI of mean difference = -0.03 – 0.02).

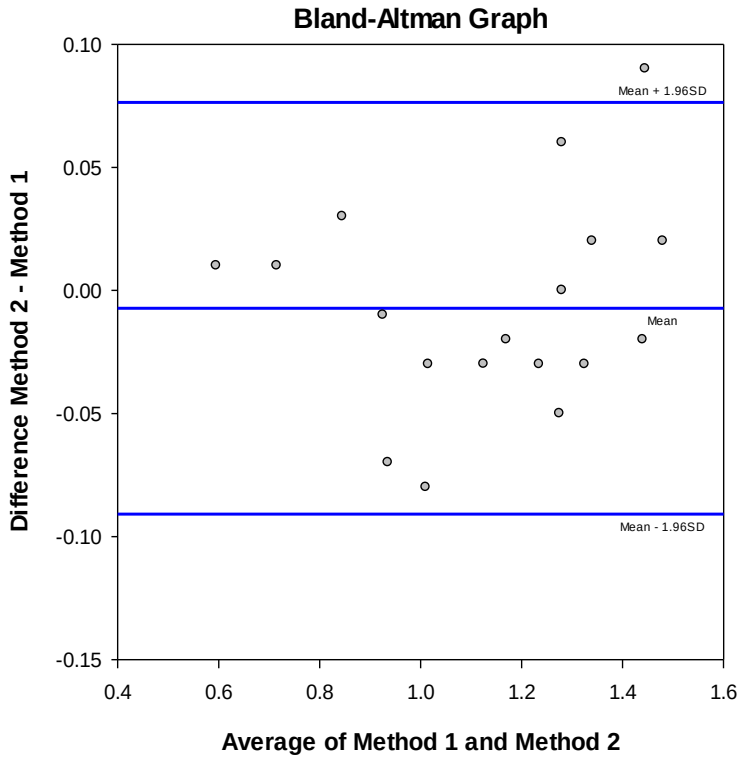

Early Quantitative Assessment

ROC analysis demonstrated that a pre-treatment ADC of > 1.26 predicted non-responders to treatment with 100% sensitivity and 80% specificity (p = 0.04, Figure 6-10). There was no correlation between Ki-67 score and pre-treatment ADC or change in ADC on treatment.

Response data from two MRI scans was captured in 12 patients using *b*-values 0, 100, 500, 900. In treatment responders mean ADC at baseline increased by 11% from 1.17 ± 0.17 $x10^{-3}$ mm^2 / s (range 0.84 - 1.39) to 1.30 ± 0.13 $x10^{-3}$ mm^2 / s (range 1.13 - 1.55, p = 0.006) after one cycle. There was no difference between ADC at baseline and after two cycles of chemotherapy (p = 0.14). Figure 6-11 illustrates the percentage change in whole tumour mean ADC on an individual patient basis in 15 patients. Tumour volume significantly decreased after first and second cycles (Table 6-10). Visible tumour shrinkage can be appreciated after one cycle of chemotherapy in Figure 6-8 and Figure 6-12.

There was a negative linear association between pre-treatment ADC and the change in ADC following one cycle of chemotherapy (Figure 6-13). The association strengthened if the dataset comprised only treatment responders; Pearson Correlation r = -0.83, p = 0.003. Mean change in mean ADC was 8.8% (median change ADC 12%, range -20 – 42%). The two patients who were recorded as showing no obvious radiological response to NAC had mean ADC changes of -1.9% and 11%. A further patient who tolerated only 1.5 cycles (MAR014) was reported as having partial response on CT but stable disease at the time of surgery; change in mean ADC was -5.4%.

Two involved lymph nodes were identified on the MRI scans. Both reduced in size after one cycle and ADC value increased by 29% and 14%, consistent with a response to treatment.

Figure 6-10: MARBLE ROC curve of pre-treatment ADC > 1.26 predicted non-responders to treatment with 100% sensitivity and 80% specificity, p=0.04.

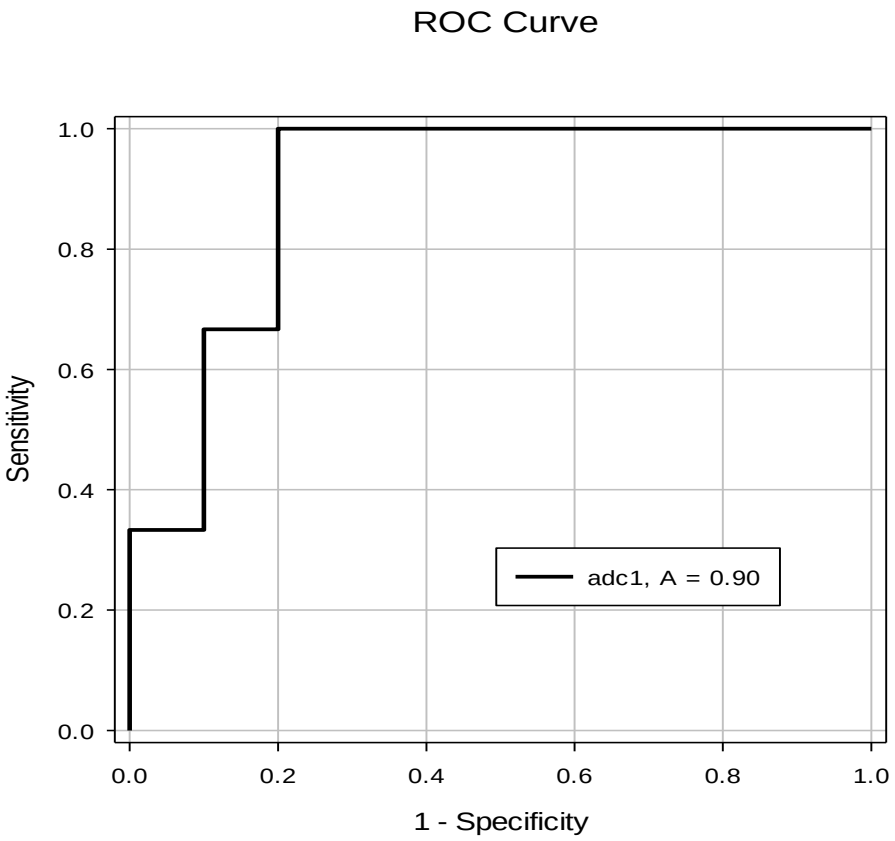

Figure 6-11: MARBLE treatment effect following 1 cycle of chemotherapy in 15 patients (treatment effect = % change in mean ADC), hatched lines = non-responders, reference y-axis at 15% repeatability value.

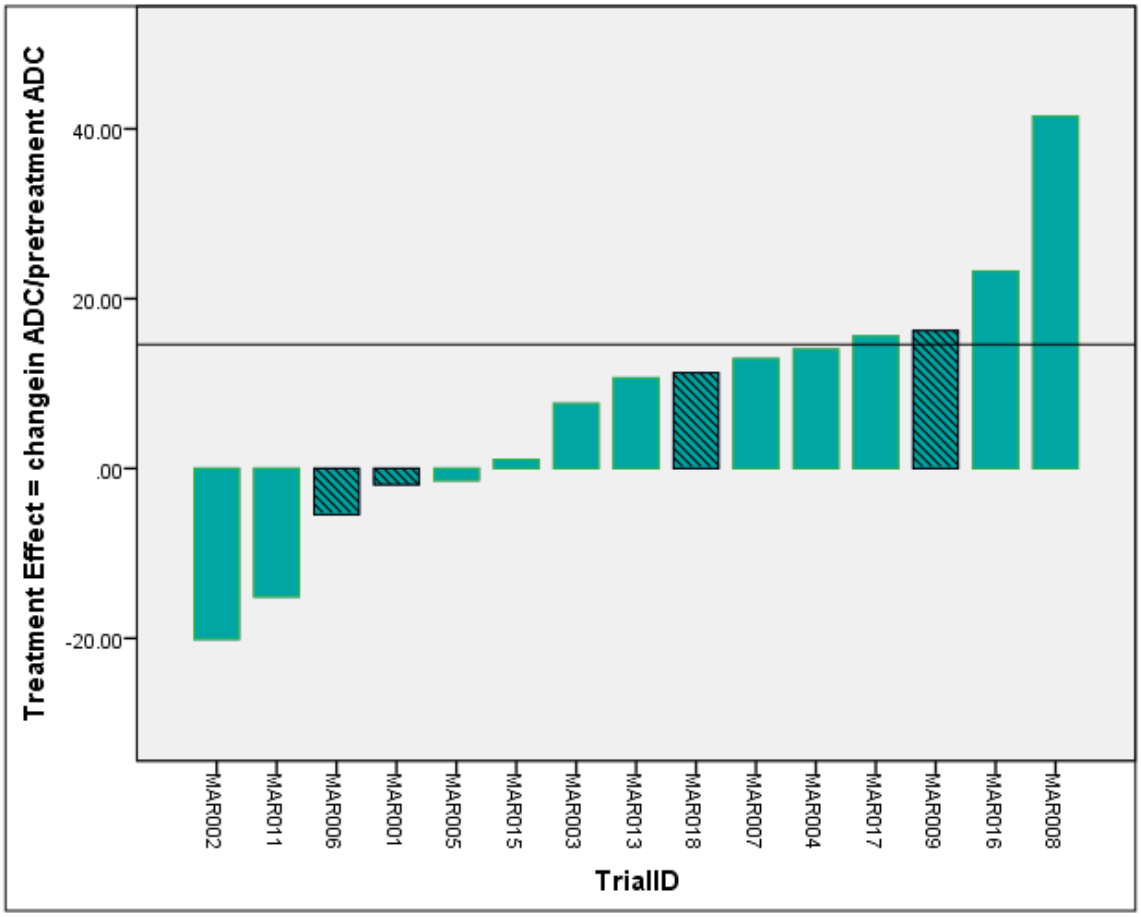

Table 6-10: MARBLE summary of quantitative measurements of 12 patients who attended for both response MRI scans using *b* = 0, 100, 500, 900 (x10^{-3} mm^2/s).

	Baseline MRI	MRI after 1 cycle	*p* value	MRI after 2 cycles	*p* value
Mean ADC (x10^{-3} mm2/s, n = 12)	1.19 ± 0.17	1.32 ± 0.14	*p* = 0.003	1.24 ± 0.16	*p* = 0.28
Mean Tumour Volume cm3 (n= 12)	11.2 ± 9.7	7.07 ± 8.73	*p* = 0.008	4.57 ± 5.41	*p*= 0.003

Figure 6-12: MARBLE serial images of anterior wall tumour responding to treatment with reduction in tumour size on T2-W images (top panel) and an increase in mean ADC calculated from ADC maps (b-values 0, 100, 500, 900 mm/s^2) with mean ADC 1.09, 1.32, 1.35 (left to right). On visual inspection, reduced restriction to diffusion can be appreciated on the response scans.

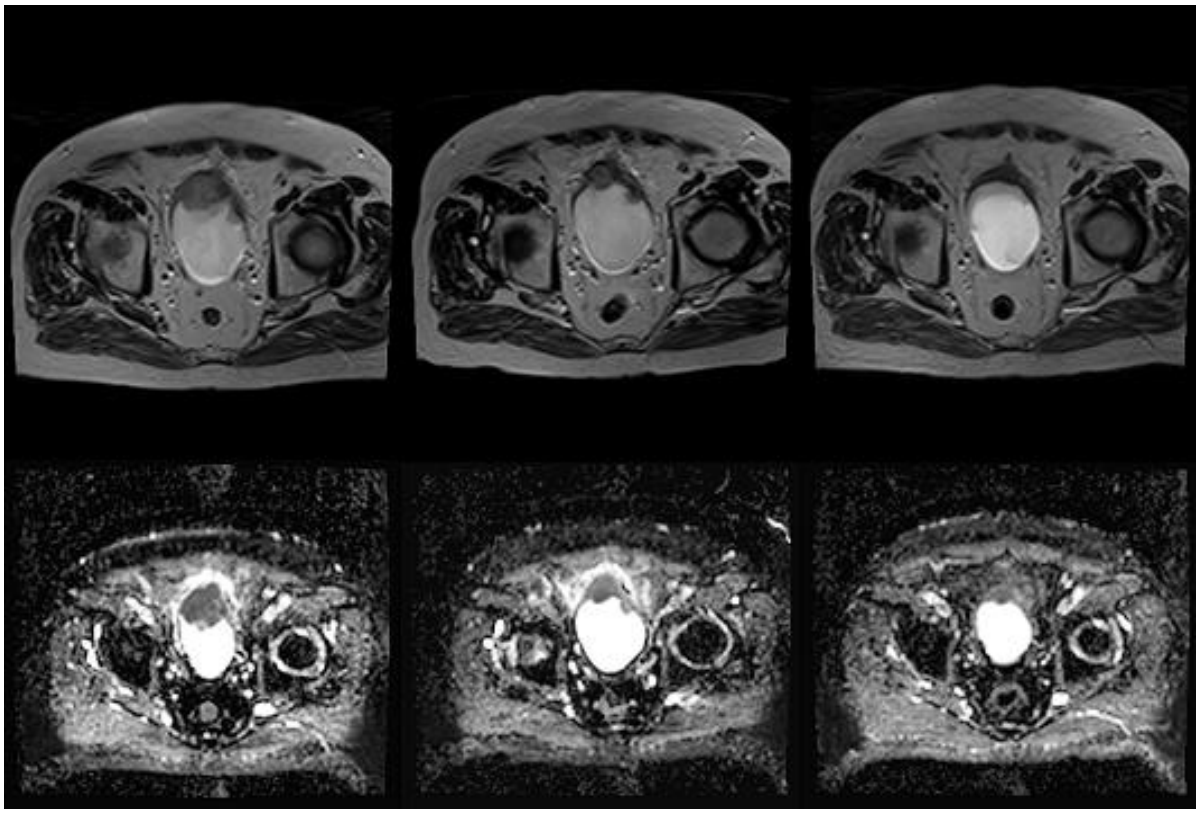

Considering the calculated repeatability figure of 15%, four patients (MAR008, MAR009, MAR016, MAR017) exhibited a > 15% change in ADC and would have been correctly identified as treatment responders after 1 cycle of chemotherapy. After two cycles, two patients (MAR003 and MAR008) would have been selected. The two patients who had no evidence of residual dysplasia at cystectomy (MAR011 and MAR013) had mean ADC changes of -15% and 11%. In the case of MAR011, tumour volume was small (2.6 cm^3) which may have influenced the accuracy of the analysis.

Table 6-11: MARBLE responders and non responders. Responders (R) and non-responders (NR) defined by RECIST 1.1 quantitative T2-W measurements (bladder thickness), and DW-MRI (whole tumour mean ADC change > 15%) after cycle 1 and 2, compared with end of treatment radiological (rResponse) +/ or pathological response (pResponse).

Patient ID	Early response assessment during chemotherapy				End of chemotherapy assessment		
	MRI2		MRI3		pResponse	rResponse	Overall
	RECIST	ADC	RECIST	ADC			
1	NR	NR	R	-	NR	NR	NR
2	R	NR	R	-	-	R	R
3	NR	NR	R	R	-	R	R
4	NR	NR	R	NR	-	R	R
5	R	NR	R	NR	-	R	R
6	NR	NR	-	-	NR	-	NR
7	R	NR	R	NR	-	R	R
8	R	R	R	R	-	R	R
9	R	R	R	NR	NR	R	NR
11	R	NR	R	NR	R	R	R
13	NR	NR	R	NR	R	R	R
15	NR	NR	R	NR	-	R	R
16	R	R	R	NR	-	R	R
17	R	R	R	NR	-	R	R
18	NR	NR	NR	NR	-	NR	NR

Table 6-12: Accuracy of early measurements at predicting overall treatment response. MRI 2 and MRI 3 performed after 1 and 2 cycles of chemotherapy respectively. PPV = positive predictive value, NPV = negative predictive value.

Parameter		Accuracy	Sensitivity	Specificity	PPV	NPV
Bladder tumour	MRI 2	10 / 15 (67%)	50%	75%	80%	43%
thickness	MRI 3	12 / 14 (86%)	80%	67%	86%	67%
Mean ADC	MRI 2	6 / 15 (40%)	28%	75%	75%	27%
	MRI 3	4 / 12 (33%)	20%	100%	100%	20%

Figure 6-13: MARBLE relationship between pre-treatment ADC and treatment effect (% change in ADC) after one cycle of chemotherapy, n = 13, r = -0.76, p = 0.003.

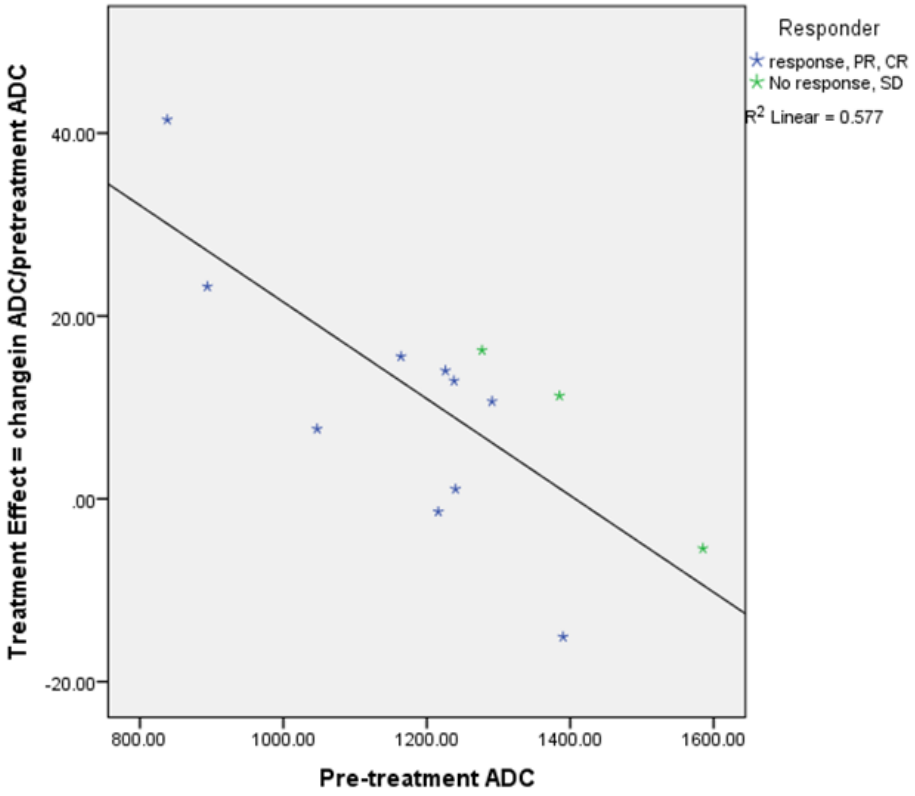

6.4.5 Patient Outcomes

Three patients were diagnosed with metastatic disease on the pre-treatment research scan and treatment intent was changed to palliative. Median time to development of metastases from completion of CRT or surgery was 9.5 months (n = 6, range 3 – 17). Eighty-two per cent of the patients who started chemotherapy survived 12 months (n = 14). 39% (7 / 18) have died during a median follow-up of 13.5 months; mean time to death from TURBT diagnosis was 17 months (range 2 – 30, ± 10), and excluding the patient who did not commence NAC, mean survival was 20 months (range 12 – 30, ± 8). All patients who died of a tumour-related death had T3 or T4 disease and Ki-67 was ≥ 75%. The patient who died within two months of diagnosis did not commence treatment due to deteriorating performance status. The three patients who survived beyond 15 months, received three or four cycles of chemotherapy followed by radiotherapy (Table 6-13). One patient died from pneumonia (MAR018).

Table 6-13: MARBLE details of tumour-related deaths

Patient ID	Age	Gender	TNM	Ki-67	Number of cycles	Definitive Treatment	pTNM	Survival after TURBT (mths)
2	67	m	T3N1	90	4	NAC-CRT	n/a	29
7	53	f	T4N0	75	3	Pall chemo	n/a	20
8	71	m	T3N0	90	4	NAC-CRT	n/a	30
9	67	f	T3N1	90	2	NAC-surgery	pT2bN1	12
10	52	f	T3N0	90	0.5	Surgery	pT3aN0	15
12	66	m	T4N0	85	0	Nil	n/a	2

Median survival for the whole cohort is 28 months (95% CI 17 – 39, Figure 6-14). Using the median Ki-67 value of 80% as a cut-off, Kaplan Meier survival analysis demonstrated clear separation of the curves with a median survival of 28 months (95% CI 15 – 41) for Ki-67 >79%, compared with median survival not reached in cohort with Ki-67≤ 79% (Figure 6-15). Half of the female (3 / 6) participants have died, accounting for three of the seven deceased. Median survival was13 months in females, in comparison to 28 months for males (Figure 6-16). Median survival was not affected by lymph node status, although the 95% CI was 11 – 45 months for node-negative compared with 2 – 54 months for node positive patients (Figure 6-17).

Figure 6-14: MARBLE Kaplan-Meier curve of overall survival, n = 18

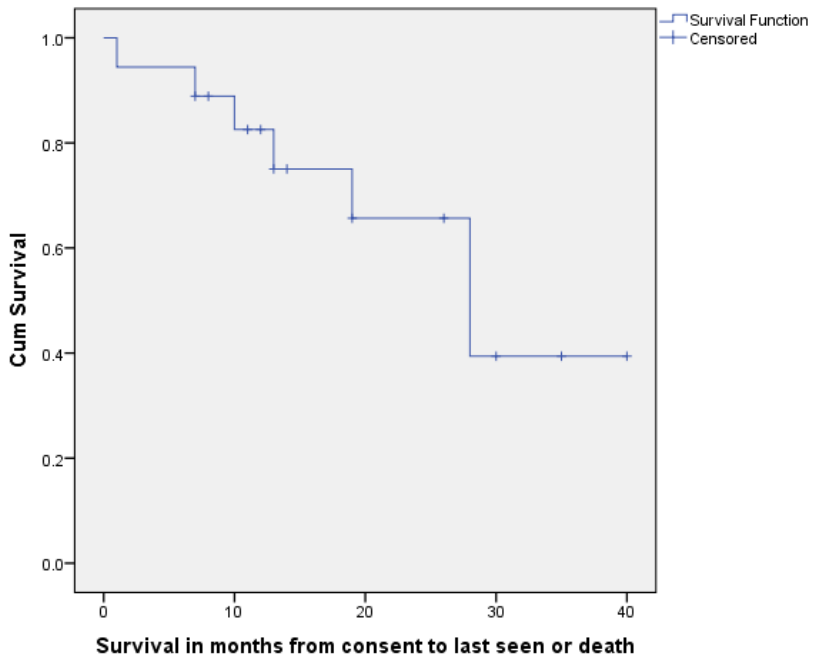

Figure 6-15: MARBLE Kaplan-Meier survival curve demonstrates survival benefit if Ki-67 is ≤ 79% (median survival not reached) compared with median survival 28 months (95% CI 15.2 – 40.8) for Ki-67 >79%.

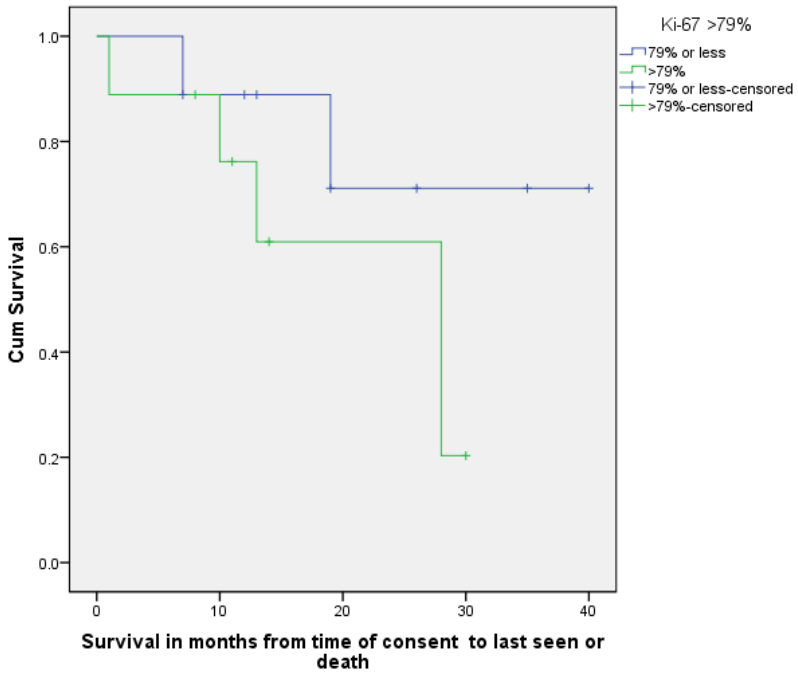

Figure 6-16: MARBLE Kaplan- Meier curve according to gender demonstrates worse survival outcomes in females. Median survival 13 months (95% CI 9 – 17) in females, compared with 28 months in males (95 % CI 17 – 39).

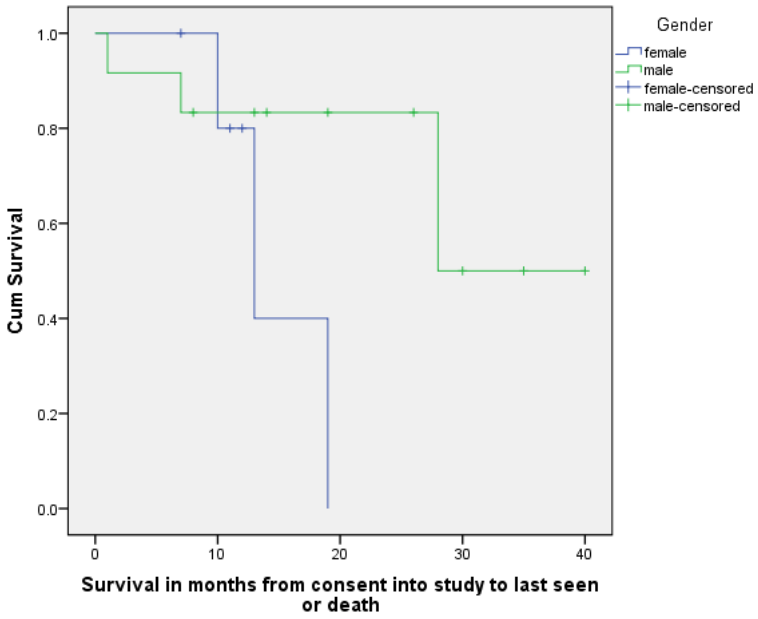

Figure 6-17: MARBLE Kaplan-Meier curve of survival according to presence or absence of nodal disease, median survival 28 months

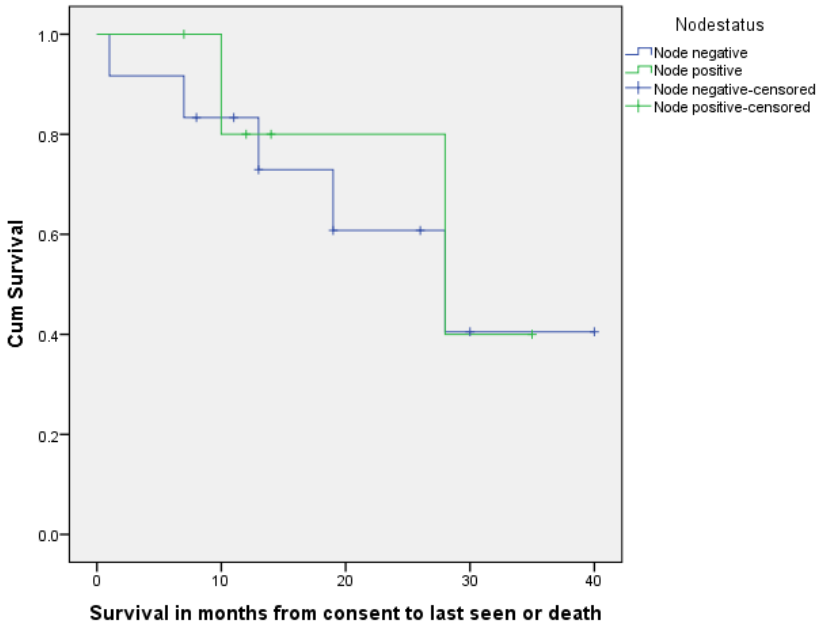

6.4.6 Additional Findings

Outcomes for patients in this cohort demonstrated a gender difference favouring males, which is comparable to the literature. Reviewing a recent statistical bulletin: Cancer Survival in England: Adults diagnosed 2009-2013 from the Office for National Statistics, the largest gender difference in one year survival was seen in bladder cancer: one-year survival 79% in males, 67% in females; similarly five-year survival 59% in males and 48% in females (Statistics, 2015).

Seventeen percent (3 / 18) of the MARBLE study cohort were diagnosed with bone or liver metastases on the baseline research MRI scan. Each patient had T3 or T4 disease, and if these patients had been scanned with FDG PET-CT, as is now recommended by NICE guidance, these patients are unlikely to have been included in the study as would have been managed palliatively. Staging with MRI or FDG PET-CT should be considered for patients at higher risk of metastases, e.g. T3b and above. According to Witjes *et al*, over a third of patients with MIBC have undetected metastases at the time of treatment of the primary tumour (Witjes *et al.*, 2015). Other review articles propose a more modest figure of 13 - 25% (NICE, 2015). Mertens *et al* reported a change in management in 13 / 95 patients as a result of upstaging following FDG PET-CT (Mertens *et al.*, 2013). The British Association of Urological Surgeons reported the average time of pathway from referral for a diagnosis to commencing treatment as > 112 days, therefore it may be >12 weeks since the original CT scan. In the MARBLE study, the delay between staging investigations and commencing treatment could account for the number of patients who were upstaged following the baseline research scan. In addition to shortening the timing of this pathway, it would be prudent to repeat baseline investigations or investigate with alternative modes of imaging in cases of advanced disease where there are symptoms consistent with clinical progression, e.g. bone pain in MAR015 and deterioration in performance status in MAR012. Additionally, a treatment response may be missed if the pre-chemotherapy scan was acquired several months before commencing chemotherapy. Currently, functional MRI in bladder cancer is not a routine staging investigation but the landscape is changing. The 2015 EAU guidelines recommend MRI for staging of bladder cancer, and suggest there may be a role for response assessment in the future but that there is no convincing evidence to this effect currently (Stenzl *et al.*, 2009). The 2015 NICE guidance for the

management of bladder cancer concluded that due to the lack of high quality evidence, it could not recommend one type of imaging (CT or MRI) over another (NICE, 2015).

6.4.7 Unexpected radiological findings

In three patients (MAR010, MAR015, and MAR016), the baseline research scan revealed unexpected findings which influenced the treatment plan: In MAR010, a suspected fistula between bladder tumour and bowel was identified on MRI. Because this can result in overwhelming sepsis a fistula is regarded a contra-indication to chemotherapy treatment. This patient did not have further chemotherapy and proceeded directly to surgery. The MRIs for MAR015 and MAR016 revealed metastases in the ilium and liver, respectively. This changed the intent of their treatment from potentially curative to palliative and favoured radiotherapy over radical cystectomy as the appropriate treatment option. The chemotherapy regime remained the same, but the number of planned cycles of treatment was increased from four to six or eight, depending on tolerance and effectiveness. In one patient (MAR018) renal function was poorer than expected and, accordingly, cisplatin was changed to the less nephrotoxic drug carboplatin. In the case of MAR012, the baseline research scan also revealed multiple bone metastases. This fit the clinical scenario of advanced disease and the patient deteriorated rapidly, therefore was unfit for any treatment. Of note, there was a delay of three months between the initial pelvic CT and the research MRI, so the metastases may have also been visible on the routine CT imaging if this had been performed nearer to the time of the MRI scan.

6.5 Discussion

6.5.1 Technical feasibility of performing serial ADC measurements in bladder cancer patients

The main objective of the MARBLE study was to investigate the feasibility of DW-MRI and DCE-MRI scanning to predict early responses to treatment in a cohort of bladder cancer patients receiving NAC in our institution. Of the 21 patients screened, two declined entry into the study due to the additional burden of visits. No study participants failed to attend a scan despite baseline scanning times of an hour, and no patients reported difficulty tolerating the scan to the research staff.

Ensuring consistent filling of the bladder is difficult to achieve during a prolonged scan time, because the bladder is continually filling. Some research groups report aiming for moderate to full bladder distension although specific details on bladder preparation for MRI scanning are relatively sparse (Barentsz *et al.*, 1998; Schrier *et al.*, 2006; Bains *et al.*, 2010; Rajesh *et al.*, 2011; Daneshmand *et al.*, 2012; Kanazawa *et al.*, 2012; Donaldson *et al.*, 2013; Hafeez and Huddart, 2013; Gupta *et al.*, 2015; Nguyen *et al.*, 2015). In the radiotherapy treatment of bladder cancer, consistent set-up is crucially important. The bladder is imaged daily to ensure delivery of the prescribed dose to the target. If the bladder varies in size there is a risk of geographical miss and surrounding organs at risk, namely rectum and small bowel, may receive excessive doses of radiotherapy resulting in excess toxicity. In our institution, to minimise variation in bladder filling, radiotherapy bladder cancer patients are instructed to empty their bladder one hour before the scan and drink 200ml of water. MARBLE study participants were encouraged to have a comfortably full bladder but, despite this, intra- and inter-patient variation in bladder filling was observed. Too full a bladder is likely to be poorly tolerated, and an empty bladder may obscure a small tumour in the folds of the bladder mucosa; therefore, in the research setting when scan times may exceed an hour, we recommend a moderately full bladder. There is no widely agreed definition of a “comfortably full” bladder. During the course of the MARBLE study, preliminary steps have been taken to optimise the scan images by reducing the duration of the scan to only acquire sequences necessary for analysis.

Eligibility of patients for the MARBLE trial stated clinically palpable disease or radiological evidence of persistent tumour post TURBT. In practice, this information was not readily available to the research team, and clinically palpable disease was difficult to visualise on some of the research MRI scans. To overcome this problem, subsequent MRI studies could have more stringent criteria for measurable disease post TURBT, and avoid serial scans if there is no convincing disease at baseline.

Muscle-invasive bladder tumours lie adjacent to urine which differs greatly in ADC and K*trans* values. The ratio of mean ADC in urine to bladder tumour was similar when different *b*-values were used (mean 2.36 -2.58). In the case of MAR011, the size of the bladder was consistently small (< 80 cm^3) for each scan, and tumour thickness perpendicular to the bladder wall measured only 3 mm pre-treatment. If the

ROI is incorrectly placed and includes urine, this will considerably affect the measurements. The likelihood of this is increased in small tumours due to human error in the registration of images. Additionally, partial volume effect and the extent of necrosis within the tumour can influence the measured parameters (Padhani *et al.*, 2009; De Robertis *et al.*, 2015). Necrosis may be present in a tumour at baseline, or may develop as a consequence of response to treatment. This can be visualised on the CT and MRI images but is more challenging in smaller tumours. Increased free fluid may artificially increase the ADC value thus some research groups recommend that only the solid areas should be included in the ROI analysis; however, this is clearly technically challenging to identify in small bladder tumours (Heijmen, 2012; De Robertis *et al.*, 2015). The value of quantitative analysis after the second cycle of chemotherapy in this group of patients is uncertain; the presence of necrosis is likely to have been higher and smaller tumours were more difficult to define accurately. In many cases, visible shrinkage in the size of tumours at this time-point was identified on standard T1- and T2-weighted sequences questioning the added value of DW-MRI and DCE-MRI sequences.

The literature cautions against the comparison of quantitative measurements derived from different sets of *b*-values due to the influence of *b*-values on the ADC value (Dale *et al.*, 2010; Donati *et al.*, 2014a). Supporting this, in MARBLE, a mean difference of 50% (range 17 – 78%) in bladder tumour and urine ADC values was recorded between the two different sets of *b*-values *(b* = 200, 800 and 1500 mm / s^2 and *b* = 0, 100, 500, 900).

At *b*-values < 100 mm/s^2, blood perfusion can be mistaken for diffusion. Excluding *b*-value = 0 mm/s^2 may improve the accuracy of the ADC calculation by omitting the contribution from blood flow (Padhani *et al.*, 2009). Acquiring more *b*-values provides a more accurate estimation of ADC but is off-set by the longer acquisition time, and must be considered fully when designing a clinical trial.

Tumours less than 15mm thick were technically challenging to evaluate therefore, the ADC values may not be accurate. T2 tumours post TURBT were particularly small and in two cases the DW-MRI aided identification of tumour which was not detected on the T2-weighted imaging. The 2009 DW-MRI consensus meeting recommended that evaluable lesions should be greater than, or equal to 2cm (Padhani *et al.*, 2009), and other research groups report a threshold of 3cm lesions (Galbraith *et al.*, 2002;

Leach *et al.*, 2005; Morgan *et al.*, 2006; Leach *et al.*, 2012). Kyriazi *et al* discounted subcentimeter ovarian lesions from analysis due to limitations within spatial resolution (Kyriazi *et al.*, 2011). Clearly, there will be situations in the response setting where tumours shrink below this 2cm size constraint and ADC measurements become unnecessary because changes in size provide the answer for response assessment.

Recommendations for acquisition of bladder MRI images for quantitative analysis

- Aim for a moderately filled bladder for quantitative assessments.
- Tumours should have a minimum thickness of 15 – 20 mm for response assessment analysis.
- Serial MRI scanning in patients undergoing chemotherapy is acceptable to patients
- Mean ADC values from a single-slice analysis is comparable to whole tumour assessment

6.5.2 Determining repeatability measurements

Repeatability refers to the precision of one operator measuring the same object on the same MRI scanner under the same conditions, in a short period of time. Reproducibility is different, and relates to the same test of the same object but on different devices, by different operators (Padhani *et al.*, 2009). A more detailed assessment of intra-patient variation through an assessment of repeatability and reproducibility would require two or more baseline scans acquired on separate visits but for the purposes of this study, a pragmatic approach was taken. To assess DW-MRI repeatability, calculation of whole tumour mean ADC and total volume from two pre-treatment DW-MRI scans generated data which were not statistically different. Consistent mean ADC values, independent of the tumour size and analysis method, within this study suggested that changes in these values were attributable to a treatment-related effect rather than inherent biological variation. Indeed, mean change in ADC across the entire tumour between the baseline and repeated scan was 1 ± 4%, generating a CoV of 7.5% and repeatability figure of 15%. This suggests that a treatment effect is required to be of greater magnitude than 15% to be reliably

detected and compares favourably with studies reported in solid tumours and myeloma where a range of CoV of between 7% and 15% is reported (Braithwaite *et al.*, 2009; Koh *et al.*, 2009; Bilgili, 2011; Messiou *et al.*, 2011). If the degree of inherent variability within a set of results can be estimated, this can be used for power calculations in future clinical trials. Accordingly, some authors suggest treatment effects of less than 27% (1.96 x CoV) are unlikely to be detected with confidence after a single MRI scan in an individual (Braithwaite *et al.*, 2009). A recent consensus meeting of DW-MRI outside the brain reported good repeatability with DW-MRI; Bland-Altman analyses have demonstrated a coefficient of repeatability of between 15 and 30% across multiple studies (Taouli *et al.*, 2016). In MARBLE treatment responders, however, the mean magnitude of ADC changes was small at 11%, less than the calculated treatment effect. When such small treatment effects are being recorded, factors which influence the measurement are important to acknowledge. For instance, across MRI vendors, repeatability of 14% has been reported (Donati *et al.*, 2014b).

A comparison of three methods to obtain ADC values using the OsiriX software programme produced results which varied by 3 – 5%. Given that the treatment effects were of small magnitude within the MARBLE study, a contribution of 5% from the software programme could result in the wrong treatment decision being made. These findings support the importance of reporting detailed data analysis methods which can be reproduced by other research groups.

6.5.3 Whole tumour assessment

The method of data analysis is important when comparing studies. Two investigators undertook the analysis of six DW-MRI datasets in ImageJ generating statistically similar results. More detailed analysis is required before commenting on inter- and intra-operator bias. Tumour heterogeneity may result in increased diffusion in one region cancelling out reduced diffusion in another, directly influencing the reliability of a technique (Metcalfe *et al.*, 2013). In an attempt to overcome this, whole tumour VOI analysis rather than single-slice assessments were conducted in MARBLE. Many studies only report data from the central tumour slice. Acquiring data only from the middle of the tumour, may reduce inaccuracies derived from partial volume effects at either end of the tumour. There is no consensus on whether single-slice or whole tumour analysis is more accurate. Other research groups have reported on data

averaged across the whole ROI: breast cancer, hepatocellular carcinoma (Wu *et al.*, 2015a) (Vandecaveye *et al.*, 2014). Hayes *et al* compared whole tumour region-of-interest analysis with histogram analysis to improve understanding of tumour heterogeneity using DCE-MRI and found that results were approximately equal (Hayes *et al.*, 2002). In MARBLE, the mean difference between the whole tumour and single-slice measurements was 1 ± 4%, similar to the repeatability measurements. This result supports the single-slice method used for tumour evaluation in a number of other studies. A major advantage of the single-slice method is that is faster to process, thus could be more easily incorporated into clinical routine practice.

Some research groups have preferred to evaluate changes in ADC and K*trans* on a voxel level using a semi-automated method to characterise intra-tumoural heterogeneity (Hayes *et al.*, 2002; Yankeelov *et al.*, 2007; Li *et al.*, 2009; Atuegwu *et al.*, 2011; Kyriazi *et al.*, 2011; Donati *et al.*, 2014c). Functional diffusional maps can be generated from voxel-based analyses to depict changes within each voxel as a result of treatment. Serial scans are co-registered and changes in the voxels at each time-point recorded. The method relies on accurate co-registration of images which is challenged by patient repositioning, and changes in tumour shape and size in response to therapy. It may be more technically feasible to generate functional diffusional maps in anatomical sites such as the breast or limb, than in a distensible organ like the bladder which is continually filling. Voxel-based analysis may be potentially useful tool to guide dose escalated radiotherapy treatment.

6.5.4 DW-MRI as a prognostic and predictive biomarker

Significant correlations between ADC values and histological grade, tumour size and muscle-invasiveness in bladder cancer have been reported (Sevcenco *et al.*, 2014a). Quantification of ADC aids prognostication of tumours; lower ADC values correlate with higher grades of prostate, pancreatic, breast, bladder, renal pelvis (Kim *et al.*, 2009; Takeuchi *et al.*, 2009; Costantini *et al.*, 2010; Nakanishi *et al.*, 2012; Kobayashi *et al.*, 2013; Donati *et al.*, 2014a; De Robertis *et al.*, 2015; Gupta *et al.*, 2015) (Kim *et al.*, 2009; Takeuchi *et al.*, 2009; Whittaker *et al.*, 2009; Costantini *et al.*, 2010; Razek *et al.*, 2010; Kobayashi *et al.*, 2011; Nakanishi *et al.*, 2012; Donati *et al.*, 2014a; De Robertis *et al.*, 2015; Gupta *et al.*, 2015). ADC values may also be used to predict more advanced disease. Rosenkrantz *et al* reported significantly lower ADC values in

bladder cancer patients with metastatic disease; using *b*-values = 0, 400, and 800 sec/mm^2, ROC curve analysis showed that an ADC cut-off of 0.94 identified patients with metastatic disease (Rosenkrantz *et al.*, 2012). Similarly, Sevcenco *et al* reported a cut-off of 0.88 predicted muscle-invasiveness, and 0.91 predicted higher grade in bladder cancer, using *b*-values = 50, 400 and 1000 s/mm^2 (Sevcenco *et al.*, 2014b).

The MARBLE results showed that a lower pre-treatment ADC resulted in larger changes in ADC value following one cycle of chemotherapy; ROC analysis demonstrated pre-treatment ADC values > 1.26 predicted non-responders to treatment. Heijmen *et al* published a review of tumour response prediction by DW-MRI in 2012, reporting similar findings from studies involving mainly colorectal, brain and cervix cancers. There was a negative correlation between pre-treatment ADC and clinical outcome (Mardor *et al.*, 2004; Koh *et al.*, 2007; Cui *et al.*, 2008; Heijmen, 2012) and pre-treatment ADC values have been shown to predict response to chemotherapy or radiotherapy in colorectal, glioma, uterine, gastric, rectal and pancreatic tumours (Cui *et al.*, 2008; Niwa *et al.*, 2009; Heijmen, 2012; Cao *et al.*, 2014). Although a negative correlation between pre-treatment ADC and treatment response was observed in responders in some studies, conflicting results have been published in other studies involving similar tumour types (Kyriazi *et al.*, 2011; Elmi *et al.*, 2013). For example, Nilsen *et al* found that in breast cancer, pre-treatment ADC did not predict treatment response (Nilsen *et al.*, 2010). Less commonly reported are mid-treatment ADC values. Higher mid-treatment ADC values have been shown to predict better outcome in cervix cancer patients assessed by DW-MRI after 2 weeks of chemoradiation (Somoye *et al.*, 2012).

Although a significant relationship between Ki-67 score and pre-treatment ADC was not found in MARBLE, there was a trend between higher Ki-67 score and poor outcome. More actively proliferating tumours respond faster to treatments but can recur, and left untreated they do badly (De Robertis *et al.*, 2015). All patients who died during the course of the study had a Ki-67 score of > 85% on the diagnostic biopsy.

6.5.5 DW-MRI as an early response biomarker

Effective treatment results in tumour necrosis and apoptosis, and membrane disruption which increases the extracellular fluid space. This promotes increased movement of water molecules and is reflected by a rise in ADC on DW-MRI (Nakayama *et al.*, 2008; Braithwaite *et al.*, 2009). Treatment evaluations may be performed using visual assessment of *b*-value images, or ADC maps. Changes in tumour ADC values which result from a treatment response as opposed to inherent normal biological variation should be defined using repeatability measurements and incorporated into the design of clinical trials (Padhani *et al.*, 2009). A more recent review of DW-MRI for the prediction of response to anticancer therapy concluded that DW-MRI holds potential for early response monitoring, but that validation has been hindered by the lack of reproducibility and standardisation studies (Heijmen, 2012). Treatment effects of less than a 27% change in ADC (1.96 x CoV) are unlikely to be detected with confidence after a single MRI scan and may have questionable clinical significance (Braithwaite *et al.*, 2009). In MARBLE, the treatment effect value was 15%. Given the small number of patients in the study, this value may change with a larger cohort. The treatment effect value was low so the sensitivity of the ADC analysis was expected to be higher and identify more of the responding patients. ADC values are influenced by factors including b-values, as demonstrated in MARBLE, field strength and sequence type, thus it is important to exercise caution when comparing results generated using varying MRI parameters. Evaluating the treatment effect rather than an absolute value is advised.

DW-MRI has been investigated as a surrogate marker of response in a variety of tumour types including breast, colorectal, cervix and primary bone tumours (Koh *et al.*, 2007) (Heijmen *et al.*; Koh *et al.*, 2007; Harry *et al.*, 2008; Kim *et al.*, 2009; Intven *et al.*, 2015). A greater increase in tumour ADC values occur in responders than non-responders, although the magnitude of this change varies between tumour sites. Nilsen *et al* found that in breast cancer, ADC increases after two cycles of neoadjuvant chemotherapy did not relate to tumour volume changes (Nilsen *et al.*, 2010).

To our knowledge there is little published on the role of DW-MRI in the response prediction and treatment evaluation of bladder cancer. Yoshida *et al* demonstrated that DW-MRI after chemoradiotherapy in 20 bladder cancer patients improved the

sensitivity, specificity and accuracy of predicting pathological complete response compared with T2W and DCE imaging (Yoshida *et al.*, 2012). Increasingly, research groups are exploring the role of functional imaging at early time-points, frequently within two weeks of commencing therapy. Demonstrating a treatment effect at the earliest opportunity could spare patients the unnecessary toxicity from ineffective treatments and contribute to personalised medicine by tailoring treatment algorithms.

Participants can be defined as treatment responders using radiological or pathological criteria. The gold standard method for validating imaging responses to treatment is pathological evaluation. There is a trend to move away from definitive surgical management and towards organ preservation with CRT due to a number of recent papers reporting equivalence in outcomes between surgical and definitive CRT treatment (Smith *et al.*, 2013; Ploussard *et al.*, 2014). The change in practice impacts on the timing and method of tissue sampling following treatment, such that a much smaller number pathological correlates are available within a couple of months of the MR and CT imaging. In MARBLE, histology samples were available from radical cystectomies in five of the eighteen participants who had ≥1 cycle of NAC, however three received suboptimal chemotherapy doses, or were given carboplatin in place of cisplatin which limits the treatment effectiveness.

Response rates to chemotherapy were higher than expected in the MARBLE study. There were 11 treatment responders, and 4 non-responders. There were two complete pathological responders. Complete response rates to either MVAC or gemcitabine/cisplatin range from 23 – 38% (Zargar *et al.*, 2015). Following TURBT, complete pathological responses occur in 15% of cases, increasing to 38% following NAC (Grossman *et al.*, 2003). In the MARBLE cohort of patients, stable radiological disease after three cycles of chemotherapy was classified as no response. Absence of tumour progression over 12 weeks, it could be argued, indicates that the chemotherapy is having some effect on the tumour but not of large enough magnitude to visibly reduce tumour size. CT assessment can be limited, and if MRI had perhaps been used for the routine restaging assessment more responses may have been identified. The restaging CT assessment defined 12 treatment responders and two with stable disease. One of the radiologically-defined treatment responders had stable disease on cystectomy due to pT2 staging, although this had been down-staged from radiological T3 staging. Applying the DW-MRI treatment effect value of

15% to the MARBLE cohort after one cycle of chemotherapy would have correctly identified four of the 11 responders. The median change was 12%, mean change 9% and range -20 – 42%. Of the four patients who showed SD, the percentage change in derived ADC values were lower (mean ADC 1.34, median -1.8, range -5 – 11). Change in mean ADC was not markedly different in the two patients with pathological complete responses. One was a T2 tumour which was difficult to define on baseline imaging, and in the other mean ADC increased by 10% after one cycle. There are likely to always be some cases where the pathological assessment does not correlate with radiological information and caution should be exercised when comparing studies which use different criteria for determining response to treatment.

Although there were statistically significant differences in mean ADC across the whole patient cohort between the pre-treatment MRI and post one-cycle MRI scans, the absolute magnitude of changes within patients was very small. As mentioned earlier, small tumour size is likely to have influenced the reliability of some of the analysis results. Percentage change in mean ADC was higher in responders than those with stable disease and this is reported widely in the literature in many tumour types. Kyriazi *et al* studied ovarian cancer patients and reported a repeatability figure of 9.4%, mean change in ADC of 14% ± 13 in responders and 2.8% ± 7.3 in non-responders to one cycle of chemotherapy, n = 42, p = 0.022 (Kyriazi *et al.*, 2011). Intven *et al* found that in 55 rectal cancer patients who received CRT, mean ADC change showed greater diagnostic accuracy than tumour volume or mean K*trans* (Intven *et al.*, 2015). The vast majority of response assessment studies comprise only 15 - 30 patients; clearly there is a need for larger, well-designed clinical trials.

The greatest changes in mean ADC after one or two cycles of chemotherapy were recorded in patients with the lower baseline ADCs. Although a number of studies have shown promising associations of low pre-treatment ADC values and better treatment outcomes, reports in the literature are varied, and more validation work is needed (Heijmen, 2012).

Evaluation of the lymph nodes with DW-MRI was not particularly helpful. The majority were subcentimeter lymph nodes. Lymph nodes less than 1 cm are not size-significant, therefore, may or may not be involved. A change in ADC consistent with treatment response was detected in the largest lymph node, but this was a solitary case. Some studies have examined the utility of DW-MRI at detecting nodal

involvement. They report a high false-negative rate using DW-MRI due to an overlap in mean ADC values between benign and malignant lymph nodes. Benign processes such as inflammation and fibrosis can cause restricted diffusion (Wang *et al.*, 2014a) (Funatsu *et al.*, 2012). Given the small size of involved nodes in bladder cancer, there is questionable value in assessing these using DW-MRI for the reasons mentioned above. In treatment responders, tumour thickness changes of > 30% were measured in 67% of patients after only one cycle of chemotherapy, suggesting this may be a more useful measure of early response to treatment than volume changes.

A volumetric response in the primary bladder tumour was observed in 33% of patients after one cycle of NAC, increasing to 88% after two cycles NAC. Changes in ADC values occurred earlier in more patients, than volumetric changes. To the surprise of the investigators, significant changes in primary bladder tumour thickness were seen ten to seventeen days following the first cycle of chemotherapy. A reduction in tumour size has not previously been demonstrated at this early time-point in this tumour group to our knowledge. After the second cycle of chemotherapy, the mean tumour size was 66% smaller than the pre-chemotherapy size and in 70% of patients maximum tumour thickness perpendicular to the bladder was less than 15mm. Additionally, in MARBLE, MRI assessment of anatomical changes after two cycles correctly predicted CT assessment after three cycles, suggesting that imaging at this earlier time-point with MRI may be appropriate.

Although the optimal time-point for early MRI imaging following treatment for most tumours is unknown, it appears that DW-MRI as early as 7 days after treatment can demonstrate a magnitude of ADC change which relates to a treatment effect in other tumour sites. In a neo-adjuvant breast cancer trial, DW-MRI demonstrated an increase in mean ADC in responding patients 7 and 12 days after cycles 1 and 2 of chemotherapy (Pickles *et al.*, 2006). Similarly, in patients with rectal tumours undergoing concurrent chemo-radiation, an increase in ADC also predicted response after 2 weeks of radiotherapy (Barbaro *et al.*, 2012). Response assessment studies should be based on feasibility studies which provide information on how the DW-MRI parameters change with time. MARBLE was designed to obtain preliminary data that would allow the magnitude of variability within and between patients to be assessed, as a prelude to the design of subsequent studies which would be statistically

powered to detect a pre-specified difference and enable the modification of patient treatment plans according to imaging findings.

Recommendations for treatment response monitoring in bladder cancer

- Early responses may be detected as early as ten days after the first cycle of chemotherapy with changes in the whole tumour size, bladder tumour thickness and mean ADC
- Delaying quantitative analysis until a time point when tumours show visible shrinkage, e.g. after two cycles, is of questionable value
- Maximal tumour thickness shows promise as an early predictor of response which could be easily incorporated into clinical practice
- MRI imaging after two cycles of chemotherapy is recommended for earlier tumour assessment than CT scanning after three cycles

6.5.6 Ki-67 as a predictive biomarker in muscle-invasive bladder cancer

Biomarker data may help select the patients who should be offered NAC. Fourteen of the eighteen study participants had Ki-67 scores of >70%, and of these five were > 90%. MARBLE did not demonstrate a clear association between Ki-67 and pre-treatment ADC or change in mean ADC value, although a number of other studies have demonstrated conflicting results. Sevcenco *et al* studied 41 bladder cancer patients and reported that ADC values correlated with cell cycle and proliferative markers: Ki-67, p21 and p53. They concluded that ADC and p53 were both independent prognostic factors for muscle invasiveness (Sevcenco *et al.*, 2014a).

There was a clear separation of the survival curves for tumours with Ki-67 scores above the median score of 80% and all patients who died had Ki-67 scores of > 75%. Ki-67 has been established as both a predictive and prognostic biomarker in bladder cancer, and although it may be used to influence treatment decisions in other malignancies, e.g. lymphoma, is not routinely measured in bladder cancer. The findings from MARBLE further support extrapolation of histopathological biomarker data, and other cell cycle markers such as p21, p27, p53, cyclin E which may play an important role forecasting outcome and selecting treatment (Krabbe *et al.*, 2014).

6.5.7 Limitations of the study

Follow-up was relatively short, the number of patients were few and there was a noteworthy absence of a cohort of patients with progressive disease. Additionally, few patients proceeded to radical cystectomy, and hence, pathological assessment of treatment response was not available within the study period.

6.6 Conclusions

Bladder DW-MRI is prone to anatomic distortion. The tumours are often small post TURBT and assessment of the primary tumour by existing imaging modalities is difficult. A scanning sequence was developed which enabled measurement of ADC values, which are influenced by *b*-values. To detect a treatment effect, repeatability data from MARBLE suggest ADC changes of 15% are required. Differences in primary bladder tumour thickness and volume were identified 10-17 days after the first cycle of chemotherapy with 67% accuracy and 50 % sensitivity, which may hold more promise than ADC measurements which had a sensitivity of 28%.

MRI imaging after two cycles of chemotherapy is recommended for earlier tumour assessment than CT scanning after three cycles, with a sensitivity of at least 86% and specificity 67%for changes in bladder tumour thickness predicting response. Low pre-treatment ADC values predicted greater changes in ADC after one cycle of chemotherapy. Ki-67 scores were high in the majority of patients, and may predict early death.

Publication bias and underpowered small clinical studies may partly explain the conflicting data in the literature. To evaluate relationships further, adequately powered studies need to be designed. Further data are required to validate DW-MRI as a useful biomarker of treatment response in bladder cancer.

In the next chapter, the role of DCE-MRI is explored in a subset of the MARBLE patients.

Chapter 7 Dynamic contrast-enhanced MRI as a predictive and early response biomarker in muscle-invasive bladder cancer: MARBLE study

7.1 Introduction

Although a role for DCE-MRI in the detection and staging of tumours has been reported for over twenty years in tumour sites including brain, breast, prostate and bladder, the technique has not been adopted into routine UK practice (Hesselink *et al.*, 1988; Hamm *et al.*, 1990; Tanimoto *et al.*, 1992; Narumi *et al.*, 1993; Boetes *et al.*, 1994; Jager *et al.*, 1997). More recently, research studies have explored DCE-MRI as a response biomarker (Boetes *et al.*, 2004; Heverhagen *et al.*, 2004; Yankeelov *et al.*, 2007; Ah-See *et al.*, 2008; Johansen *et al.*, 2009; Petralia *et al.*, 2011; Barrett *et al.*, 2012; Abramson *et al.*, 2013; Etxano *et al.*, 2014; Li *et al.*, 2014; Schmitz *et al.*, 2015). Qualitative assessments of DCE-MRI images report the extent of any abnormal areas of enhancement and how these change in response to treatment. Clinical trials investigating the effect of anti-vascular agents have commonly reported the quantitative parameters K*trans* and AUC60 as endpoints. Effective treatment results in a fall in K*trans,* and observations of the signal-intensity curves show a delay in enhancement, less steep slope and lower signal maximum intensity, the latter effect being explained by a reduction in blood vessel diameter (Barentsz *et al.*, 1998; Tofts *et al.*, 1999).

Estimating the concentration of contrast agent in blood plasma over time (arterial input function, AIF) is an important measurement required in quantitative models but is technically challenging to acquire. The AIF can be calculated in several ways: obtained from insertion of an arterial catheter; measured on the DCE-MRI data sets; or derived from a cohort of subjects, named the population-based AIF (Yankeelov and Gore, 2009).

There is a lack of literature on the utility of DCE-MRI as an early response imaging biomarker, where the effect of treatment is assessed after a few days. Typically, radiological response assessments are undertaken after two to three months.

7.2 Objectives

The MARBLE study was designed to investigate the predictive, prognostic and early response potential of DWI and DCE-MRI in a cohort of bladder cancer patients planned to receive gemcitabine-based chemotherapy. The primary objective was to assess the feasibility of performing serial quantitative MRI scans in patients with bladder tumours, prior to and early in the course of cytotoxic treatment. Secondary objectives included relating baseline MRI parameters and Ki-67 to pathological or radiological assessment of response at two – three months, progression-free survival and overall survival; and investigating whether the early changes in MRI parameters after one or two cycles of chemotherapy related to treatment response, overall survival and progression-free survival. The DCE-MRI sequence was optimised in the first cohort of patients attending for DW-MRI. Therefore, there were ten patients who underwent the same DCE-MRI protocol and the results are reported in this chapter.

7.3 Methods

7.3.1 Study Participants

The MARBLE study was conducted in accordance with The Code of Ethics of the World Medical Association (Declaration of Helsinki) for experiments involving humans. Ethical approval was gained from the local ethics committee (REC reference 13/NE/0007 and IRAS project ID 100429). The study was sponsored by Newcastle upon Tyne Hospitals NHS Foundation Trust (NUTH) and was undertaken at the Northern Centre for Cancer Care (NCCC), Freeman Hospital, Newcastle upon Tyne, UK. Participants for DCE-MRI assessment were identified in the NUTH Urology Multidisciplinary Team Meeting between 29 July 2014 and 22 October 2015.

Eligibility criteria were:

- T2-T4a N0-2 M0 muscle-invasive bladder cancer according to UICC TNM Seventh Edition (2009)
- Residual disease post transurethral resection of bladder tumour (TURBT) determined by examination under anaesthetic at time of TURBT or on staging CT

- Patients scheduled to receive three or four cycles of neo-adjuvant or down-staging cisplatin-based chemotherapy followed by radical cystectomy or radiotherapy
- Adequate renal function (GFR > 50 ml / min)

Patients were excluded if they were unable to give fully informed consent or tolerate an MRI scan. Participants were classed as treatment responders if there was obvious shrinkage in tumour volume measurements. Non-responders were identified by stable or progressive disease on a CT scan acquired after two or three cycles of chemotherapy, or greater than pT2 disease at time of cystectomy.

7.3.2 Ki-67 measurements

Details on the Ki-67 measurements can be found in Chapter 6.

7.3.3 DCE-MRI scanning details

Serial MRI scans were acquired before and during neoadjuvant chemotherapy treatment (10-17 days after the first and second cycles). All MRI scans were performed on a Siemens 1.5-Tesla Espree system using a body array 6-element coil with six integrated preamplifiers. Patients were requested to have a comfortably full bladder. T1-weighted, T2-weighted, DW-MRI and DCE-MRI sequences were acquired. Images were obtained of the pelvis up to lumbar vertebrae level L3/4, ensuring bladder and local pelvic lymph nodes were encompassed. Images were obtained in two blocks:

- inferior - symphysis pubis to L5/S1 or S1/2;
- superior – S1/2 to L2/3

T1-weighted (repetition time TR 541 / echo time TE 13 ms, 3mm slices) and T2-weighted sequences (TR 3500 ms / TE 109 ms, matrix 384x332, 3mm slices) with field of view (FOV) 380 x 332 mm were anatomically matched to the DW-MRI sequences. A smaller field of view was positioned over the bladder for the contrast-enhanced images and a second T2-weighted sequence acquired (TR 3570 / TE 109, 5 mm slices, FOV 250 x 250 mm) which was anatomically matched for the DCE-analysis. The scanning protocol was optimised for quantitative analysis in healthy volunteers and two bladder cancer patients; pre- and post-contrast images were acquired over 5 minutes using a sequence with temporal resolution of 30 seconds, 3mm slices, TR 7.84 ms / TE 2.84 ms, matrix 256x256, and 28 images per series

The sequence was subsequently modified as follows: DCE scans were acquired over 6 minutes using 3D gradient echo sequence with temporal resolution of 3.5 sec, 5mm slices, TR 2.7ms / TE 1 ms (Figure 7-2). Pre- and post-contrast images for T1 calculation were obtained from six repeats of multiple flip angles (1, 2, 5, 10, and 15 degrees). After 5 baseline series had been acquired, 20ml (ten mmoles) of Gadoteric acid contrast agent was administered as a bolus intravenous injection (3ml / second) using an automatic power injector, followed by a 20ml saline flush (3 ml / second) (Dotarem, relaxivity 4.6units s^{-1} mM^{-1} ('Package leaflet DOTAREM 0.5 mmol/ml,')).

Figure 7-1: MARBLE trigone bladder tumour (denoted by arrow) acquired pre and post contrast (left, middle and right panel: before, 30 and 60 secs). TR 7.84 ms, TE 2.84 ms, temporal resolution 30s. Note superior spatial resolution and contrast of images compared to Figure 7-2.

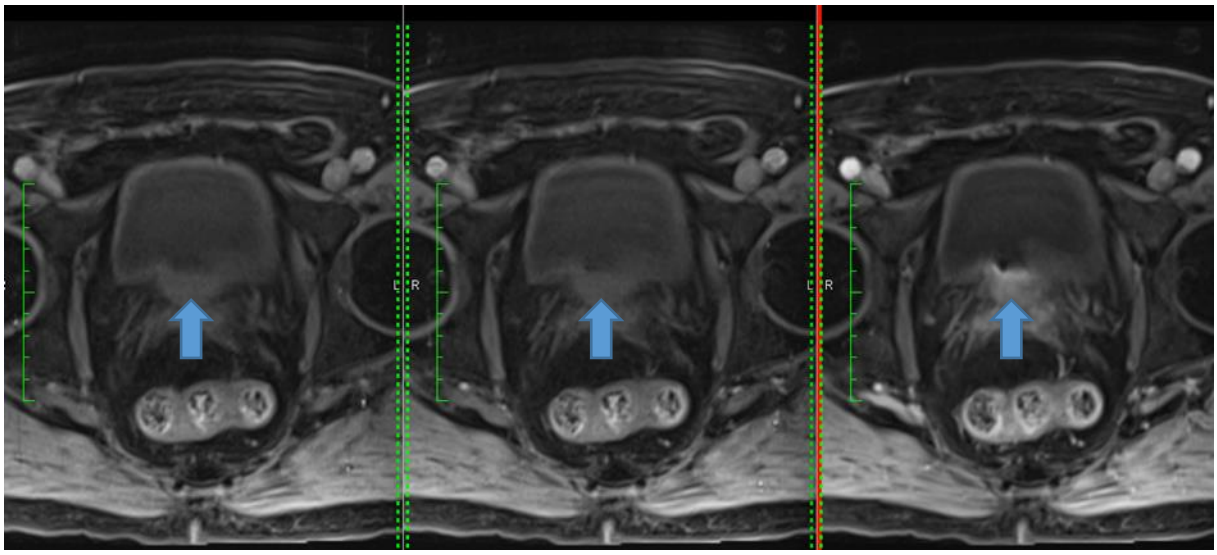

Figure 7-2: MARBLE tumour pre and post contrast. T4N1 tumour right bladder wall (arrowed), from left to right images taken before, 28 and 62 seconds post iv contrast administration (TR 2.7 ms, TE 1 ms, temporal resolution 3.5s)

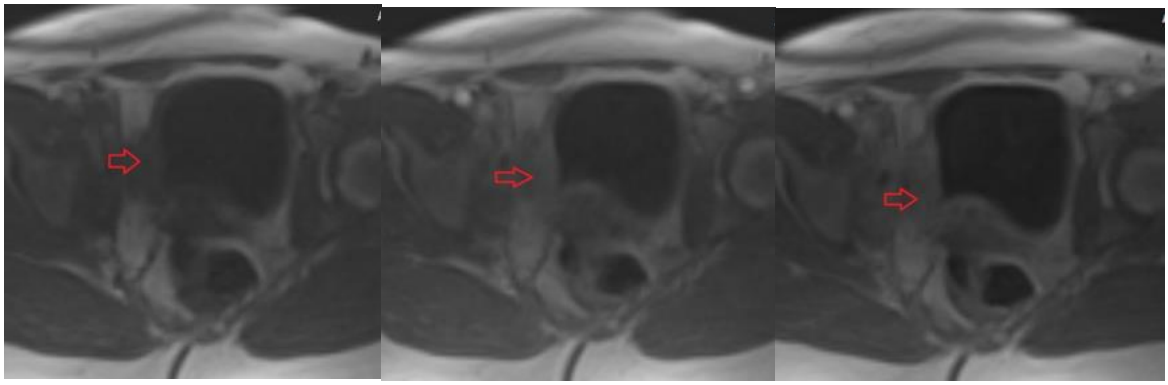

7.3.4 DCE-MRI analysis

DCE-MRI volumes of interest (VOIs) were defined using an anatomically-matched T2-weighted image acquired immediately prior to the DCE-MRI series. Data acquisition for pre-contrast T1 mapping involved six repeats, each using five different flip angles. For each flip angle, one of these repeats (excluding the first one) was used for calculation of the T1 map. Initially, ROIs were defined over the external iliac artery to give an arterial input function. A preliminary study compared results obtained using Fritz-Hansen and modified Fritz-Hansen population-based AIFs, and the subject-based AIF (Walker-Samuel *et al.*, 2007; Woolf *et al.*, 2016). There was considerable variability in the results using the subject-based AIF, and they showed little agreement with results obtained using the population-based AIFs on ROI analysis (see appendix). The modified Fritz-Hansen AIF is used in a number of oncological studies and for this and the above reasons, was selected for the MARBLE DCE analysis (Li *et al.*, 2011; Coolens *et al.*, 2015). A maximum of 99 images in a dynamic series could be analysed using the open-source medical image processing software (OsiriX v.5.8.2 32-bit, revision 20131218, www.pixmeo.pixmeo.com). Final analysis comprised fitting the Tofts extended model to region of interest data with a population-based modified Fritz-Hansen arterial input function, using the OsiriX DCE Tool plugin. Gadolinium concentration curves were calculated for 345 seconds (99 series), and estimates for K*trans*, K*ep*, Ve and V*p* were derived. Figure 7-3 demonstrates the DCE analysis workflow.

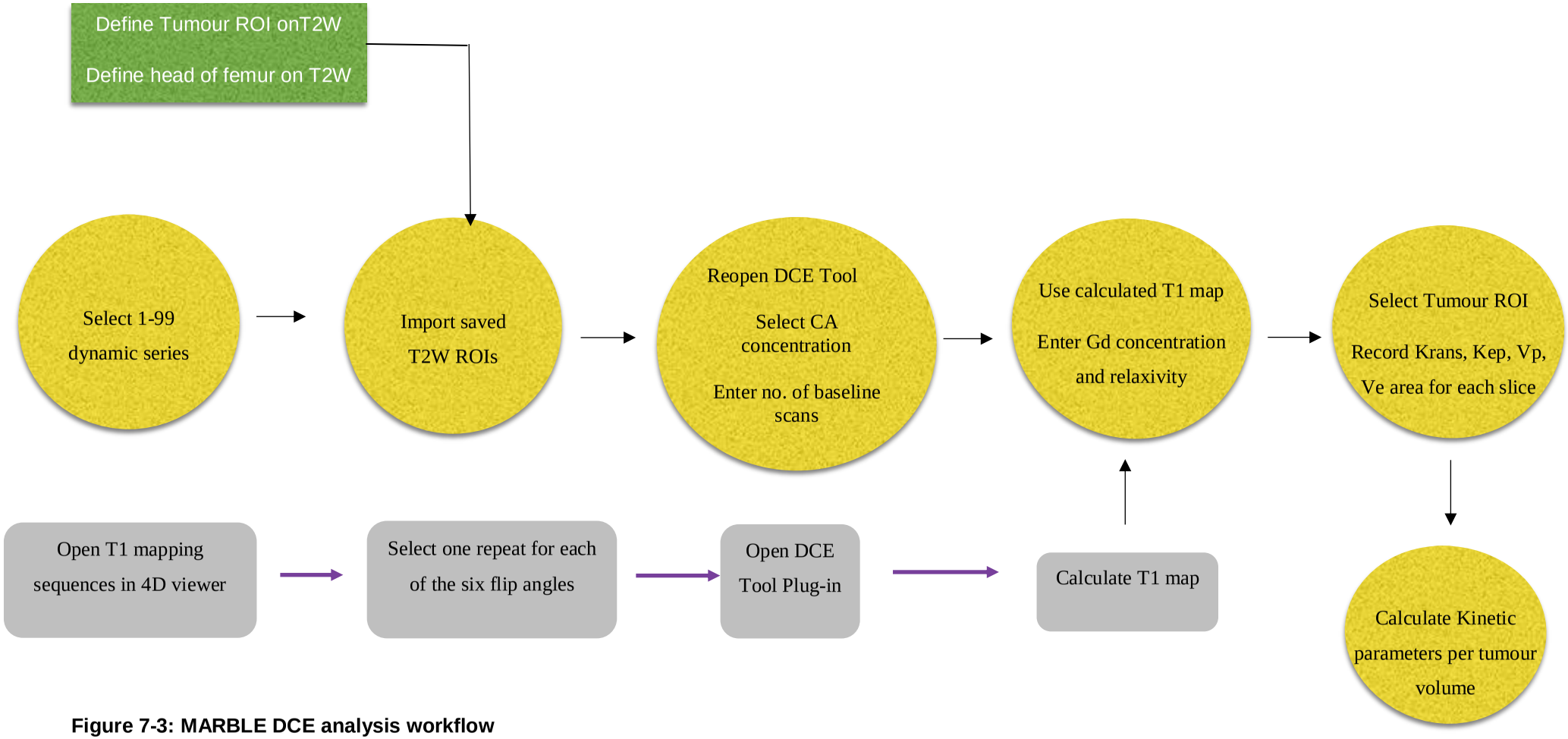

Figure 7-3: MARBLE DCE analysis workflow

7.3.5 Treatment response evaluation

Repeatability figures of 15% for DW-MRI (from MARBLE DW-MRI data) and 14% for DCE-MRI (from the literature) were used to determine the cut-off value for determining treatment response from inherent biological variation. Treatment response was defined by ADC increases of greater than 15%; K*trans* decreases of greater than 14%; and reduction in primary tumour thickness by greater than 30% (as per RECIST criteria, Table 1.1).

7.3.6 Statistical analysis

The demographic, treatment and imaging details of the study participants were analysed using the SPSS v22 statistical package (IBM UK Ltd, Portsmouth). Mean change and CoV of K*trans* were calculated and expressed as percentages. To test for differences between the baseline and each response scan, the Wilcoxon signed ranks test was applied. Correlation analysis was undertaken to assess the association between the following parameters: Ki-67 score, tumour volume, mean K*trans,* change in K*trans*, baseline mean ADC, change in volume between the scans, and length of follow-up. Excluding Ki-67 score, data were not of normal distribution so Spearman's correlation coefficient was calculated. Receiver Operating Curve (ROC) analysis was performed to compare the percentage decrease in K*trans* with pathological / radiological assessment of partial or complete response, and to determine the optimal cut-point for percentage change in K*trans* associated with the highest specificity, sensitivity, positive and negative predictive values, as similar research studies have used (Elmi *et al.*, 2013; Ashraf *et al.*, 2015). These measurements were compared with CT or MRI qualitative assessments after two or three cycles of chemotherapy to calculate sensitivity, specificity, negative and positive predictive values, and negative and positive likelihood ratios. Findings were reported as significant at the 0.05 level (2-tailed).

7.4 Results

7.4.1 Study Participants

Ten patients were recruited to the DCE-MRI MARBLE trial. Characteristics of the patients are described in Table 7-1 and Table 7-2. Four patients did not complete the intended courses of chemotherapy for the following reasons: deterioration in

performance status and not fit enough to commence chemotherapy (n = 1); allergic reaction to two regimes of chemotherapy (n = 1); identification on baseline MRI of a fistula between bladder and bowel which is a contra-indication to chemotherapy (n = 1); discontinued chemotherapy after two cycles due to side-effects (n = 1). Seven patients received more than one cycle of chemotherapy and attended for one or more follow up research scans. Each patient was classified according to response radiologically (n = 4), or at surgery (n = 3). There were 5 treatment responders, and 2 non-responders. Two of the five treatment responders had complete pathological responses at cystectomy after chemotherapy (Table 7-2). The non-responders had either no appreciable shrinkage in tumour volume, or ≥ pT2 tumour staging at surgery. One was defined on imaging, and had received four cycles of carboplatin-based chemotherapy instead of cisplatin, due to renal insufficiency. The other patient received 1.5 cycles of cisplatin-gemcitabine chemotherapy. Median follow-up was 10.5 months (range 1 - 14) from date of consent into the study to last follow-up appointment or date of death (censored 24 September 2016). Four patients have died (one cancer-unrelated death); MAR009, 010 and 012 died 15, 12 and 2 months after TURBT respectively. Two patients are alive 7 and 11 months after being diagnosed with metastatic disease on the baseline MRI. Four patients are free from disease.

Table 7-1: MARBLE characteristics of DCE-MRI cohort

	n	%
Gender		
Male	5	50%
Female	5	50%
Age (years)	Median 65 years	Range 37 – 68 years
T stage		
T2	1	10%
T3/4	9	90%
N-stage		
N0	6	60%
N1/2	4	40%
Ki-67	Median 85%	Range 30 – 90%
Definitive Treatment		
NAC - CRT	2	20%
NAC - S	5	50%
Other	3	30%
NAC dose intensity (n = 7)	Median 3 cycles	Mean 2.6 cycles
No. of tumour-related events		
Distant metastases	4	40%
Tumour-related death	3	30%

Table 7-2: MARBLE treatment response according to modality: r = radiological, p = pathological, PR = partial response, CR = complete response, NR = non-responder, R = responder.

Patient ID	Response		
	Radiological	Pathological	Overall
9	rPR	Downstaged from T3 to pT2	NR
11	rPR	pCR	R
13	rCR	pCR	R
15	rPR	-	R
16	rPR	-	R
17	rPR	-	R
18	rSD	-	NR

7.4.2 Semi-quantitative DCE-MRI

DCE-MRI scans were acquired in ten patients. Of these, seven patients attended for one or two response scans. In two cases (MAR011 and MAR017), the tumours were difficult to identify on the baseline MRI scans due to collapse of the bladder wall obscuring the area of malignant thickening, and small tumour size relative to the size of the bladder. In both cases, the DW-MRI and DCE-MRI sequences aided identification of tumour. Figures 7-4 and 7-5 illustrate an example of signal intensity and gadolinium contrast agent uptake curves within tumour ROI on four axial MRI slices in one patient. Contrast agent was injected after five baseline series (approximately 17 seconds) and all curves show uptake which rises sharply after 30 seconds, excluding one patient where uptake was more gradual. Tumour Ki-67 score was 30% in this case. The enhancement curves demonstrate similar times to peak (TTP) on each slice but there is considerable variation in the areas under the signal intensity and gadolinium contrast agent curves (AUC), represented graphically.

Figure 7-4: MARBLE signal intensity over time in a single patient. MAR014. Each line represents a tumour ROI from a different slice.

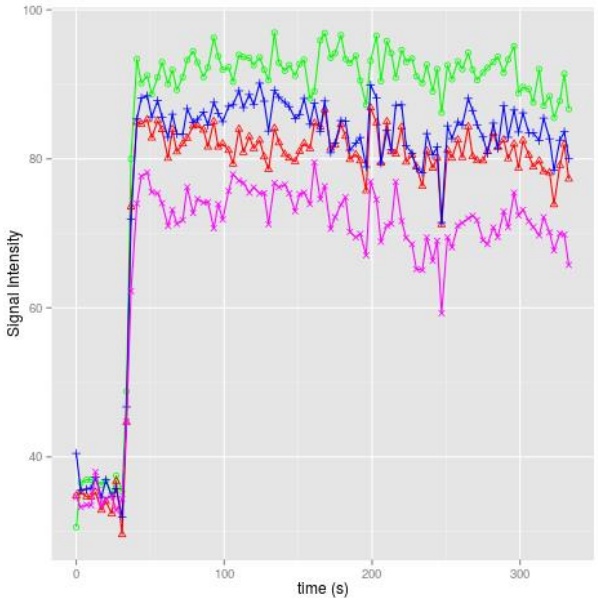

Figure 7-5: MARBLE gadolinium uptake curves in a single patient over time -MAR014. Each line represents a tumour ROI from a different slice.

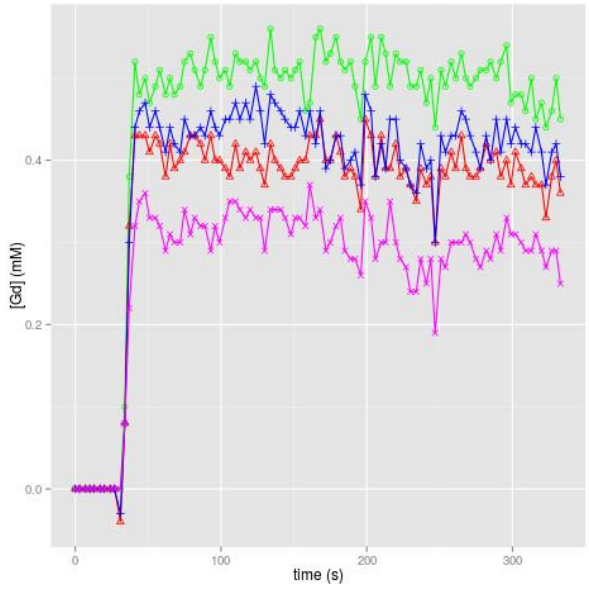

Figure 7-6 demonstrates the difference in baseline measurement in three patients: MAR014, MAR015, and MAR018. There is a more rapid TTP and AUC in MAR014 compared with MAR015 and MAR018. Following treatment, there were changes in the TTP and AUC parameters. Represented in Figure 7-7 is an example of a patient who responded well to treatment, and in Figure 7-8 a non-responder where there was no appreciable change in tumour volume after treatment. The Ki-67 score was 90% in the responder and 30% in the non-responder. The TTP and AUC are considerably greater on the baseline scan compared with the curves acquired following each cycle of chemotherapy in the treatment responder (Figure 7-7). These curves represent a single slice within the tumour ROI. Figure 7-9 represents a single slice of a patient who responded to 2 cycles of chemotherapy according to CT, but had progressive disease after a further 2 cycles. An increase in the amplitude of the contrast agent enhancement curves was observed after each cycle of chemotherapy (see case report for further details).

Figure 7-6: MARBLE comparison of gadolinium contrast agent uptake curves in a single slice of the baseline MRI scan in three patients (MAR014 green, MAR015 red, MAR018 blue).

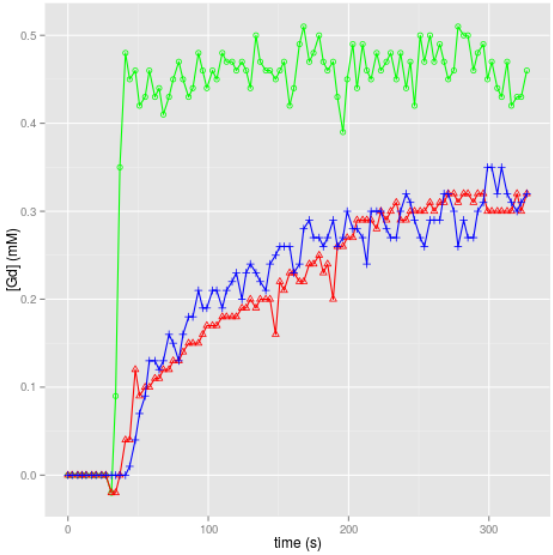

Figure 7-7: MARBLE contrast agent uptake curve in treatment responder. 37-year old female with T4N0 bladder tumour (red=baseline, blue=after 1 cycle, green=after 2 cycles). Ki-67 score 90% on TURBT. The fall in contrast uptake was consistent with a good treatment response and serial K*trans* results were 0.25, 0.1, and 0.11.

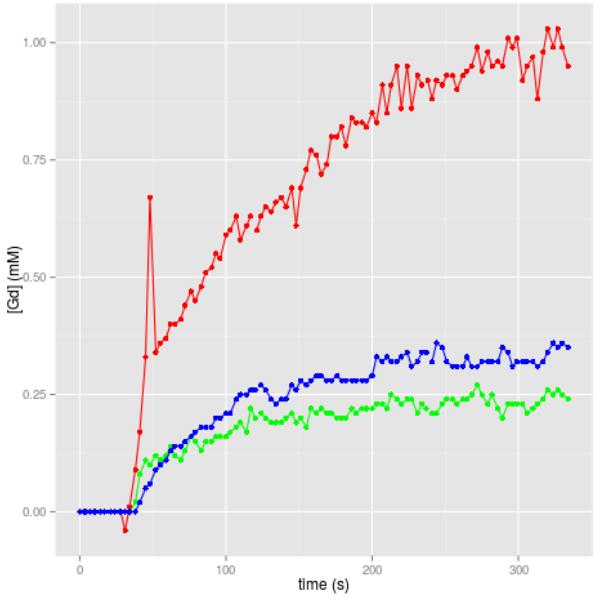

Figure 7-8: MARBLE contrast agent uptake curve over time in treatment non responder. 67-year old male with T4N0 muscle-invasive bladder tumour. CT showed stable disease after chemotherapy (green = baseline, red = after 1 cycle, blue = after 2 cycles). Ki-67 score 30% on TURBT. Serial K*trans* were 0.1, 0.1, and 0.09.

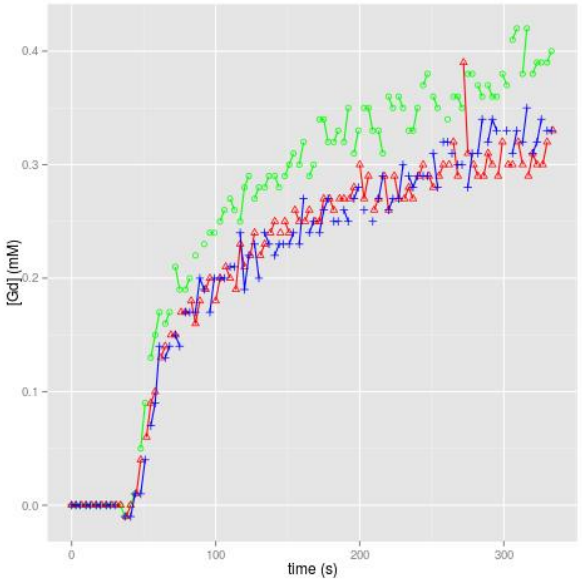

Figure 7-9: MARBLE contrast agent uptake curve in 68 year-old female with T4N1M1 bladder cancer demonstrating an increase in the amplitude of the enhancement curve after the first and second cycles of NAC (green = baseline, red = after 1 cycle, blue = after 2 cycles), MAR016, Ki-67 45%. This patient responded to the first two cycles of chemotherapy, but CT scan after four cycles showed progressive disease.

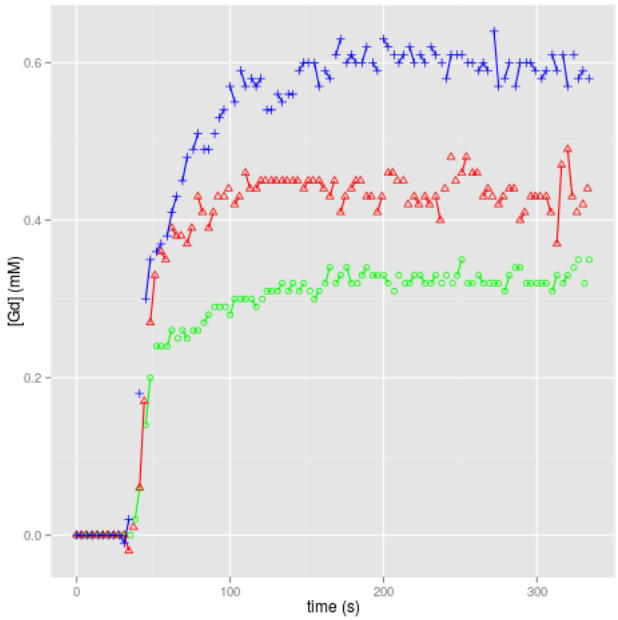

7.4.3 Quantitative assessment of baseline tumour parameters and clinical outcome

Results of mean ADC and kinetic parameters for the bladder tumours of ten patients who attended for baseline MRI are summarised in Table 7-3. Baseline K*ep* was found to have a negative correlation with mean baseline ADC score (r = -0.63, p = 0.02) and baseline K*trans* (r = -0.78, p = 0.01). There was no significant correlation between baseline mean ADC and baseline K*trans* (r = -0.6, p = 0.08, n=10). The pre-treatment K*trans* in each of the patients who have died a cancer - related death during the study was ≥ 0.38, and in the remaining seven alive patients, < 0.38 (Figure 7-10).

Table 7-3: MARBLE baseline quantitative MRI parameters (n = 10).

	Mean ADC (x 10^{-3} mm^2/s)	Mean K*trans*	Mean K*ep*	Mean V*e*
Mean	1.19	0.30	0.79	0.44
Median	1.26	0.31	0.62	0.37
Minimum	0.89	0.09	0.29	0.20
Maximum	1.39	0.57	1.88	0.87

Figure 7-10: MARBLE dot histogram demonstrating cut-off of pretreatment K*trans* 0.38 which distinguished the patients who died with 100% sensitivity, 100% specificity, p= 0.02, n=10. Black dots represent the patients who died, and white dots represent the patients alive.

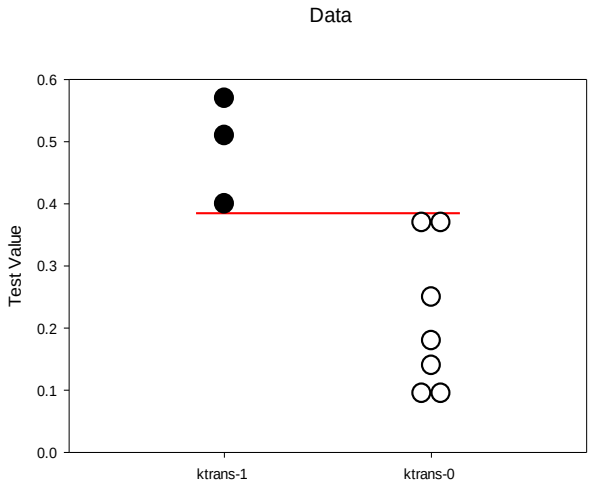

7.4.4 Quantitative assessment of changes in MRI parameters after one and two cycles of chemotherapy

As discussed in the previous chapter, quantitative measurements were technically more challenging to undertake in small tumours or where there was poor bladder distension (Figure 7-11). In general, decreases were observed in K*trans*, K*ep* and tumour volume after one cycle of chemotherapy (Table 7-4). Although not significant, there was a trend with tumour mean ADC increasing and volume decreasing after one cycle of chemotherapy in the DCE cohort (p = 0.09 and p = 0.06, respectively), consistent with findings from the larger cohort of MARBLE patients (Table 7-5). After one cycle of chemotherapy a median fall of 29% (range -28% to 60%) in whole tumour mean K*trans* was recorded in the responding patients (n = 5), compared with 0% and 84% decrease in the two non-responders. Of note, one of these non-responders was the patient previously mentioned in Chapter 6 who was classed as a radiological responder due to tumour shrinkage but at cystectomy had pT2 disease, defining non-responder status. In these two patients, mean tumour ADC increased by 16% and 11% after one cycle. In another patient, the tumour demonstrated shrinkage on CT after 2 cycles but progressed after 4 cycles (Refer to case report, MAR016). Tumour volume continued to decrease after two cycles of chemotherapy; however, K*trans, Kep* values showed no consistent change.

Table 7-4: MARBLE DCE-MRI parameters after 1 and 2 cycles of chemotherapy (n = 7). Wilcoxon signed ranks test comparison of mean K*trans*, K*ep* and tumour volume between scans. A 30 - 50% fall in K*trans* was observed after the first cycle but was not significant. The *p*-value relates to the changes in MRI parameters after 1 or 2 cycles compared to the baseline measurement.

	Baseline			**After 1 cycle chemotherapy**			**After 2 cycles chemotherapy**		
	K*trans*	**K*ep***	**Tumour volume (cm^3)**	**K*trans***	**K*ep***	**Tumour volume (cm^3)**	**K*trans***	**K*ep***	**Tumour volume (cm^3)**
Mean	0.24	0.65	19.7	0.17	0.47	13.2	0.21	0.35	6.16
Median	0.18	0.41	6.44	0.10	0.31	3.85	0.11	0.18	2.61
Minimum	0.09	0.29	1.70	0.06	0.28	0.60	0.04	0.04	0.35
Maximum	0.57	1.88	87.3	0.41	1.01	59.8	0.60	0.86	27.3
***p*-value**				0.25	0.13	0.03	0.40	0.24	0.4

Table 7-5: MARBLE response DWI-MRI parameters for DCE cohort (n = 7).

	Baseline		After 1 cycle chemotherapy		After 2 cycles chemotherapy	
	ADC ($x10^{-3}$ mm^2/s)	**Tumour volume (cm^3)**	**ADC** ($x10^{-3}$ mm^2/s	**Tumour volume (cm^3)**	**ADC** ($x10^{-3}$ mm^2/s	**Tumour volume (cm^3)**
Mean	1.23	10.07	1.36	6.79	1.21	4.41
p-value			0.09	0.06	0.87	0.28
Minimum	0.89	2.62	1.14	0.43	0.84	0.86
Maximum	1.39	26.3	1.55	28.9	1.47	11.3

Tables 7-6 to 7-9 display the qualitative and quantitative response assessments after each cycle of chemotherapy, including data on number of cycles of chemotherapy delivered, and baseline tumour volume. Treatment response was defined pathologically, or in the absence of this data, radiologically.

Table 7-6: MARBLE summary of response assessments after 1 cycle of chemotherapy (mean 12 days). MRI2 = MRI performed after one cycle chemotherapy. R = treatment response, SD = stable disease, U = unclear from imaging due to poor bladder distension; Y = treatment responder, N = non-responder defined by restaging CT or cystectomy.

Patient ID	No of chemo cycles	Qualitative assessment MRI2	% Change mean ADC MRI2	% Change K*trans* MRI2	Treatment Response
9	1.5	R	16	-84	N
11	4	SD	-15	-33	Y
13	3	SD	11	-29	Y
15	6	SD	1	-60	Y
16	4	R	23	128	Y
17	3	U	16	-19	Y
18	4	SD	11	0	N

Figure 7-11: MARBLE T2W images of left-sided bladder tumour (denoted by arrow) at baseline (left panel), after 1 (middle panel) and 2 cycles of chemotherapy (right panel). Note poorly filled bladder on second scan hinders assessment of treatment response and final scan demonstrates response.

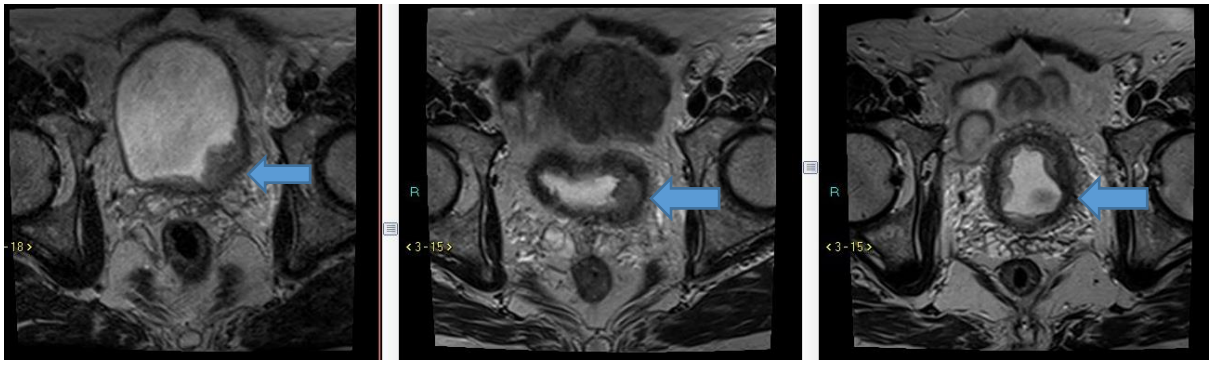

Table 7-7: MARBLE summary of response assessments after 2 cycles of chemotherapy. MRI3 performed after two cycles of chemotherapy. R = treatment response, SD = stable disease, Y = treatment responder, N = non-responder defined by restaging CT or cystectomy.

Patient ID	Baseline Vol	Visual Assessment MRI3	% Change mean ADC MRI3	% Change K*trans* MRI3	Treatment Response
9	7.10	R	4	5	N
11	2.62	R	-15	-44	Y
13	6.06	R	-5	-71	Y
15	39.4	R	-3	-56	Y
16	5.65	R	12	122	Y
17	2.53	R	-26	-51	Y
18	5.88	SD	10	-10	N

Table 7-8: MARBLE individual patient data showing % change in ADC, K*trans* and volume after 1 cycle of chemotherapy (MRI2). Pt 9 was defined as a non-responder due to ≥ pT2 at cystectomy although had regression of disease on CT. Pt 18 was a non-responder due to radiological stable disease on CT after three cycles.

Patient ID		% Change ADC MRI2	% Change K*trans* MRI2	% Change vol MRI2	Treatment response
9		16	-84	-49	N
11		-15	-33	-35	Y
13		11	-29	-56	Y
15		1	-60	-32	Y
16		23	128	-24	Y
17		16	-19	-79	Y
18		11	0	2	N
All cases	**Mean change (%)**	9	-14	-39	
	CoV (%)	1.39	-4.9	-0.66	

Table 7-9: MARBLE individual patient data showing % change in ADC, K*trans* and volume after 2 cycles of chemotherapy (MRI3), Y = treatment responder, N = treatment non-responder.

Patient ID		% change ADC MRI3	% change K*trans* MRI3	% change vol MRI3	Treatment Response
9		4	5	-87	N
11		-15	-44	-59	Y
13		-5	-71	-59	Y
15		-3	-56	-69	Y
16		12	122	-81	Y
17		-26	-51	-88	Y
18		10	-10	61	N
All cases	**Mean change (%)**	-3.29	-15	-54.6	
	CoV (%)	-4.16	-4.4	-0.96	

Table 7-10: MARBLE comparison of early versus end of treatment response assessments. RECIST criteria applied to change in primary tumour thickness, ADC change > 15% = Response, K*trans* change > 14% = Response, ND = not performed. pResponse = pathological response determine at cystectomy, r Response = radiological response determined on MRI or CT after 2 – 3 cycles.

Patient ID	Early response assessment during chemotherapy						End of treatment		
	MRI2			MRI3			pResponse	rResponse	Overall
	RECIST	ADC	K*trans*	RECIST	ADC	K*trans*			
9	PR	R	R	PR	NR	NR	NR	R	NR
11	PR	NR	R	PR	R	R	R	R	R
13	SD	NR	R	PR	NR	R	R	R	R
15	SD	NR	R	PR	NR	R	ND	R	R
16	PR	R	NR	PR	NR	NR	ND	R	R
17	PR	R	R	PR	R	R	ND	R	R
18	SD	NR	NR	SD	NR	NR	ND	NR	NR

All the DCE-MRI and DW-MRI metrics were evaluated for a potential relationship with Ki-67 and survival. Correlations were demonstrated between the percentage change in K*trans* value after one cycle and both Ki-67 score and survival. Higher Ki-67 scores were related to greater decreases in mean tumour K*trans* as seen in Figure 7-12. Furthermore, reviewing the treatment effect measured by change in K*trans*, a correlation with survival was observed with greater falls in K*trans* after only one cycle of chemotherapy in patients who survived longer (Figure 7-13).

Figure 7-12: MARBLE scatterplot of Ki67 score and change in Ktrans after one cycle of chemotherapy, Spearman's correlation coefficient r = -0.78, p = 0.04, n = 7

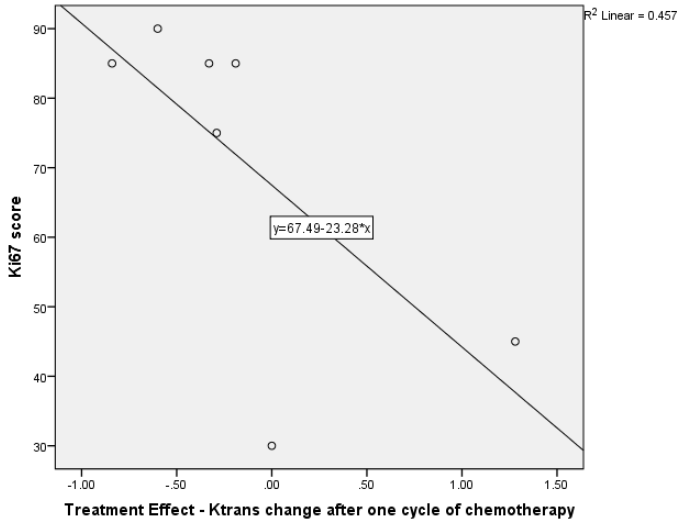

Figure 7-13: MARBLE scatterplot demonstrating negative trend between change in mean K*trans* value after one cycle of chemotherapy and overall survival, r = -0.818, p = 0.02, n = 7.

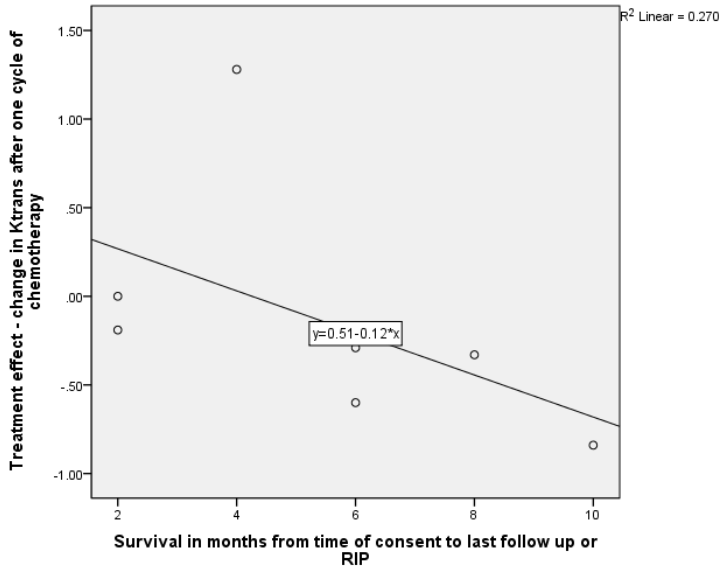

Tables 7-10 and 7-11 list the treatment responses on a per-patient basis, using qualitative and quantitative parameters. Tables 7-12 and 7-13 list the data from each of the early research measurements compared with the routine scan performed at the end of treatment. If one of the non-responders (MAR009) was considered instead as a responder, given tumour downsizing from T3 to T2 and radiological regression, then RECIST measurements of primary tumour thickness would have increased sensitivity from 67% sensitivity after one cycle to 100% after two cycles, and specificity would have been 100% after one and two cycles. Specificity and positive

predictive value would also have increased to 100% after one cycle, and sensitivity would have decreased, for both the DW-MRI and DCE-MRI quantitative parameters under evaluation.

Table 7-11: MARBLE research and routine radiological response assessments performed by a radiologist who visually assessed all MRI scans, but did not undertake quantitative measurements, n = 15, ND = not performed, U = radiologist unable to determine response due to poor visualisation of primary on baseline scan, * denotes CT scan performed after two cycles of chemotherapy.

Patient ID	Chemo cycles	MRI2	MRI3	Restaging CT	Cystectomy	Check Cyst
9	1.5	R	R	R*	SD	ND
11	4	SD	R	R	CR	ND
13	3	SD	R	R	CR	ND
15	6	SD	R	R	ND	ND
16	4	R	R	R*	ND	ND
17	3	U	R	R	ND	NAD
18	4	SD	SD	SD	ND	ND

Table 7-12: MARBLE evaluating change in tumour thickness on T2-W imaging, DCE-MRI and DW-MRI as a measure of early response to treatment after 1 cycle of chemotherapy

	After one cycle		
	RECIST	**DW-MRI (ADC)**	**DCE-MRI (K*trans*)**
Sensitivity	60%	40%	80%
Specificity	50%	50%	50%
Positive Predictive Value	75%	67%	80%
Negative Predictive Value	33%	25%	50%
Positive Likelihood Ratio	1.2	0.8	1.6
Negative Likelihood Ratio	0.8	1.2	0.4
Response Prevalence	72%	71%	71%

Table 7-13: MARBLE evaluating change in tumour thickness on T2-W imaging, DCE-MRI and DW-MRI as a measure of early response to treatment after 2 cycles of chemotherapy

	After two cycles		
	RECIST	**DW-MRI (ADC)**	**DCE-MRI (K*trans*)**
Sensitivity	100%	40%	80%
Specificity	50%	100%	100%
Positive Predictive Value	83%	100%	100%
Negative Predictive Value	100%	40%	66.7%
Positive Likelihood Ratio	2	0	0
Negative Likelihood Ratio	0	0.6	0.2
Response Prevalence	71%	71%	71%

7.5 Discussion

7.5.1 Technical aspects

DCE-MRI is not an established imaging modality in bladder cancer. Whilst some studies report that DCE-MRI imaging provides valuable staging information, the degree of diagnostic accuracy is not statistically superior to images from T2-weighted sequences (Kim *et al.*, 1994; Barentsz *et al.*, 1998; Nguyen *et al.*, 2014). The current European Association of Urology (EAU) guidelines recognise that DCE-MRI may be useful in distinguishing between normal tissue and tumour in the post biopsy setting, but does not recommend it as a routine staging modality or for response assessment outwith clinical trials (Witjes *et al.*, 2015). One aim of the MARBLE study was to assess the feasibility of serial scanning with DCE-MRI in patients with muscle-invasive bladder carcinoma undergoing chemotherapy, in addition to the aims discussed in Chapter 6.

According to the literature, K*trans* is sufficiently reproducible to detect treatment effects of 14 – 20% (Galbraith *et al.*, 2002; Morgan *et al.*, 2006; Lankester *et al.*, 2007). After one and two cycles of chemotherapy, K*trans* changes were between 19% and 128%, and between 44% and 122%, respectively, in treatment responders. Reproducibility is, however, likely to be dependent on the tumour site being imaged. As discussed previously, there are a number of technical challenges, to consider when imaging the bladder of this cohort of patients, which may affect the accuracy of measurements. A repeatability study of DCE was not undertaken within MARBLE for pragmatic reasons but should be evaluated in future work. The MARBLE study

demonstrated that it is possible to obtain tissue-enhancement curves and estimates for K*trans* using a DCE-MRI sequence. Intratumour variability in these parameters was observed, supporting whole tumour *versus* single-slice tumour assessment. The AIF is required for most kinetic models but subject-based estimation can be difficult leading to systematic errors. Considerable variability in subject-based AIF results was demonstrated in MARBLE. To overcome this, we support using a population-based AIF such as the modified Fritz-Hansen method in the analysis, as other research groups have done (Cheng, 2008; Mendichovszky *et al.*, 2009; Li *et al.*, 2011). More recently, the modified Fritz-Hansen AIF has been reported as one of the best performing models for AIF (Woolf *et al.*, 2016).

7.5.2 Baseline DCE – MRI as a prognostic and predictive imaging biomarker

Semi-quantitative analyses methods are simpler and quicker because they can be performed in real time using standard MRI scanning software by the radiologist. Quantitative methods, particularly if they require whole-tumour assessments and specialist software or expertise are logistically more difficult to integrate into routine clinical practice.

Contrast agent is taken up more readily by tumours due to abnormal vasculature, including leaky and dilated vessels, and increased vascular density. Previous studies have demonstrated that following intravenous administration of gadolinium, bladder tumours enhance earlier than inflammatory tissue (Barentsz *et al.*, 1998; Donaldson *et al.*, 2013; Chakiba *et al.*, 2015). Early enhancement can also differentiate higher stage tumours from lower stage lesions (Narumi *et al.*, 1993). Consistent with these results, a more rapid and higher amplitude of enhancement was observed in the tumours with higher Ki-67 scores in the MARBLE study.

Predictive imaging biomarkers may permit personalised medicine. There are little data on the predictive value of kinetic parameters in bladder cancer patients. Despite the low number of patients in the MARBLE study, some interesting findings for K*trans* were observed; pretreatment K*trans* of > 0.38 identified patients who died during the study, with 100% sensitivity and specificity ($p = 0.02$). These patients received none, or only one full cycle of chemotherapy. Several studies have investigated relationships between K*trans*, K*ep,* V*e,* and histological prognostic factors. K*trans* and K*ep* were higher in aggressive breast tumours than in low-grade tumours and Yi

et al reported a strong correlation between K*ep* and high nuclear grade breast tumours, compared with K*trans* (Radjenovic *et al.*, 2008; Yi *et al.*, 2014). Higher histological grade tumours are more aggressive, with poorer prognoses, but if treated, often respond faster to treatment. Accordingly, a number of studies have shown promising associations of high K*trans* and treatment response. In metastatic renal cell carcinoma, higher baseline K*trans* measurements predicted longer progression free survival in patients receiving pazopanib (Sweis *et al.*, 2016). In 2002, Loncaster *et al* found that in 50 patients with cervix cancer, large volume and poor tumour enhancement resulted in poorer outcome following radiotherapy than smaller, better enhancing tumours (Loncaster *et al.*, 2002). It is well recognised that well oxygenated and better vascularised cervical and head and neck tumours respond better to radiotherapy than hypoxic tumours. Hence a correlation between greater degrees of tumour enhancement and better outcome is hypothesised. The ability to predict a better tumour response to chemotherapy or radiotherapy using baseline MRI measurements may guide a patient towards these modalities rather than surgery.

7.5.3 DCE-MRI for Response Assessment

In the absence of marked tumour shrinkage, distinguishing treatment response from chemotherapy-related inflammation in bladder cancer can be challenging on T2-weighted MRI. Furthermore, assessment on CT is difficult and in MARBLE the primary tumour could not be assessed in 3 / 7 patients due to inadequate bladder distension and poor quality images. There is an unmet need for better radiological assessment, and determining the sensitivity and specificity of imaging techniques is a necessary component of evaluation.

Persisting contrast enhancement after a course of treatment may indicate neovascularity, consistent with a poor response to chemotherapy. Enhancement of bladder tissue within 10 seconds of arterial enhancement, or abnormal areas of persisting contrast enhancement indicated treatment failures (Barentsz *et al.*, 1998). In further work, this group showed that after 2 cycles of methotrexate, vinblastine, adriamycin and cisplatin (MVAC) chemotherapy, ADC increased by 14% and fast DCE-MRI correctly determined treatment response in 33 of the 36 patients, generating a positive predicative value of 87% for DCE (Schrier *et al.*, 2006). Cisplatin gemcitabine chemotherapy has demonstrated similar survival figures as

MVAC, but with less toxicity (von der Maase *et al.*, 2000), and has been adopted by many oncological centres as the standard of care.

Donaldson and colleagues measured relative signal intensity (rSI) in 21 bladder cancer patients and reported its use in differentiating residual tumour from treatment effect (Donaldson *et al.*, 2013). Another group reported that rSI at 80 seconds before and after two cycles of chemotherapy was significantly different between pathological complete responders and non-pathological complete responders, with a cut-off value of 40% (Chakiba *et al.*, 2015). This group also reported a reduction in tumour thickness and diameter in treatment responders.

An objective of the MARBLE study was to evaluate model-based kinetic parameters as imaging biomarkers. K*trans* appeared the superior quantitative parameter in the MARBLE study demonstrating 80% sensitivity and 50% specificity after one cycle, increasing to 100% specificity after two cycles, with no loss in sensitivity. The classification used to determine response is currently not standardised and varies between studies. Changing the classification of one patient (MAR009) in a small study such as MARBLE, increased the response rate from 71% to 86% resulting in 83% sensitivity after one cycle and 100% specificity, and compared to 67% and 50% for RECIST tumour thickness and ADC measurements, respectively. As expected, sensitivity for the RECIST tumour measurements increased over time, to 100% after two cycles.

The fully quantitative analysis proved challenging for reasons explained previously so an alternative method employing tissue enhancement curves was evaluated in a sub-group of patients. From the data obtained, TTP and AUC were of smaller magnitude in the early follow-up scans in responders. Similar findings have been reported in responding breast cancer patients (Yi *et al.*, 2014). Furthermore, in MARBLE non-responders, contrast agent uptake curves showed faster and stronger tumour enhancement after one or two cycles of chemotherapy, compared with pre-treatment imaging. Li *et al* reported that the signal enhancement washout ratio and K*ep* were significantly different between pathological complete responders and non-responders after one cycle of chemotherapy in breast cancer patients (Li *et al.*, 2014). Ashraf *et al* reported greater peak enhancement, more rapid wash-out and heterogeneous uptake in the responding tumours, resulting from a greater arterial supply and a more aggressive tumour (Ashraf *et al.*, 2015).

Alternative DCE-MRI analysis methods have been reported. Recently, in a study of bladder cancer patients, K-means clustering of 3T-derived DCE kinetic parameters has shown some promise predicting treatment responses mid-chemotherapy cycle with good sensitivity/specificity/accuracy (96% / 100% / 97%) (Nguyen *et al.*, 2015). Although the timing of the mid-cycle MRI was not clear, the authors reported a further advantage of K-means clustering is the ability to evaluate whole tumour heterogeneity by measuring microcirculatory changes. The response rate of the study participants to chemotherapy was similar to the MARBLE study cohort, with 23 / 27 treatment responders, and 10 / 27 developed a complete pathological response.

Fewer studies have evaluated K*trans* in bladder cancer. In MARBLE, K*trans* estimates decreased within 12 days of Day 1 of the first cycle of chemotherapy. Evaluation of chemotherapeutic response at this early stage is unreported in bladder cancer, to the best of our knowledge. To understand the rate of the decrease in K*trans* requires multiple time-point imaging with serial scans, yet the literature base is sparse. In the MARBLE study, a median fall in K*trans* of 33% was recorded after one cycle of chemotherapy. The magnitude of the fall after one cycle is similar to previous studies which scanned at a later time-point. For example, in breast cancer, after two cycles of chemotherapy, a median fall in K*trans* of 40% and median increase of 18% was reported in treatment responders and non-responders, respectively (Ah-See *et al.*, 2008).

One of the non-responding MARBLE patients, who had stable disease after three cycles of chemotherapy, demonstrated no change in K*trans* after one cycle, and a 10% change (less than the reproducibility value of 12 – 20%) was measured after two cycles. ADC changes were also less than the threshold for repeatability of 15%, described in the previous chapter.

Patient MAR016 is worthy of particular mention. Despite an increase in mean ADC after one cycle of chemotherapy, which is suggestive of a treatment response, mean K*trans* considerably increased, which is more consistent with treatment failure. Additionally, the contrast enhancement curve showed progressive rises in the amplitude of enhancement after the both the first and second cycles of chemotherapy. The restaging CT after two cycles of treatment demonstrated shrinkage in tumour volume. After a further two cycles of chemotherapy, the tumour volume had increased, suggesting that the tumour which initially responded quickly

became resistant requiring termination of chemotherapy. The Ki-67 score was 45%. In this case, although the DCE data yielded results which contradicted the initial anatomical assessment after two cycles, they predicted the ultimate response suggesting that the DCE may have detected early functional changes consistent with treatment failure. Perhaps, if the patient had been scanned after three cycles in line with the protocol, the findings would have been consistent. Given the relatively low Ki-67 score, with respect to the trial cohort, it may not be surprising that the TTP was longer and the peak enhancement curve was lower than other tumours with higher Ki-67 scores.

Further discussion of the third patient classed as a treatment non-responder is also warranted. K*trans* decreased by 84% suggesting treatment response, and ADC was a borderline response with a calculated increase of 14%. MRI imaging demonstrated tumour shrinkage; however, the patient was recorded as a non-responder to treatment, due to TNM stage greater than pT2, despite down-staging. Although using a recognised scoring system to classify treatment responders and non-responders allows comparison between studies, this score could be criticized for under-estimating treatment effects. In the case of this particular patient, an inadequate dose of chemotherapy was delivered (1.5 cycles), but this nevertheless resulted in tumour shrinkage. If the patient had tolerated further chemotherapy, continued response to treatment may have redefined the patient as a responder, and from a “false positive” treatment responder to a “true positive” responder. Other research groups have defined treatment response as > 50% decrease in the summed products of the longest perpendicular diameters and the absence of new lesions (Schrier *et al.*, 2006). Lack of a consensus on this topic challenges the comparison of response assessments between research studies.

A greater understanding of the relationship between semi-quantitative tissue enhancement measurements and K*trans* is required. Hayes *et al* reported that changes in the rate of tumour enhancement correlated strongly with K*trans* values but that the shape of the enhancement curve only changed when the K*trans* value changed by more than 50%. Additionally, a larger decrease in the higher pre-treatment K*trans* values was observed, particularly in responding patients (Hayes *et al.*, 2002). High median V*e* pre-treatment was associated with the greatest tumour shrinkage in one small study of eight patients (O'Connor *et al.*, 2011). Yi *et al*

demonstrated a significant correlation between model-based (K*trans*, K*ep* and V*e*) and model-free kinetic parameters (signal intensity curves) in breast cancer patients (Yi *et al.*, 2014). Mean K*ep* was higher in tumours with an early rapid and delayed washout pattern. K*ep* was associated with TTP, K*ep* with washout slope and V*e* with TTP. They did not find a correlation between K*ep* and K*trans,* and hypothesised that this was due to K*trans* reflecting microvascular blood flow, vessel permeability and vessel density, whereas Kep reflects vessel permeability and is not subject to variable factors such as hypertension, cardiac output.

Organ-preservation is an important consideration for patients with bladder, rectal, oesophageal and gastric tumours. Lower mean K*trans* after chemoradiotherapy correlated with pathological complete response in a cohort of rectal cancer patients (Gollub *et al.*, 2012). Ultimately, changes in the kinetic parameters need to correlate with patient outcomes and be clinically relevant, prior to being incorporated into routine practice. A greater than 40% decrease in K*trans* after five cycles of bevacizumab treatment was associated with longer progression free survival in metastatic colorectal cancer (De Bruyne *et al.*, 2012). In MARBLE, the change in mean K*trans* after one cycle of chemotherapy was statistically significant and there was a trend towards better survival in the patients with greatest changes in K*trans.* Studies require long follow-up periods to enable collection of survival data, and it is anticipated that further data on this topic will follow in the next five to ten years, as studies report their longer-term outcomes.

Currently, reports in the literature are varied, and Intven *et al* did not find that changes in K*trans* predicted response to chemoradiotherapy in rectal cancer patients (Intven *et al.*, 2015). Further to studying 55 patients, they found that change in ADC value on DW-MRI had the best accuracy for predicting pathological responders, compared to DCE-MRI and tumour volume shrinkage.

Mechanistic modelling of tumour heterogeneity using DCE parameters in the assessment of treatment response is another analysis method which has been performed in breast cancer patients (Venkatasubramanian *et al.*, 2010). These authors observed that vascular transport heterogeneity was associated with increased tumour growth and poor response to treatment. A comparison of histogram analysis of pixel maps against whole tumour ROI-analysis on a single-slice

to derive changes in K*trans* measurements concluded that the two methods generated approximately equal results (Hayes *et al.*, 2002).

7.5.4 Ki-67 scores

Ki-67 has been established as both a predictive and prognostic biomarker in bladder cancer and although it has been used to influence treatment decisions in other malignancies, e.g. lymphoma, is not widely used in bladder cancer. In MARBLE, of the tissue enhancement curves analysed, there was a trend observed between high Ki-67 score and more rapid TTP and higher AUC. High pre-treatment Ki-67 scores may have a role in predicting early treatment responses due to the strong association with change in K*trans* value after one cycle of NAC in treatment responders in the MARBLE cohort of patients. The higher pre-treatment Ki-67 scores resulted in a greater change in mean K*trans* which was associated with greater survival. These findings are supported by Tanabe *et al* who found that high Ki-67 expression favoured treatment with CRT as a multimodality treatment, and was associated with improved survival (Tanabe *et al.*, 2015). As a prognostic biomarker, Lara *et al* evaluated Ki-67 scores in 55 bladder cancer patients and found that 5-year survival in tumours with Ki-67 > 27% was 32% compared with 69% if Ki67 was <27% (Lara *et al.*, 1998). Margulis and colleagues' review of more than 700 patients found that Ki-67 expression > 20% was independently associated with 5-year cancer specific survival of 23% compared to 36% p = 0.001 if Ki-67 was <20% (Margulis *et al.*, 2009). Accordingly, there may be a role for including Ki-67 score in a prognostic tool in bladder cancer, as is the case in other malignancies, e.g. breast, lymphoma, cervix, head and neck. Currently, it does not form part of the routine pathological examination of bladder specimens in our institution and is not mentioned in the EAU guidelines (Wang *et al.*, 2014b; Engelberg *et al.*, 2015; Witjes *et al.*, 2015; Wu *et al.*, 2015b). The findings from the latter studies further support evaluation of histopathological biomarker data, and other cell cycle markers such as p21, p27, p53, cyclin E which may play an important role forecasting outcome (Krabbe *et al.*, 2014).

7.6 Conclusions

The MARBLE study demonstrated that it was technically feasible to acquire DCE-MRI serial images of bladder tumours to derive kinetic parameters. In some patients, the DCE-MRI sequences aided localisation of the tumours.

More aggressive tumours are reported to be characterised by low ADC, high K*trans* and high Ki67 levels (Ashraf *et al*., 2015). Supporting these data, a negative correlation between mean ADC and K*trans* estimate was recorded in MARBLE.

Mean K*trans* decreased after 1 cycle of NAC (with a sensitivity of 80% and 50% specificity) consistent with treatment response according to literature, and longer survival was observed in the patients with greatest changes in K*trans*. The DCE-MRI parameters were superior to the DW-MRI in the MARBLE cohort in predicting treatment response.

Semi-quantitative DCE analysis is more feasible than fully quantitative K*trans* measurements and does not require offline processing. DCE-MRI (particularly semi-quantitative contrast uptake curves) looks promising but further investigation is required. Intra- and inter-tumour variability was observed in the contrast uptake curves between tumour slices. Further data analysis is required before firm conclusions can be made on single-slice versus whole tumour assessments. Future work will investigate if these relationships can be reproduced in a larger patient population, and quantify the predictive value of MRI kinetic parameters for treatment outcome. Some results suggest that DCE-MRI and DW-MRI are complementary techniques, and this could be explored further.

This chapter concludes the reports from the clinical trials portfolio and is followed by final concluding remarks.

Chapter 8 Final Discussion

8.1 Development of Imaging Biomarkers

Functional imaging techniques may permit personalised medicine within oncology. Many palliative oncological treatments have only a 20 - 30% response rate, thus it is desirable to discontinue ineffective treatments at an early stage to minimise side-effects, and direct the patient to an alternative treatment, or best supportive care. Routine CT / MRI assessments for treatment response are typically performed after two or three months of treatment. PET tracers and functional MRI techniques are sensitive to changes in tumour biology within shorter time-frames of hours or days, enabling the early assessment of treatment response. Imaging biomarkers are an appealing alternative to the collection of biomarker data from invasive procedures and can provide whole tumour in-situ evaluation. Furthermore, in the development of novel drugs, early pharmacodynamic endpoints can be derived from imaging biomarkers. In the tumour sites investigated in this dissertation (pancreas, head and neck, bladder and thyroid), targeted agents are yet to have a significant impact on survival. Thus, there is considerable research potential for the development of imaging biomarkers to facilitate the development of promising drug targets in these cancers.

Prior to incorporation into clinical practice, an imaging technique needs be: evaluated *in vitro*, in animals and humans; and address specific clinical questions. O'Connor *et al* refer to the process as crossing two translational gaps (O'Connor *et al.*, 2016). After the period of evaluation, the imaging biomarker must pass the first translational gap to become a robust imaging tool. Fewer imaging biomarkers pass the second gap which requires demonstration of the technique as a reliable method to test specific hypotheses in clinical research. This dissertation has evaluated FLT PET-CT, DW-MRI and DCE-MRI at different stages in the development pathway. Detection of selected tumours using the FLT PET-CT imaging technique was first performed, followed by a series of experiments to optimise imaging in a tumour cell line which has poor FLT uptake. To advance knowledge on three tumour groups which have been previously studied using one or more of the imaging modalities under investigation, unanswered questions relating to the evaluation of, and quantification of treatment response, and optimal time-point for imaging were addressed in clinical studies.

8.2 Chapter conclusions and planned future work

8.2.1 FLT PET-CT

In the MARBLE-FLT study, pre-treatment FLT PET-CT scans were acquired of patients with muscle-invasive transitional cell bladder carcinomas to evaluate if the tumours were FLT-avid, and if a trial-specific scanning protocol could reduce the urinary activity of the radiotracer sufficiently to enable detection of the bladder wall tumours. Using a dilution protocol of intravenous low-dose furosemide, oral hydration and delayed imaging reduced the SUVmax of urine by mean 72% (range 48 – 86%, n = 5, $p<0.01$), resulting in a test sensitivity of 80% and a positive predictive value of 100%. Detection of nodal disease was less accurate, with sensitivity 67%. Mean SUVmax of tumours was 7.7 (range 4.4 – 11, n = 4) and mean Ki-67 score 70% (range 45 – 90%, n=4).

There is a 20 - 40% relapse rate within three years of radical surgery or chemoradiotherapy in bladder cancer (Solsona *et al.*, 2003; Cagiannos and Morash, 2009; Mitra *et al.*, 2012). Early identification of relapse using non-invasive PET imaging may improve the current median survival of six months by accelerating the treatment pathway (James *et al.*, 2012; Mitra *et al.*, 2012). Using the MARBLE-FLT scanning protocol, the FLT PET-CT scan could be used to assess treatment responses in both the primary bladder cancer and the metastatic disease. PET-MRI may overcome the problem of poor registration of CT with PET images of a filling bladder. Multiple-time-point anatomical images of the bladder can be acquired with no radiation exposure concerns, and may be a promising area to investigate further. One of the practical considerations for further studies with FLT, however, is its limited availability. Modifying a scanning protocol similar to the one used in MARBLE-FLT for the more readily available FDG may be a more pragmatic option, and a recent funding application led by the author to evaluate this further has been successful.

There is increasing interest in the incorporation of PET or functional MRI imaging to personalise radiotherapy treatment plans. However, how to achieve this remains a subject of debate. To reduce the inter-observer variability in gross tumour volume (GTV) definition, a number of image processing methods are under investigation. Appropriate segmentation of the images is required. The International Atomic Energy Agency (IAEA) guidance on PET-CT in radiotherapy planning suggests that a useful

metric in delineating tumours is the background cut-off approach whereby a tumour volume is grown from the maximum value to 3 standard deviations (SD) above the background level (Watanabe and Jeremic, 2008). In MARBLE-FLT, the relevant background was the normal bladder and for patients 002 and 016, the tumour signal was greater than three standard deviations (3SDs) above the background, therefore suggesting that ROIs for these tumours could be drawn using an auto-contour methodology.

Demonstrating that either FDG PET or a research tracer such as FLT can be used to assess primary bladder tumours has the potential therefore to: minimise the number of scans a patient needs to attend; upstage a small group of patients and prevent futile surgery with significant associated morbidity; assess response early with subsequent tailoring of treatment programmes; and detect early regional or metastatic recurrences.

PET imaging of pelvic tumours such as cervix, endometrial, and rectum is also limited by high urinary concentrations of the PET tracer, so an enhanced imaging protocol which reduces this activity may have transferrable applications to other primary tumour sites.

Clearly, imaging pelvic tumours with renally excreted tracers is technically challenging. However, progress is being made towards inclusion of PET as a useful imaging modality in bladder cancer. Recognition that imaging protocols need to be modified according to the tracer being used, dose administered, the constituents of the urinary system and the patient's general fitness, is likely to contribute to making gains in this field.

The THRIFT study imaged two patients with differentiated thyroid cancers, which had low Ki-67 scores on biopsy samples; FLT uptake was minimal, thus, FLT-guided radiotherapy plans were not technically feasible. More promising data is expected to be achieved in anaplastic thyroid cancers where the histological samples show Ki-67 scores of 12 - 70% (Katoh *et al.*, 1995). These patients are rarely treated with radically intended radiotherapy due to poor performance status from a rapidly progressive tumour. Typically RT is delivered in the adjuvant setting postoperatively, when there is no radiologically visible disease, or for symptom control. If tumours can be identified at an earlier stage when patients are fit for chemoradiation, there may

be a role for FLT PET-CT scans for treatment planning or early response assessment.

Pancreatic cancers are an example of tumours with higher Ki-67 scores. In the response assessment study discussed in Chapter 3, increases in the SUVmax of greater than 12% after one cycle of chemotherapy predicted for poor response to chemotherapy. Applying a kinetic filter to the dynamic images improved visualisation of primary and secondary tumours, if size was greater than 2cm. This study has provided preliminary data to enable design of a later phase study where the on-treatment algorithm is influenced by the early imaging results.

Although SUVmax increases were identified in pancreatic cancer patients receiving chemotherapy, all oropharyngeal cancers showed a decrease in the SUVmax of primary and nodal regions after a median of 7 fractions of radiotherapy. Across the cohort, for each patient the most avid FLT lesion decreased from a median of SUVmax 7.3 on scan 1 to SUVmax 4 on scan 2. However, decreases in the FLT uptake did not predict clinical response in all patients. The two patients with baseline SUVmax of greater than 9.9 developed metastases and died within the median follow-up of 31 months (range 16-37 months). The 2-year survival of FLAIRE study patients was 88%, and there was only one patient in the cohort who had residual disease after chemoradiotherapy, thus collection of further imaging data on non-responders would be valuable. Scanning 6-weeks after completion of treatment resulted in a negative predictive value of 100%. Many of the patients had oedema on clinical examination post treatment, which may mask response, and imaging at this time-point may be clinically relevant as discussed in Chapter 4. A reported appealing property of FLT is that it is taken up less readily by inflammatory tissue, and is more specific to neoplasia; in FLAIRE, false positive uptake was observed in patients who had a recent history of dental extraction, which is a common occurrence in these patients prior to chemoradiotherapy. This finding may limit the utility of FLT in this setting. The Ki-67 score was unknown in this cohort, hence work is planned to evaluate the relationship between Ki-67 score and FLT uptake.

Extending the application of FLT PET-CT to guide radiotherapy treatment plans was studied in FLAIRE. A 70% SUVmax subvolume was defined and boosted to 75 Gy on simulated radiotherapy plans in several patients. Dose volume histograms for the boost plan met radiotherapy planning constraints for the planning target volume and

organs at risk suggesting it is feasible to dose-escalate a proliferative sub-volume using pre-treatment FLT PET-CT imaging acquired in the radiotherapy treatment planning position. How this impacts on radiotherapy side-effects, specifically acute mucositis, warrants further evaluation in a clinical trial.

FLT uptake is known to be influenced by endogenous thymidine levels, thymidine kinase-1, thymidine phosphorylase and equilibrative nucleoside transporter-1. Endogenous tumour thymidine competes with fluorothymidine affecting the uptake, irrespective of cell cycle stage (Zhang *et al.*, 2012b). No plasma thymidine was detectable in eight FLAIRE patients, using the assay described in Chapter 5; data on tumour thymidine were not collected. The SW-620 colorectal tumour xenografts are FLT poorly-avid, hence a study to optimise the FLT PET-CT images was devised. Administration of exogenous thymidine phosphorylase to nude mice increased the FLT uptake within tumours, improving the potential for response assessment using FLT PET-CT. A further pre-clinical experiment to evaluate the ability of FLT PET-CT to detect treatment responses in underway in collaboration with Imperial College. Providing the administration of TP does not demonstrate increased tumour growth, a clinical study is planned to improve FLT PET-CT imaging in selected tumours.

Levels of TK1 are high in proliferating and malignant cells, and FLT PET-CT scans demonstrate raised uptake in proliferating regions. Earlier studies have demonstrated higher levels of serum TK1 in patients with solid tumours than in healthy individuals presumably due to leakage of TK1 from tumour into the blood (Li *et al.*, 2010; Jagarlamudi *et al.*, 2015). High levels of tumour TK1 are a poor prognostic indicator and levels may reflect tumour size and degree of proliferation (Nisman *et al.*, 2010; Chen *et al.*, 2013; Xu *et al.*, 2014). Serum TK1 activity has been investigated as a prognostic and response biomarker, but recent studies have demonstrated that a serum TK1 protein assay is more sensitive and may have improved clinical utility (Gronowitz *et al.*, 1983; He *et al.*, 2005; Li *et al.*, 2010; Chen *et al.*, 2015b; Jagarlamudi *et al.*, 2015) . An ELISA for measuring serum TK1 protein which can be used for prognosis and early detection of relapse is available, and the author is leading a further study within Newcastle to evaluate if there is a relationship between serum levels of TK1 and tumour FLT-PET uptake, independent of tumour volume. Initially, inter- and intra-patient variability in TK1 levels will be determined in a small cohort of patients with non-small cell lung cancer (NSCLC) or breast cancer (10

patients of each tumour type with 2-3 pre-treatment serum samples taken at the same time as routine bloods). The relationship to tumour burden, measured on CT will be studied. The second part of the study will evaluate the relationship between pre-treatment serum TK1 levels and tumour FLT-PET uptake in a small cohort of patients with NSCLC and breast cancer. If the data generated are promising, an application to the CRUK Biomarker Panel to evaluate serum TK1 as a screening tool for FLT PET-CT will be submitted.

An interesting area of clinical research which is important to mention, is the identification of a tumour flare response on FLT PET-CT imaging. Kenny *et al* observed an increase in breast tumour FLT uptake as early as 1 h after capecitabine administration, concluding that FLT PET-CT could be used to measure the effect of thymidylate synthase (TS) inhibitors, e.g. capecitabine (Kenny *et al.*, 2009). Further studies of tumour flare response characterised by FLT PET-CT imaging are awaited.

8.2.2 DW-MRI and DCE-MRI

Serial imaging with PET-CT has a number of drawbacks including: the exposure of patients to additional radiation; an out-patient visit of several hours duration; the high financial cost of the PET radiotracer and the PET-CT scan which may be in excess of £1000; availability of the radiotracer; and the number of staff required to arrange, perform and report the scan. Serial MRI imaging does not involve ionising radiation, and is generally a less costly and more widely available investigation. However, off-line processing of images may be more complex and more time-consuming than for PET-CT.

In the MARBLE study two functional MRI modalities were investigated for early assessment of treatment response in bladder cancer, employing fully quantitative and semi-quantitative approaches. Technical challenges of imaging tumours less than 20mm thick post-surgical resection were encountered. The MRI sequences were less accurate at identifying involved lymph nodes than the staging CT in the cohort studied. Scanning parameters were optimised separately for DW-MRI and DCE-MRI to enable acquisition of data which could be analysed to derive quantitative parameters. DW-MRI repeatability data indicated that an ADC increase of greater than 15% is required to detect a treatment effect. In MARBLE the mean ADC change was small in responders (mean 8.8%, median 12%); yet the literature suggests

treatment effects of less than 27% are unlikely to be detected with confidence. Mean ADC measurements of the central single-slice was found to be representative of the mean of ADC measurements from the whole tumour, and it is recommended that future studies should be directed to single-slice analysis which will reduce the workload of off-line processing.

As a predictive biomarker, pre-treatment mean ADC of greater than 1.26 predicted the non-responders to treatment with 100% sensitivity and 80% specificity. A greater change in ADC was seen in the tumours with lower pre-treatment ADC after one cycle of chemotherapy. In the DCE-MRI cohort, a pre-treatment K*trans* of greater than 0.38 predicted the patients who died with 100% sensitivity and 100% specificity.

Patients are usually imaged with CT after three cycles of chemotherapy. Tumour shrinkage was observed in 33% of patients after a median of 12 days from the first cycle of chemotherapy. Quantitative DW-MRI improved the detection of early treatment response after one cycle. After two cycles, responding tumours had shrunk further and the added value of DW-MRI is unclear. Mean K*trans* decreased after one cycle, consistent with treatment response. After one cycle of chemotherapy K*trans* predicted more treatment responders than DW-MRI and tumour thickness assessment, with sensitivity 80% and specificity 50%, increasing to sensitivity 80% and specificity 100% after two cycles.

Fully quantitative DCE-MRI is technically challenging to undertake, requiring administration of intravenous contrast, the need for robust quality assurance processes and more complex analysis. Semi-quantitative approaches are less demanding potentially providing more rapid answers on response assessment; the uptake curves studied demonstrated clear changes in contrast agent uptake consistent with treatment responses in several patients. The main focus of the MARBLE study was the derivation of quantitative parameters, thus the analysis of contrast-agent uptake curves was limited. In view of the challenges encountered with robust quantification of kinetic parameters (described in more detail in Chapter 7), further work is ongoing to complete collection of contrast agent uptake data on a larger cohort of patients; TTP and AUC at 60, 90, and 120 seconds, is being measured.

For the purposes of standardising radiological reports and generating an objective score of response, a trial-specific proforma for MARBLE has been devised by the author. This is being completed independently by two radiologists who are blinded to the clinical details of the patients. Images will be analysed for maximal tumour thickness perpendicular to the bladder wall, nodal involvement, comment on the extent of restricted diffusion and contrast enhancement within the known tumour, any evidence of necrosis, and document changes in tumour size. In view of concerns that the RECIST 1.1 score is of limited use in this clinical setting, two four-point scores have been devised to record the extent of the primary tumour prior to treatment, and the effect of treatment (Tables 8-1 and 8-2). In the case of discordant responses, a consensus score will be allocated. Collection of these data are ongoing and will be presented at a later date.

Table 8-1: Newcastle Bladder Score - baseline MRI assessment

Score	MRI findings
0	No abnormal thickening or evidence of disease
1	Minor stranding probably benign or treatment related
2	Thickening of bladder wall suspicious for malignancy
3	Presence of primary tumour

Table 8-2: Newcastle Bladder Sore - MRI response assessment

Score	MRI findings
0	No abnormal thickening or evidence of disease = Complete response
1	Residual thickening = PR
2	No change = SD
3	Increase in tumour bulk or new lesions = PD

Within the UK bladder community, there is concern that for patients with muscle-invasive disease the wait for a TURBT introduces unnecessary delays in the treatment pathway. This hypothesis forms the basis for the clinical trial BladderPATH which is due to open to recruitment shortly. The investigators are introducing parametric MRI in place of TURBT to assess for extent of muscle invasion, with the

hope that this will reduce treatment delays. One of the main advantages of DW-MRI is that it is considered truly non-invasive. No intravenous access is required. Conversely, gadolinium-based contrast agents are more labour-intensive for staff. They may cause an allergic reaction, and cannot be given to patients with severe renal impairment as may cause nephrogenic systemic fibrosis. There have been reports of gadolinium deposition in the cerebellum following repeated administration, but the clinical significance of this is unclear (Olchowy *et al.*, 2017). The author's institution is considering participating in the BladderPATH study. Timing the MRI prior to TURBT when the tumours are larger may overcome some of the technical challenges faced in the MARBLE study.

Building on the work described the author is collaborating with a research group led by Professor Robert Huddart at the Institute of Cancer Research to deliver a clinical study using functional bladder MRI to plan and assess radiotherapy treatment. The study protocol is being drafted and will form an imaging sub-study for the multicentre Phase III RAIDER study in bladder cancer patients which opened to recruitment in 2015.

Ki-67 score is not routinely tested in the author's institution but the MARBLE study found that a Ki-67 score above the median predicted for worse outcome; median survival was 28 months if Ki-67 score was greater than 79%, but has not been not reached if the Ki-67 score was less than the median. This histopathological biomarker could be used to identify patients with an anticipated poorer outcome who may be better suited by an alternative treatment strategy, or entry into a clinical trial.

8.3 Limitations

There were a number of limitations to the studies described in the dissertation. In the MARBLE trial, it would have been preferable to run an optimisation study for the development of the DW-MRI and DCE-MRI protocols before recruiting patients. The number of patients was small and in the MARBLE and FLAIRE studies there were particularly few non-responders to treatment. The number of events due to recurrence or death would increase with a longer duration of follow-up. When the MARBLE study was designed it was anticipated all patients would have radical cystectomies and there would be pathological correlation for the imaging. However, due to a change in the standard of care, radiological assessments were required for

those who did not have cystectomies. CT imaging of the bladder for restaging is limited, thus MRI is suggested as an alternative for local assessment of treatment response, and either surgery or radiology chosen for all the response assessments in future studies.

8.4 Future directions – PET-MRI

The increasing capabilities of hybrid-imaging and an increasing interest in the oncological and neurological applications of functional imaging have facilitated the installation of PET-MRI and SPECT-CT scanners which are enabled for radiotherapy planning, by Newcastle University and the Newcastle upon Tyne Hospitals NHS Foundation Trust. PET-MRI provides higher soft tissue contrast than PET-CT, using reduced radiation. Within the radiotherapy department at the Northern Centre for Cancer Care, the author is involved in a research collaboration to evaluate MR-only radiotherapy planning. PET-MRI proof-of-concept studies are encouraging prompting interested in clinical validation studies. Building on the work undertaken for this PhD, the author plans to evaluate FLT PET-MRI in head and neck cancer radiotherapy planning. Combining novel targeted agents with radiotherapy is an exciting area that could be developed further using FLT, DWI-MRI or DCE-MRI imaging biomarkers to provide the surrogate end-points to guide the ‘go and no-go’ decisions faced by the drug developers.

8.5 Final Conclusions

Whether FLT PET-CT, DWI-MRI and DCE-MRI will be incorporated into routine clinical pathways, or hold a pivotal role in drug development in the future is unclear. However, the scientific work described in this dissertation provides a foundation to support the further development of novel imaging biomarkers in larger clinical trials to robustly clinically validate their use.

Appendix

List of abbreviations

ADC - apparent diffusion coefficient

AIF – arterial input function

AUC_{60} – area under the curve at 60 seconds

BM - biomarker

CoV – coefficient of variation

CR – complete response

pCR – pathological complete response

CRT - chemoradiotherapy

CT – computed tomography

CTV – clinical target volume

DTC – differentiated thyroid cancer

DW-MRI – diffusion weighted magnetic resonance imaging

DCE-MRI- dynamic contrast-enhanced magnetic resonance imaging

DFS – disease free survival

DTC – differentiated thyroid cancer

EANM – European Association of Nuclear Medicine

EAU – European Association of Urology

EES – extravascular extracellular space

EE-TP – erythrocyte encapsulated thymidine phosphorylase

EORTC – European Organisation for Research and Treatment of Cancer

FDG – 18F-fluorodeoxyglucose

FLT – 18F-fluorothymidine

FMISO – 18F-fluoromisonidazole

FNA – fine needle aspiration

G-CSG – granulocyte stimulating factor

GIST – gastrointestinal stromal tumours

GMP – good manufacturing process

GTV – gross tumour volume

Gy – gray, measurement of absorbed dose of ionising radiation, 1 Gy = 1 J/Kg

HANSCC – head and neck squamous cell cancer

HE – haematoxylin and eosin

HPLC – high performance liquid chromatography

IAEA – International Atomic Energy Agency

IdUrd - iododeoxyuridine

IHC - immunohistochemistry

IMRT – intensity modulated radiotherapy

IV - intravenous

K*trans* – volume transfer constant between blood plasma and extravascular extracellular space

K*ep* – rate constant of exchange between extravascular extracellular space and plasma

L5 – fifth lumbar vertebra

LRC – loco-regional control

LN – lymph node

MIBC – muscle-invasive bladder cancer

MMM – mucosal malignant melanoma

MMT – multimodality treatment (TURBT, chemotherapy and radiotherapy)

MRI- magnetic resonance imaging

MTV – metabolic tumour volume

NAC – neoadjuvant chemotherapy

NAD – no abnormality detected

NCCC – Northern Centre for Cancer Care

NCI – National Cancer Institute

NCRI – National Cancer Research Institute

ND – scan not performed

NICE – National Institute for Health and Care Excellence

NMIBC – non muscle-invasive bladder cancer

NUTH – Newcastle upon Tyne Hospitals NHS Foundation Trust

OAR – organ at risk

OS – overall survival

PCNA – proliferating cell nuclear antigen

PD – progressive disease

PD-ECGF – platelet-derived endothelial cell growth factor

PERCIST – PET response evaluation criteria in solid tumours

PET – positron emission tomography

PFS – progression free survival

PRV – planning risk volume

PTV – planning target volume

RECIST – response evaluation criteria in solid tumours

RF – radiofrequency

RIA - radio-iodine ablation

ROI – region of interest

RT – radiotherapy

SD – stable disease

SNR – signal to noise ratio

SUV – standard uptake value

TAC – time activity curves

TE – echo time

Tg – thyroglobulin tumour marker

TK1 – thymidine kinase 1

TLP – total lesion proliferation

TNM – tumour nodal metastasis staging

TP – thymidine phosphorylase

TR – repetition time

TS – thymidine synthase

TSH – thyroid stimulating hormone

TTP – time to peak

TURBT – transurethral resection of bladder tumour

USS – ultrasound scan

V*e* – fractional volume of extravascular extracellular space, K*trans*/K*ep*

V*p* – fractional plasma volume

VOI – volume of interest

VZ – varicella zoster

WBS – whole body scan

5FU- 5-fluorouracil

MARBLE Additional scanning details and quantitative results

DW-MRI Scanning details

The scanning protocols were reviewed during the course of the study following detailed image analysis. For the final patients on the study a considerably shorter scanning acquisition protocol was followed. Only sequences from the original protocol which were necessary for the qualitative radiological review and quantitative analysis were acquired. Changes were made as follows:

- the superior block of T1-weighted, T2-weighted and DW-MRI images were not obtained in the repeatability scan
- pre-contrast multiple flip angles were obtained from two repeats instead of six
- a series of 99 DCE images were acquired instead of 111
- post-contrast multiple flip angles were not obtained
- the superior block of T1-weighted, T2-weighted and DW-MRI images was excluded in the second and third scans in node negative patients. This resulted in reducing the initial scan time by 17 minutes to 30 minutes, and subsequent scans by eight minutes to 22 minutes
- in line with new multicentre trial protocols of DWI-MRI, a coronal DW-MRI sequence was acquired in one patient for the purpose of comparison with axial images

Tables A-1: Comparison of signal intensity using low and high *b*-values for two DWI-MRI sequences

ROI	*b*-value (mm/s^2)							
	0				**200**			
	mean signal	**SD**	**min**	**max**	**mean signal**	**SD**	**min**	**max**
Urine	416	4	408	426	80	3	72	86
Femur	6.4	1.5	3	9	9.1		8	11
Muscle	62.8	19	40	142	61	3.5	26	48
Tumour	13	4	6	21	9.7	0.9	8	11
	900				**1500**			
Urine	18.5	1.9	15	23	19.7	1.9	18	25
Femur	5.8	1.3	3	9	14.2	1.3	12	17
Muscle	5.5	1.1	3	8	43	7	34	57
Tumour	79.8	9	63	93	11.4	0.9	9	13

Table A-2: Comparison of mean ADC values of normal tissues and bladder tumour in MARBLE patients. (Hong *et al.*, 2005; Kilickesmez *et al.*, 2009; Khoo *et al.*, 2011; Halefoglu *et al.*, 2013)[1-4] Normal bladder wall is thin and challenging to identify and analyse using the methods employed in the study.

		Mean ADC (x10^{-3}mm^2/s)	**Literature mean ADC**
Bone	Femur (n = 9)	0.26	0.47[1]
	Ilium (n = 4)	0.41	0.67[3]
Urine	(n = 4)	3.27	3.12[3]
Normal Bladder Wall	(n = 4)	1.22	1.98 – 2.08[2,4]
Bladder Tumour	(n = 16)	1.19	1.28[3]

Table A-3: Comparison of mean ADC values in normal tissues and tumour in an individual patient (MAR002) highlighting the difference in measurements using different sets of b-values.

ROI	*b*-value (mm/s^2)							
	0, 100, 500, 900				200, 800, 1500			
	mean ADC	SD	min	max	mean ADC	SD	min	max
Urine	3.49	0.11	3.22	3.78	1.06	0.08	0.9	1.26
Femur	0.17	0.15	0	0.58	0.24	0.04	0	1.62
Muscle	0.53	0.34	0	1.22	0.42	0.05	0.1	1.74
Tumour	1.35	0.20	0.95	1.71	0.45	0.01	0.28	0.63
Ratio urine : tumour	2.58				2.36			

Table A-4: Comparison of mean ADC values obtained using three different methods within OsiriX

	OsiriX		
	Siemens ADC (a)	Plug-in ADC (b)	Plug-in generated ADC (d)
MAR011	1.51	1.70	1.59
	1.52	1.62	1.62
	1.31	1.32	1.34
MAR013	0.99	1.00	1.02
	1.47	1.55	1.54
	1.47	1.54	1.55
MAR014	1.08	1.13	1.15
	1.05	1.07	1.08
MAR015	1.28	1.29	1.31
	1.34	1.37	1.38
	1.43	1.46	1.49
MAR016	0.84	0.85	0.86
	0.91	1.04	1.06
MAR017	1.09	1.12	1.24
	1.11	1.01	1.15
	1.24	1.37	1.35
All cases	CoV	(a - b) 3%	
		(a – d) 5%	
		(b – d) 2%	

Table A-5: Early treatment assessment data from Image J analysis showing a significant increase in mean ADC after one cycle of chemotherapy, and minimum ADC after two cycles.

	MRI 1 Scan (n = 6)	MRI 2 (n = 6)	*p* value (MRI1 – MRI 2)	MRI 3 (n = 5)	*p* value (MRI1 – MRI 3)
Mean ADC (range, x10^{-3} mm^2/s)	1.31 (0.99 - 1.69)	1.43 (1.18 - 1.6)	*p*= 0.016	1.39 (1.27 - 1.49)	-
Minimum ADC (range, x10^{-3} mm^2/s)	0.57 (0.33 - 0.79)	0.6 (0.37 - 0.75)	-	0.8 (0.59 - 1.12)	*p* = 0.019

Table A-6: Absolute change in ADC measurement between baseline and response scans

Patient ID	Absolute change in ADC Scan 1 and 2 (x10^{-3} mm^2/s)	Absolute change in ADC Scan 1 and 3 (x10^{-3} mm^2/s)
MAR001	-0.01	-
MAR002	-0.14	-
MAR003	0.08	0.08
MAR004	0.12	0.17
MAR005	0.05	-0.02
MAR006	-0.19	-0.08
MAR007	0.18	0.16
MAR008	0.34	0.35
MAR009	0.18	0.20
MAR011	-0.16	-0.22
MAR013	0.26	0.15
MAR015	0.09	0.01
MAR016	0.25	0.22
MAR017	0.15	0.18
MAR018	0.11	0.15
Mean	0.09	0.06
SD	0.16	0.18
Min	-0.19	-0.22
Max	0.34	0.35

Table A-7: Inter-patient CoV for quantitative parameters (CV = SD / mean)

	Inter-patient Coefficient of Variation
MRI1 mean ADC	17%
Repeatable MRI1 mean ADC	16%
mean ADC MRI2	10%
mean ADC MRI3	13%
Baseline mean Ktrans	57%
mean Ktrans MRI2	81%
mean Ktrans MRI3	105%

Figure A-1: Variability in intra- and inter-patient bladder size between scans

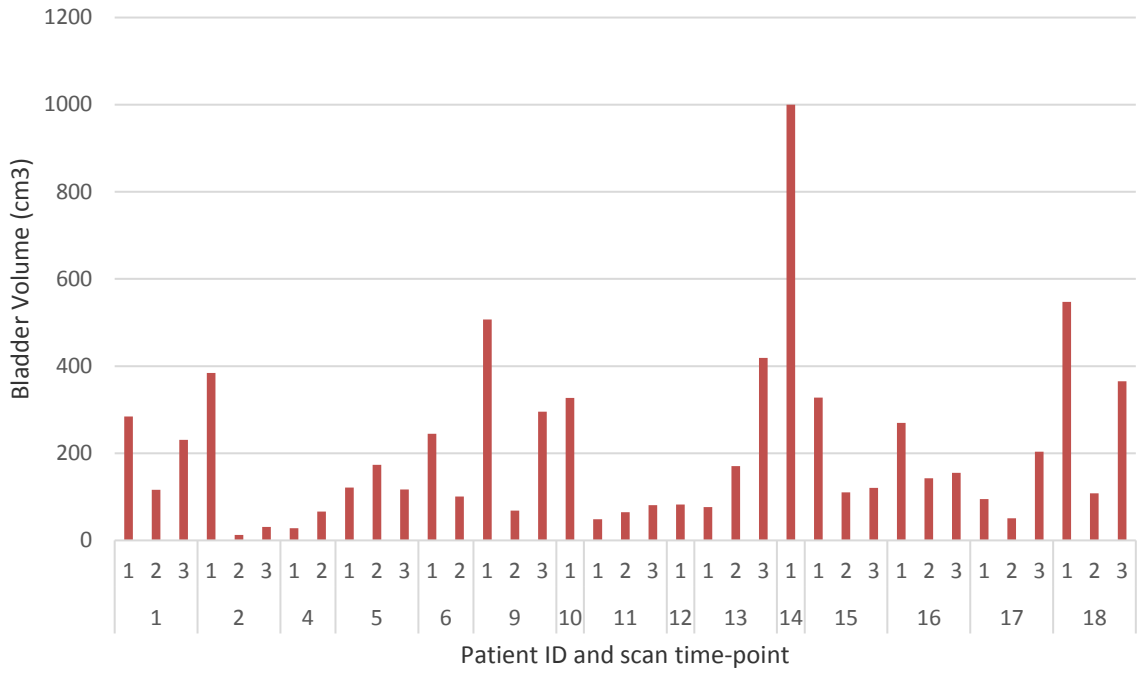

Table A-8: Tumour thickness perpendicular to bladder wall

	Tumour thickness (cm)		
	Scan 1	**Scan 2**	**Scan 3**
	n = 15	n = 12	n = 10
mean	1.78	1.61	1.23
SD	1.43	1.71	0.95
min	0.30	0.40	0.30
max	6.00	5.70	3.00

Table A-9: Bladder dimensions and tumour thickness

Patient ID	Scan	Bladder dimensions (cm)				Tumour thickness (cm) n=29
		transverse	anterior-posterior	height	volume (cm^3)	
MAR001	1	7.3	7.8	5.0	285	1.4
	2	5.8	4.0	5.0	116	1.2
	3	7.0	6.6	5.0	231	1.0
MAR002	1	6.4	10.0	6.0	384	1.4
	2	3.5	2.1	1.7	13	0.8
	3	2.9	4.3	2.5	31	0.8
MAR004	1	2.8	5.0	2.0	28	1.0
	2	3.0	5.5	4.0	66	1.0
MAR005	1	6.0	7.2	2.8	121	1.7
	2	6.8	6.9	3.7	174	0.8
	3	6.0	6.7	2.9	116.6	1.0
MAR006	1	7.0	7.0	5.0	245.0	0.5
	2	6.0	6.0	2.8	100.8	0.5
MAR009	1	8.7	11.0	5.3	507.2	1.5
	2	6.6	6.5	1.6	68.6	1.8
	3	7.9	6.8	5.5	295.5	0.9
MAR010	1	8.5	5.5	7.0	327.3	3.0
MAR011	1	6.4	5.4	1.4	48.4	3.0
	2	6.7	5.7	1.7	64.9	0.4
	3	7.2	5.6	2.0	80.6	0.3
MAR012	1	5.6	8.2	1.8	82.7	1.0
MAR013	1	5.3	4.8	3.0	76.3	0.8
	2	8.2	4.0	5.2	170.6	0.7
	3	7.2	9.7	6.0	419.0	0.3
MAR014	1	10.0	10.0	10.0	1000.0	1.0
MAR015	1	7.5	7.8	5.6	*327.6	6.0
	2	6.0	5.4	3.4	110.2	5.7
	3	6.0	6.7	3.0	120.6	3.0
MAR016	1	6.0	6.0	7.5	270.0	2
	2	7.0	6.0	3.4	142.8	1
	3	6.0	7.0	3.7	155.4	0.9
MAR017	1	6.7	4.7	3.0	94.5	1.3
	2	6.0	5.0	1.7	51.0	0.5
	3	6.0	7.7	4.4	203.3	0.5
MAR018	1	8.0	9.0	7.6	547.2	1.8
	2	6.0	3.6	5.0	108.0	2
	3	8.3	8.0	5.5	365.2	1.7
All cases	(n=37)			**mean**	**204.0**	**1.7**

AIF measurements

Table A-10: Comparison of kinetic parameters acquired using a range of AIF methods. Considerable variability recorded between subject-based (SB) and population-derived (Fritz Hansen (FH) and modified Fritz Hansen (mFH)) AIF measurements.

Patient ID	Scan	AIF Method	Mean Ktrans	Mean Kep	Mean Vp	Mean Ve
MAR009	1	mFH	0.61	0.72	0.01	0.85
		FH	0.75	0.75	0.19	1.00
	2	mFH	0.27	0.71	0	0.38
		FH	0.37	0.56	0.01	0.66
		SB AIF	1.18	1.18	1	1.00
	3	mFH	0.69	0.8	0	0.86
		FH	0.81	0.81	0.19	1
		SB AIF	0.69	0.69	0.1	1
MAR010	1	mFH	0.65	1.85	0	0.35
		FH	0.73	1.31	0.01	0.56
MAR011	1	mFH	0.05	0.34	0	0.15
		FH	0.08	0.27	0	0.30
		SB AIF	0.85	0.85	1	1.00
MAR012	1	mFH	0.32	0.64	0	0.49
		FH	0.44	0.51	0	0.87
		SB AIF	0.6	0.67	0.33	0.89
MAR013	1	mFH	0.31	0.73	0	0.42
		FH	0.27	0.33	0	0.81
		SB AIF	0.21	0.28	0	0.75
	2	mFH	0.09	0.29	0	0.30
		FH	0.13	0.22	0	0.58
		SB AIF	0.1	0.17	0	0.58
	3	mFH	0.03	0.03	0	1.00
		FH	0.05	0.05	0	1.00
		SB AIF	0.77	0.77	0.5	1.00
MAR014	1	mFH	0.44	0.69	0.01	0.64
		FH	0.61	0.61	0.01	1.00

Patient ID	Scan	AIF Method	Mean Ktrans	Mean Kep	Mean Vp	Mean Ve
MAR015	1	mFH	0.18	0.85	0	0.33
		FH	0.12	0.23	0	0.58
		SB AIF	0.18	0.52	0	0.62
	2	mFH	0.21	0.52	0	0.40
		FH	0.29	0.42	0	0.70
		SB AIF	1.11	1.11	1	1.00
	3	mFH	0.14	0.42	0.01	0.32
		FH	0.19	0.33	0.01	0.58
		SB AIF	0.67	0.71	0.51	0.95
MAR016	1	mFH	0.23	0.68	0	0.33
		FH	0.31	0.53	0	0.58
		SB AIF	0.23	0.42	0.02	0.54
	2	mFH	0.38	0.75	0	0.50
		FH	0.49	0.59	0	0.83
		SB AIF	1.06	1.06	1	1.00

Thirteen participants received the intended number of chemotherapy cycles, although several received dose modifications and dose delays due to treatment-related toxicity. One patient did not receive any chemotherapy due to rapid deterioration in clinical condition. Of the four patients who started but did not complete chemotherapy, two patients tolerated 1.5 cycles and the remaining two patients received a single dose. One of these four patients had a restaging CT prior to surgery. Consequently, restaging CT scans were available in 14 patients to compare with the early response MRI scans. To further evaluate newly diagnosed liver metastatic disease, the restaging CT scan was performed three weeks earlier than planned in one case.

Case Report MAR007

53-year old female who presented with frank haematuria and investigations revealed a large TCC muscle-invasive bladder cancer obstructing the right upper tract with gross right hydronephrosis and hydroureter; stage T4 N0 and Ki-67 score was 75%. Tumour was inoperable and she commenced downstaging chemotherapy with cisplatin and gemcitabine chemotherapy. Baseline MRI demonstrated a large enhancing soft tissue mass involving the right ureter, extending to pelvic side wall, uterus and rectal wall but not lymph nodes.

After three cycles of chemotherapy, despite shrinkage in the primary tumour, new pulmonary lesions were considered suspicious for metastases. Given the initial bulk of the tumour and this radiological finding, the patient was switched to second line palliative chemotherapy and no further biopsies from the bladder were taken. The lung lesions were later determined not to be metastases and the patient is therefore classified as a responder for the purposes of this study, due to primary tumour response.

Case Report MAR016

68-year old female who presented with haematuria and lower urinary tract symptoms. Staging CT showed a large irregular tumour centred on the posterior bladder wall, inseparable from and probably invading anterior vaginal wall, stage T4 N1 (9 mm

right external iliac lymph node) and Ki-67 score was 45%. Additionally, there were two small indeterminate liver lesions. Baseline MRI scan performed four weeks later confirmed liver metastases and a 19mm lymph node with restricted diffusion. FLT PET-CT scan demonstrated a 4 x 4.2 x 5.5 cm tumour with SUVmax 8.6 and external iliac lymph node with SUVmax 6.6. Urinary SUVmax was 5.3 after delayed scanning, oral hydration and diuretics. MRI scan on day 10 cycle 1 chemotherapy showed a slight reduction in size of tumour but assessment was hindered due to poor distension of the bladder. The iliac lymph node was also smaller. MRI day 13 of cycle two showed further decrease in tumour from 3.8 x 2.8 x 4.8 cm to 3.8 x 1.7 x 3.2 cm and resolution of the lymph node. The diffusion-weighted signal intensity had decreased, indicating reduced restricted diffusion. Restaging CT was performed after two cycles of chemotherapy (day 19) to assess liver lesions. It confirmed a reduction in the bladder tumour size but an increase in the size of liver lesions compared with baseline CT. Of note, the baseline CT was performed two months before starting chemotherapy, and the interval increase in lesions is likely to represent growth between staging CT and cycle 1, rather than continued growth on chemotherapy. This patient poorly tolerated four cycles of chemotherapy and declined further treatment with radiotherapy. CT scan after four cycles of chemotherapy demonstrated progressive disease. Reviewing the contrast uptake curves from the DCE-MRI scans, an increase in contrast uptake after both cycles of chemotherapy consistent with poor treatment response was observed.

Figure A-2: MAR016- T4N1 on staging CT

Figure A-3: MAR016 FLT PET-CT illustrating primary tumour

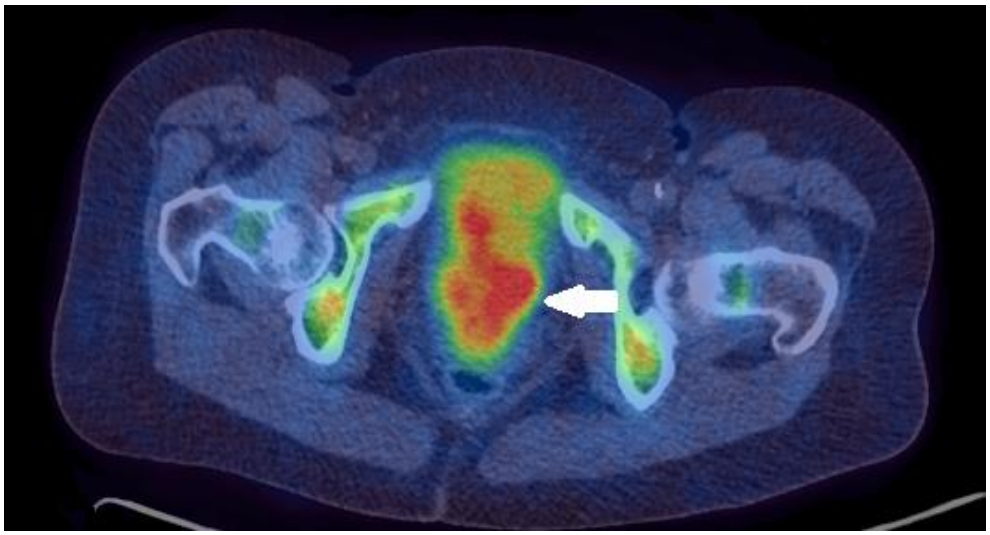

Figure A-4: MAR016 FLT PET-CT illustrating FLT avidity in iliac lymph node.

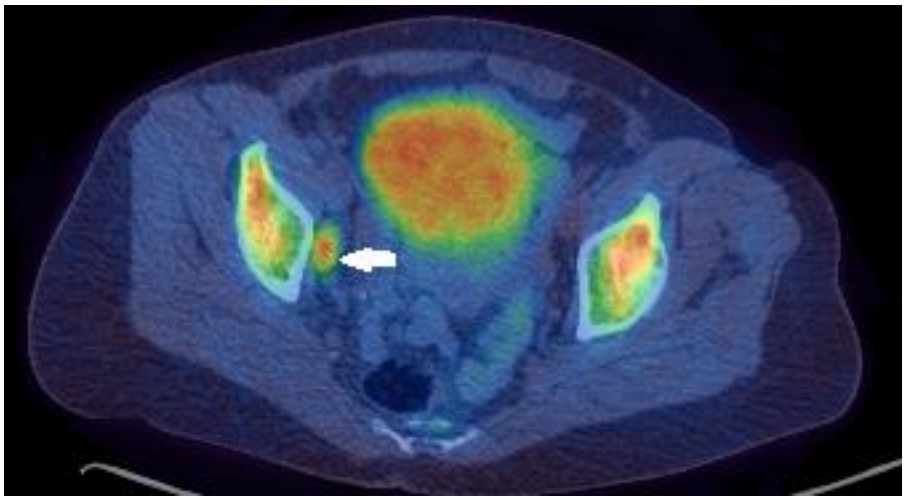

Figure A-5: MAR016 Contrast agent uptake curve demonstrating an increase in the amplitude of the enhancement curve after the first and second cycles of NAC (green = baseline, red = after first cycle, blue = after second cycle).

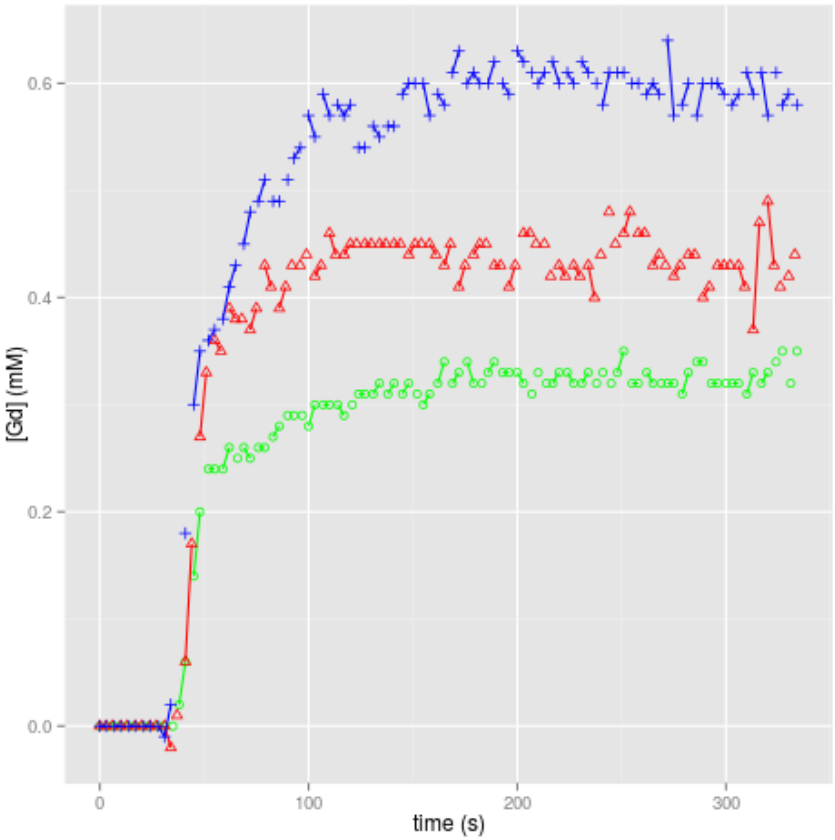

Case Report MAR008

71-year old man who presented with a two-year history of intermittent haematuria. On baseline CT there were several large bladder tumours, largest measuring 7 x 3.1 cm, with extravesical nodularity and stranding, and he was staged as T3 N0 M0 and planned for 4 cycles of downstaging gemcitabine / cisplatin chemotherapy. Baseline MRI demonstrated a lobulated irregular 6cm mass involving anterior wall of the urinary bladder, extending into the remnant of the urachus. On DW-MRI, tumour showed inhomogeneous, restricted diffusion and there was marked enhancement after contrast injection. Second MRI was performed day 15 of cycle 1 chemotherapy and moderate reduction in the bulk of multifocal bladder tumours was identified. The third MRI scan was performed day 11 of cycle 2 chemotherapy and showed further decrease in size of the bladder tumour, with a reduced number of foci with restricted diffusion. Restaging CT performed after cycle 3 chemotherapy showed irregular thickening and enhancement of the bladder wall but no definitive information on response to treatment was available. The patient was then treated with chemoradiotherapy to the bladder (55-Gy in 20 # with concurrent 5FU/ Mitomycin C week 1 and 5 of radiotherapy). First check cystoscopy was performed seven months later (the latest time-point of all MARBLE patients) and showed three tumours within the site of original disease. He proceeded to an urgent TURBT and salvage cystectomy which showed pT3 N0 high grade TCC bladder and a pT1a prostate cancer. He was followed up with 3-monthly CT scans but was diagnosed with liver metastases after 9 months and died two months later. In this case, there was a rapid response to the initial chemotherapy (Ki-67 was 90%), however, at some point in the following 9 months disease relapsed within the bladder and he required salvage treatment but died a year later.

Bibliography

Aboagye, E.O. and Price, P.M. (2003) 'Use of positron emission tomography in anticancer drug development', *Invest New Drugs*, 21(2), pp. 169-81.

Abramson, R.G., Li, X., Hoyt, T.L., Su, P.F., Arlinghaus, L.R., Wilson, K.J., Abramson, V.G., Chakravarthy, A.B. and Yankeelov, T.E. (2013) 'Early assessment of breast cancer response to neoadjuvant chemotherapy by semi-quantitative analysis of high-temporal resolution DCE-MRI: preliminary results', *Magn Reson Imaging*, 31(9), pp. 1457-64.

Ackland, S.P. and Peters, G.J. (1999) 'Thymidine phosphorylase: its role in sensitivity and resistance to anticancer drugs', *Drug Resist Updat*, 2(4), pp. 205-214.

Agool, A., Slart, R.H., Thorp, K.K., Glaudemans, A.W., Cobben, D.C., Been, L.B., Burlage, F.R., Elsinga, P.H., Dierckx, R.A., Vellenga, E. and Holter, J.L. (2011) 'Effect of radiotherapy and chemotherapy on bone marrow activity: a 18F-FLT-PET study', *Nucl Med Commun*, 32(1), pp. 17-22.

Ah-See, M.L., Makris, A., Taylor, N.J., Harrison, M., Richman, P.I., Burcombe, R.J., Stirling, J.J., d'Arcy, J.A., Collins, D.J., Pittam, M.R., Ravichandran, D. and Padhani, A.R. (2008) 'Early changes in functional dynamic magnetic resonance imaging predict for pathologic response to neoadjuvant chemotherapy in primary breast cancer', *Clin Cancer Res*, 14(20), pp. 6580-9.

Akamatsu, G., Ishikawa, K., Mitsumoto, K., Taniguchi, T., Ohya, N., Baba, S., Abe, K. and Sasaki, M. (2012) 'Improvement in PET/CT image quality with a combination of point-spread function and time-of-flight in relation to reconstruction parameters', *J Nucl Med*, 53(11), pp. 1716-22.

Allen, M.D., Luong, P., Hudson, C., Leyton, J., Delage, B., Ghazaly, E., Cutts, R., Yuan, M., Syed, N., Lo Nigro, C., Lattanzio, L., Chmielewska-Kassassir, M., Tomlinson, I., Roylance, R., Whitaker, H.C., Warren, A.Y., Neal, D., Frezza, C., Beltran, L., Jones, L.J., Chelala, C., Wu, B.W., Bomalaski, J.S., Jackson, R.C., Lu, Y.J., Crook, T., Lemoine, N.R., Mather, S., Foster, J., Sosabowski, J., Avril, N., Li, C.F. and Szlosarek, P.W. (2014) 'Prognostic and therapeutic impact of argininosuccinate synthetase 1 control in bladder cancer as monitored longitudinally by PET imaging', *Cancer Res*, 74(3), pp. 896-907.

Alonzi, R. and Hoskin, P. (2006) 'Functional imaging in clinical oncology: magnetic resonance imaging- and computerised tomography-based techniques', *Clin Oncol (R Coll Radiol)*, 18(7), pp. 555-70.

American Thyroid Association Guidelines Taskforce on Thyroid, N., Differentiated Thyroid, C., Cooper, D.S., Doherty, G.M., Haugen, B.R., Kloos, R.T., Lee, S.L., Mandel, S.J., Mazzaferri, E.L., McIver, B., Pacini, F., Schlumberger, M., Sherman, S.I., Steward, D.L. and Tuttle, R.M. (2009) 'Revised American Thyroid Association management guidelines for patients with thyroid nodules and differentiated thyroid cancer', *Thyroid*, 19(11), pp. 1167-214.

Andrade, R.S., Heron, D.E., Degirmenci, B., Filho, P.A., Branstetter, B.F., Seethala, R.R., Ferris, R.L. and Avril, N. (2006) 'Posttreatment assessment of response using

FDG-PET/CT for patients treated with definitive radiation therapy for head and neck cancers', *Int J Radiat Oncol Biol Phys*, 65(5), pp. 1315-22.

Ang, K.K., Harris, J., Wheeler, R., Weber, R., Rosenthal, D.I., Nguyen-Tan, P.F., Westra, W.H., Chung, C.H., Jordan, R.C., Lu, C., Kim, H., Axelrod, R., Silverman, C.C., Redmond, K.P. and Gillison, M.L. (2010) 'Human papillomavirus and survival of patients with oropharyngeal cancer', *N Engl J Med*, 363(1), pp. 24-35.

Anjos, D.A., Etchebehere, E.C., Ramos, C.D., Santos, A.O., Albertotti, C. and Camargo, E.E. (2007) '18F-FDG PET/CT delayed images after diuretic for restaging invasive bladder cancer', *J Nucl Med*, 48(5), pp. 764-70.

Aras, M., Erdil, T.Y., Dane, F., Gungor, S., Ones, T., Dede, F., Inanir, S. and Turoglu, H.T. (2016) 'Comparison of WHO, RECIST 1.1, EORTC, and PERCIST criteria in the evaluation of treatment response in malignant solid tumors', *Nucl Med Commun*, 37(1), pp. 9-15.

Arens, A.I., Troost, E.G., Hoeben, B.A., Grootjans, W., Lee, J.A., Gregoire, V., Hatt, M., Visvikis, D., Bussink, J., Oyen, W.J., Kaanders, J.H. and Visser, E.P. (2014) 'Semiautomatic methods for segmentation of the proliferative tumour volume on sequential FLT PET/CT images in head and neck carcinomas and their relation to clinical outcome', *Eur J Nucl Med Mol Imaging*, 41(5), pp. 915-24.

Ashraf, A., Gaonkar, B., Mies, C., DeMichele, A., Rosen, M., Davatzikos, C. and Kontos, D. (2015) 'Breast DCE-MRI Kinetic Heterogeneity Tumor Markers: Preliminary Associations With Neoadjuvant Chemotherapy Response', *Transl Oncol*, 8(3), pp. 154-62.

Atkinson, D.M., Clarke, M.J., Mladek, A.C., Carlson, B.L., Trump, D.P., Jacobson, M.S., Kemp, B.J., Lowe, V.J. and Sarkaria, J.N. (2008) 'Using fluorodeoxythymidine to monitor anti-EGFR inhibitor therapy in squamous cell carcinoma xenografts', *Head Neck*, 30(6), pp. 790-9.

Atuegwu, N.C., Arlinghaus, L.R., Li, X., Welch, E.B., Chakravarthy, B.A., Gore, J.C. and Yankeelov, T.E. (2011) 'Integration of diffusion-weighted MRI data and a simple mathematical model to predict breast tumor cellularity during neoadjuvant chemotherapy', *Magn Reson Med*, 66(6), pp. 1689-96.

Bains, L.J., McGrath, D.M., Naish, J.H., Cheung, S., Watson, Y., Taylor, M.B., Logue, J.P., Parker, G.J., Waterton, J.C. and Buckley, D.L. (2010) 'Tracer kinetic analysis of dynamic contrast-enhanced MRI and CT bladder cancer data: A preliminary comparison to assess the magnitude of water exchange effects', *Magn Reson Med*, 64(2), pp. 595-603.

Barbaro, B., Vitale, R., Valentini, V., Illuminati, S., Vecchio, F.M., Rizzo, G., Gambacorta, M.A., Coco, C., Crucitti, A., Persiani, R., Sofo, L. and Bonomo, L. (2012) 'Diffusion-Weighted Magnetic Resonance Imaging in Monitoring Rectal Cancer Response to Neoadjuvant Chemoradiotherapy', *International Journal of Radiation Oncology*Biology*Physics*, 83(2), pp. 594-599.

Barentsz, J.O., Berger-Hartog, O., Witjes, J.A., Hulsbergen-van der Kaa, C., Oosterhof, G.O., VanderLaak, J.A., Kondacki, H. and Ruijs, S.H. (1998) 'Evaluation of chemotherapy in advanced urinary bladder cancer with fast dynamic contrast-enhanced MR imaging', *Radiology*, 207(3), pp. 791-7.

Barrett, T., Gill, A.B., Kataoka, M.Y., Priest, A.N., Joubert, I., McLean, M.A., Graves, M.J., Stearn, S., Lomas, D.J., Griffiths, J.R., Neal, D., Gnanapragasam, V.J. and

Sala, E. (2012) 'DCE and DW MRI in monitoring response to androgen deprivation therapy in patients with prostate cancer: a feasibility study', *Magn Reson Med*, 67(3), pp. 778-85.

Barrington, S. and Scarsbrook, A. (2013) *Evidence-based indications for the use of PET-CT in the UK*. London: The Royal College of Physicians and the Royal College of Radiologists Physicians, R.C.o.

Barthel, H., Cleij, M.C., Collingridge, D.R., Hutchinson, O.C., Osman, S., He, Q., Luthra, S.K., Brady, F., Price, P.M. and Aboagye, E.O. (2003) '3'-deoxy-3'-[18F]fluorothymidine as a new marker for monitoring tumor response to antiproliferative therapy in vivo with positron emission tomography', *Cancer Res*, 63(13), pp. 3791-8.

Barthel, H., Perumal, M., Latigo, J., He, Q., Brady, F., Luthra, S.K., Price, P.M. and Aboagye, E.O. (2005) 'The uptake of 3'-deoxy-3'-[18F]fluorothymidine into L5178Y tumours in vivo is dependent on thymidine kinase 1 protein levels', *Eur J Nucl Med Mol Imaging*, 32(3), pp. 257-63.

Bax, B.E., Bain, M.D., Scarpelli, M., Filosto, M., Tonin, P. and Moran, N. (2013) 'Clinical and biochemical improvements in a patient with MNGIE following enzyme replacement', *Neurology*, 81(14), pp. 1269-71.

Been, L.B., Elsinga, P.H., de Vries, J., Cobben, D.C., Jager, P.L., Hoekstra, H.J. and Suurmeijer, A.J. (2006) 'Positron emission tomography in patients with breast cancer using (18)F-3'-deoxy-3'-fluoro-l-thymidine ((18)F-FLT)-a pilot study', *Eur J Surg Oncol*, 32(1), pp. 39-43.

Belohlavek, O., Fencl, P., Majovsky, M., Jaruskova, M. and Benes, V. (2014) 'FLT-PET in previously untreated patients with low-grade glioma can predict their overall survival', *Nucl Med Rev Cent East Eur*, 17(1), pp. 7-12.

Benz, M.R., Czernin, J., Allen-Auerbach, M.S., Dry, S.M., Sutthiruangwong, P., Spick, C., Radu, C., Weber, W.A., Tap, W.D. and Eilber, F.C. (2012) '3′-deoxy-3′-[18F]fluorothymidine positron emission tomography for response assessment in soft tissue sarcoma', *Cancer*, 118(12), pp. 3135-3144.

Bertz, S., Otto, W., Denzinger, S., Wieland, W.F., Burger, M., Stohr, R., Link, S., Hofstadter, F. and Hartmann, A. (2014) 'Combination of CK20 and Ki-67 immunostaining analysis predicts recurrence, progression, and cancer-specific survival in pT1 urothelial bladder cancer', *Eur Urol*, 65(1), pp. 218-26.

Bilgili, M.Y. (2011) 'Reproductibility of apparent diffusion coefficients measurements in diffusion-weighted MRI of the abdomen with different b values', *Eur J Radiol*.

Boellaard, R., Delgado-Bolton, R., Oyen, W.J.G., Giammarile, F., Tatsch, K., Eschner, W., Verzijlbergen, F.J., Barrington, S.F., Pike, L.C., Weber, W.A., Stroobants, S., Delbeke, D., Donohoe, K.J., Holbrook, S., Graham, M.M., Testanera, G., Hoekstra, O.S., Zijlstra, J., Visser, E., Hoekstra, C.J., Pruim, J., Willemsen, A., Arends, B., Kotzerke, J., Bockisch, A., Beyer, T., Chiti, A. and Krause, B.J. (2015) 'FDG PET/CT: EANM procedure guidelines for tumour imaging: version 2.0', *European Journal of Nuclear Medicine and Molecular Imaging*, 42(2), pp. 328-354.

Boetes, C., Barentsz, J.O., Mus, R.D., van der Sluis, R.F., van Erning, L.J., Hendriks, J.H., Holland, R. and Ruys, S.H. (1994) 'MR characterization of suspicious breast lesions with a gadolinium-enhanced TurboFLASH subtraction technique', *Radiology*, 193(3), pp. 777-81.

Boetes, C., Veltman, J., van Die, L., Bult, P., Wobbes, T. and Barentsz, J.O. (2004) 'The role of MRI in invasive lobular carcinoma', *Breast Cancer Res Treat*, 86(1), pp. 31-7.

Bollineni, V.R., Kramer, G., Liu, Y., Melidis, C. and deSouza, N.M. (2015) 'A literature review of the association between diffusion-weighted MRI derived apparent diffusion coefficient and tumour aggressiveness in pelvic cancer', *Cancer Treat Rev*, 41(6), pp. 496-502.

Bossi, P., Orlandi, E., Miceli, R., Perrone, F., Guzzo, M., Mariani, L., Granata, R., Locati, L., Fallai, C., Cortelazzi, B., Pilotti, S., Scaramellini, G., Gloghini, A. and Licitra, L. (2014) 'Treatment-related outcome of oropharyngeal cancer patients differentiated by HPV dictated risk profile: a tertiary cancer centre series analysis', *Ann Oncol*, 25(3), pp. 694-9.

Bouchet, F., Geworski, L., Knoop, B.O., Ferrer, L., Barriolo-Riedinger, A., Millardet, C., Fourcade, M., Martineau, A., Belly-Poinsignon, A., Djoumessi, F., Tendero, K., Keros, L., Montoya, F., Mesleard, C., Martin, A.L., Lacoeuille, F. and Couturier, O. (2013) 'Calibration test of PET scanners in a multi-centre clinical trial on breast cancer therapy monitoring using 18F-FLT', *PLoS One*, 8(3), p. e58152.

Bourgeaux, V., Lanao, J.M., Bax, B.E. and Godfrin, Y. (2016) 'Drug-loaded erythrocytes: on the road toward marketing approval', *Drug Des Devel Ther*, 10, pp. 665-76.

Braithwaite, A.C., Dale, B.M., Boll, D.T. and Merkle, E.M. (2009) 'Short- and midterm reproducibility of apparent diffusion coefficient measurements at 3.0-T diffusion-weighted imaging of the abdomen', *Radiology*, 250(2), pp. 459-65.

Brockenbrough, J.S., Souquet, T., Morihara, J.K., Stern, J.E., Hawes, S.E., Rasey, J.S., Leblond, A., Wiens, L.W., Feng, Q., Grierson, J. and Vesselle, H. (2011) 'Tumor 3'-deoxy-3'-(18)F-fluorothymidine ((18)F-FLT) uptake by PET correlates with thymidine kinase 1 expression: static and kinetic analysis of (18)F-FLT PET studies in lung tumors', *J Nucl Med*, 52(8), pp. 1181-8.

Bronckaers, A., Gago, F., Balzarini, J. and Liekens, S. (2009) 'The dual role of thymidine phosphorylase in cancer development and chemotherapy', *Med Res Rev*, 29(6), pp. 903-53.

Buck, A.K., Halter, G., Schirrmeister, H., Kotzerke, J., Wurziger, I., Glatting, G., Mattfeldt, T., Neumaier, B., Reske, S.N. and Hetzel, M. (2003) 'Imaging proliferation in lung tumors with PET: F-18-FLT versus F-18-FDG', *Journal of Nuclear Medicine*, 44(9), pp. 1426-1431.

Cagiannos, I. and Morash, C. (2009) 'Surveillance strategies after definitive therapy of invasive bladder cancer', *Can Urol Assoc J*, 3(6 Suppl 4), pp. S237-42.

Campbell, B.A., Callahan, J., Bressel, M., Simoens, N., Everitt, S., Hofman, M.S., Hicks, R.J., Burbury, K. and MacManus, M. (2015) 'Distribution Atlas of Proliferating Bone Marrow in Non-Small Cell Lung Cancer Patients Measured by FLT-PET/CT Imaging, With Potential Applicability in Radiation Therapy Planning', *Int J Radiat Oncol Biol Phys*, 92(5), pp. 1035-43.

Cao, M.Q., Suo, S.T., Zhang, X.B., Zhong, Y.C., Zhuang, Z.G., Cheng, J.J., Chi, J.C. and Xu, J.R. (2014) 'Entropy of T2-weighted imaging combined with apparent diffusion coefficient in prediction of uterine leiomyoma volume response after uterine artery embolization', *Acad Radiol*, 21(4), pp. 437-44.

Carmeliet, P. and Jain, R.K. (2000) 'Angiogenesis in cancer and other diseases', *Nature*, 407(6801), pp. 249-57.

Ceriani, L., Suriano, S., Ruberto, T. and Giovanella, L. (2011) 'Could different hydration protocols affect the quality of 18F-FDG PET/CT images?', *J Nucl Med Technol*, 39(2), pp. 77-82.

Chakiba, C., Cornelis, F., Descat, E., Gross-Goupil, M., Sargos, P., Roubaud, G. and Houede, N. (2015) 'Dynamic contrast enhanced MRI-derived parameters are potential biomarkers of therapeutic response in bladder carcinoma', *Eur J Radiol*, 84(6), pp. 1023-8.

Chalkidou, A., Landau, D.B., Odell, E.W., Cornelius, V.R., O'Doherty, M.J. and Marsden, P.K. (2012) 'Correlation between Ki-67 immunohistochemistry and 18F-fluorothymidine uptake in patients with cancer: A systematic review and meta-analysis', *Eur J Cancer*, 48(18), pp. 3499-513.

Challapalli, A., Barwick, T., Pearson, R.A., Merchant, S., Mauri, F., Howell, E.C., Sumpter, K., Maxwell, R.J., Aboagye, E.O. and Sharma, R. (2015) '3'-Deoxy-3'-(1)(8)F-fluorothymidine positron emission tomography as an early predictor of disease progression in patients with advanced and metastatic pancreatic cancer', *Eur J Nucl Med Mol Imaging*, 42(6), pp. 831-40.

Chatterjee, S., Frew, J., Mott, J., McCallum, H., Stevenson, P., Maxwell, R., Wilsdon, J. and Kelly, C.G. (2012) 'Variation in Radiotherapy Target Volume Definition, Dose to Organs at Risk and Clinical Target Volumes using Anatomic (Computed Tomography) versus Combined Anatomic and Molecular Imaging (Positron Emission Tomography/Computed Tomography): Intensity-modulated Radiotherapy Delivered using a Tomotherapy Hi Art Machine: Final Results of the VortigERN Study', *Clin Oncol (R Coll Radiol)*, 24(10), pp. e173-9.

Chen, F., Tang, L., Xia, T., He, E., Hu, G., Li, Y., Zhang, M., Zhou, J., Eriksson, S. and Skog, S. (2013) 'Serum thymidine kinase 1 levels predict cancer-free survival following neoadjuvant, surgical and adjuvant treatment of patients with locally advanced breast cancer', *Mol Clin Oncol*, 1(5), pp. 894-902.

Chen, W., Cloughesy, T., Kamdar, N., Satyamurthy, N., Bergsneider, M., Liau, L., Mischel, P., Czernin, J., Phelps, M.E. and Silverman, D.H. (2005) 'Imaging proliferation in brain tumors with 18F-FLT PET: comparison with 18F-FDG', *J Nucl Med*, 46(6), pp. 945-52.

Chen, W.J., He, D.S., Tang, R.X., Ren, F.H. and Chen, G. (2015a) 'Ki-67 is a valuable prognostic factor in gliomas: evidence from a systematic review and meta-analysis', *Asian Pac J Cancer Prev*, 16(2), pp. 411-20.

Chen, Z., Guan, H., Yuan, H., Cao, X., Liu, Y., Zhou, J.I., He, E. and Skog, S. (2015b) 'Serum thymidine kinase 1 is a reliable maker for the assessment of the risk of developing malignancy: A case report', *Oncol Lett*, 10(3), pp. 1669-1673.

Chenevert, T.L., Brunberg, J.A. and Pipe, J.G. (1990) 'Anisotropic diffusion in human white matter: demonstration with MR techniques in vivo', *Radiology*, 177(2), pp. 401-405.

Cheng, H.L. (2008) 'Investigation and optimization of parameter accuracy in dynamic contrast-enhanced MRI', *J Magn Reson Imaging*, 28(3), pp. 736-43.

Choudhury, A. and Cowan, R. (2011) 'Bladder preservation multimodality therapy as an alternative to radical cystectomy for treatment of muscle invasive bladder cancer', *BJU Int*, 108(9), p. E313.

Contractor, K., Aboagye, E.O., Jacob, J., Challapalli, A., Coombes, R.C. and Stebbing, J. (2012) 'Monitoring early response to taxane therapy in advanced breast cancer with circulating tumor cells and [(18)F] 3 -deoxy-3 -fluorothymidine PET: a pilot study', *Biomark Med*, 6(2), pp. 231-3.

Coolens, C., Driscoll, B., Foltz, W. and Chung, C. (2015) 'SU-D-303-02: Impact of Arterial Input Function Selection and T10 Correction On DCE-MRI Tumour Response Prediction Using Compared to Volumetric DCE CT', *Med Phys*, 42(6), p. 3215.

Costantini, M., Belli, P., Rinaldi, P., Bufi, E., Giardina, G., Franceschini, G., Petrone, G. and Bonomo, L. (2010) 'Diffusion-weighted imaging in breast cancer: relationship between apparent diffusion coefficient and tumour aggressiveness', *Clin Radiol*, 65(12), pp. 1005-12.

CRUK (2016) 'Oral Cancer Incidence'. Cancer Research UK 24 March 2016. Available at: http://www.cancerresearchuk.org/health-professional/cancer-statistics/statistics-by-cancer-type/oral-cancer/incidence#heading-Three.

Cui, Y., Zhang, X.P., Sun, Y.S., Tang, L. and Shen, L. (2008) 'Apparent diffusion coefficient: potential imaging biomarker for prediction and early detection of response to chemotherapy in hepatic metastases', *Radiology*, 248(3), pp. 894-900.

Daisne, J.F., Duprez, T., Weynand, B., Lonneux, M., Hamoir, M., Reychler, H. and Gregoire, V. (2004) 'Tumor volume in pharyngolaryngeal squamous cell carcinoma: comparison at CT, MR imaging, and FDG PET and validation with surgical specimen', *Radiology*, 233(1), pp. 93-100.

Dale, B.M., Braithwaite, A.C., Boll, D.T. and Merkle, E.M. (2010) 'Field strength and diffusion encoding technique affect the apparent diffusion coefficient measurements in diffusion-weighted imaging of the abdomen', *Invest Radiol*, 45(2), pp. 104-8.

Daneshmand, S., Ahmadi, H., Huynh, L.N. and Dobos, N. (2012) 'Preoperative staging of invasive bladder cancer with dynamic gadolinium-enhanced magnetic resonance imaging: results from a prospective study', *Urology*, 80(6), pp. 1313-8.

De Bruyne, S., Van Damme, N., Smeets, P., Ferdinande, L., Ceelen, W., Mertens, J., Van de Wiele, C., Troisi, R., Libbrecht, L., Laurent, S., Geboes, K. and Peeters, M. (2012) 'Value of DCE-MRI and FDG-PET/CT in the prediction of response to preoperative chemotherapy with bevacizumab for colorectal liver metastases', *Br J Cancer*, 106(12), pp. 1926-33.

De Felice, F., Thomas, C., Barrington, S., Pathmanathan, A., Lei, M. and Urbano, T.G. (2015) 'Analysis of loco-regional failures in head and neck cancer after radical radiation therapy', *Oral Oncol*, 51(11), pp. 1051-5.

de Haas, R.J., Steyvers, M.J. and Fütterer, J.J. (2014) 'Multiparametric MRI of the Bladder: Ready for Clinical Routine?', *American Journal of Roentgenology*, 202(6), pp. 1187-1195.

de Langen, A.J., Klabbers, B., Lubberink, M., Boellaard, R., Spreeuwenberg, M.D., Slotman, B.J., de Bree, R., Smit, E.F., Hoekstra, O.S. and Lammertsma, A.A. (2009) 'Reproducibility of quantitative 18F-3'-deoxy-3'-fluorothymidine measurements using positron emission tomography', *Eur J Nucl Med Mol Imaging*, 36(3), pp. 389-95.

De Robertis, R., Tinazzi Martini, P., Demozzi, E., Puntel, G., Ortolani, S., Cingarlini, S., Ruzzenente, A., Guglielmi, A., Tortora, G., Bassi, C., Pederzoli, P. and D'Onofrio, M. (2015) 'Prognostication and response assessment in liver and pancreatic tumors: The new imaging', *World J Gastroenterol*, 21(22), pp. 6794-808.

Ding, W., Gou, Y., Sun, C., Xia, G., Wang, H., Chen, Z., Tan, J., Xu, K. and Qiang, D. (2014) 'Ki-67 is an independent indicator in non-muscle invasive bladder cancer (NMIBC); combination of EORTC risk scores and Ki-67 expression could improve the risk stratification of NMIBC', *Urol Oncol*, 32(1), pp. 42 e13-9.

Dittmann, H., Jusufoska, A., Dohmen, B.M., Smyczek-Gargya, B., Fersis, N., Pritzkow, M., Kehlbach, R., Vonthein, R., Machulla, H.J. and Bares, R. (2009) '3'-Deoxy-3'-[(18)F]fluorothymidine (FLT) uptake in breast cancer cells as a measure of proliferation after doxorubicin and docetaxel treatment', *Nucl Med Biol*, 36(2), pp. 163-9.

Donaldson, S.B., Bonington, S.C., Kershaw, L.E., Cowan, R., Lyons, J., Elliott, T. and Carrington, B.M. (2013) 'Dynamic contrast-enhanced MRI in patients with muscle-invasive transitional cell carcinoma of the bladder can distinguish between residual tumour and post-chemotherapy effect', *Eur J Radiol*, 82(12), pp. 2161-8.

Donati, O.F., Afaq, A., Vargas, H.A., Mazaheri, Y., Zheng, J., Moskowitz, C.S., Hricak, H. and Akin, O. (2014a) 'Prostate MRI: evaluating tumor volume and apparent diffusion coefficient as surrogate biomarkers for predicting tumor Gleason score', *Clin Cancer Res*, 20(14), pp. 3705-11.

Donati, O.F., Chong, D., Nanz, D., Boss, A., Froehlich, J.M., Andres, E., Seifert, B. and Thoeny, H.C. (2014b) 'Diffusion-weighted MR imaging of upper abdominal organs: field strength and intervendor variability of apparent diffusion coefficients', *Radiology*, 270(2), pp. 454-63.

Donati, O.F., Mazaheri, Y., Afaq, A., Vargas, H.A., Zheng, J., Moskowitz, C.S., Hricak, H. and Akin, O. (2014c) 'Prostate cancer aggressiveness: assessment with whole-lesion histogram analysis of the apparent diffusion coefficient', *Radiology*, 271(1), pp. 143-52.

Dong, M.J., Liu, Z.F., Zhao, K., Ruan, L.X., Wang, G.L., Yang, S.Y., Sun, F. and Luo, X.G. (2009) 'Value of 18F-FDG-PET/PET-CT in differentiated thyroid carcinoma with radioiodine-negative whole-body scan: a meta-analysis', *Nucl Med Commun*, 30(8), pp. 639-50.

Duprez, F., De Neve, W., De Gersem, W., Coghe, M. and Madani, I. (2011) 'Adaptive dose painting by numbers for head-and-neck cancer', *Int J Radiat Oncol Biol Phys*, 80(4), pp. 1045-55.

Eisenhauer, E.A., Therasse, P., Bogaerts, J., Schwartz, L.H., Sargent, D., Ford, R., Dancey, J., Arbuck, S., Gwyther, S., Mooney, M., Rubinstein, L., Shankar, L., Dodd, L., Kaplan, R., Lacombe, D. and Verweij, J. (2009) 'New response evaluation criteria in solid tumours: revised RECIST guideline (version 1.1)', *Eur J Cancer*, 45(2), pp. 228-47.

Elmi, A., Hedgire, S.S., Covarrubias, D., Abtahi, S.M., Hahn, P.F. and Harisinghani, M. (2013) 'Apparent diffusion coefficient as a non-invasive predictor of treatment response and recurrence in locally advanced rectal cancer', *Clin Radiol*, 68(10), pp. e524-31.

Engelberg, J.A., Retallack, H., Balassanian, R., Dowsett, M., Zabaglo, L., Ram, A.A., Apple, S.K., Bishop, J.W., Borowsky, A.D., Carpenter, P.M., Chen, Y.Y., Datnow, B., Elson, S., Hasteh, F., Lin, F., Moatamed, N.A., Zhang, Y. and Cardiff, R.D. (2015) '"Score the Core" Web-based pathologist training tool improves the accuracy of breast cancer IHC4 scoring', *Hum Pathol*, 46(11), pp. 1694-704.

Etxano, J., Insausti, L.P., Elizalde, A., Lopez Vega, J.M., Plazaola, A. and Martinez, P. (2014) 'Analysis of the changes induced by bevacizumab using a high temporal resolution DCE-MRI as prognostic factors for response to further neoadjuvant chemotherapy', *Acta Radiol*.

Everitt, S.J., Ball, D.L., Hicks, R.J., Callahan, J., Plumridge, N., Collins, M., Herschtal, A., Binns, D., Kron, T., Schneider, M. and MacManus, M. (2014) 'Differential (18)F-FDG and (18)F-FLT Uptake on Serial PET/CT Imaging Before and During Definitive Chemoradiation for Non-Small Cell Lung Cancer', *J Nucl Med*, 55(7), pp. 1069-74.

Fodor, A., Fiorino, C., Dell'Oca, I., Broggi, S., Pasetti, M., Cattaneo, G.M., Gianolli, L., Calandrino, R. and Di Muzio, N.G. (2011) 'PET-guided dose escalation tomotherapy in malignant pleural mesothelioma', *Strahlenther Onkol*, 187(11), pp. 736-43.

Folkman, J. (2002) 'Role of angiogenesis in tumor growth and metastasis', *Semin Oncol*, 29(6 Suppl 16), pp. 15-8.

Fox, S.B., Engels, K., Comley, M., Whitehouse, R.M., Turley, H., Gatter, K.C. and Harris, A.L. (1997) 'Relationship of elevated tumour thymidine phosphorylase in node-positive breast carcinomas to the effects of adjuvant CMF', *Ann Oncol*, 8(3), pp. 271-5.

Funatsu, H., Imamura, A., Takano, H., Ueda, T. and Uno, T. (2012) 'Can pretreatment ADC values predict recurrence of bladder cancer after transurethral resection?', *Eur J Radiol*, 81(11), pp. 3115-9.

Galbraith, S.M., Lodge, M.A., Taylor, N.J., Rustin, G.J., Bentzen, S., Stirling, J.J. and Padhani, A.R. (2002) 'Reproducibility of dynamic contrast-enhanced MRI in human muscle and tumours: comparison of quantitative and semi-quantitative analysis', *NMR Biomed*, 15(2), pp. 132-42.

Gallamini, A., Zwarthoed, C. and Borra, A. (2014) 'Positron Emission Tomography (PET) in Oncology', *Cancers (Basel)*, 6(4), pp. 1821-89.

Garcia Vicente, A.M., Nunez Garcia, A., Palomar Munoz, A., Pilkington Woll, J.P., Bellon Guardia, M.E., Gonzalez Garcia, B. and Soriano Castrejon, A. (2011) '[18F-FDG PET/CT with retrograde filling of the urinary bladder in the assessment of malignant pelvic disease]', *Rev Esp Med Nucl*, 30(2), pp. 71-6.

Gasparini, G., Toi, M., Miceli, R., Vermeulen, P.B., Dittadi, R., Biganzoli, E., Morabito, A., Fanelli, M., Gatti, C., Suzuki, H., Tominaga, T., Dirix, L.Y. and Gion, M. (1999) 'Clinical relevance of vascular endothelial growth factor and thymidine phosphorylase in patients with node-positive breast cancer treated with either adjuvant chemotherapy or hormone therapy', *Cancer J Sci Am*, 5(2), pp. 101-11.

Geets, X., Tomsej, M., Lee, J.A., Duprez, T., Coche, E., Cosnard, G., Lonneux, M. and Gregoire, V. (2007) 'Adaptive biological image-guided IMRT with anatomic and functional imaging in pharyngo-laryngeal tumors: impact on target volume delineation and dose distribution using helical tomotherapy', *Radiother Oncol*, 85(1), pp. 105-15.

Gollub, M.J., Gultekin, D.H., Akin, O., Do, R.K., Fuqua, J.L., 3rd, Gonen, M., Kuk, D., Weiser, M., Saltz, L., Schrag, D., Goodman, K., Paty, P., Guillem, J., Nash, G.M., Temple, L., Shia, J. and Schwartz, L.H. (2012) 'Dynamic contrast enhanced-MRI for the detection of pathological complete response to neoadjuvant chemotherapy for locally advanced rectal cancer', *Eur Radiol*, 22(4), pp. 821-31.

Gong, J., Tuli, R., Shinde, A. and Hendifar, A.E. (2016) 'Meta-analyses of treatment standards for pancreatic cancer', *Mol Clin Oncol*, 4(3), pp. 315-325.

Gray, K.R., Contractor, K.B., Kenny, L.M., Al-Nahhas, A., Shousha, S., Stebbing, J., Wasan, H.S., Coombes, R.C., Aboagye, E.O., Turkheimer, F.E. and Rosso, L. (2010) 'Kinetic filtering of [(18)F]Fluorothymidine in positron emission tomography studies', *Phys Med Biol*, 55(3), pp. 695-709.

Gregoire, V., Ang, K., Budach, W., Grau, C., Hamoir, M., Langendijk, J.A., Lee, A., Le, Q.T., Maingon, P., Nutting, C., O'Sullivan, B., Porceddu, S.V. and Lengele, B. (2014) 'Delineation of the neck node levels for head and neck tumors: a 2013 update. DAHANCA, EORTC, HKNPCSG, NCIC CTG, NCRI, RTOG, TROG consensus guidelines', *Radiother Oncol*, 110(1), pp. 172-81.

Grierson, J.R. and Shields, A.F. (2000) 'Radiosynthesis of 3'-deoxy-3'-[(18)F]fluorothymidine: [(18)F]FLT for imaging of cellular proliferation in vivo', *Nucl Med Biol*, 27(2), pp. 143-56.

Gronowitz, J.S., Hagberg, H., Kallander, C.F. and Simonsson, B. (1983) 'The use of serum deoxythymidine kinase as a prognostic marker, and in the monitoring of patients with non-Hodgkin's lymphoma', *Br J Cancer*, 47(4), pp. 487-95.

Grossman, H.B., Natale, R.B., Tangen, C.M., Speights, V.O., Vogelzang, N.J., Trump, D.L., deVere White, R.W., Sarosdy, M.F., Wood, D.P., Jr., Raghavan, D. and Crawford, E.D. (2003) 'Neoadjuvant chemotherapy plus cystectomy compared with cystectomy alone for locally advanced bladder cancer', *N Engl J Med*, 349(9), pp. 859-66.

Guerrero Urbano, T., Clark, C.H., Hansen, V.N., Adams, E.J., A'Hern, R., Miles, E.A., McNair, H., Bidmead, M., Warrington, A.P., Dearnaley, D.P., Harrington, K.J. and Nutting, C.M. (2007) 'A phase I study of dose-escalated chemoradiation with accelerated intensity modulated radiotherapy in locally advanced head and neck cancer', *Radiother Oncol*, 85(1), pp. 36-41.

Gunn, G.B., Debnam, J.M., Fuller, C.D., Morrison, W.H., Frank, S.J., Beadle, B.M., Sturgis, E.M., Glisson, B.S., Phan, J., Rosenthal, D.I. and Garden, A.S. (2013) 'The impact of radiographic retropharyngeal adenopathy in oropharyngeal cancer', *Cancer*, 119(17), pp. 3162-9.

Gupta, N., Sureka, B., Kumar, M.M., Malik, A., Bhushan, T.B. and Mohanty, N.K. (2015) 'Comparison of dynamic contrast-enhanced and diffusion weighted magnetic resonance image in staging and grading of carcinoma bladder with histopathological correlation', *Urol Ann*, 7(2), pp. 199-204.

Hafeez, S., Horwich, A., Omar, O., Mohammed, K., Thompson, A., Kumar, P., Khoo, V., Van As, N., Eeles, R., Dearnaley, D. and Huddart, R. (2016) 'Selective organ preservation with neo-adjuvant chemotherapy for the treatment of muscle invasive transitional cell carcinoma of the bladder', *Br J Cancer*, 114(12), p. e24.

Hafeez, S. and Huddart, R. (2013) 'Advances in bladder cancer imaging', *BMC Med*, 11, p. 104.

Halefoglu, A.M., Sen, E.Y., Tanriverdi, O. and Yilmaz, F. (2013) 'Utility of diffusion-weighted MRI in the diagnosis of bladder carcinoma', *Clin Imaging*, 37(6), pp. 1077-83.

Hamberg, L.M., Hunter, G.J., Alpert, N.M., Choi, N.C., Babich, J.W. and Fischman, A.J. (1994) 'The dose uptake ratio as an index of glucose metabolism: useful parameter or oversimplification?', *J Nucl Med*, 35(8), pp. 1308-12.

Hamm, B., Laniado, M. and Saini, S. (1990) 'Contrast-enhanced magnetic resonance imaging of the abdomen and pelvis', *Magn Reson Q*, 6(2), pp. 108-35.

Han, D., Yu, J., Zhong, X., Fu, Z., Mu, D., Zhang, B., Xu, G., Yang, W. and Zhao, S. (2012) 'Comparison of the diagnostic value of 3-deoxy-3-18F-fluorothymidine and 18F-fluorodeoxyglucose positron emission tomography/computed tomography in the assessment of regional lymph node in thoracic esophageal squamous cell carcinoma: a pilot study', *Dis Esophagus*, 25(5), pp. 416-26.

Harkirat, S., Anand, S. and Jacob, M. (2010) 'Forced diuresis and dual-phase F-fluorodeoxyglucose-PET/CT scan for restaging of urinary bladder cancers', *Indian J Radiol Imaging*, 20(1), pp. 13-9.

Harry, V.N., Semple, S.I., Gilbert, F.J. and Parkin, D.E. (2008) 'Diffusion-weighted magnetic resonance imaging in the early detection of response to chemoradiation in cervical cancer', *Gynecol Oncol*, 111(2), pp. 213-20.

Hayes, C., Padhani, A.R. and Leach, M.O. (2002) 'Assessing changes in tumour vascular function using dynamic contrast-enhanced magnetic resonance imaging', *NMR Biomed*, 15(2), pp. 154-63.

Hayman, J.A., Callahan, J.W., Herschtal, A., Everitt, S., Binns, D.S., Hicks, R.J. and Mac Manus, M. (2011) 'Distribution of proliferating bone marrow in adult cancer patients determined using FLT-PET imaging', *Int J Radiat Oncol Biol Phys*, 79(3), pp. 847-52.

He, Q., Zhang, P., Zou, L., Li, H., Wang, X., Zhou, S., Fornander, T. and Skog, S. (2005) 'Concentration of thymidine kinase 1 in serum (S-TK1) is a more sensitive proliferation marker in human solid tumors than its activity', *Oncol Rep*, 14(4), pp. 1013-9.

Heijmen, L. (2012) 'Tumour response prediction by diffusion-weighted MR imaging: Ready for clinical use?', *Critical Reviews in Oncology Haematology*.

Heijmen, L., Verstappen, M.C.H.M., ter Voert, E.E.G.W., Punt, C.J.A., Oyen, W.J.G., de Geus-Oei, L.-F., Hermans, J.J., Heerschap, A. and van Laarhoven, H.W.M. 'Tumour response prediction by diffusion-weighted MR imaging: Ready for clinical use?', *Critical Reviews in Oncology/Hematology*, (0).

Heinzmann, K., Honess, D.J., Lewis, D.Y., Smith, D.M., Cawthorne, C., Keen, H., Heskamp, S., Schelhaas, S., Witney, T.H., Soloviev, D., Williams, K.J., Jacobs, A.H., Aboagye, E.O., Griffiths, J.R. and Brindle, K.M. (2016) 'The relationship between endogenous thymidine concentrations and [(18)F]FLT uptake in a range of preclinical tumour models', *EJNMMI Res*, 6(1), p. 63.

Hendee, W.R. and Morgan, C.J. (1984) 'Magnetic resonance imaging. Part II--Clinical applications', *West J Med*, 141(5), pp. 638-48.

Herrmann, K., Buck, A.K., Schuster, T., Junger, A., Wieder, H.A., Graf, N., Ringshausen, I., Rudelius, M., Wester, H.J., Schwaiger, M., Keller, U. and Dechow,

T. (2011a) 'Predictive value of initial 18F-FLT uptake in patients with aggressive non-Hodgkin lymphoma receiving R-CHOP treatment', *J Nucl Med*, 52(5), pp. 690-6.

Herrmann, K., Buck, A.K., Schuster, T., Rudelius, M., Wester, H.J., Graf, N., Scheuerer, C., Peschel, C., Schwaiger, M., Dechow, T. and Keller, U. (2011b) 'A pilot study to evaluate 3'-deoxy-3'-18F-fluorothymidine pet for initial and early response imaging in mantle cell lymphoma', *J Nucl Med*, 52(12), pp. 1898-902.

Herrmann, K., Eckel, F., Schmidt, S., Scheidhauer, K., Krause, B.J., Kleeff, J., Schuster, T., Wester, H.J., Friess, H., Schmid, R.M., Schwaiger, M. and Buck, A.K. (2008) 'In vivo characterization of proliferation for discriminating cancer from pancreatic pseudotumors', *J Nucl Med*, 49(9), pp. 1437-44.

Herrmann, K., Erkan, M., Dobritz, M., Schuster, T., Siveke, J.T., Beer, A.J., Wester, H.J., Schmid, R.M., Friess, H., Schwaiger, M., Kleeff, J. and Buck, A.K. (2012) 'Comparison of 3'-deoxy-3'-[(1)(8)F]fluorothymidine positron emission tomography (FLT PET) and FDG PET/CT for the detection and characterization of pancreatic tumours', *Eur J Nucl Med Mol Imaging*, 39(5), pp. 846-51.

Hesselink, J.R., Healy, M.E., Press, G.A. and Brahme, F.J. (1988) 'Benefits of Gd-DTPA for MR imaging of intracranial abnormalities', *J Comput Assist Tomogr*, 12(2), pp. 266-74.

Heuveling, D.A., de Bree, R. and van Dongen, G.A. (2011) 'The potential role of non-FDG-PET in the management of head and neck cancer', *Oral Oncol*, 47(1), pp. 2-7.

Heverhagen, J.T., von Tengg-Kobligk, H., Baudendistel, K.T., Jia, G., Polzer, H., Henry, H., Levine, A.L., Rosol, T.J. and Knopp, M.V. (2004) 'Benign prostate hyperplasia: evaluation of treatment response with DCE MRI', *MAGMA*, 17(1), pp. 5-11.

Hingorani, A.D., Windt, D.A., Riley, R.D., Abrams, K., Moons, K.G., Steyerberg, E.W., Schroter, S., Sauerbrei, W., Altman, D.G., Hemingway, H. and Group, P. (2013) 'Prognosis research strategy (PROGRESS) 4: Stratified medicine research', *BMJ*, 346, p. e5793.

Hoeben, B.A., Troost, E.G., Span, P.N., van Herpen, C.M., Bussink, J., Oyen, W.J. and Kaanders, J.H. (2013) '18F-FLT PET during radiotherapy or chemoradiotherapy in head and neck squamous cell carcinoma is an early predictor of outcome', *J Nucl Med*, 54(4), pp. 532-40.

Hong, N., Du, X., Nie, Z. and Li, S. (2005) 'Diffusion-weighted MR study of femoral head avascular necrosis in severe acute respiratory syndrome patients', *J Magn Reson Imaging*, 22(5), pp. 661-4.

Hoshikawa, H., Kishino, T., Mori, T., Nishiyama, Y., Yamamoto, Y., Inamoto, R., Akiyama, K. and Mori, N. (2012) 'Comparison of (18) F-FLT PET and (18) F-FDG PET for detection of cervical lymph node metastases in head and neck cancers', *Acta Otolaryngol*, 132(12), pp. 1347-54.

Hoshikawa, H., Mori, T., Yamamoto, Y., Kishino, T., Fukumura, T., Samukawa, Y., Mori, N. and Nishiyama, Y. (2015) 'Prognostic value comparison between (18)F-FLT PET/CT and (18)F-FDG PET/CT volume-based metabolic parameters in patients with head and neck cancer', *Clin Nucl Med*, 40(6), pp. 464-8.

Hoshikawa, H., Nishiyama, Y., Kishino, T., Yamamoto, Y., Haba, R. and Mori, N. (2011) 'Comparison of FLT-PET and FDG-PET for visualization of head and neck squamous cell cancers', *Mol Imaging Biol*, 13(1), pp. 172-7.

Huang, S.H., Xu, W., Waldron, J., Siu, L., Shen, X., Tong, L., Ringash, J., Bayley, A., Kim, J., Hope, A., Cho, J., Giuliani, M., Hansen, A., Irish, J., Gilbert, R., Gullane, P., Perez-Ordonez, B., Weinreb, I., Liu, F.F. and O'Sullivan, B. (2015) 'Refining American Joint Committee on Cancer/Union for International Cancer Control TNM stage and prognostic groups for human papillomavirus-related oropharyngeal carcinomas', *J Clin Oncol*, 33(8), pp. 836-45.

Intven, M., Monninkhof, E.M., Reerink, O. and Philippens, M.E. (2015) 'Combined T2w volumetry, DW-MRI and DCE-MRI for response assessment after neo-adjuvant chemoradiation in locally advanced rectal cancer', *Acta Oncol*, pp. 1-8.

Inubushi, M., Saga, T., Koizumi, M., Takagi, R., Hasegawa, A., Koto, M., Wakatuki, M., Morikawa, T., Yoshikawa, K., Tanimoto, K., Fukumura, T., Yamada, S. and Kamada, T. (2013) 'Predictive value of 3'-deoxy-3'-[18F]fluorothymidine positron emission tomography/computed tomography for outcome of carbon ion radiotherapy in patients with head and neck mucosal malignant melanoma', *Ann Nucl Med*, 27(1), pp. 1-10.

Jagarlamudi, K.K., Hansson, L.O. and Eriksson, S. (2015) 'Breast and prostate cancer patients differ significantly in their serum Thymidine kinase 1 (TK1) specific activities compared with those hematological malignancies and blood donors: implications of using serum TK1 as a biomarker', *BMC Cancer*, 15, p. 66.

Jager, G.J., Ruijter, E.T., van de Kaa, C.A., de la Rosette, J.J., Oosterhof, G.O., Thornbury, J.R., Ruijs, S.H. and Barentsz, J.O. (1997) 'Dynamic TurboFLASH subtraction technique for contrast-enhanced MR imaging of the prostate: correlation with histopathologic results', *Radiology*, 203(3), pp. 645-52.

James, N.D., Hussain, S.A., Hall, E., Jenkins, P., Tremlett, J., Rawlings, C., Crundwell, M., Sizer, B., Sreenivasan, T., Hendron, C., Lewis, R., Waters, R., Huddart, R.A. and Investigators, B.C. (2012) 'Radiotherapy with or without chemotherapy in muscle-invasive bladder cancer', *N Engl J Med*, 366(16), pp. 1477-88.

Johansen, R., Jensen, L.R., Rydland, J., Goa, P.E., Kvistad, K.A., Bathen, T.F., Axelson, D.E., Lundgren, S. and Gribbestad, I.S. (2009) 'Predicting survival and early clinical response to primary chemotherapy for patients with locally advanced breast cancer using DCE-MRI', *J Magn Reson Imaging*, 29(6), pp. 1300-7.

Johnston, K.C., Wagner, D.P., Wang, X.Q., Newman, G.C., Thijs, V., Sen, S., Warach, S., Gain, C. and Investigators, A. (2007) 'Validation of an acute ischemic stroke model: does diffusion-weighted imaging lesion volume offer a clinically significant improvement in prediction of outcome?', *Stroke*, 38(6), pp. 1820-5.

Kahraman, D., Scheffler, M., Zander, T., Nogova, L., Lammertsma, A.A., Boellaard, R., Neumaier, B., Ullrich, R.T., Holstein, A., Dietlein, M., Wolf, J. and Kobe, C. (2011) 'Quantitative Analysis of Response to Treatment with Erlotinib in Advanced Non-Small Cell Lung Cancer Using 18F-FDG and 3'-Deoxy-3'-18F-Fluorothymidine PET', *J Nucl Med*, 52(12), pp. 1871-7.

Kamel, E.M., Jichlinski, P., Prior, J.O., Meuwly, J.Y., Delaloye, J.F., Vaucher, L., Malterre, J., Castaldo, S., Leisinger, H.J. and Delaloye, A.B. (2006) 'Forced diuresis

improves the diagnostic accuracy of 18F-FDG PET in abdominopelvic malignancies', *J Nucl Med*, 47(11), pp. 1803-7.

Kanazawa, Y., Miyati, T. and Sato, O. (2012) 'Hemodynamic analysis of bladder tumors using T1-dynamic contrast-enhanced fast spin-echo MRI', *Eur J Radiol*, 81(8), pp. 1682-7.

Katoh, R., Bray, C.E., Suzuki, K., Komiyama, A., Hemmi, A., Kawaoi, A., Oyama, T., Sugai, T. and Sasou, S. (1995) 'Growth activity in hyperplastic and neoplastic human thyroid determined by an immunohistochemical staining procedure using monoclonal antibody MIB-1', *Hum Pathol*, 26(2), pp. 139-46.

Kenny, L., Coombes, R.C., Vigushin, D.M., Al-Nahhas, A., Shousha, S. and Aboagye, E.O. (2007) 'Imaging early changes in proliferation at 1 week post chemotherapy: a pilot study in breast cancer patients with 3'-deoxy-3'-[18F]fluorothymidine positron emission tomography', *Eur J Nucl Med Mol Imaging*, 34(9), pp. 1339-47.

Kenny, L.M., Contractor, K.B., Stebbing, J., Al-Nahhas, A., Palmieri, C., Shousha, S., Coombes, R.C. and Aboagye, E.O. (2009) 'Altered tissue 3'-deoxy-3'-[18F]fluorothymidine pharmacokinetics in human breast cancer following capecitabine treatment detected by positron emission tomography', *Clin Cancer Res*, 15(21), pp. 6649-57.

Kenny, L.M., Vigushin, D.M., Al-Nahhas, A., Osman, S., Luthra, S.K., Shousha, S., Coombes, R.C. and Aboagye, E.O. (2005) 'Quantification of cellular proliferation in tumor and normal tissues of patients with breast cancer by [18F]fluorothymidine-positron emission tomography imaging: evaluation of analytical methods', *Cancer Res*, 65(21), pp. 10104-12.

Kety, S.S. (1951) 'The theory and applications of the exchange of inert gas at the lungs and tissues', *Pharmacol Rev*, 3(1), pp. 1-41.

Khalifa, F., Soliman, A., El-Baz, A., Abou El-Ghar, M., El-Diasty, T., Gimel'farb, G., Ouseph, R. and Dwyer, A.C. (2014) 'Models and methods for analyzing DCE-MRI: a review', *Med Phys*, 41(12), p. 124301.

Khoo, M.M., Tyler, P.A., Saifuddin, A. and Padhani, A.R. (2011) 'Diffusion-weighted imaging (DWI) in musculoskeletal MRI: a critical review', *Skeletal Radiol*, 40(6), pp. 665-81.

Kibel, A.S., Dehdashti, F., Katz, M.D., Klim, A.P., Grubb, R.L., Humphrey, P.A., Siegel, C., Cao, D., Gao, F. and Siegel, B.A. (2009) 'Prospective study of [18F]fluorodeoxyglucose positron emission tomography/computed tomography for staging of muscle-invasive bladder carcinoma', *J Clin Oncol*, 27(26), pp. 4314-20.

Kilickesmez, O., Cimilli, T., Inci, E., Kayhan, A., Bayramoglu, S., Tasdelen, N. and Gurmen, N. (2009) 'Diffusion-weighted MRI of urinary bladder and prostate cancers', *Diagn Interv Radiol*, 15(2), pp. 104-10.

Kim, B., Semelka, R.C., Ascher, S.M., Chalpin, D.B., Carroll, P.R. and Hricak, H. (1994) 'Bladder tumor staging: comparison of contrast-enhanced CT, T1- and T2-weighted MR imaging, dynamic gadolinium-enhanced imaging, and late gadolinium-enhanced imaging', *Radiology*, 193(1), pp. 239-45.

Kim, S.H., Cha, E.S., Kim, H.S., Kang, B.J., Choi, J.J., Jung, J.H., Park, Y.G. and Suh, Y.J. (2009) 'Diffusion-weighted imaging of breast cancer: correlation of the

apparent diffusion coefficient value with prognostic factors', *J Magn Reson Imaging*, 30(3), pp. 615-20.

Kishino, T., Hoshikawa, H., Nishiyama, Y., Yamamoto, Y. and Mori, N. (2012) 'Usefulness of 3'-deoxy-3'-18F-fluorothymidine PET for predicting early response to chemoradiotherapy in head and neck cancer', *J Nucl Med*, 53(10), pp. 1521-7.

Klein, W.M., Hruban, R.H., Klein-Szanto, A.J. and Wilentz, R.E. (2002) 'Direct correlation between proliferative activity and dysplasia in pancreatic intraepithelial neoplasia (PanIN): additional evidence for a recently proposed model of progression', *Mod Pathol*, 15(4), pp. 441-7.

Kobayashi, S., Koga, F., Kajino, K., Yoshita, S., Ishii, C., Tanaka, H., Saito, K., Masuda, H., Fujii, Y., Yamada, T. and Kihara, K. (2013) 'Apparent diffusion coefficient value reflects invasive and proliferative potential of bladder cancer', *Journal of Magnetic Resonance Imaging*, pp. n/a-n/a.

Kobayashi, S., Koga, F., Yoshida, S., Masuda, H., Ishii, C., Tanaka, H., Komai, Y., Yokoyama, M., Saito, K., Fujii, Y., Kawakami, S. and Kihara, K. (2011) 'Diagnostic performance of diffusion-weighted magnetic resonance imaging in bladder cancer: potential utility of apparent diffusion coefficient values as a biomarker to predict clinical aggressiveness', *Eur Radiol*, 21(10), pp. 2178-86.

Koh, D.M., Blackledge, M., Collins, D.J., Padhani, A.R., Wallace, T., Wilton, B., Taylor, N.J., Stirling, J.J., Sinha, R., Walicke, P., Leach, M.O., Judson, I. and Nathan, P. (2009) 'Reproducibility and changes in the apparent diffusion coefficients of solid tumours treated with combretastatin A4 phosphate and bevacizumab in a two-centre phase I clinical trial', *Eur Radiol*, 19(11), pp. 2728-38.

Koh, D.M., Scurr, E., Collins, D., Kanber, B., Norman, A., Leach, M.O. and Husband, J.E. (2007) 'Predicting response of colorectal hepatic metastasis: value of pretreatment apparent diffusion coefficients', *AJR Am J Roentgenol*, 188(4), pp. 1001-8.

Kong, X.B., Vidal, P., Tong, W.P., Chiang, J., Gloff, C.A. and Chou, T.C. (1992) 'Preclinical pharmacology and pharmacokinetics of the anti-hepatitis virus agent 2'-fluoro-5-ethyl-1-beta-D-arabinofuranosyluracil in mice and rats', *Antimicrob Agents Chemother*, 36(7), pp. 1472-7.

Kosuda, S., Kison, P.V., Greenough, R., Grossman, H.B. and Wahl, R.L. (1997) 'Preliminary assessment of fluorine-18 fluorodeoxyglucose positron emission tomography in patients with bladder cancer', *Eur J Nucl Med*, 24(6), pp. 615-20.

Koyama, K., Okamura, T., Kawabe, J., Ozawa, N., Torii, K., Umesaki, N., Miyama, M., Ochi, H. and Yamada, R. (2003) 'Evaluation of 18F-FDG PET with bladder irrigation in patients with uterine and ovarian tumors', *J Nucl Med*, 44(3), pp. 353-8.

Krabbe, L.M., Lotan, Y., Bagrodia, A., Gayed, B.A., Darwish, O.M., Youssef, R.F., Bolenz, C., Sagalowsky, A.I., Raj, G.V., Shariat, S.F., Kapur, P. and Margulis, V. (2014) 'Prospective comparison of molecular signatures in urothelial cancer of the bladder and the upper urinary tract--is there evidence for discordant biology?', *J Urol*, 191(4), pp. 926-31.

Kyriazi, S., Collins, D.J., Messiou, C., Pennert, K., Davidson, R.L., Giles, S.L., Kaye, S.B. and Desouza, N.M. (2011) 'Metastatic ovarian and primary peritoneal cancer: assessing chemotherapy response with diffusion-weighted MR imaging--value of histogram analysis of apparent diffusion coefficients', *Radiology*, 261(1), pp. 182-92.

Lallemand, D., Gooding, C.A., Wesbey, G.E., Brasch, R.C., Botvinick, E., Lanzer, P. and McNamara, M.T. (1985) 'Magnetic resonance (MR) imaging of aorta and pulmonary circulation. Initial experience with ECG-gating', *Ann Radiol (Paris)*, 28(3-4), pp. 289-98.

Lamarca, A., Asselin, M.-C., Manoharan, P., McNamara, M.G., Trigonis, I., Hubner, R., Saleem, A. and Valle, J.W. (2016) '18F-FLT PET imaging of cellular proliferation in pancreatic cancer', *Critical Reviews in Oncology/Hematology*, 99, pp. 158-169.

Langen, P., Etzold, G., Hintsche, R. and Kowollik, G. (1969) '3'-Deoxy-3'-fluorothymidine, a new selective inhibitor of DNA-synthesis', *Acta Biol Med Ger*, 23(6), pp. 759-66.

Lankester, K.J., Taylor, J.N., Stirling, J.J., Boxall, J., d'Arcy, J.A., Collins, D.J., Walker-Samuel, S., Leach, M.O., Rustin, G.J. and Padhani, A.R. (2007) 'Dynamic MRI for imaging tumor microvasculature: comparison of susceptibility and relaxivity techniques in pelvic tumors', *J Magn Reson Imaging*, 25(4), pp. 796-805.

Lara, P.C., Rey, A., Santana, C., Afonso, J.L., Diaz, J.M., Gonzalez, G.J. and Apolinario, R. (1998) 'The role of Ki67 proliferation assessment in predicting local control in bladder cancer patients treated by radical radiation therapy', *Radiother Oncol*, 49(2), pp. 163-7.

Lassen, P., Eriksen, J.G., Krogdahl, A., Therkildsen, M.H., Ulhoi, B.P., Overgaard, M., Specht, L., Andersen, E., Johansen, J., Andersen, L.J., Grau, C., Overgaard, J., Danish, H. and Neck Cancer, G. (2011) 'The influence of HPV-associated p16-expression on accelerated fractionated radiotherapy in head and neck cancer: evaluation of the randomised DAHANCA 6&7 trial', *Radiother Oncol*, 100(1), pp. 49-55.

Lauve, A., Morris, M., Schmidt-Ullrich, R., Wu, Q., Mohan, R., Abayomi, O., Buck, D., Holdford, D., Dawson, K., Dinardo, L. and Reiter, E. (2004) 'Simultaneous integrated boost intensity-modulated radiotherapy for locally advanced head-and-neck squamous cell carcinomas: II--clinical results', *Int J Radiat Oncol Biol Phys*, 60(2), pp. 374-87.

Le Bihan, D., Breton, E., Lallemand, D., Aubin, M.L., Vignaud, J. and Laval-Jeantet, M. (1988) 'Separation of diffusion and perfusion in intravoxel incoherent motion MR imaging', *Radiology*, 168(2), pp. 497-505.

Leach, M.O., Brindle, K.M., Evelhoch, J.L., Griffiths, J.R., Horsman, M.R., Jackson, A., Jayson, G.C., Judson, I.R., Knopp, M.V., Maxwell, R.J., McIntyre, D., Padhani, A.R., Price, P., Rathbone, R., Rustin, G.J., Tofts, P.S., Tozer, G.M., Vennart, W., Waterton, J.C., Williams, S.R. and Workman, P. (2005) 'The assessment of antiangiogenic and antivascular therapies in early-stage clinical trials using magnetic resonance imaging: issues and recommendations', *Br J Cancer*, 92(9), pp. 1599-610.

Leach, M.O., Morgan, B., Tofts, P.S., Buckley, D.L., Huang, W., Horsfield, M.A., Chenevert, T.L., Collins, D.J., Jackson, A., Lomas, D., Whitcher, B., Clarke, L., Plummer, R., Judson, I., Jones, R., Alonzi, R., Brunner, T., Koh, D.M., Murphy, P., Waterton, J.C., Parker, G., Graves, M.J., Scheenen, T.W., Redpath, T.W., Orton, M., Karczmar, G., Huisman, H., Barentsz, J., Padhani, A. and Experimental Cancer Medicine Centres Imaging Network Steering, C. (2012) 'Imaging vascular function for early stage clinical trials using dynamic contrast-enhanced magnetic resonance imaging', *Eur Radiol*, 22(7), pp. 1451-64.

Leclerc, M., Lartigau, E., Lacornerie, T., Daisne, J.F., Kramar, A. and Gregoire, V. (2015) 'Primary tumor delineation based on (18)FDG PET for locally advanced head and neck cancer treated by chemo-radiotherapy', *Radiother Oncol*, 116(1), pp. 87-93.

Leclerc, M., Maingon, P., Hamoir, M., Dalban, C., Calais, G., Nuyts, S., Serre, A. and Gregoire, V. (2013) 'A dose escalation study with intensity modulated radiation therapy (IMRT) in T2N0, T2N1, T3N0 squamous cell carcinomas (SCC) of the oropharynx, larynx and hypopharynx using a simultaneous integrated boost (SIB) approach', *Radiother Oncol*, 106(3), pp. 333-40.

Lee, H., Kim, S.K., Kim, Y.I., Kim, T.S., Kang, S.H., Park, W.S., Yun, T. and Eom, H.S. (2014a) 'Early determination of prognosis by interim 3'-deoxy-3'-18F-fluorothymidine PET in patients with non-Hodgkin lymphoma', *J Nucl Med*, 55(2), pp. 216-22.

Lee, N.Y., Mechalakos, J.G., Nehmeh, S., Lin, Z., Squire, O.D., Cai, S., Chan, K., Zanzonico, P.B., Greco, C., Ling, C.C., Humm, J.L. and Schoder, H. (2008) 'Fluorine-18-labeled fluoromisonidazole positron emission and computed tomography-guided intensity-modulated radiotherapy for head and neck cancer: a feasibility study', *Int J Radiat Oncol Biol Phys*, 70(1), pp. 2-13.

Lee, S.J., Kang, H.Y., Kim, S.Y., Chung, J.H., Oh, S.J., Ryu, J.S., Kim, S.B., Kang, J.S., Park, S.K., Kim, H.M., Kim, M.H. and Moon, D.H. (2011) 'Early assessment of tumor response to JAC106, an anti-tubulin agent, by 3'-deoxy-3'-[(1)(8)F]fluorothymidine in preclinical tumor models', *Eur J Nucl Med Mol Imaging*, 38(8), pp. 1436-48.

Lee, S.J., Kim, S.Y., Chung, J.H., Oh, S.J., Ryu, J.S., Hong, Y.S., Kim, T.W. and Moon, D.H. (2010) 'Induction of thymidine kinase 1 after 5-fluorouracil as a mechanism for 3'-deoxy-3'-[18F]fluorothymidine flare', *Biochem Pharmacol*, 80(10), pp. 1528-36.

Lee, S.J., Yeo, J.S., Lee, H.J., Lee, E.J., Kim, S.Y., Jang, S.J., Lee, J.J., Ryu, J.S. and Moon, D.H. (2014b) 'Thymidine phosphorylase influences [F]fluorothymidine uptake in cancer cells and patients with non-small cell lung cancer', *Eur J Nucl Med Mol Imaging*.

Leimgruber, A., Moller, A., Everitt, S.J., Chabrot, M., Ball, D.L., Solomon, B., MacManus, M. and Hicks, R.J. (2014) 'Effect of Platinum-Based Chemoradiotherapy on Cellular Proliferation in Bone Marrow and Spleen, Estimated by (18)F-FLT PET/CT in Patients with Locally Advanced Non-Small Cell Lung Cancer', *J Nucl Med*, 55(7), pp. 1075-80.

Levene, M., Coleman, D.G., Kilpatrick, H.C., Fairbanks, L.D., Gangadharan, B., Gasson, C. and Bax, B.E. (2013) 'Preclinical toxicity evaluation of erythrocyte-encapsulated thymidine phosphorylase in BALB/c mice and beagle dogs: an enzyme-replacement therapy for mitochondrial neurogastrointestinal encephalomyopathy', *Toxicol Sci*, 131(1), pp. 311-24.

Leyton, J., Latigo, J.R., Perumal, M., Dhaliwal, H., He, Q. and Aboagye, E.O. (2005) 'Early detection of tumor response to chemotherapy by 3'-deoxy-3'-[18F]fluorothymidine positron emission tomography: the effect of cisplatin on a fibrosarcoma tumor model in vivo', *Cancer Res*, 65(10), pp. 4202-10.

Li, X., Arlinghaus, L.R., Ayers, G.D., Chakravarthy, A.B., Abramson, R.G., Abramson, V.G., Atuegwu, N., Farley, J., Mayer, I.A., Kelley, M.C., Meszoely, I.M., Means-

Powell, J., Grau, A.M., Sanders, M., Bhave, S.R. and Yankeelov, T.E. (2014) 'DCE-MRI analysis methods for predicting the response of breast cancer to neoadjuvant chemotherapy: pilot study findings', *Magn Reson Med*, 71(4), pp. 1592-602.

Li, X., Dawant, B.M., Welch, E.B., Chakravarthy, A.B., Freehardt, D., Mayer, I., Kelley, M., Meszoely, I., Gore, J.C. and Yankeelov, T.E. (2009) 'A nonrigid registration algorithm for longitudinal breast MR images and the analysis of breast tumor response', *Magn Reson Imaging*, 27(9), pp. 1258-70.

Li, X., Welch, E.B., Arlinghaus, L.R., Chakravarthy, A.B., Xu, L., Farley, J., Loveless, M.E., Mayer, I.A., Kelley, M.C., Meszoely, I.M., Means-Powell, J.A., Abramson, V.G., Grau, A.M., Gore, J.C. and Yankeelov, T.E. (2011) 'A novel AIF tracking method and comparison of DCE-MRI parameters using individual and population-based AIFs in human breast cancer', *Phys Med Biol*, 56(17), pp. 5753-69.

Li, Z., Wang, Y., He, J., Ma, J., Zhao, L., Chen, H., Li, N., Zhou, J., He, E. and Skog, S. (2010) 'Serological thymidine kinase 1 is a prognostic factor in oesophageal, cardial and lung carcinomas', *Eur J Cancer Prev*, 19(4), pp. 313-8.

Lill, C., Kornek, G., Bachtiary, B., Selzer, E., Schopper, C., Mittlboeck, M., Burian, M., Wrba, F. and Thurnher, D. (2011) 'Survival of patients with HPV-positive oropharyngeal cancer after radiochemotherapy is significantly enhanced', *Wien Klin Wochenschr*, 123(7-8), pp. 215-21.

Lin, C., Itti, E., Haioun, C., Petegnief, Y., Luciani, A., Dupuis, J., Paone, G., Talbot, J.N., Rahmouni, A. and Meignan, M. (2007) 'Early 18F-FDG PET for prediction of prognosis in patients with diffuse large B-cell lymphoma: SUV-based assessment versus visual analysis', *J Nucl Med*, 48(10), pp. 1626-32.

Lin, M., Pellerin, O., Bhagat, N., Rao, P.P., Loffroy, R., Ardon, R., Mory, B., Reyes, D.K. and Geschwind, J.F. (2012) 'Quantitative and volumetric European Association for the Study of the Liver and Response Evaluation Criteria in Solid Tumors measurements: feasibility of a semiautomated software method to assess tumor response after transcatheter arterial chemoembolization', *J Vasc Interv Radiol*, 23(12), pp. 1629-37.

Linecker, A., Kermer, C., Sulzbacher, I., Angelberger, P., Kletter, K., Dudczak, R., Ewers, R. and Becherer, A. (2008) 'Uptake of (18)F-FLT and (18)F-FDG in primary head and neck cancer correlates with survival', *Nuklearmedizin*, 47(2), pp. 80-5; quiz N12.

Loncaster, J.A., Carrington, B.M., Sykes, J.R., Jones, A.P., Todd, S.M., Cooper, R., Buckley, D.L., Davidson, S.E., Logue, J.P., Hunter, R.D. and West, C.M. (2002) 'Prediction of radiotherapy outcome using dynamic contrast enhanced MRI of carcinoma of the cervix', *Int J Radiat Oncol Biol Phys*, 54(3), pp. 759-67.

Lu, Y.Y., Chen, J.H., Liang, J.A., Wang, H.Y., Lin, C.C., Lin, W.Y. and Kao, C.H. (2011) 'Clinical value of FDG PET or PET/CT in urinary bladder cancer: A systemic review and meta-analysis', *Eur J Radiol*.

MacManus, M.P., Seymour, J.F. and Hicks, R.J. (2007) 'Overview of early response assessment in lymphoma with FDG-PET', *Cancer Imaging*, 7, pp. 10-8.

Madani, I., Duprez, F., Boterberg, T., Van de Wiele, C., Bonte, K., Deron, P., Gersem, W.D., Coghe, M. and Neve, W.D. (2011) 'Maximum tolerated dose in a phase I trial on adaptive dose painting by numbers for head and neck cancer', *Radiother Oncol*, 101(3), pp. 351-5.

Madani, I., Duthoy, W., Derie, C., De Gersem, W., Boterberg, T., Saerens, M., Jacobs, F., Gregoire, V., Lonneux, M., Vakaet, L., Vanderstraeten, B., Bauters, W., Bonte, K., Thierens, H. and De Neve, W. (2007a) 'Positron emission tomography-guided, focal-dose escalation using intensity-modulated radiotherapy for head and neck cancer', *Int J Radiat Oncol Biol Phys*, 68(1), pp. 126-35.

Madani, I., Duthoy, W., Derie, C., De Gersem, W., Boterberg, T., Saerens, M., Jacobs, F., Gregoire, V., Lonneux, M., Vakaet, L., Vanderstraeten, B., Bauters, W., Bonte, K., Thierens, H. and De Neve, W. (2007b) 'Positron emission tomography-guided, focal-dose escalation using intensity-modulated radiotherapy for head and neck cancer', *International Journal of Radiation Oncology Biology Physics*, 68(1), pp. 126-135.

Maeda, K., Chung, Y.S., Ogawa, Y., Takatsuka, S., Kang, S.M., Ogawa, M., Sawada, T., Onoda, N., Kato, Y. and Sowa, M. (1996) 'Thymidine phosphorylase/platelet-derived endothelial cell growth factor expression associated with hepatic metastasis in gastric carcinoma', *Br J Cancer*, 73(8), pp. 884-8.

Mahadevan, V. and Hart, I.R. (1990) 'Metastasis and angiogenesis', *Acta Oncol*, 29(1), pp. 97-103.

Maiorana, A. and Gullino, P.M. (1978) 'Acquisition of angiogenic capacity and neoplastic transformation in the rat mammary gland', *Cancer Res*, 38(12), pp. 4409-14.

Mankoff, D.A., Muzi, M. and Zaidi, H. (2006) 'Quantitative Analysis in Nuclear Imaging', in Zaidi, H. (ed.) Singapore: Springer, p. 592.

Mankoff, D.A., Shields, A.F. and Krohn, K.A. (2005) 'PET imaging of cellular proliferation', *Radiol Clin North Am*, 43(1), pp. 153-67.

Mardor, Y., Roth, Y., Ochershvilli, A., Spiegelmann, R., Tichler, T., Daniels, D., Maier, S.E., Nissim, O., Ram, Z., Baram, J., Orenstein, A. and Pfeffer, R. (2004) 'Pretreatment prediction of brain tumors' response to radiation therapy using high b-value diffusion-weighted MRI', *Neoplasia*, 6(2), pp. 136-42.

Margulis, V., Lotan, Y., Karakiewicz, P.I., Fradet, Y., Ashfaq, R., Capitanio, U., Montorsi, F., Bastian, P.J., Nielsen, M.E., Muller, S.C., Rigaud, J., Heukamp, L.C., Netto, G., Lerner, S.P., Sagalowsky, A.I. and Shariat, S.F. (2009) 'Multi-institutional validation of the predictive value of Ki-67 labeling index in patients with urinary bladder cancer', *J Natl Cancer Inst*, 101(2), pp. 114-9.

Margulis, V., Shariat, S.F., Ashfaq, R., Sagalowsky, A.I. and Lotan, Y. (2006) 'Ki-67 Is an Independent Predictor of Bladder Cancer Outcome in Patients Treated with Radical Cystectomy for Organ-Confined Disease', *Clinical Cancer Research*, 12(24), pp. 7369-7373.

Martiat, P., Ferrant, A., Labar, D., Cogneau, M., Bol, A., Michel, C., Michaux, J.L. and Sokal, G. (1988) 'In vivo measurement of carbon-11 thymidine uptake in non-Hodgkin's lymphoma using positron emission tomography', *J Nucl Med*, 29(10), pp. 1633-7.

Mazzaferri, E.L. and Massoll, N. (2002) 'Management of papillary and follicular (differentiated) thyroid cancer: new paradigms using recombinant human thyrotropin', *Endocr Relat Cancer*, 9(4), pp. 227-47.

McGuire, S.M., Menda, Y., Boles Ponto, L.L., Gross, B., TenNapel, M., Smith, B.J. and Bayouth, J.E. (2014) 'Spatial mapping of functional pelvic bone marrow using FLT PET', *J Appl Clin Med Phys*, 15(4), p. 4780.

Meeks, J.J., Bellmunt, J., Bochner, B.H., Clarke, N.W., Daneshmand, S., Galsky, M.D., Hahn, N.M., Lerner, S.P., Mason, M., Powles, T., Sternberg, C.N. and Sonpavde, G. (2012) 'A Systematic Review of Neoadjuvant and Adjuvant Chemotherapy for Muscle-invasive Bladder Cancer', *European Urology*, 62(3), pp. 523-533.

Menda, Y., Boles Ponto, L.L., Dornfeld, K.J., Tewson, T.J., Watkins, G.L., Schultz, M.K., Sunderland, J.J., Graham, M.M. and Buatti, J.M. (2009) 'Kinetic analysis of 3'-deoxy-3'-(18)F-fluorothymidine ((18)F-FLT) in head and neck cancer patients before and early after initiation of chemoradiation therapy', *J Nucl Med*, 50(7), pp. 1028-35.

Mendichovszky, I.A., Cutajar, M. and Gordon, I. (2009) 'Reproducibility of the aortic input function (AIF) derived from dynamic contrast-enhanced magnetic resonance imaging (DCE-MRI) of the kidneys in a volunteer study', *European Journal of Radiology*, 71(3), pp. 576-581.

Mertens, L.S., Fioole-Bruining, A., Vegt, E., Vogel, W.V., van Rhijn, B.W. and Horenblas, S. (2013) 'Impact of (18) F-fluorodeoxyglucose (FDG)-positron-emission tomography/computed tomography (PET/CT) on management of patients with carcinoma invading bladder muscle', *BJU Int*, 112(6), pp. 729-34.

Messiou, C., Collins, D.J., Morgan, V.A. and Desouza, N.M. (2011) 'Optimising diffusion weighted MRI for imaging metastatic and myeloma bone disease and assessing reproducibility', *Eur Radiol*, 21(8), pp. 1713-8.

Metcalfe, P., Liney, G.P., Holloway, L., Walker, A., Barton, M., Delaney, G.P., Vinod, S. and Tome, W. (2013) 'The potential for an enhanced role for MRI in radiation-therapy treatment planning', *Technol Cancer Res Treat*, 12(5), pp. 429-46.

Miah, A.B., Bhide, S.A., Guerrero-Urbano, M.T., Clark, C., Bidmead, A.M., St. Rose, S., Barbachano, Y., A'Hern, R., Tanay, M., Hickey, J., Nicol, R., Newbold, K.L., Harrington, K.J. and Nutting, C.M. (2012) 'Dose-Escalated Intensity-Modulated Radiotherapy Is Feasible and May Improve Locoregional Control and Laryngeal Preservation in Laryngo-Hypopharyngeal Cancers', *International Journal of Radiation Oncology*Biology*Physics*, 82(2), pp. 539-547.

Miszczak-Zaborska, E., Smolarek, M. and Bartkowiak, J. (2010) '[Influence of the thymidine phosphorylase (platelet-derived endothelial cell growth factor) on tumor angiogenesis. Catalytic activity of enzyme inhibitors]', *Postepy Biochem*, 56(1), pp. 61-6.

Mitra, A.P., Quinn, D.I., Dorff, T.B., Skinner, E.C., Schuckman, A.K., Miranda, G., Gill, I.S. and Daneshmand, S. (2012) 'Factors influencing post-recurrence survival in bladder cancer following radical cystectomy', *BJU Int*, 109(6), pp. 846-54.

Miwa, M., Ura, M., Nishida, M., Sawada, N., Ishikawa, T., Mori, K., Shimma, N., Umeda, I. and Ishitsuka, H. (1998) 'Design of a novel oral fluoropyrimidine carbamate, capecitabine, which generates 5-fluorouracil selectively in tumours by enzymes concentrated in human liver and cancer tissue', *Eur J Cancer*, 34(8), pp. 1274-81.

Moller, D.S., Khalil, A.A., Knap, M.M., Muren, L.P. and Hoffmann, L. (2011) 'A planning study of radiotherapy dose escalation of PET-active tumour volumes in non-small cell lung cancer patients', *Acta Oncol*, 50(6), pp. 883-8.

Monazzam, A., Josephsson, R., Blomqvist, C., Carlsson, J., Langstrom, B. and Bergstrom, M. (2007) 'Application of the multicellular tumour spheroid model to screen PET tracers for analysis of early response of chemotherapy in breast cancer', *Breast Cancer Res*, 9(4), p. R45.

Morgan, B., Utting, J.F., Higginson, A., Thomas, A.L., Steward, W.P. and Horsfield, M.A. (2006) 'A simple, reproducible method for monitoring the treatment of tumours using dynamic contrast-enhanced MR imaging', *Br J Cancer*, 94(10), pp. 1420-1427.

Muijs, C.T., Beukema, J.C., Widder, J., van den Bergh, A.C., Havenga, K., Pruim, J. and Langendijk, J.A. (2011) '18F-FLT-PET for detection of rectal cancer', *Radiother Oncol*, 98(3), pp. 357-9.

Munch-Petersen, B., Cloos, L., Jensen, H.K. and Tyrsted, G. (1995) 'Human thymidine kinase 1. Regulation in normal and malignant cells', *Adv Enzyme Regul*, 35, pp. 69-89.

Muzaffar, R., Fesler, M. and Osman, M.M. (2013) 'Active Shingles Infection as Detected on (18)F-FDG PET/CT', *Front Oncol*, 3, p. 103.

Muzi, M., Mankoff, D.A., Grierson, J.R., Wells, J.M., Vesselle, H. and Krohn, K.A. (2005a) 'Kinetic modeling of 3'-deoxy-3'-fluorothymidine in somatic tumors: mathematical studies', *J Nucl Med*, 46(2), pp. 371-80.

Muzi, M., Vesselle, H., Grierson, J.R., Mankoff, D.A., Schmidt, R.A., Peterson, L., Wells, J.M. and Krohn, K.A. (2005b) 'Kinetic analysis of 3'-deoxy-3'-fluorothymidine PET studies: validation studies in patients with lung cancer', *J Nucl Med*, 46(2), pp. 274-82.

Nakajo, M., Kajiya, Y., Jinguji, M., Mori, S., Aridome, K., Suenaga, T. and Tanaka, S. (2012) 'High FDG and low FLT uptake in a thyroid papillary carcinoma incidentally discovered by FDG PET/CT', *Clin Nucl Med*, 37(6), pp. 607-8.

Nakajo, M., Nakajo, M., Jinguji, M., Tani, A., Kajiya, Y., Tanabe, H., Fukukura, Y., Nakabeppu, Y. and Koriyama, C. (2013) 'Diagnosis of Metastases from Postoperative Differentiated Thyroid Cancer: Comparison between FDG and FLT PET/CT Studies', *Radiology*.

Nakanishi, M., Chuma, M., Hige, S., Omatsu, T., Yokoo, H., Nakanishi, K., Kamiyama, T., Kubota, K., Haga, H., Matsuno, Y., Onodera, Y., Kato, M. and Asaka, M. (2012) 'Relationship between diffusion-weighted magnetic resonance imaging and histological tumor grading of hepatocellular carcinoma', *Ann Surg Oncol*, 19(4), pp. 1302-9.

Nakayama, T., Yoshida, S., Fujii, Y., Koga, F., Saito, K., Masuda, H., Kobayashi, T., Kawakami, S. and Kihara, K. (2008) '[Use of diffusion-weighted MRI in monitoring response of lymph node metastatic bladder cancer treated with chemotherary]', *Nihon Hinyokika Gakkai Zasshi*, 99(7), pp. 737-41.

Narumi, Y., Kadota, T., Inoue, E., Kuriyama, K., Fujita, M., Hosomi, N., Sawai, Y., Kuroda, M., Kotake, T. and Kuroda, C. (1993) 'Bladder tumors: staging with gadolinium-enhanced oblique MR imaging', *Radiology*, 187(1), pp. 145-50.

Nayak, B., Dogra, P.N., Naswa, N. and Kumar, R. (2013) 'Diuretic 18F-FDG PET/CT imaging for detection and locoregional staging of urinary bladder cancer: prospective evaluation of a novel technique', *Eur J Nucl Med Mol Imaging*, 40(3), pp. 386-93.

Nguyen, H.T., Jia, G., Shah, Z.K., Pohar, K., Mortazavi, A., Zynger, D.L., Wei, L., Yang, X., Clark, D. and Knopp, M.V. (2015) 'Prediction of chemotherapeutic response in bladder cancer using K-means clustering of dynamic contrast-enhanced (DCE)-MRI pharmacokinetic parameters', *J Magn Reson Imaging*, 41(5), pp. 1374-82.

Nguyen, H.T., Pohar, K.S., Jia, G., Shah, Z.K., Mortazavi, A., Zynger, D.L., Wei, L., Clark, D., Yang, X. and Knopp, M.V. (2014) 'Improving Bladder Cancer Imaging Using 3-T Functional Dynamic Contrast-Enhanced Magnetic Resonance Imaging', *Invest Radiol*.

NICE (2002) *Guidance on the use of trastuzumab for the treatmentof advanced breast cancer (TA34)* (TA34). London: NICE. [Online]. Available at: http://guidance.nice.org.uk/TA34/Guidance.

NICE (2012) *NICE Guideline 151 - Neutropenic sepsis: prevention and management of cancer patients [CG151]*. NATIONAL INSTITUTE FOR HEALTH AND CARE EXCELLENCE.

NICE (2015) *NICE Guideline 2 Bladder Cancer: Diagnosis and Management*. London. [Online]. Available at: http://www.nice.org.uk/guidance/ng2/evidence/full-guideline-3744109.

Nilsen, L., Fangberget, A., Geier, O., Olsen, D.R. and Seierstad, T. (2010) 'Diffusion-weighted magnetic resonance imaging for pretreatment prediction and monitoring of treatment response of patients with locally advanced breast cancer undergoing neoadjuvant chemotherapy', *Acta Oncol*, 49(3), pp. 354-60.

Nisman, B., Allweis, T., Kaduri, L., Maly, B., Gronowitz, S., Hamburger, T. and Peretz, T. (2010) 'Serum thymidine kinase 1 activity in breast cancer', *Cancer Biomark*, 7(2), pp. 65-72.

Niwa, T., Ueno, M., Ohkawa, S., Yoshida, T., Doiuchi, T., Ito, K. and Inoue, T. (2009) 'Advanced pancreatic cancer: the use of the apparent diffusion coefficient to predict response to chemotherapy', *Br J Radiol*, 82(973), pp. 28-34.

O'Connor, J.P., Aboagye, E.O., Adams, J.E., Aerts, H.J., Barrington, S.F., Beer, A.J., Boellaard, R., Bohndiek, S.E., Brady, M., Brown, G., Buckley, D.L., Chenevert, T.L., Clarke, L.P., Collette, S., Cook, G.J., deSouza, N.M., Dickson, J.C., Dive, C., Evelhoch, J.L., Faivre-Finn, C., Gallagher, F.A., Gilbert, F.J., Gillies, R.J., Goh, V., Griffiths, J.R., Groves, A.M., Halligan, S., Harris, A.L., Hawkes, D.J., Hoekstra, O.S., Huang, E.P., Hutton, B.F., Jackson, E.F., Jayson, G.C., Jones, A., Koh, D.M., Lacombe, D., Lambin, P., Lassau, N., Leach, M.O., Lee, T.Y., Leen, E.L., Lewis, J.S., Liu, Y., Lythgoe, M.F., Manoharan, P., Maxwell, R.J., Miles, K.A., Morgan, B., Morris, S., Ng, T., Padhani, A.R., Parker, G.J., Partridge, M., Pathak, A.P., Peet, A.C., Punwani, S., Reynolds, A.R., Robinson, S.P., Shankar, L.K., Sharma, R.A., Soloviev, D., Stroobants, S., Sullivan, D.C., Taylor, S.A., Tofts, P.S., Tozer, G.M., van Herk, M., Walker-Samuel, S., Wason, J., Williams, K.J., Workman, P., Yankeelov, T.E., Brindle, K.M., McShane, L.M., Jackson, A. and Waterton, J.C. (2016) 'Imaging biomarker roadmap for cancer studies', *Nat Rev Clin Oncol*.

O'Connor, J.P., Rose, C.J., Jackson, A., Watson, Y., Cheung, S., Maders, F., Whitcher, B.J., Roberts, C., Buonaccorsi, G.A., Thompson, G., Clamp, A.R., Jayson, G.C. and Parker, G.J. (2011) 'DCE-MRI biomarkers of tumour heterogeneity predict CRC liver metastasis shrinkage following bevacizumab and FOLFOX-6', *Br J Cancer*, 105(1), pp. 139-45.

Olchowy, C., Cebulski, K., Lasecki, M., Chaber, R., Olchowy, A., Kalwak, K. and Zaleska-Dorobisz, U. (2017) 'The presence of the gadolinium-based contrast agent depositions in the brain and symptoms of gadolinium neurotoxicity - A systematic review', *PLoS One*, 12(2), p. e0171704.

Orlandi, E., Palazzi, M., Pignoli, E., Fallai, C., Giostra, A. and Olmi, P. (2010) 'Radiobiological basis and clinical results of the simultaneous integrated boost (SIB) in intensity modulated radiotherapy (IMRT) for head and neck cancer: A review', *Crit Rev Oncol Hematol*, 73(2), pp. 111-25.

Ott, K., Herrmann, K., Lordick, F., Wieder, H., Weber, W.A., Becker, K., Buck, A.K., Dobritz, M., Fink, U., Ulm, K., Schuster, T., Schwaiger, M., Siewert, J.R. and Krause, B.J. (2008) 'Early metabolic response evaluation by fluorine-18 fluorodeoxyglucose positron emission tomography allows in vivo testing of chemosensitivity in gastric cancer: long-term results of a prospective study', *Clin Cancer Res*, 14(7), pp. 2012-8.

Ott, K., Herrmann, K., Schuster, T., Langer, R., Becker, K., Wieder, H.A., Wester, H.J., Siewert, J.R., zum Buschenfelde, C.M., Buck, A.K., Wilhelm, D., Ebert, M.P., Peschel, C., Schwaiger, M., Lordick, F. and Krause, B.J. (2011) 'Molecular imaging of proliferation and glucose utilization: utility for monitoring response and prognosis after neoadjuvant therapy in locally advanced gastric cancer', *Ann Surg Oncol*, 18(12), pp. 3316-23.

'Package leaflet DOTAREM 0.5 mmol/ml'. February 2014. Solihull: Guerbet Laboratories.

Padhani, A.R., Liu, G., Koh, D.M., Chenevert, T.L., Thoeny, H.C., Takahara, T., Dzik-Jurasz, A., Ross, B.D., Van Cauteren, M., Collins, D., Hammoud, D.A., Rustin, G.J., Taouli, B. and Choyke, P.L. (2009) 'Diffusion-weighted magnetic resonance imaging as a cancer biomarker: consensus and recommendations', *Neoplasia*, 11(2), pp. 102-25.

Perros, P. (2007) 'Introduction to the updated guidelines on the management of thyroid cancer', *Clin Med*, 7(4), pp. 321-2.

Perros, P., Boelaert, K., Colley, S., Evans, C., Evans, R.M., Gerrard Ba, G., Gilbert, J., Harrison, B., Johnson, S.J., Giles, T.E., Moss, L., Lewington, V., Newbold, K., Taylor, J., Thakker, R.V., Watkinson, J., Williams, G.R. and British Thyroid, A. (2014) 'Guidelines for the management of thyroid cancer', *Clin Endocrinol (Oxf)*, 81 Suppl 1, pp. 1-122.

Perumal, M., Pillai, R.G., Barthel, H., Leyton, J., Latigo, J.R., Forster, M., Mitchell, F., Jackman, A.L. and Aboagye, E.O. (2006) 'Redistribution of nucleoside transporters to the cell membrane provides a novel approach for imaging thymidylate synthase inhibition by positron emission tomography', *Cancer Res*, 66(17), pp. 8558-64.

Petralia, G., Bonello, L., Priolo, F., Summers, P. and Bellomi, M. (2011) 'Breast MR with special focus on DW-MRI and DCE-MRI', *Cancer Imaging*, 11, pp. 76-90.

Pickles, M.D., Gibbs, P., Lowry, M. and Turnbull, L.W. (2006) 'Diffusion changes precede size reduction in neoadjuvant treatment of breast cancer', *Magnetic Resonance Imaging*, 24(7), pp. 843-847.

Pio, B.S., Park, C.K., Pietras, R., Hsueh, W.A., Satyamurthy, N., Pegram, M.D., Czernin, J., Phelps, M.E. and Silverman, D.H. (2006) 'Usefulness of 3'-[F-18]fluoro-3'-deoxythymidine with positron emission tomography in predicting breast cancer response to therapy', *Mol Imaging Biol*, 8(1), pp. 36-42.

Plotnik, D.A., McLaughlin, L.J., Krohn, K.A. and Schwartz, J.L. (2012) 'The effects of 5-fluoruracil treatment on 3'-fluoro-3'-deoxythymidine (FLT) transport and metabolism in proliferating and non-proliferating cultures of human tumor cells', *Nucl Med Biol*, 39(7), pp. 970-6.

Ploussard, G., Daneshmand, S., Efstathiou, J.A., Herr, H.W., James, N.D., Rodel, C.M., Shariat, S.F., Shipley, W.U., Sternberg, C.N., Thalmann, G.N. and Kassouf, W. (2014) 'Critical analysis of bladder sparing with trimodal therapy in muscle-invasive bladder cancer: a systematic review', *Eur Urol*, 66(1), pp. 120-37.

Popov, Z., Hoznek, A., Colombel, M., Bastuji-Garin, S., Lefrere-Belda, M.A., Bellot, J., Abboh, C.C., Mazerolles, C. and Chopin, D.K. (1997) 'The prognostic value of p53 nuclear overexpression and MIB-1 as a proliferative marker in transitional cell carcinoma of the bladder', *Cancer*, 80(8), pp. 1472-81.

Porceddu, S.V., Jarmolowski, E., Hicks, R.J., Ware, R., Weih, L., Rischin, D., Corry, J. and Peters, L.J. (2005) 'Utility of positron emission tomography for the detection of disease in residual neck nodes after (chemo)radiotherapy in head and neck cancer', *Head Neck*, 27(3), pp. 175-81.

Proctor, I., Stoeber, K. and Williams, G.H. (2010) 'Biomarkers in bladder cancer', *Histopathology*, 57(1), pp. 1-13.

Pytynia, K.B., Dahlstrom, K.R. and Sturgis, E.M. (2014) 'Epidemiology of HPV-associated oropharyngeal cancer', *Oral Oncol*, 50(5), pp. 380-6.

Quon, A., Chang, S.T., Chin, F., Kamaya, A., Dick, D.W., Loo, B.W., Jr., Gambhir, S.S. and Koong, A.C. (2008) 'Initial evaluation of 18F-fluorothymidine (FLT) PET/CT scanning for primary pancreatic cancer', *Eur J Nucl Med Mol Imaging*, 35(3), pp. 527-31.

Radjenovic, A., Dall, B.J., Ridgway, J.P. and Smith, M.A. (2008) 'Measurement of pharmacokinetic parameters in histologically graded invasive breast tumours using dynamic contrast-enhanced MRI', *Br J Radiol*, 81(962), pp. 120-8.

Rajesh, A., Sokhi, H.K., Fung, R., Mulcahy, K.A. and Bankart, M.J. (2011) 'Bladder cancer: evaluation of staging accuracy using dynamic MRI', *Clin Radiol*, 66(12), pp. 1140-5.

Rasey, J.S., Grierson, J.R., Wiens, L.W., Kolb, P.D. and Schwartz, J.L. (2002) 'Validation of FLT uptake as a measure of thymidine kinase-1 activity in A549 carcinoma cells', *J Nucl Med*, 43(9), pp. 1210-7.

Razek, A.A., Gaballa, G., Denewer, A. and Nada, N. (2010) 'Invasive ductal carcinoma: correlation of apparent diffusion coefficient value with pathological prognostic factors', *NMR Biomed*, 23(6), pp. 619-23.

Rosenkrantz, A.B., Mussi, T.C., Spieler, B., Melamed, J., Taneja, S.S. and Huang, W.C. (2012) 'High-grade bladder cancer: association of the apparent diffusion

coefficient with metastatic disease: preliminary results', *J Magn Reson Imaging*, 35(6), pp. 1478-83.

Saga, T., Kawashima, H., Araki, N., Takahashi, J.A., Nakashima, Y., Higashi, T., Oya, N., Mukai, T., Hojo, M., Hashimoto, N., Manabe, T., Hiraoka, M. and Togashi, K. (2006) 'Evaluation of primary brain tumors with FLT-PET: usefulness and limitations', *Clin Nucl Med*, 31(12), pp. 774-80.

Sanghera, B., Wong, W.L., Sonoda, L.I., Beynon, G., Makris, A., Woolf, D. and Ardeshna, K. (2014) 'FLT PET-CT in evaluation of treatment response', *Indian J Nucl Med*, 29(2), pp. 65-73.

Schelhaas, S., Wachsmuth, L., Viel, T., Honess, D.J., Heinzmann, K., Smith, D.M., Hermann, S., Wagner, S., Kuhlmann, M.T., Muller-Tidow, C., Kopka, K., Schober, O., Schafers, M., Schneider, R., Aboagye, E.O., Griffiths, J., Faber, C. and Jacobs, A.H. (2014a) 'Variability of Proliferation and Diffusion in Different Lung Cancer Models as Measured by 3'-Deoxy-3'-18F-Fluorothymidine PET and Diffusion-Weighted MR Imaging', *J Nucl Med*, 55(6), pp. 983-988.

Schelhaas, S., Wachsmuth, L., Viel, T., Honess, D.J., Heinzmann, K., Smith, D.M., Hermann, S., Wagner, S., Kuhlmann, M.T., Muller-Tidow, C., Kopka, K., Schober, O., Schafers, M., Schneider, R., Aboagye, E.O., Griffiths, J., Faber, C. and Jacobs, A.H. (2014b) 'Variability of Proliferation and Diffusion in Different Lung Cancer Models as Measured by 3'-Deoxy-3'-(1)(8)F-Fluorothymidine PET and Diffusion-Weighted MR Imaging', *J Nucl Med*, 55(6), pp. 983-8.

Schmitz, A.M., Veldhuis, W.B., Menke-Pluijmers, M.B., van der Kemp, W.J., van der Velden, T.A., Kock, M.C., Westenend, P.J., Klomp, D.W. and Gilhuijs, K.G. (2015) 'Multiparametric MRI With Dynamic Contrast Enhancement, Diffusion-Weighted Imaging, and 31-Phosphorus Spectroscopy at 7 T for Characterization of Breast Cancer', *Invest Radiol*, 50(11), pp. 766-71.

Schoder, H., Fury, M., Lee, N. and Kraus, D. (2009) 'PET monitoring of therapy response in head and neck squamous cell carcinoma', *J Nucl Med*, 50 Suppl 1, pp. 74S-88S.

Schrier, B.P., Peters, M., Barentsz, J.O. and Witjes, J.A. (2006) 'Evaluation of chemotherapy with magnetic resonance imaging in patients with regionally metastatic or unresectable bladder cancer', *Eur Urol*, 49(4), pp. 698-703.

Seitz, U., Wagner, M., Neumaier, B., Wawra, E., Glatting, G., Leder, G., Schmid, R.M. and Reske, S.N. (2002) 'Evaluation of pyrimidine metabolising enzymes and in vitro uptake of 3'-[(18)F]fluoro-3'-deoxythymidine ([(18)F]FLT) in pancreatic cancer cell lines', *Eur J Nucl Med Mol Imaging*, 29(9), pp. 1174-81.

Sevcenco, S., Haitel, A., Ponhold, L., Susani, M., Fajkovic, H., Shariat, S.F., Hiess, M., Spick, C., Szarvas, T. and Baltzer, P.A. (2014a) 'Quantitative apparent diffusion coefficient measurements obtained by 3-Tesla MRI are correlated with biomarkers of bladder cancer proliferative activity', *PLoS One*, 9(9), p. e106866.

Sevcenco, S., Ponhold, L., Heinz-Peer, G., Fajkovic, H., Haitel, A., Susani, M., Shariat, S.F., Szarvas, T. and Baltzer, P.A. (2014b) 'Prospective evaluation of diffusion-weighted MRI of the bladder as a biomarker for prediction of bladder cancer aggressiveness', *Urol Oncol*, 32(8), pp. 1166-71.

Shah, C., Miller, T.W., Wyatt, S.K., McKinley, E.T., Olivares, M.G., Sanchez, V., Nolting, D.D., Buck, J.R., Zhao, P., Ansari, M.S., Baldwin, R.M., Gore, J.C., Schiff,

R., Arteaga, C.L. and Manning, H.C. (2009) 'Imaging biomarkers predict response to anti-HER2 (ErbB2) therapy in preclinical models of breast cancer', *Clin Cancer Res*, 15(14), pp. 4712-21.

Sherif, A., Holmberg, L., Rintala, E., Mestad, O., Nilsson, J., Nilsson, S., Malmstrom, P.U. and Nordic Urothelial Cancer, G. (2004) 'Neoadjuvant cisplatinum based combination chemotherapy in patients with invasive bladder cancer: a combined analysis of two Nordic studies', *Eur Urol*, 45(3), pp. 297-303.

Sherley, J.L. and Kelly, T.J. (1988) 'Regulation of human thymidine kinase during the cell cycle', *J Biol Chem*, 263(17), pp. 8350-8.

Shields, A.F. (2012) 'PET imaging of tumor growth: not as easy as it looks', *Clin Cancer Res*, 18(5), pp. 1189-91.

Shields, A.F., Briston, D.A., Chandupatla, S., Douglas, K.A., Lawhorn-Crews, J., Collins, J.M., Mangner, T.J., Heilbrun, L.K. and Muzik, O. (2005) 'A simplified analysis of [18F]3'-deoxy-3'-fluorothymidine metabolism and retention', *Eur J Nucl Med Mol Imaging*, 32(11), pp. 1269-75.

Shields, A.F., Grierson, J.R., Dohmen, B.M., Machulla, H.J., Stayanoff, J.C., Lawhorn-Crews, J.M., Obradovich, J.E., Muzik, O. and Mangner, T.J. (1998) 'Imaging proliferation in vivo with [F-18]FLT and positron emission tomography', *Nat Med*, 4(11), pp. 1334-6.

Skougaard, K., Nielsen, D., Jensen, B.V. and Hendel, H.W. (2013) 'Comparison of EORTC criteria and PERCIST for PET/CT response evaluation of patients with metastatic colorectal cancer treated with irinotecan and cetuximab', *J Nucl Med*, 54(7), pp. 1026-31.

Smith, T.J., Bohlke, K., Lyman, G.H., Carson, K.R., Crawford, J., Cross, S.J., Goldberg, J.M., Khatcheressian, J.L., Leighl, N.B., Perkins, C.L., Somlo, G., Wade, J.L., Wozniak, A.J. and Armitage, J.O. (2015) 'Recommendations for the Use of WBC Growth Factors: American Society of Clinical Oncology Clinical Practice Guideline Update', *J Clin Oncol*, 33(28), pp. 3199-212.

Smith, Z.L., Christodouleas, J.P., Keefe, S.M., Malkowicz, S.B. and Guzzo, T.J. (2013) 'Bladder preservation in the treatment of muscle-invasive bladder cancer (MIBC): a review of the literature and a practical approach to therapy', *BJU Int*, 112(1), pp. 13-25.

Solsona, E., Iborra, I., Rubio, J., Casanova, J., Dumont, R. and Monros, J.L. (2003) 'Late oncological occurrences following radical cystectomy in patients with bladder cancer', *Eur Urol*, 43(5), pp. 489-94.

Somoye, G., Harry, V., Semple, S., Plataniotis, G., Scott, N., Gilbert, F.J. and Parkin, D. (2012) 'Early diffusion weighted magnetic resonance imaging can predict survival in women with locally advanced cancer of the cervix treated with combined chemo-radiation', *Eur Radiol*, 22(11), pp. 2319-27.

Sonpavde, G., Goldman, B.H., Speights, V.O., Lerner, S.P., Wood, D.P., Vogelzang, N.J., Trump, D.L., Natale, R.B., Grossman, H.B. and Crawford, E.D. (2009) 'Quality of pathologic response and surgery correlate with survival for patients with completely resected bladder cancer after neoadjuvant chemotherapy', *Cancer*, 115(18), pp. 4104-9.

Statistics, O.f.N. 44 (2015) 'Statistical Bulletin: Cancer Survival in England: adults diagnosed in 2009 to 2013, followed up to 2014'. 19 November 2015. England: Office for National Statistics. Available at: http://www.ons.gov.uk/ons/rel/cancer-unit/cancer-survival/cancer-survival-in-england--adults-diagnosed--2009-to-2013--followed-up-to-2014/stb-cancer-survival.html.

Stein, J.P. (2006) 'Improving outcomes with radical cystectomy for high-grade invasive bladder cancer', *World J Urol*, 24(5), pp. 509-16.

Stejskal, E.O. and Tanner, J.E. (1965) 'Spin Diffusion Measurements: Spin Echoes in the Presence of a Time-Dependent Field Gradient', *The Journal of Chemical Physics*, 42(1), pp. 288-292.

Stenzl, A., Cowan, N.C., De Santis, M., Jakse, G., Kuczyk, M.A., Merseburger, A.S., Ribal, M.J., Sherif, A. and Witjes, J.A. (2009) 'The updated EAU guidelines on muscle-invasive and metastatic bladder cancer', *Eur Urol*, 55(4), pp. 815-25 [Online].

Sultana, A., Smith, C.T., Cunningham, D., Starling, N., Neoptolemos, J.P. and Ghaneh, P. (2007) 'Meta-analyses of chemotherapy for locally advanced and metastatic pancreatic cancer', *J Clin Oncol*, 25(18), pp. 2607-15.

Sutterluety, H., Bartl, S., Doetzlhofer, A., Khier, H., Wintersberger, E. and Seiser, C. (1998) 'Growth-regulated antisense transcription of the mouse thymidine kinase gene', *Nucleic Acids Res*, 26(21), pp. 4989-95.

Sweis, R.F., Medved, M., Towey, S., Karczmar, G.S., Oto, A., Szmulewitz, R.Z., O'Donnell, P.H., Fishkin, P., Karrison, T. and Stadler, W.M. (2016) 'Dynamic Contrast-Enhanced Magnetic Resonance Imaging as a Pharmacodynamic Biomarker for Pazopanib in Metastatic Renal Carcinoma', *Clin Genitourin Cancer*.

Swinnen, G., Maes, A., Pottel, H., Vanneste, A., Billiet, I., Lesage, K. and Werbrouck, P. (2010) 'FDG-PET/CT for the preoperative lymph node staging of invasive bladder cancer', *Eur Urol*, 57(4), pp. 641-7.

Sylvester, R.J., van der Meijden, A.P., Oosterlinck, W., Witjes, J.A., Bouffioux, C., Denis, L., Newling, D.W. and Kurth, K. (2006) 'Predicting recurrence and progression in individual patients with stage Ta T1 bladder cancer using EORTC risk tables: a combined analysis of 2596 patients from seven EORTC trials', *Eur Urol*, 49(3), pp. 466-5; discussion 475-7.

Tahari, A.K., Alluri, K.C., Quon, H., Koch, W., Wahl, R.L. and Subramaniam, R.M. (2014) 'FDG PET/CT imaging of oropharyngeal squamous cell carcinoma: characteristics of human papillomavirus-positive and -negative tumors', *Clin Nucl Med*, 39(3), pp. 225-31.

Takeuchi, M., Sasaki, S., Ito, M., Okada, S., Takahashi, S., Kawai, T., Suzuki, K., Oshima, H., Hara, M. and Shibamoto, Y. (2009) 'Urinary bladder cancer: diffusion-weighted MR imaging--accuracy for diagnosing T stage and estimating histologic grade', *Radiology*, 251(1), pp. 112-21.

Tanabe, K., Yoshida, S., Koga, F., Inoue, M., Kobayashi, S., Ishioka, J., Tamura, T., Sugawara, E., Saito, K., Akashi, T., Fujii, Y. and Kihara, K. (2015) 'High Ki-67 Expression Predicts Favorable Survival in Muscle-Invasive Bladder Cancer Patients Treated With Chemoradiation-Based Bladder-Sparing Protocol', *Clin Genitourin Cancer*, 13(4), pp. e243-51.

Tanimoto, A., Yuasa, Y., Imai, Y., Izutsu, M., Hiramatsu, K., Tachibana, M. and Tazaki, H. (1992) 'Bladder tumor staging: comparison of conventional and gadolinium-enhanced dynamic MR imaging and CT', *Radiology*, 185(3), pp. 741-7.

Taouli, B., Beer, A.J., Chenevert, T., Collins, D., Lehman, C., Matos, C., Padhani, A.R., Rosenkrantz, A.B., Shukla-Dave, A., Sigmund, E., Tanenbaum, L., Thoeny, H., Thomassin-Naggara, I., Barbieri, S., Corcuera-Solano, I., Orton, M., Partridge, S.C. and Koh, D.-M. (2016) 'Diffusion-weighted imaging outside the brain: Consensus statement from an ISMRM-sponsored workshop', *Journal of Magnetic Resonance Imaging*, pp. n/a-n/a.

Thorwarth, D., Eschmann, S.M., Paulsen, F. and Alber, M. (2007) 'Hypoxia dose painting by numbers: a planning study', *Int J Radiat Oncol Biol Phys*, 68(1), pp. 291-300.

Tofts, P.S., Brix, G., Buckley, D.L., Evelhoch, J.L., Henderson, E., Knopp, M.V., Larsson, H.B., Lee, T.Y., Mayr, N.A., Parker, G.J., Port, R.E., Taylor, J. and Weisskoff, R.M. (1999) 'Estimating kinetic parameters from dynamic contrast-enhanced T(1)-weighted MRI of a diffusable tracer: standardized quantities and symbols', *J Magn Reson Imaging*, 10(3), pp. 223-32.

Tokunaga, Y., Hosogi, H., Hoppou, T., Nakagami, M., Tokuka, A. and Ohsumi, K. (2002) 'Prognostic value of thymidine phosphorylase/platelet-derived endothelial cell growth factor in advanced colorectal cancer after surgery: evaluation with a new monoclonal antibody', *Surgery*, 131(5), pp. 541-7.

Troost, E.G., Bussink, J., Hoffmann, A.L., Boerman, O.C., Oyen, W.J. and Kaanders, J.H. (2010) '18F-FLT PET/CT for early response monitoring and dose escalation in oropharyngeal tumors', *J Nucl Med*, 51(6), pp. 866-74.

Troost, E.G., Bussink, J., Oyen, W.J. and Kaanders, J.H. (2009) '18F-FDG and 18F-FLT do not discriminate between reactive and metastatic lymph nodes in oral cancer', *J Nucl Med*, 50(3), pp. 490-1.

Troost, E.G., Vogel, W.V., Merkx, M.A., Slootweg, P.J., Marres, H.A., Peeters, W.J., Bussink, J., van der Kogel, A.J., Oyen, W.J. and Kaanders, J.H. (2007) '18F-FLT PET does not discriminate between reactive and metastatic lymph nodes in primary head and neck cancer patients', *J Nucl Med*, 48(5), pp. 726-35.

Trusheim, M.R., Berndt, E.R. and Douglas, F.L. (2007) 'Stratified medicine: strategic and economic implications of combining drugs and clinical biomarkers', *Nat Rev Drug Discov*, 6(4), pp. 287-93.

Vale, C.L. (2005) 'Neoadjuvant Chemotherapy in Invasive Bladder Cancer: Update of a Systematic Review and Meta-Analysis of Individual Patient Data: Advanced Bladder Cancer (ABC) Meta-analysis Collaboration', *Eur Urol*, 48(2), pp. 202-206.

Vallius, T., Peter, A., Auranen, A., Carpen, O., Kemppainen, J., Matomaki, J., Oksa, S., Roering, P., Seppanen, M., Grenman, S. and Hynninen, J. (2016) '18F-FDG-PET/CT can identify histopathological non-responders to platinum-based neoadjuvant chemotherapy in advanced epithelial ovarian cancer', *Gynecol Oncol*, 140(1), pp. 29-35.

van Heijl, M., Omloo, J.M., van Berge Henegouwen, M.I., Hoekstra, O.S., Boellaard, R., Bossuyt, P.M., Busch, O.R., Tilanus, H.W., Hulshof, M.C., van der Gaast, A., Nieuwenhuijzen, G.A., Bonenkamp, H.J., Plukker, J.T., Cuesta, M.A., Ten Kate, F.J., Pruim, J., van Dekken, H., Bergman, J.J., Sloof, G.W. and van Lanschot, J.J. (2011)

'Fluorodeoxyglucose positron emission tomography for evaluating early response during neoadjuvant chemoradiotherapy in patients with potentially curable esophageal cancer', *Ann Surg*, 253(1), pp. 56-63.

van Waarde, A., Cobben, D.C., Suurmeijer, A.J., Maas, B., Vaalburg, W., de Vries, E.F., Jager, P.L., Hoekstra, H.J. and Elsinga, P.H. (2004) 'Selectivity of 18F-FLT and 18F-FDG for differentiating tumor from inflammation in a rodent model', *J Nucl Med*, 45(4), pp. 695-700.

van Westreenen, H.L., Cobben, D.C., Jager, P.L., van Dullemen, H.M., Wesseling, J., Elsinga, P.H. and Plukker, J.T. (2005) 'Comparison of 18F-FLT PET and 18F-FDG PET in esophageal cancer', *J Nucl Med*, 46(3), pp. 400-4.

Vandecaveye, V., Michielsen, K., De Keyzer, F., Laleman, W., Komuta, M., Op de beeck, K., Roskams, T., Nevens, F., Verslype, C. and Maleux, G. (2014) 'Chemoembolization for hepatocellular carcinoma: 1-month response determined with apparent diffusion coefficient is an independent predictor of outcome', *Radiology*, 270(3), pp. 747-57.

Venkatasubramanian, R., Arenas, R.B., Henson, M.A. and Forbes, N.S. (2010) 'Mechanistic modelling of dynamic MRI data predicts that tumour heterogeneity decreases therapeutic response', *Br J Cancer*, 103(4), pp. 486-97.

Verma, S., Rajesh, A., Prasad, S.R., Gaitonde, K., Lall, C.G., Mouraviev, V., Aeron, G., Bracken, R.B. and Sandrasegaran, K. (2012) 'Urinary Bladder Cancer: Role of MR Imaging', *Radiographics*, 32(2), pp. 371-387.

Vesselle, H., Grierson, J., Muzi, M., Pugsley, J.M., Schmidt, R.A., Rabinowitz, P., Peterson, L.M., Vallieres, E. and Wood, D.E. (2002) 'In vivo validation of 3'deoxy-3'-[(18)F]fluorothymidine ([(18)F]FLT) as a proliferation imaging tracer in humans: correlation of [(18)F]FLT uptake by positron emission tomography with Ki-67 immunohistochemistry and flow cytometry in human lung tumors', *Clin Cancer Res*, 8(11), pp. 3315-23.

Vesselle, H., Grierson, J., Peterson, L.M., Muzi, M., Mankoff, D.A. and Krohn, K.A. (2003) '18F-Fluorothymidine radiation dosimetry in human PET imaging studies', *J Nucl Med*, 44(9), pp. 1482-8.

Vesselle, H., Salskov, A., Turcotte, E., Wiens, L., Schmidt, R., Jordan, C.D., Vallieres, E. and Wood, D.E. (2008) 'Relationship between non-small cell lung cancer FDG uptake at PET, tumor histology, and Ki-67 proliferation index', *J Thorac Oncol*, 3(9), pp. 971-8.

Vineeth Kumar, P.M., Verma, G.R., Mittal, B.R., Agrawal, K., Gupta, R., Kochhar, R., Singh, V., Kaman, L. and Singh, R. (2016) 'FLT PET/CT Is Better Than FDG PET/CT in Differentiating Benign From Malignant Pancreatobiliary Lesions', *Clin Nucl Med*.

von der Maase, H., Hansen, S.W., Roberts, J.T., Dogliotti, L., Oliver, T., Moore, M.J., Bodrogi, I., Albers, P., Knuth, A., Lippert, C.M., Kerbrat, P., Sanchez Rovira, P., Wersall, P., Cleall, S.P., Roychowdhury, D.F., Tomlin, I., Visseren-Grul, C.M. and Conte, P.F. (2000) 'Gemcitabine and cisplatin versus methotrexate, vinblastine, doxorubicin, and cisplatin in advanced or metastatic bladder cancer: results of a large, randomized, multinational, multicenter, phase III study', *J Clin Oncol*, 18(17), pp. 3068-77.

Wahl, R.L., Jacene, H., Kasamon, Y. and Lodge, M.A. (2009) 'From RECIST to PERCIST: Evolving Considerations for PET response criteria in solid tumors', *J Nucl Med*, 50 Suppl 1, pp. 122S-50S.

Walker-Samuel, S., Parker, C.C., Leach, M.O. and Collins, D.J. (2007) 'Reproducibility of reference tissue quantification of dynamic contrast-enhanced data: comparison with a fixed vascular input function', *Phys Med Biol*, 52(1), pp. 75-89.

Wang, H.J., Pui, M.H., Guo, Y., Yang, D., Pan, B.T. and Zhou, X.H. (2014a) 'Diffusion-weighted MRI in bladder carcinoma: the differentiation between tumor recurrence and benign changes after resection', *Abdom Imaging*, 39(1), pp. 135-41.

Wang, L., Feng, C., Ding, G., Ding, Q., Zhou, Z., Jiang, H. and Wu, Z. (2014b) 'Ki67 and TP53 expressions predict recurrence of non-muscle-invasive bladder cancer', *Tumour Biol*, 35(4), pp. 2989-95.

Wang, M.Y., Cheng, J.L., Han, Y.H., Li, Y.L., Dou, S.W., Yan, F.S. and Shi, D.P. (2011) 'Comparison of volumetric methods for tumor measurements on two and three dimensional MRI in adult glioblastoma', *Neuroradiology*, 53(8), pp. 565-9.

Warth, A., Cortis, J., Soltermann, A., Meister, M., Budczies, J., Stenzinger, A., Goeppert, B., Thomas, M., Herth, F.J., Schirmacher, P., Schnabel, P.A., Hoffmann, H., Dienemann, H., Muley, T. and Weichert, W. (2014) 'Tumour cell proliferation (Ki-67) in non-small cell lung cancer: a critical reappraisal of its prognostic role', *Br J Cancer*, 111(6), pp. 1222-9.

Watanabe, N. and Jeremic, B. (2008) *The Role of PET/CT in Radiation Treatment Planning for Cancer Patient Treatment* (IAEA-TECDOC-1603). Vienna, Austria: International Atomic Energy Agency. [Online]. Available at: http://www-pub.iaea.org/MTCD/publications/PDF/te_1603_web.pdf.

Weber, W.A., Ott, K., Becker, K., Dittler, H.J., Helmberger, H., Avril, N.E., Meisetschlager, G., Busch, R., Siewert, J.R., Schwaiger, M. and Fink, U. (2001) 'Prediction of response to preoperative chemotherapy in adenocarcinomas of the esophagogastric junction by metabolic imaging', *J Clin Oncol*, 19(12), pp. 3058-65.

Wells, P., Aboagye, E., Gunn, R.N., Osman, S., Boddy, A.V., Taylor, G.A., Rafi, I., Hughes, A.N., Calvert, A.H., Price, P.M. and Newell, D.R. (2003) '2-[11C]thymidine positron emission tomography as an indicator of thymidylate synthase inhibition in patients treated with AG337', *J Natl Cancer Inst*, 95(9), pp. 675-82.

Welsh, J.L., Bodeker, K., Fallon, E., Bhatia, S.K., Buatti, J.M. and Cullen, J.J. (2012) 'Comparison of response evaluation criteria in solid tumors with volumetric measurements for estimation of tumor burden in pancreatic adenocarcinoma and hepatocellular carcinoma', *Am J Surg*, 204(5), pp. 580-5.

Whittaker, C.S., Coady, A., Culver, L., Rustin, G., Padwick, M. and Padhani, A.R. (2009) 'Diffusion-weighted MR imaging of female pelvic tumors: a pictorial review', *Radiographics*, 29(3), pp. 759-74; discussion 774-8.

Willaime, J.M., Turkheimer, F.E., Kenny, L.M. and Aboagye, E.O. (2013) 'Quantification of intra-tumour cell proliferation heterogeneity using imaging descriptors of 18F fluorothymidine-positron emission tomography', *Phys Med Biol*, 58(2), pp. 187-203.

Witjes, J.A., Comperat, E., Cowan, N.C., De Santis, M., Gakis, G., James, N., Lebret, T., Sherif, A., van der Heijden, A.G. and Ribal, M.J. (2015) *Guidelines on Muscle-Invasive and Metastatic Bladder Cancer*. European Association of Urology.

Woolf, D.K., Taylor, N.J., Makris, A., Tunariu, N., Collins, D.J., Li, S.P., Ah-See, M.L., Beresford, M. and Padhani, A.R. (2016) 'Arterial input functions in dynamic contrast-enhanced magnetic resonance imaging: which model performs best when assessing breast cancer response?', *Br J Radiol*, 89(1063), p. 20150961.

Wu, L.A., Chang, R.F., Huang, C.S., Lu, Y.S., Chen, H.H., Chen, J.Y. and Chang, Y.C. (2015a) 'Evaluation of the treatment response to neoadjuvant chemotherapy in locally advanced breast cancer using combined magnetic resonance vascular maps and apparent diffusion coefficient', *J Magn Reson Imaging*, 42(5), pp. 1407-20.

Wu, P., Liu, S., Zhang, W., Zhang, Y., Zhu, G., Wei, D., Wan, B. and Wang, J. (2015b) 'Low-level Ki-67 expression as an independent predictor of bladder tumour recurrence in patients with primary upper tract urothelial carcinoma after radical nephroureterectomy', *Jpn J Clin Oncol*, 45(12), pp. 1175-81.

Wu, T.T., Chen, J.H., Lee, Y.H. and Huang, J.K. (2000) 'The role of bcl-2, p53, and ki-67 index in predicting tumor recurrence for low grade superficial transitional cell bladder carcinoma', *J Urol*, 163(3), pp. 758-60.

Xu, Y., Liu, B., Shi, Q.L., Huang, P.L., Zhou, X.J., Ma, H.H., Lu, Z.F., Bo, Y., Eriksson, S., He, E. and Skog, S. (2014) 'Thymidine kinase 1 is a better prognostic marker than Ki-67 for pT1 adenocarcinoma of the lung', *Int J Clin Exp Med*, 7(8), pp. 2120-8.

Yang, X. and Knopp, M.V. (2011) 'Quantifying tumor vascular heterogeneity with dynamic contrast-enhanced magnetic resonance imaging: a review', *J Biomed Biotechnol*, 2011, p. 732848.

Yankeelov, T.E. and Gore, J.C. (2009) 'Dynamic Contrast Enhanced Magnetic Resonance Imaging in Oncology: Theory, Data Acquisition, Analysis, and Examples', *Curr Med Imaging Rev*, 3(2), pp. 91-107.

Yankeelov, T.E., Lepage, M., Chakravarthy, A., Broome, E.E., Niermann, K.J., Kelley, M.C., Meszoely, I., Mayer, I.A., Herman, C.R., McManus, K., Price, R.R. and Gore, J.C. (2007) 'Integration of quantitative DCE-MRI and ADC mapping to monitor treatment response in human breast cancer: initial results', *Magn Reson Imaging*, 25(1), pp. 1-13.

Yi, B., Kang, D.K., Yoon, D., Jung, Y.S., Kim, K.S., Yim, H. and Kim, T.H. (2014) 'Is there any correlation between model-based perfusion parameters and model-free parameters of time-signal intensity curve on dynamic contrast enhanced MRI in breast cancer patients?', *Eur Radiol*, 24(5), pp. 1089-96.

Yoshida, S., Koga, F., Kobayashi, S., Ishii, C., Tanaka, H., Tanaka, H., Komai, Y., Saito, K., Masuda, H., Fujii, Y., Kawakami, S. and Kihara, K. (2012) 'Role of diffusion-weighted magnetic resonance imaging in predicting sensitivity to chemoradiotherapy in muscle-invasive bladder cancer', *Int J Radiat Oncol Biol Phys*, 83(1), pp. e21-7.

Yue, J., Chen, L., Cabrera, A.R., Sun, X., Zhao, S., Zheng, F., Han, A., Zheng, J., Teng, X., Ma, L., Ma, Y., Han, D., Zhao, X., Mu, D., Yu, J. and Li, Y. (2010) 'Measuring tumor cell proliferation with 18F-FLT PET during radiotherapy of esophageal squamous cell carcinoma: a pilot clinical study', *J Nucl Med*, 51(4), pp. 528-34.

Zaidi, H., Abdoli, M., Fuentes, C.L. and El Naqa, I.M. (2012) 'Comparative methods for PET image segmentation in pharyngolaryngeal squamous cell carcinoma', *Eur J Nucl Med Mol Imaging*, 39(5), pp. 881-91.

Zaidi, H. and El Naqa, I. (2010) 'PET-guided delineation of radiation therapy treatment volumes: a survey of image segmentation techniques', *Eur J Nucl Med Mol Imaging*, 37(11), pp. 2165-87.

Zargar, H., Espiritu, P.N., Fairey, A.S., Mertens, L.S., Dinney, C.P., Mir, M.C., Krabbe, L.M., Cookson, M.S., Jacobsen, N.E., Gandhi, N.M., Griffin, J., Montgomery, J.S., Vasdev, N., Yu, E.Y., Youssef, D., Xylinas, E., Campain, N.J., Kassouf, W., Dall'Era, M.A., Seah, J.A., Ercole, C.E., Horenblas, S., Sridhar, S.S., McGrath, J.S., Aning, J., Shariat, S.F., Wright, J.L., Thorpe, A.C., Morgan, T.M., Holzbeierlein, J.M., Bivalacqua, T.J., North, S., Barocas, D.A., Lotan, Y., Garcia, J.A., Stephenson, A.J., Shah, J.B., van Rhijn, B.W., Daneshmand, S., Spiess, P.E. and Black, P.C. (2015) 'Multicenter assessment of neoadjuvant chemotherapy for muscle-invasive bladder cancer', *Eur Urol*, 67(2), pp. 241-9.

Zhang, C.C., Yan, Z., Li, W., Kuszpit, K., Painter, C.L., Zhang, Q., Lappin, P.B., Nichols, T., Lira, M.E., Affolter, T., Fahey, N.R., Cullinane, C., Spilker, M., Zasadny, K., O'Brien, P., Buckman, D., Wong, A. and Christensen, J.G. (2012a) '[(18)F]FLT-PET imaging does not always "light up" proliferating tumor cells', *Clin Cancer Res*, 18(5), pp. 1303-12.

Zhang, C.C., Yan, Z., Li, W., Kuszpit, K., Painter, C.L., Zhang, Q., Lappin, P.B., Nichols, T., Lira, M.E., Affolter, T., Fahey, N.R., Cullinane, C., Spilker, M., Zasadny, K., O'Brien, P., Buckman, D., Wong, A. and Christensen, J.G. (2012b) '[18F]FLT–PET Imaging Does Not Always “Light Up” Proliferating Tumor Cells', *Clinical Cancer Research*, 18(5), pp. 1303-1312.

Zhang, X., Zheng, Z., Shin, Y.K., Kim, K.Y., Rha, S.Y., Noh, S.H., Chung, H.C. and Jeung, H.C. (2014) 'Angiogenic factor thymidine phosphorylase associates with angiogenesis and lymphangiogenesis in the intestinal-type gastric cancer', *Pathology*, 46(4), pp. 316-24.

Zhao, B., Tan, Y., Bell, D.J., Marley, S.E., Guo, P., Mann, H., Scott, M.L., Schwartz, L.H. and Ghiorghiu, D.C. (2013) 'Exploring intra- and inter-reader variability in uni-dimensional, bi-dimensional, and volumetric measurements of solid tumors on CT scans reconstructed at different slice intervals', *Eur J Radiol*, 82(6), pp. 959-68.

Zhou, M., Wang, C., Hu, S., Zhang, Y., Yao, Z., Li, J., Guo, W. and Zhang, Y. (2013) '18F-FLT PET/CT imaging is not competent for the pretreatment evaluation of metastatic gastric cancer: a comparison with 18F-FDG PET/CT imaging', *Nucl Med Commun*, 34(7), pp. 694-700.

Zygogianni, A., Kyrgias, G., Kouvaris, J., Pistevou-Gompaki, K. and Kouloulias, V. (2012) 'A new role of PET/CT for target delineation for radiotherapy treatment planning for head and neck carcinomas', *Hell J Nucl Med*, 15(2), pp. 139-43.